

DISS. ETH NO. 17724

Light-induced dissolution of iron(III) (hydr)oxides in the presence and absence of siderophores

A dissertation submitted to
ETH ZURICH

for the degree of
Doctor of Sciences

presented by

Paul Michael Borer
Dipl. Umwelt-Natw. ETH
Born April 8, 1977
citizen of Erschwil, SO

accepted on the recommendation of

Prof. Dr. Ruben Kretzschmar, examiner
Prof. Dr. Stephan M. Kraemer, co-examiner
PD. Dr. Barbara Sulzberger, co-examiner
Dr. Stephan Hug, co-examiner

Zürich, 2008

This Ph.D thesis was conducted at ETH Zürich and at the Swiss Federal Institute of Aquatic Science and Technology (Eawag) in Dübendorf. It was financially supported by Eawag and by the Swiss National Science Foundation (project No. 200021-105268).

Table of contents

SUMMARY	VII
ZUSAMMENFASSUNG	IX
INTRODUCTION	1
CHAPTER 1: EFFECT OF SIDEROPHORES ON THE LIGHT-INDUCED DISSOLUTION OF COLLOIDAL IRON(III) (HYDR)OXIDES	9
Introduction	10
Roles of siderophores in the light-induced redox cycling of dissolved iron	11
Roles of siderophores in the thermal dissolution of iron oxides	12
Mechanism and rate law of light-induced dissolution of iron oxides	13
Purpose of this study	14
Materials and methods	14
Materials	14
Dissolution experiments	15
Photolysis of dissolved Fe(III)-siderophore complexes	16
Results	16
Photolysis of Fe(III)-siderophore complexes in homogeneous and heterogeneous systems	16
Effects of DFOB or aerobactin and light on the dissolution of lepidocrocite and goethite	18
Photodissolution of lepidocrocite and goethite in the presence of DFOB and/or oxalate	18
Non-steady-state experiments with lepidocrocite and goethite in the two-ligand system DFOB/oxalate	22
Discussion	24
Photolysis of Fe(III)-siderophore complexes	24
Thermal and photodissolution of lepidocrocite by DFOB and aerobactin	26
Thermal and photodissolution of goethite and lepidocrocite in the two-ligand system DFOB/oxalate	27
Conclusions	29
References	30

CHAPTER 2: PHOTOLYSIS OF CITRATE ON THE SURFACE OF LEPIDOCROCITE: AN IN SITU ATR-FTIR STUDY	37
Introduction	38
Experimental section	39
Synthesis of lepidocrocite	39
Batch dissolution experiments	40
Preparation of lepidocrocite thin film layers for ATR-FTIR experiments	41
ATR-FTIR adsorption and photoirradiation experiments	41
Results and discussion	43
Batch photoirradiation experiments with ¹⁴ C-labeled citrate	43
Decomposition of the photoproduct	45
Readsorption of Fe(II)	46
ATR-FTIR photoirradiation experiments	48
ATR-FTIR spectra of adsorbed citrate and acetonedicarboxylic acid	49
Heat generation during ATR-FTIR photoirradiation experiments	50
ATR-FTIR photoirradiation experiment at pH 4	52
ATR-FTIR photoirradiation experiment at pH 6	52
Parallel and consecutive reactions during photoirradiation experiments	54
Ligand-exchange reactions	55
Decomposition of the intermediate photoproduct(s)	57
Conclusions	60
References	60
CHAPTER 3: ATR-FTIR SPECTROSCOPIC STUDY OF THE ADSORPTION OF DESFERRIOXAMINE B AND AEROBACTIN TO THE SURFACE OF LEPIDOCROCITE (γ-FeOOH)	65
Introduction	66
Materials and methods	68
Samples	68
ATR-FTIR spectra of solution species	69
ATR-FTIR spectra of adsorbed species	70
ATR-FTIR photoirradiation experiments	71
Results and discussion	71
IR spectra of DFOB in aqueous solutions	71
IR spectra of aerobactin in aqueous solutions	74
IR spectra of aqueous Fe(III)-DFOB and Fe(III)-aerobactin complexes	77

Assessment of surface interactions of siderophore functional groups	78
IR spectra of DFOB adsorbed to lepidocrocite	80
IR spectra of aerobactin adsorbed to lepidocrocite	83
Photoirradiation of adsorbed DFOB and adsorbed aerobactin	85
Summary and conclusions	87
References	89
Supporting Information	93

CHAPTER 4: PHOTODISSOLUTION OF LEPIDOCROCITE (γ -FeOOH) IN THE PRESENCE OF DESFERRIOXAMINE B AND AEROBACTIN 97

Introduction	98
Experimental section	100
Samples	100
Adsorption of siderophores	100
Readsorption of Fe(III)-siderophore complexes	102
(Photo)dissolution experiments	103
Adsorption and dissolution experiments with citrate	104
Results and discussion	104
Adsorption of DFOB and aerobactin to lepidocrocite	104
Effect of ionic strength on the adsorption of DFOB and aerobactin	107
Adsorption of aqueous Fe(III)-siderophore complexes	108
Proton-promoted (photo)dissolution of lepidocrocite	110
Siderophore-promoted (photo)dissolution of lepidocrocite	112
Non-linear dissolution kinetics in the presence of aerobactin	113
The mechanism of siderophore-controlled dissolution in the dark	117
The mechanism of photoreductive dissolution	121
Summary and conclusions	124
References	125
Supporting Information	131

CHAPTER 5: PHOTOREDUCTIVE DISSOLUTION IRON(III) (HYDR) OXIDES IN THE ABSENCE OF ORGANIC LIGANDS: EXPERIMENTAL STUDIES AND KINETIC MODELING 137

Introduction	138
Experimental section	139

Materials	139
Synthesis of iron(III) (hydr)oxides	139
Analytical methods	140
Experimental procedure	140
Kinetic modeling	141
Results and discussion	141
Photoreductive dissolution of lepidocrocite	141
Formation of reactive oxygen species (ROS)	143
Kinetic modeling of Fe(II) and ROS formation	145
Effect of radical scavengers and organic ligands on photoreductive dissolution	147
Photoreactivity of other iron (hydr)oxides	150
Environmental significance	152
References	152
Supporting Information	155

CHAPTER 6: WAVELENGTH-DEPENDENCE OF PHOTOREDUCTIVE DISSOLUTION OF LEPIDOCROCITE (γ-FEOOH) IN THE ABSENCE AND PRESENCE OF THE SIDEROPHORE DFOB	167
Introduction	168
Experimental section	169
Materials	169
Analytical methods	170
Experimental setup	170
Calculation of normalized photoreductive dissolution rates	172
Results and discussion	172
Photoreductive dissolution of lepidocrocite in the absence of organic ligands	172
Photoreductive dissolution of lepidocrocite in the presence of desferrioxamine B	176
Environmental significance	179
References	180
Supporting Information	185

CONCLUSIONS AND OUTLOOK	199
Siderophore-promoted dissolution iron(III) hydroxide phases	199
Environmental significance	201
Outlook	202
References	203
ACKNOWLEDGEMENTS	205
CURRICULUM VITAE	207

Summary

Iron is essential for phytoplankton growth, and recent research has confirmed that it is a limiting micronutrient in large parts of the oceans. An important pathway by which new iron is introduced into surface waters is by atmospheric deposition of iron containing aerosols (e.g., mineral dust). Particulate iron is however not directly available to most phytoplankton species. Since iron bioavailability is primarily controlled by dissolved iron, any process that facilitates the transformation of particulate iron into dissolved forms of iron may increase the bioavailable amount of this limited micronutrient. To overcome iron starvation, microorganisms have evolved different iron acquisition and uptake systems. One of the strategies is to exude strong iron binding ligands, so called siderophores, into the water column. Due to the high affinity and specificity of these chelate compounds for iron, siderophores are able to retain iron from iron-bearing minerals or iron(III) (hydr)oxide phases by dissolving these phases and preventing the loss of dissolved iron in the water column by precipitation and scavenging processes. Iron bound to siderophores may be utilized by phytoplankton by different uptake mechanisms.

In sunlit surface waters, the dissolution of iron-bearing minerals or iron(III) (hydr)oxides can be significantly enhanced by photoreductive processes leading to the formation of kinetically labile Fe(II). Hitherto, photoreductive dissolution of iron(III) (hydr)oxides in the presence of siderophores has not been investigated. The aim of this thesis was to investigate the effect of (sun)light on siderophore-controlled dissolution of iron(III) (hydr)oxide phases under controlled laboratory conditions.

Interactions of siderophores with iron(III) (hydr)oxide surfaces is key to understanding the dissolution reactivity of these compounds. The interactions of two siderophores, desferrioxamine B and aerobactin, with the surface of lepidocrocite (γ -FeOOH) were investigated at the macroscopic and also at the molecular level by ATR-FTIR spectroscopy. In addition, rates of siderophore-promoted dissolution were studied as a function of the surface concentrations of siderophores. Dissolution experiments were also performed with other iron(III) (hydr)oxides phases in the presence and absence of these siderophores. Furthermore, we investigated siderophore-promoted dissolution of lepidocrocite under irradiation of artificial sunlight at different wavelengths.

The spectroscopic and macroscopic adsorption experiments suggested that DFOB is predominantly coordinated to the surface of lepidocrocite at acidic pH by inner-

sphere coordination of two to three hydroxamate groups. In the case of aerobactin, the experimental findings suggested that the carboxylic acid groups are involved in the coordination of aerobactin to the surface of lepidocrocite. The surface interactions of the hydroxamate groups, however, could not be determined in these experiments.

Rate constants determined for the dissolution of lepidocrocite revealed that DFOB is far more effective than aerobactin in promoting dissolution of lepidocrocite. This was explained by the formation of less dissolution active surface complexes of aerobactin at the surface of lepidocrocite as compared to DFOB. In this study, we provided evidence for the photoreactivity of solution Fe(III)-aerobactin complexes. Dissolution experiments conducted under simulated sunlight indicated that the potentially photoreactive iron binding group of aerobactin (α -hydroxycarboxylic acid) might form a photoreactive surface complex leading to photoreductive dissolution of lepidocrocite. Interestingly, dissolution rates determined under irradiation increased similarly in the presence of DFOB and aerobactin as compared to the rates determined in the dark. This observation was explained by the formation of Fe(II) at the surface of lepidocrocite by photochemical mechanisms intrinsic to the lepidocrocite solid, (i) by surface scavenging of photoelectrons generated in the semiconducting bulk and (ii) by photolysis of surface Fe(III)-hydroxo groups. Evidence for these processes was provided by dissolution experiments showing that dissolved Fe(II) is formed in irradiated lepidocrocite suspensions in the absence of organic ligands. Concomitant with the formation of Fe(II), we also observed the formation of reactive oxygen species.

Despite the observed photostability of aqueous Fe(III)-DFOB complexes, dissolution experiments conducted at pH 8 and under irradiation of light with different wavelengths indicated that the specific coordination of DFOB at the surface of lepidocrocite facilitates a light-induced ligand-to-metal charge-transfer resulting in photoreductive dissolution of lepidocrocite. The major conclusion of this thesis was that both the photoreactive properties of lepidocrocite and the formation of photoreactive surface complexes of siderophores with α -hydroxycarboxylic acid and unexpectedly hydroxamic acid groups may contribute to the enhancement of dissolution rates under irradiation. Based on the high response of photoreductive dissolution of lepidocrocite observed in the visible range (395-435 nm) in the presence of DFOB, we suggested that photoreduction of particulate iron in the presence of hydroxamate siderophores may occur deep into the photic zone of oceanic waters.

Zusammenfassung

In vielen ozeanischen Gewässern wird das Wachstum von Phytoplankton von der geringen Verfügbarkeit des Mikronährstoffs Eisen limitiert, welches unter anderem als eisenhaltige Aerosolpartikel über atmosphärische Deposition in eisenlimitierte Oberflächengewässer eingetragen wird. Partikuläres Eisen kann jedoch von den meisten marinen Mikroorganismen nicht aufgenommen werden. Da die Bioverfügbarkeit von Eisen generell durch den gelösten Anteil bestimmt wird, tragen biotische und abiotische Prozesse, welche partikuläres Eisen in gelöstes Eisen überführen, zur Erhöhung der Bioverfügbarkeit bei. Eine wesentliche Strategie von Mikroorganismen, die Bioverfügbarkeit von Eisen zu erhöhen, besteht in der Ausscheidung von Siderophoren. Siderophore sind niedermolekulare organische Liganden mit hoher Affinität und Selektivität für gelöstes Eisen. Aufgrund dieser hohen Affinität für Eisen, können Siderophore partikuläres Eisen in Form von Fe(III) (Hydr)oxiden in gelöste und damit bioverfügbare Eisenkomplexe überführen, welche eine wichtige Eisen-Quelle für eine Vielzahl von marinen Mikroorganismen darstellen.

Die Auflösung von Fe(III)-haltigen Mineralen kann über die Bildung von Fe(II) an der Mineraloberfläche, z.B., durch die Photolyse von adsorbierten Liganden, beschleunigt werden. Bisher ist jedoch nicht bekannt, ob und wie stark natürliches Sonnenlicht die Siderophor-induzierte Auflösung von Fe(III) (Hydr)oxiden über einen reduktiven Mechanismus beschleunigt.

Ziel dieser Arbeit war es, die Siderophor-induzierte Auflösung von Eisen(hydr)oxiden in Gegenwart von Licht unter kontrollierten Laborbedingungen zu untersuchen.

Die Interaktionen zwischen Siderophoren und der Oberfläche von Eisen(hydr)oxiden bestimmen maßgeblich die Geschwindigkeit ihrer Auflösung. Daher wurde in dieser Arbeit die Adsorption von zwei Siderophoren, Desferrioxamin B (DFOB) und Aerobaktin, auf Lepidokrokit (γ -FeOOH) sowohl auf der makroskopischen wie auch auf der molekularen Ebene mittels ATR-FTIR Spektroskopie untersucht. Zusätzlich wurden Auflösungsdaten von Lepidokrokit als Funktion der adsorbierten Menge an DFOB oder Aerobaktin bestimmt. Auflösungsexperimente mit anderen Eisenhydroxiden wurden ebenfalls durchgeführt. Desweiteren wurde der Einfluss von Licht unterschiedlicher Wellenlängen auf die DFOB-induzierte Auflösung von Lepidokrokit untersucht.

Die Befunde der Adsorptionsexperimente sowie der spektroskopischen Untersuchungen zeigen, dass zwei bis drei Hydroxamatgruppen des DFOB-Moleküls

vorwiegend über innersphärische Komplexierung an der Oberfläche von Lepidokrokit koordiniert sind. Während die Carboxylgruppen von Aerobaktin definitiv an der Bindung des Moleküls an Lepidokrokit beteiligt sind, ist eine Aussage über das Bindungsverhalten der Hydroxamatgruppen in Aerobactin auf der Basis unserer Experimente nicht möglich.

Im Vergleich zu Aerobaktin löste DFOB den Lepidokrokit deutlich schneller auf. Diese Beobachtung wurde dadurch erklärt, dass Aerobaktin Oberflächenkomplexe bildet, die eine geringere Auflösungsreaktivität aufweisen.

In dieser Arbeit konnte zudem gezeigt werden, dass Fe(III)-Aerobaktinkomplexe in Lösung photoreaktiv sind und unter Lichteinstrahlung ein Elektronentransfer zwischen der α -Hydroxycarboxylgruppe und Fe(III) stattfindet. Die Auflösungsexperimente mit Lepidokrokit und Aerobaktin deuten auf einen photoreduktiven Auflösungsmechanismus hin, ausgelöst durch einen Elektronentransfer zwischen der koordinierten α -Hydroxycarboxylgruppe und der Oberfläche von Lepidokrokit. Unter Lichteinstrahlung wurde Lepidokrokit durch DFOB und Aerobaktin stärker aufgelöst als im Dunkeln. Diese Beobachtung legt einen photoreduktiven Auflösungsmechanismus nahe, welcher von der Mineralphase bestimmt wird. Die Beschleunigung der Liganden-induzierten Auflösung unter Lichteinfluss kann durch einen Halbleitermechanismus in der Mineralphase oder direkt an der Oberfläche erklärt werden. In Abwesenheit von Siderophoren wurde die Bildung von Fe(II) in Lösung unter Lichteinfluss nachgewiesen, und damit konnte der Mechanismus der photoreduktiven Auflösung bestätigt werden. Die photoreduktive Bildung von Fe(II) Spezies in Abwesenheit von Siderophoren ging mit der Bildung reaktiver Sauerstoffspezies einher.

Trotz der bekannten Photostabilität von Fe(III)-DFOB Komplexen in wässriger Lösung, deuteten Auflösungsexperimente unter Lichteinstrahlung unterschiedlicher Wellenlänge darauf hin, dass DFOB an der photoreduktiven Auflösung von Lepidokrokit durch einen licht-induzierten Elektronentransfer von koordinierten Hydroxamatgruppen zu Oberflächen-Fe(III) direkt beteiligt ist.

Zusammenfassend kann festgestellt werden, dass sowohl die intrinsische Photoreaktivität von Lepidokrokit als auch die Photoreaktivität von Siderophor-Oberflächenkomplexen, an denen α -Hydroxycarboxyl- und auch Hydroxamatgruppen beteiligt sind, zur beschleunigten Auflösung von Lepidokrokit unter Lichteinstrahlung beitragen. Die starke DFOB-induzierte Auflösung von Lepidokrokit unter Lichteinstrahlung im Wellenlängenbereich von 395-435 nm zeigt, dass die Auflösung von partikulärem Eisen durch Siderophore mit Hydroxamatgruppen bis tief in die euphotische Zone ozeanischer Gewässer stattfinden kann.

Introduction

Iron is an essential micronutrient for almost all known organisms. While iron is the fourth most abundant element in the Earth's crust, the insolubility of iron at neutral pH limits the availability of this nutrient in many terrestrial and aquatic systems [1-4]. The oceanic environment is particularly extreme from the standpoint of iron scarcity. In remote oceanic waters dissolved iron concentrations are in the sub-nanomolar range [5]. It has been shown by in-situ iron addition experiments that especially oceanic areas classified as high-nutrient, low-chlorophyll regions (Northeast Pacific, Equatorial Pacific and Southern Ocean) are iron-limited [6-8]. The extent to which iron limits primary productivity in open ocean waters depends on both the abundance of iron and its bioavailability. Forms of iron that are more kinetically labile are regarded as being more biologically available [9]. Dissolved Fe(II), dissolved inorganic Fe(III) species with a low degree of hydrolysis, and weak iron-organic species are examples of kinetically labile iron. In contrast, crystalline iron(III) (hydr)oxides phases are not considered bioavailable to microorganisms [10-12], but may still serve as a nutrient source after transformation to more labile iron forms. To overcome iron starvation, microorganisms have developed different mechanisms to acquire iron. One of these mechanisms is the exudation of siderophores, low-molecular weight chelate compounds (0.5-1.5 kDa) which form extremely strong Fe(III)-complexes and thus retain dissolved iron in the water column and prevent inorganic precipitation and scavenging removal. The uptake of iron bound to siderophores involves cellular transport systems or enzymatic systems facilitating the release and uptake of iron [13-17].

The speciation and solubility of dissolved iron in seawater is strongly affected by organic complexation [18-23]. It has been revealed in numerous studies that > 99% of dissolved iron is organically complexed [18, 22-24]. Due to experimental and analytical limitations, the nature of these organic complexes is largely unknown, but these complexes are presumed to be of biological origin [25]. Recently, evidence has been provided which suggests that some component of the natural organic Fe-binding ligands in surface seawater consists of siderophores [26, 27]. Over 500 different siderophores from culturable organisms are known today [28]. Iron binding groups in siderophores include hydroxamate and catecholate groups, and less commonly α -hydroxycarboxylate and carboxylate groups [14].

Siderophores are assumed to play a key role in the transformation of iron(III) (hydr)

oxide mineral phases into more bioavailable iron forms. Recent studies have shown that siderophores are able to promote dissolution of iron(III) (hydr)oxides and to prevent precipitation of dissolved Fe(III) [29-33]. Siderophore-promoted dissolution of colloidal iron is an important process in remote ocean waters where the input of new iron is strongly determined by atmospheric deposition of iron-bearing aerosols (e.g. dust). Dust deposition events have been observed to lead to an increase in primary productivity in some ocean regions, however the biological response to dust deposition events was not strong in all cases [34-36].

Dissolution rates of iron(III) (hydr)oxides or Fe(III)-bearing minerals can be significantly enhanced in sunlit surface waters, if photoreductive processes leading to kinetic labile Fe(II) are involved. In the presence of photoreductive ligands, which might be associated with microbial exudates [37] or with photochemically transformed anthropogenic precursors of deposited aerosols [38, 39], iron(III) (hydr)oxides phases can undergo photoreductive dissolution. Numerous laboratory studies have investigated photoreductive dissolution of iron(III) (hydr)oxides in the presence of photoreductive ligands such as carboxylic acids and α -hydroxycarboxylic acids [40-43], but the effect of siderophores on photoreductive dissolution has not been investigated before this PhD project was initiated. Siderophores are known to interact with the surface of iron(III) (hydr)oxides and may facilitate the transfer of photochemically produced surface Fe(II) into solution. It has been proposed that siderophores might be directly involved in the photoreductive dissolution of iron(III) (hydr)oxide phases, by forming photoreactive Fe(III) complexes at the surface of these phases [9]. This assumption is based on the observation that siderophores containing α -hydroxycarboxylic acid functional groups form photoreactive Fe(III)-siderophore complexes in which the Fe(III) center is reduced by a light-induced ligand-to-metal charge-transfer reaction [44, 45]. Photoreductive dissolution of iron(III) (hydr)oxide phases may be promoted even in the absence of any organic ligands. It was observed that dissolved Fe(II) accumulated under irradiation of organic-free suspensions of lepidocrocite (γ -FeOOH) at pH 4 [46]. Even at pH 8, it has been recently reported that photoreductive dissolution of freshly formed amorphous ferric hydroxides in artificial and organic-free seawater samples results in measurable dissolved Fe(II) concentrations [47].

The overall objective of this thesis was the investigation of the light-induced dissolution of iron(III) (hydr)oxides in the presence of siderophores. The specific research objectives were:

- (i) to investigate the interactions of two model siderophores, desferrioxamine B (DFOB) and aerobactin, with the surface of lepidocrocite (γ -FeOOH) at the

molecular level by ATR-FTIR spectroscopy.

(ii) to investigate if the α -hydroxycarboxylic acid group in aerobactin is coordinated to the surface of lepidocrocite such that photolysis of the surface Fe(III)-complex formed by this functional group is feasible.

(iii) to investigate the dissolution of lepidocrocite as a function of the adsorbed amount of siderophores (DFOB, aerobactin) and thus to assess the dissolution reactivity of the siderophores in the dark and under irradiation of artificial sunlight.

(iv) to investigate the mechanisms of photoreductive dissolution in the absence of organic ligands.

(v) to investigate the effect of light at different wavelengths on photoreductive dissolution in the absence and presence of siderophores.

The results of this work are divided into 7 chapters:

- Chapter 1 is based on work that was conducted during my diploma thesis “Effect of siderophores on the light-induced dissolution of colloidal Fe(III) (hydr)oxides”. The manuscript for publication was written during the initial phase of this PhD project and was the starting point for further experimental work. The main focus was the interplay between siderophores and an additional photoreductive ligand (oxalate) in the siderophore-promoted dissolution of lepidocrocite and goethite at pH 6.
- Chapter 2 reports an ATR-FTIR spectroscopic investigation of a model α -hydroxycarboxylic acid ligand (citrate) at the surface of lepidocrocite. The aim of this chapter was to assess the possibility of investigating photoredox reactions of surface complexes of adsorbed organic ligands by ATR-FTIR spectroscopy. This chapter focuses on the surface-mediated photolysis of the α -hydroxycarboxylate functional group in citrate, which is also a functional metal binding group in many siderophores (e.g., in aerobactin).
- Chapter 3 describes an ATR-FTIR spectroscopic study on the interactions of DFOB

and aerobactin at the surface of lepidocrocite. Adsorption of these siderophores was investigated in a broad pH range. The aim of this work was to determine the coordination of siderophore functional groups to the surface. In addition, it was tested if the α -hydroxycarboxylate group in aerobactin is coordinated and is photolyzed at the surface of lepidocrocite under UV-visible irradiation.

- Chapter 4 presents the results of a kinetic study on the dissolution of lepidocrocite by DFOB and aerobactin. In contrast to Chapter 1, the investigated pH range was extended to pH 3-8. Dissolution experiments were performed in the dark and under artificial sunlight. The aim of this work was to provide information on the dissolution reactivity of adsorbed siderophores. This was achieved by parameterizing dissolution rates according to the rate law of ligand-promoted dissolution.
- Chapter 5 describes a kinetic and modeling study of photoreductive dissolution of lepidocrocite and other iron(III) (hydr)oxides in the absence of any organic ligands. The aim of this work was to provide information on the processes leading to the formation of dissolved Fe(II) and reactive oxygen species in irradiated organic-free suspensions of lepidocrocite. A central focus in this work was the development of a kinetic model describing the numerous processes involved during photoreductive dissolution of iron(III) (hydr)oxides in the absence of siderophores.
- Chapter 6 is related to a study investigating the wavelength dependence of photoreductive dissolution in the absence and presence of DFOB. The aim of this study was to provide information on the spectral quality of light required to induce photodissolution of lepidocrocite in the absence or presence of DFOB.
- Chapter 7 presents the overall conclusions of this thesis.

Not included in this thesis is the co-authored review article “Siderophores and dissolution of iron-bearing minerals in marine systems” [48].

References

- [1] Martin, J. H. and Fitzwater, S. E. **1988**. Iron-deficiency limits phytoplankton growth in the northeast Pacific Subarctic. *Nature* 331: 341-343.
- [2] Martin, J. H., Coale, K. H., Johnson, K. S., Fitzwater, S. E., Gordon, R. M., Tanner, S. J., Hunter, C. N., Elrod, V. A., Nowicki, J. L., Coley, T. L., Barber, R. T., Lindley, S., Watson, A. J., Vanscoy, K., Law, C. S., Liddicoat, M. I., Ling, R., Santon, T., Stockel, J., Collins, C., Anderson, A., Bidigare, R., Ondrusek, M., Latasa, M., Millero, F. J., Lee, K., Yao, W., Zhang, J. Z., Friederich, G., Sakamoto, C., Chavez, F., Buck, K., Kolber, Z., Greene, R., Falkowski, P., Chisholm, S. W., Hoge, F., Swift, R., Yungel, J., Turner, S., Nightingale, P., Hatton, A., Liss, P. and Tindale, N. W. **1994**. Testing the iron hypothesis in ecosystems of the equatorial Pacific-Ocean. *Nature* 371: 123-129.
- [3] Römheld, V. (1987). Existence of two different strategies for the acquisition of iron in higher plants. In: *Microbes, Plants and Animals*. G. Winkelmann, D. Van der Helm and J. B. Neilands, Eds. VHC, Weinheim: 353-374.
- [4] Kraemer, S. M., Crowley, D. E. and Kretzschmar, R. **2006**. Geochemical aspects of phytosiderophore-promoted iron acquisition by plants. *Adv. Agron.* 91: 1-46.
- [5] Johnson, K. S., Gordon, R. M. and Coale, K. H. **1997**. What controls dissolved iron concentrations in the world ocean? *Mar. Chem.* 57: 137-161.
- [6] Butler, A. and Martin, J. D. (2005). The marine biogeochemistry of iron. In: *Metal Ions in Biological Systems, Vol 44*. A. S. Sigel, H. and R. K. O. Sigel, Eds. Taylor & Francis, Boca Raton, FL: 21-46.
- [7] Boyd, P. W. **2002**. The role of iron in the biogeochemistry of the Southern Ocean and equatorial Pacific: a comparison of in situ iron enrichments. *Deep-Sea Res.* 49: 1803-1821.
- [8] Boyd, P. W., Jickells, T., Law, C. S., Blain, S., Boyle, E. A., Buesseler, K. O., Coale, K. H., Cullen, J. J., de Baar, H. J. W., Follows, M., Harvey, M., Lancelot, C., Levasseur, M., Owens, N. P. J., Pollard, R., Rivkin, R. B., Sarmiento, J., Schoemann, V., Smetacek, V., Takeda, S., Tsuda, A., Turner, S. and Watson, A. J. **2007**. Mesoscale iron enrichment experiments 1993-2005: Synthesis and future directions. *Science* 315: 612-617.
- [9] Barbeau, K. **2006**. Photochemistry of organic iron(III) complexing ligands in oceanic systems. *Photochem. Photobiol.* 82: 1505-1516.
- [10] Wells, M. L., Zorkin, N. G. and Lewis, A. G. **1983**. The role of colloid chemistry in providing a source of iron to phytoplankton. *J. Mar. Res.* 41: 731-746.
- [11] Finden, D. A. S., Tipping, E., Jaworski, G. H. M. and Reynolds, C. S. **1984**. Light-

- induced reduction of natural iron(III) oxide and its relevance to phytoplankton. *Nature* 309: 783-784.
- [12] Rich, H. W. and Morel, F. M. M. **1990**. Availability of well-defined iron colloids to the marine diatom *Thalassiosira weissflogii*. *Limnol. Oceanogr.* 35: 652-662.
- [13] Byers, B. R. and Arceneaux, J. E. L. (1998). Microbial iron transport: iron acquisition by pathogenic microorganisms In: *Metal Ions in Biological Systems*. A. Sigel and H. Sigel, Eds. Marcel Dekker, New York: 37-66.
- [14] Winkelmann, G. **1991**. *Handbook of microbial iron chelates*. CRC Press: Boca Raton, Florida.
- [15] Maldonado, M. T. and Price, N. M. **2001**. Reduction and transport of organically bound iron by *Thalassiosira oceanica* (Bacillariophyceae). *J. Phycol.* 37: 298-309.
- [16] Maldonado, M. T. and Price, N. M. **1999**. Utilization of iron bound to strong organic ligands by plankton communities in the subarctic Pacific Ocean. *Deep-Sea Res.* 46: 2447-2473.
- [17] Armstrong, E., Granger, J., Mann, E. L. and Price, N. M. **2004**. Outer-membrane siderophore receptors of heterotrophic oceanic bacteria. *Limnol. Oceanogr.* 49: 579-587.
- [18] Powell, R. T. and Donat, J. R. **2001**. Organic complexation and speciation of iron in the South and Equatorial Atlantic. *Deep-Sea Res.* 48: 2877-2893.
- [19] Rue, E. L. and Bruland, K. W. **1997**. The role of organic complexation on ambient iron chemistry in the equatorial Pacific Ocean and the response of a mesoscale iron addition experiment. *Limnol. Oceanogr.* 42: 901-910.
- [20] Kuma, K., Katsumoto, A., Kawakami, H., Takatori, F. and Matsunaga, K. **1998**. Spatial variability of Fe(III) hydroxide solubility in the water column of the northern North Pacific Ocean. *Deep-Sea Res.* 45: 91-113.
- [21] Kuma, K., Katsumoto, A., Shiga, N., Sawabe, T. and Matsunaga, K. **2000**. Variation of size-fractionated Fe concentrations and Fe(III) hydroxide solubilities during a spring phytoplankton bloom in Funaka Bay (Japan). *Mar. Chem.* 71: 111-123.
- [22] Wu, J. F. and Luther, G. W. **1995**. Complexation of Fe(III) by natural organic ligands in the Northwest Atlantic Ocean by a competitive ligand equilibration method and a kinetic approach. *Mar. Chem.* 50: 159-177.
- [23] Nolting, R. F., Gerringa, L. J. A., Swagerman, M. J. W., Timmermans, K. R. and de Baar, H. J. W. **1998**. Fe (III) speciation in the high nutrient, low chlorophyll Pacific region of the Southern Ocean. *Mar. Chem.* 62: 335-352.
- [24] Gledhill, M. and Vandenberg, C. M. G. **1994**. Determination of Complexation of

- Iron(III) with Natural Organic Complexing Ligands in Seawater Using Cathodic Stripping Voltammetry. *Mar. Chem.* 47: 41-54.
- [25] Tortell, P. D., Maldonado, M. T., Granger, J. and Price, N. M. **1999**. Marine bacteria and biogeochemical cycling of iron in the oceans. *FEMS Microbiol. Ecol.* 29: 1-11.
- [26] Macrellis, H. M., Trick, C. G., Rue, E. L., Smith, G. and Bruland, K. W. **2001**. Collection and detection of natural iron-binding ligands from seawater. *Mar. Chem.* 76: 175-187.
- [27] Gledhill, M., McCormack, P., Ussher, S., Achterberg, E. P., Mantoura, R. F. C. and Worsfold, P. J. **2004**. Production of siderophore type chelates by mixed bacterioplankton populations in nutrient enriched seawater incubations. *Mar. Chem.* 88: 75-83.
- [28] Boukhalfa, H. and Crumbliss, A. L. **2002**. Chemical aspects of siderophore mediated iron transport. *Biometals* 15: 325-339.
- [29] Hersman, L., Lloyd, T. and Sposito, G. **1995**. Siderophore-promoted dissolution of hematite. *Geochim. Cosmochim. Acta* 59: 3327-3330.
- [30] Reichard, P. U., Kraemer, S. M., Frazier, S. W. and Kretzschmar, R. **2005**. Goethite dissolution in the presence of phytosiderophores: Rates, mechanisms, and the synergistic effect of oxalate. *Plant Soil* 276: 115-132.
- [31] Cheah, S. F., Kraemer, S. M., Cervini-Silva, J. and Sposito, G. **2003**. Steady-state dissolution kinetics of goethite in the presence of desferrioxamine B and oxalate ligands: implications for the microbial acquisition of iron. *Chem. Geol.* 198: 63-75.
- [32] Yoshida, T., Hayashi, K. and Ohmoto, H. **2002**. Dissolution of iron hydroxides by marine bacterial siderophore. *Chem. Geol.* 184: 1-9.
- [33] Kraemer, S. M. **2004**. Iron oxide dissolution and solubility in the presence of siderophores. *Aquat. Sci.* 66: 3-18.
- [34] Bishop, J. K. B., Davis, R. E. and Sherman, J. T. **2002**. Robotic observations of dust storm enhancement of carbon biomass in the North Pacific. *Science* 298: 817-821.
- [35] Johnson, K. S., Elrod, V. A., Fitzwater, S. E., Plant, J. N., Chavez, F. P., Tanner, S. J., Gordon, R. M., Westphal, D. L., Perry, K. D., Wu, J. F. and Karl, D. M. **2003**. Surface ocean-lower atmosphere interactions in the Northeast Pacific Ocean Gyre: Aerosols, iron, and the ecosystem response. *Glob. Biogeochem. Cycles* 17.
- [36] Lenes, J. M., Darrow, B. P., Cattrall, C., Heil, C. A., Callahan, M., Vargo, G. A., Byrne, R. H., Prospero, J. M., Bates, D. E., Fanning, K. A. and Walsh, J. J.

- 2001.** Iron fertilization and the Trichodesmium response on the West Florida shelf. *Limnol. Oceanogr.* 46: 1261-1277.
- [37] Kuma, K., Nalabayashi, S., Suzuki, Y., Kudo, I. and Matsunaga, K. **1992.** Photo-reduction of Fe(III) by dissolved organic substances and existence of Fe(II) in seawater during spring blooms. *Mar. Chem.* 37: 15-27.
- [38] Sempere, R. and Kawamura, K. **1996.** Low molecular weight dicarboxylic acids and related polar compounds in the remote marine rain samples collected from western Pacific. *Atmos. Environ.* 30: 1609-1619.
- [39] Sempere, R. and Kawamura, K. **2003.** Trans-hemispheric contribution of C₂-C₁₀ α, ω-dicarboxylic acids, and related polar compounds to water-soluble organic carbon in the western Pacific aerosols in relation to photochemical oxidation reactions. *Glob. Biogeochem. Cycles* 17: 1069.
- [40] Sulzberger, B. and Laubscher, H. **1995.** Reactivity of various types of iron(III) (hydr)oxides towards light-induced dissolution. *Mar. Chem.* 50: 103-115.
- [41] Waite, T. D. and Morel, F. M. M. **1984.** Photoreductive dissolution of colloidal iron-oxide - Effect of citrate. *J. Colloid Interface Sci.* 102: 121-137.
- [42] Siffert, C. and Sulzberger, B. **1991.** Light-induced dissolution of hematite in the presence of oxalate - a case-study. *Langmuir* 7: 1627-1634.
- [43] Kuma, K., Nakabayashi, S. and Matsunaga, K. **1995.** Photoreduction of Fe(III) by hydroxycarboxylic acids in seawater. *Water Res.* 29: 1559-1569.
- [44] Barbeau, K., Rue, E. L., Trick, C. G., Bruland, K. T. and Butler, A. **2003.** Photochemical reactivity of siderophores produced by marine heterotrophic bacteria and cyanobacteria based on characteristic Fe(III) binding groups. *Limnol. Oceanogr.* 48: 1069-1078.
- [45] Kuepper, F. C., Carrano, C. J., Kuhn, J. U. and Butler, A. **2006.** Photoreactivity of iron(III)-aerobactin: Photoproduct structure and iron(III) coordination. *Inorg. Chem.* 45: 6028-6033.
- [46] Waite, T. D. and Morel, F. M. M. **1984.** Photoreductive dissolution of colloidal iron oxides in natural waters. *Environ. Sci. Technol.* 18: 860-868.
- [47] Rijkenberg, M. J. A. (2005). Photochemistry and organic complexation of iron: interactions in the Southern Ocean. PhD Thesis, University of Groningen.
- [48] Kraemer, S. M., Butler, A., Borer, P. and Cervini-Silva, J. **2005.** Siderophores and the dissolution of iron-bearing minerals in marine systems. *Rev. Mineral. Geochem.* 59: 53-84.

Chapter 1

Effect of siderophores on the light-induced dissolution of colloidal iron(III)(hydr)oxides

Paul M. Borer, Barbara Sulzberger, Petra Reichard, Stephan M. Kraemer

Published in Marine Chemistry (2005), 93, 179-193.

Abstract

Siderophores play an important role in biological iron acquisition in iron limited aquatic systems. While it is widely accepted that the solubilization of iron bearing mineral phases is a key function of siderophores, the mechanism of siderophore-promoted mineral dissolution in aquatic systems is largely unknown. In this study, we investigated the effect of siderophores (desferrioxamine B (DFOB) and aerobactin) on light-induced dissolution of goethite and lepidocrocite in the presence or absence of oxalate in aerated and deaerated suspensions at pH 6. For the irradiated two-ligand system (oxalate/siderophore) the experimental results suggest that oxalate acts as the electron donor for the formation of surface Fe(II), and the siderophore acts as an efficient shuttle for the transfer of surface Fe(II) into solution. Furthermore, even in the absence of an electron donor such as oxalate, both DFOB and aerobactin accelerated the light-induced dissolution of lepidocrocite as compared to the thermal dissolution. Experiments with dissolved Fe(III)-DFOB and Fe(III)-aerobactin complexes suggest that this enhancing effect is not due to photolysis of corresponding surface complexes but to efficient transfer of reduced surface Fe(II) into solution, where surface Fe(II) may be formed, e.g. through photolysis of surface Fe(III)-hydroxo groups. Based on this study we conclude that the interplay of light and siderophores may play a key role in the dissolution of colloidal iron(III) (hydr) oxides in marine systems, particularly in the presence of efficient electron donors.

1. Introduction

Iron bioavailability has been shown to limit or co-limit primary productivity in several oceanic waters, particularly in ‘High Nutrient, Low Chlorophyll’ (HNLC) regions [1, 2]. A significant external iron source to these and other oceanographic regimes is atmospheric input [1, 2]. For example, it has been estimated that atmospheric deposition of aeolian iron-containing mineral dust accounts for 84-93 % of the external iron input to the subarctic Pacific, which lies in the path of an extended aerosol plume that originates in China [3]. At the relatively low pH values (3 - 6) of atmospheric waters, solid iron phases (e.g. crystalline iron oxides and iron aluminium silicates) in the aerosols are subject to photoreductive dissolution [4-10]. Besides crystalline iron oxides (this term will be used for the various Fe(III) oxides, Fe(III) oxo-hydroxides, and Fe(III) hydroxides), photoproduced Fe(II) also enters open ocean surface waters by wet deposition. However, without significant stabilization of Fe(II) by some organic ligands, Fe(II) undergoes fast oxidative precipitation in seawater [11].

The extent to which iron limits primary production in open ocean waters depends on both the abundance of iron and its bioavailability. Particulate and colloidal iron is believed to be unavailable to phytoplankton [12-14], and the solubility of iron in open ocean waters is extremely low, $\log [\text{Fe(III)}] < -9$ [15]. Regarding dissolved iron, it has been proposed that eukaryotic phytoplankton species utilize only inorganic iron species [16]. However, more recent studies have shown that some eukaryotic algae are able to utilize iron bound to (strong) organic chelators via a cell surface reductase mechanism [17-22].

Unlike eukaryotic algae, marine bacteria acquire iron through a siderophore-mediated uptake system [23]. Siderophores are low-molecular-weight organic ligands (0.5–1.5 kDa) with a high affinity and specificity for iron. Under iron-limiting conditions, siderophores are excreted by cyano- and heterotrophic bacteria [24-28]. The stability constants of Fe(III)-siderophore complexes are in the range of $\log K = 25-50$ [29]. Besides increasing the solubility of iron, siderophores also accelerate iron oxide dissolution [30-33]. Iron binding groups of bacterial siderophores typically include hydroxamate, catecholate, α -hydroxycarboxylate, and less often carboxylate groups [23].

Hitherto, there is no clear picture of the roles of siderophores for iron acquisition by the phytoplankton community. The acquisition of iron from iron-siderophore complexes by eukaryotic phytoplankton (e.g. diatoms) is obscure and controversially discussed in literature. Although eukaryotic phytoplankton generally do not produce siderophores, it has been shown that some species may utilize siderophore bound iron under iron-

limiting conditions, by a cell surface reductase mechanism [18, 21]. Other studies however have pointed out, that strong iron-siderophore complexes are not available to eukaryotic phytoplankton in iron-replete waters [34, 35]. For an in-depth discussion of these contrasting results, we refer to Maldonado et al. [21].

It has been reported, that most (>99%) dissolved ferric iron in the HNLC upper ocean water is complexed by strong organic ligands having conditional stability constants in seawater similar to siderophores [36-40]. The nature of these ligands was partly elucidated by Macrellis et al. [41]. They have determined size classes as well as conditional Fe-binding affinities of iron binding compounds collected in the central California coastal upwelling system. The size class and conditional stability constants of these ligands were similar to known siderophores. Moreover, hydroxamate as well as catecholate Fe(III)-binding groups were found in all compounds for which strong iron binding was detected.

1.1 Roles of siderophores in the light-induced redox cycling of dissolved iron

The effect of siderophores on the redox chemistry of dissolved iron is dominated by two processes: (i) stabilization of the trivalent state of iron due to the much higher affinity of siderophores for Fe(III) compared to Fe(II), and (ii) photolysis of certain Fe(III)-siderophore complexes resulting in the formation of Fe(II). It has been demonstrated that Fe(III) complexes with the marine siderophores petrobactin (Fig. 1) [42] and various aquachelins [43] are photolyzed under irradiation, yielding Fe(II) and increased bioavailability of iron to phytoplankton (as has been demonstrated for the photolysis of the Fe(III)-aquachelin B complex). The photoreactivity of Fe(III)-petrobactin and Fe(III)-aquachelin complexes is imparted by the α -hydroxycarboxylate functional group, which decarboxylates under irradiation. This is consistent with earlier observations of the photoreactivity of α -hydroxycarboxylic acids complexed to transition metals [44, 45]. According to a recent study of the photochemical reactivity of siderophores based on characteristic iron(III)-binding groups, siderophores containing only hydroxamate groups such as DFOB (Fig. 1) form photostable iron complexes [46].

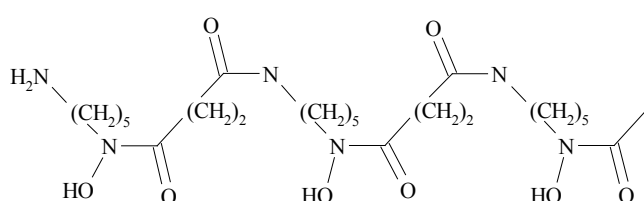
The stabilization of the trivalent redox state of iron by siderophores can be related to the stability constants of the Fe(II)- and Fe(III)-complexes [47]:

$$E_{Fe_{std}^{III/II}}^{\circ} = E_{aq}^{\circ} - 59.15 * \log \left(\frac{\beta_{110}^{Fe(III)}}{\beta_{110}^{Fe(II)}} \right) \quad (1)$$

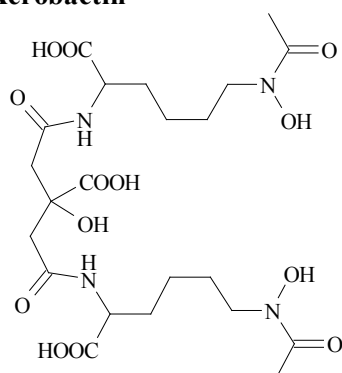
where the redox potential of the hexaaquated iron E_{aq}° is +770 mV (vs. normal hydrogen electrode). Due to the much higher affinity of siderophores to Fe(III) than to Fe(II)

($\beta_{110}^{\text{Fe(III)}} \gg \beta_{110}^{\text{Fe(II)}}$), redox potentials observed for most Fe-siderophore complexes are in the range of -350 to -750 mV. These strongly negative redox potentials facilitate Fe(II) oxidation in the presence of oxygen. In the reported case of Fe(II)-DFOB complexes, the oxidation to Fe(III)-DFOB is instantaneous [48]. Based on above consideration, measured Fe(II) concentrations may not be a suitable indicator for photoreductive dissolution of iron oxides in the presence of siderophores in the laboratory or in marine in situ studies.

Desferrioxamine B (DFOB)



Aerobactin



Petrobactin

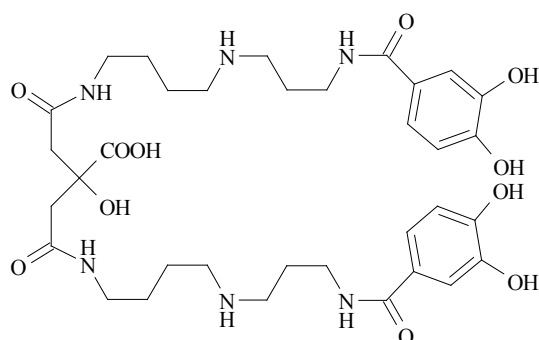


Fig. 1: Chemical structures of the microbial siderophores DFOB, aerobactin, and petrobactin [73].

1.2 Roles of siderophores in the thermal dissolution of iron oxides

The dissolution of iron oxides requires the breaking of bonds between surface Fe(III) and lattice neighbors (e.g. lattice oxygen). Surface chemical processes that weaken these bonds can accelerate iron oxide dissolution. Protonation of surface sites, adsorption of ligands, and (photo)reduction of surface sites by reductive agents all lead to polarization of metal-oxygen bonds and therefore promote dissolution [49].

Siderophores react with iron oxides in the dark via a ligand-controlled dissolution mechanism [33] with a rate law proposed by Furrer and Stumm [50]:

$$R_L = k_L \cdot [L]_{ads} \quad (2)$$

where R_L is the dissolution rate, k_L is a first order rate constant and $[L]_{ads}$ is the adsorbed ligand concentration. Siderophores also accelerate other ligand controlled dissolution mechanisms. A recent study of thermal steady-state dissolution kinetics of goethite in the presence of DFOB and oxalate at near neutral pH has revealed that the rate determining step in the overall dissolution reaction is the detachment of surface Fe(III) by oxalate, followed by a ligand exchange reaction between DFOB and Fe(III)-oxalate complexes in solution [32].

1.3 Mechanism and rate law of light-induced dissolution of iron oxides

Photodissolution of iron oxides has been subject to many studies [4, 5, 8, 9, 51-53]. The dissolution process generally involves two steps:

- Photoexcitation and charge transfer resulting in the reduction of surface Fe(III) to Fe(II)
- detachment of reduced surface Fe(II) from the mineral surface.

Different mechanisms can result in the formation of surface Fe(II): (i) ligand-to-metal charge transfer (LMCT) within organic Fe(III) surface complexes or within surface Fe(III)-hydroxo groups, leading to the reduction of surface Fe(III) and the oxidation of the ligand, and (ii) generation of photo-electrons and photo-holes within the iron oxide lattice (semiconductor mechanism) through photoexcitation of $O^{2-} \rightarrow Fe^{3+}$ charge transfer bands and migration of photo-electrons to surface Fe(III) and photo-holes to an adsorbed electron donor. (Di)carboxylate and hydroxycarboxylate functional groups are important electron donors and are ubiquitous in biogenic organic compounds. Furthermore, (di)carboxylic and hydroxycarboxylic acids are also introduced to remote ocean surface waters by wet deposition of photochemically transformed anthropogenic precursors [54, 55].

Irrespective of the mechanism involved, the rate determining step in the dissolution of crystalline iron oxides is the detachment of Fe(II) from the mineral surface [53, 56, 57], and the rate of Fe(II) formation is linearly dependent on the concentration of the adsorbed ligand, acting as an electron donor (see Eq. (2)). In the presence of oxygen and depending on pH, detachment of reduced surface iron may be outcompeted by reoxidation of surface Fe(II). Unless stabilized by ligands, detached Fe(II) is subject

to oxidative precipitation in circumneutral surface waters, resulting in the formation of amorphous iron oxide phases [58]. These freshly formed amorphous iron oxide phases are more readily dissolved than crystalline iron oxides. Hence, photoreductive dissolution is an important process, potentially increasing the bioavailability of iron in circumneutral surface waters [13, 58-60].

1.4 Purpose of this study

Solubilization of crystalline iron oxides originating from tropospheric deposition increases the pool of iron that may be available to the marine biota. Several studies have shown that photoreductive dissolution of crystalline iron oxides phases in the presence of humic substances or model compounds such as oxalate, acting as electron donors, is extremely slow above acidic pH values [9, 51, 61]. Hitherto, the effect of siderophores on photoreductive dissolution has not yet been studied. Although we did not attempt to mimic natural conditions in iron deficient areas of the open ocean, we have investigated the interplay of siderophores and oxalate in photodissolution of iron oxides. In this study, we worked with two model siderophores: DFOB, a trihydroxamate siderophore and aerobactin, a dihydroxamate / α -hydroxycarboxylate siderophore (Fig. 1).

2. Materials and methods

2.1 Materials

Desferrioxamine B was obtained as mesylate salt [$C_{25}H_{46}N_5O_8NH_3^+(CH_3SO_3^-)$] from Ciba Geigy (Desferal®). Iron-free aerobactin ($C_{22}H_{32}O_{12}N_4$) was purchased from EMC microcollections GmbH in Tübingen, Germany and used as received. All other chemicals were reagent grade and solutions were prepared with high purity 18.2 M Ω .cm water (Milli-Q, Millipore). pH measurements were carried out with a combined glass electrode (Metrohm), standardized with pH-buffer solutions (Merck). Goethite (α -FeOOH) was synthesized using a method described by Schwertmann and Cornell [62], dialyzed and freeze-dried. Lepidocrocite (γ -FeOOH) was prepared according to a procedure developed by Brauer [63] by oxidation of $FeCl_2$ with $NaNO_2$ in the presence of hexamethylenetetraamine at 60 °C for 3 h. In order to remove excess chloride, the lepidocrocite suspension was washed several times by centrifugation and resuspension in high purity water. The precipitate was freeze-dried. Powder X-ray diffraction confirmed that the synthesized solids are goethite and lepidocrocite. The specific surface area as

determined by the BET method is 170 m²/g for lepidocrocite and 38 m²/g for goethite. The point of zero charge (PZC) of lepidocrocite produced according to the method by Brauer is 7.5 [64]. For goethite, an isoelectric point (IEP) of 8.3 was determined by measuring the electrophoretic mobility of suspended particles.

2.2 Dissolution experiments

Dissolution experiments were performed with two experimental systems. The first set-up (solar simulator) consisted of a 1000 W, high pressure xenon lamp (OSRAM), from which the originating light (spectrum similar to that of sunlight) was filtered by the bottom window of the Pyrex glass vessel acting as a cutoff filter at 305 nm [53]. All experiments were carried out in a Pyrex glass vessel with a water jacket at constant temperature (25 ± 1 °C). The incident light intensity, I_0 , was 1200 W/m², as measured by ferrioxalate actinometry. The reaction volume was typically 350 ml and the irradiated surface area was 50 cm². The solutions were vigorously stirred with a Teflon-coated stirrer. The ionic medium used for the dissolution experiments was 0.01 M KClO₄. Suspensions of 0.08 g/L goethite or 0.02 g/L lepidocrocite were irradiated for several hours in the presence of 80 μM DFOB and/or 200 μM K-oxalate. Goethite suspensions including organic ligands were prepared 17 h before irradiation and stored in the dark to circumvent thermal fast initial dissolution reactions during irradiation experiments. By adding appropriate amounts of diluted HCl or NaOH, the pH of the solutions was kept constant at pH 6 during the entire experiments. Two different types of experiments were performed: steady-state experiments, in which DFOB and oxalate were both added to goethite or lepidocrocite suspensions before irradiation; and non-steady-state experiments in which oxalate reacted with the iron oxides under irradiation before adding DFOB. Oxygen-free (deaerated) conditions were maintained by purging N₂ through the suspensions and sporadically applying a weak vacuum.

The second experimental set-up was a light box equipped with 8 Philips TL20W/05 lamps (spectrum ranging from 300 to 460 nm with a maximum at 365 nm) on two opposite sides inside the box. Dissolution experiments were carried out in 4 ml polymethylmethacrylat (PMMA) cuvettes with two optical sides with excellent transmission in the range of 280 – 800 nm. The cuvettes with dimensions of 1 cm × 1 cm × 4 cm were always placed on a magnetic stirrer plate at the same height. Because light transmission also occurred through the two non-optical sides of the cuvettes, an incident light intensity I_0 of approximately 55 W/m² was estimated by ferrioxalate actinometry. An average photolysis quantum yield of 1.16 was used for the light intensity calculation. Suspensions containing 0.02 g/L lepidocrocite, 0.01 M KClO₄,

45 μM DFOB or aerobactin at pH 6 were irradiated for over 4 h. The suspensions were stirred with small magnet bars. An integrated ventilator kept the temperature at about 32 $^{\circ}\text{C}$ to 34 $^{\circ}\text{C}$. Dark experiments were carried out at the same temperature in a temperature controlled water bath.

In all dissolution experiments, samples of the suspensions were periodically taken, immediately filtered, and acidified with a small amount of 65 % suprapure HNO_3 (Merck). Single use syringe filters with 0.2- μm pore size (Sartorius) were used for goethite suspensions. Preliminary tests showed that significant fractions of a lepidocrocite suspension passed through membrane filters with 0.2- μm pore size. Therefore membrane filters with a pore size of 0.025 μm (Schleicher and Schuell) were used to filter lepidocrocite suspensions. We operationally define iron that passes through these filters as total dissolved iron [Fe_{tot}]. Total dissolved iron was measured by ICP-MS (Agilent 7500 Series; iron standards from Fluka).

2.3 Photolysis of dissolved Fe(III)-siderophore complexes

Solutions of 45 μM 1:1-Fe(III)-DFOB and 1:1-Fe(III)-aerobactin complexes were prepared by adding the equivalent amount of siderophore to a solution of 45 μM $\text{FeCl}_3 \cdot 6\text{H}_2\text{O}$ at pH 1. The pH of the solutions was varied by titrating these unbuffered solutions manually with NaOH. No electrolyte was added. The ionic strength of solutions with pH > 3 was approximately 0.1 M, due to the initial acidification to pH 1 with HCl and titration with NaOH back to higher pH. Light and dark experiments were performed with the second experimental set-up. UV-visible absorption of the irradiated and non-irradiated solutions were recorded with a UV-visible spectrophotometer (Cary 1E) using a micro-cuvette (5 cm pathlength, 0.7 ml volume). Analogous experiments were carried out with 0.15 g/L lepidocrocite suspensions in the presence of 45 μM aerobactin and 0.01 M KClO_4 . After irradiation, samples were filtered and the spectra of the filtered solutions were recorded.

3. Results

3.1 Photolysis of Fe(III)-siderophore complexes in homogeneous and heterogeneous systems

Aqueous Fe(III)-aerobactin complexes exhibited pH-dependent peak shifts in the UV-visible spectrum consistent with published results [65]. Decreasing the pH from 6 to 3.5 led to a shift of the absorption peak maximum from 395 nm to about 430 nm.

Similar peak shifts were observed upon irradiation of a solution of 1:1 Fe(III)-aerobactin at constant pH of 6.3 for two and six hours (Fig. 2), whereas the spectrum of the non-irradiated Fe(III)-aerobactin solution did not change over time. The irradiated solution (pH 6.3) exhibited a UV-visible spectrum similar to that of a non-irradiated solution at pH 3.5 (with absorption maximum at 430 nm), which is consistent with a light-induced change in the coordination sphere of Fe(III)-aerobactin complexes analogous to the pH-dependent change in the coordination sphere. We have also observed peak shifts in irradiated solutions of Fe(III)-aerobactin complexes at lower pH. At pH 5 a peak shift from 402 nm to 427 nm occurred upon irradiation, whereas at pH 4 a peak shift from 423 nm to 430 nm was observed. Irradiation of a Fe(III)-DFOB solution for 6 h at pH 6 did not result in changes in the UV-visible absorption spectra (data not shown), which is in agreement with recent reports [46].

To investigate photolysis of Fe(III)-aerobactin complexes at the lepidocrocite surface, lepidocrocite suspensions were irradiated in the presence of aerobactin for 6 h at pH 6. The spectra of two filtered solutions (independent replicates) showed an absorption maxima at 430 nm (Fig. 3) which also was found for an irradiated homogeneous Fe(III)-aerobactin solution at pH 6.3 (Fig. 2).

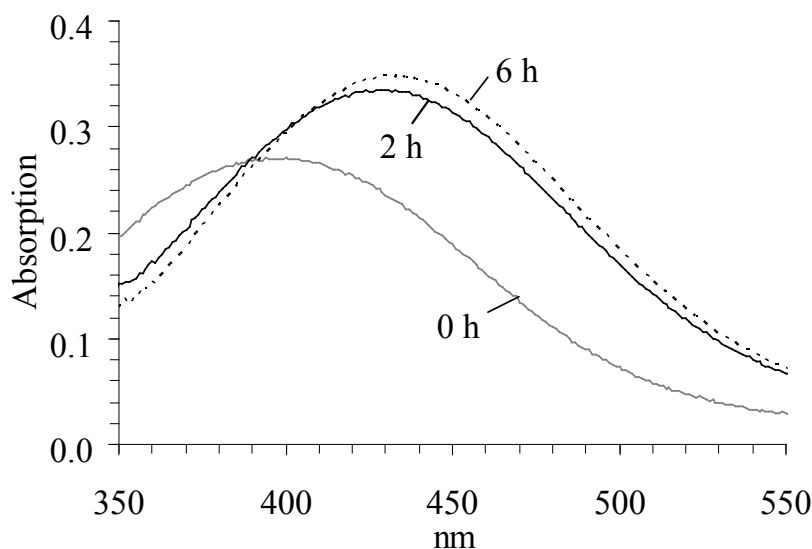


Fig. 2: UV-visible spectra of 1:1 Fe(III)-aerobactin complexes (45 μ M) irradiated for 2 and 6 hours or kept in the dark. $I_0 = 55 \text{ W/m}^2$ (blue actinic light source with a spectral range between 300 - 460 nm). $T = 32 \text{ }^\circ\text{C}$, pH 6.3, ionic strength $\sim 0.1 \text{ M}$.

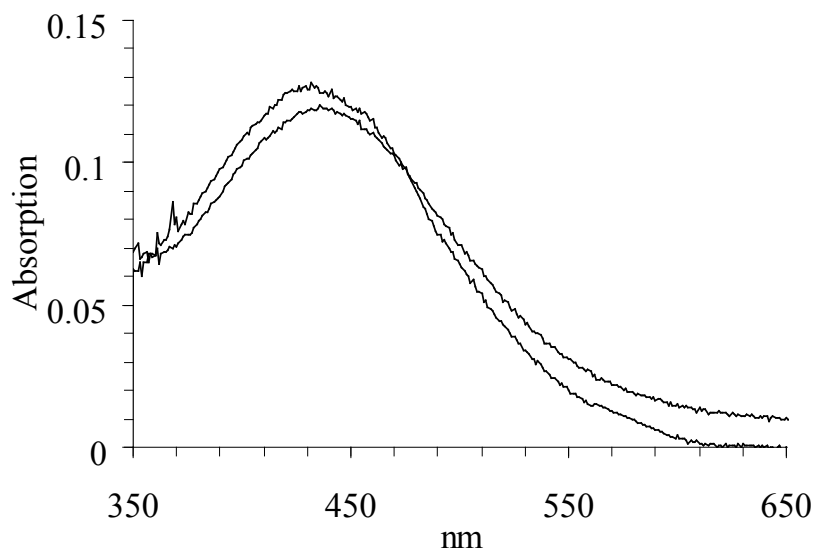


Fig. 3: UV-visible spectra of two filtered suspensions (independent replicates) containing 0.15 g/L lepidocrocite and 45 μM aerobactin, after 6 h irradiation with $I_0 = 55 \text{ W/m}^2$ (blue actinic light source with a spectral range between 300 - 460 nm). $T = 32 \text{ }^\circ\text{C}$, pH 6, electrolyte = 0.01 M KClO_4 .

3.2 Effects of DFOB or aerobactin and light on the dissolution of lepidocrocite and goethite

The results of lepidocrocite dissolution experiments in the presence of aerobactin or DFOB are shown in Fig. 4. No significant dissolution was observed in the absence of these siderophores, even in a deaerated, irradiated lepidocrocite suspension. Thermal lepidocrocite dissolution rates were accelerated in the presence of DFOB and aerobactin (2.0 and 2.8 $\text{nmol min}^{-1} \text{ m}^{-2}$, respectively). Irradiation caused further acceleration of dissolution rates relative to thermal dissolution rates by a factor of four (8.2 and 11.5 $\text{nmol min}^{-1} \text{ m}^{-2}$) in the presence of DFOB and aerobactin, respectively.

No thermal or photodissolution of goethite was observed in the presence of DFOB as the only organic ligand (detection limit $\sim 0.1 \mu\text{M Fe}$) under aerated or deaerated conditions on the time scale of the dissolution experiments (data not shown).

3.3 Photodissolution of lepidocrocite and goethite in the presence of DFOB and/or oxalate

Dissolution rates of lepidocrocite in the presence or absence of DFOB and oxalate are summarized in Table 1 and Fig. 5. Under aerated conditions at pH 6, oxalate did not promote significant photodissolution, whereas DFOB did (see also Fig. 4). However,

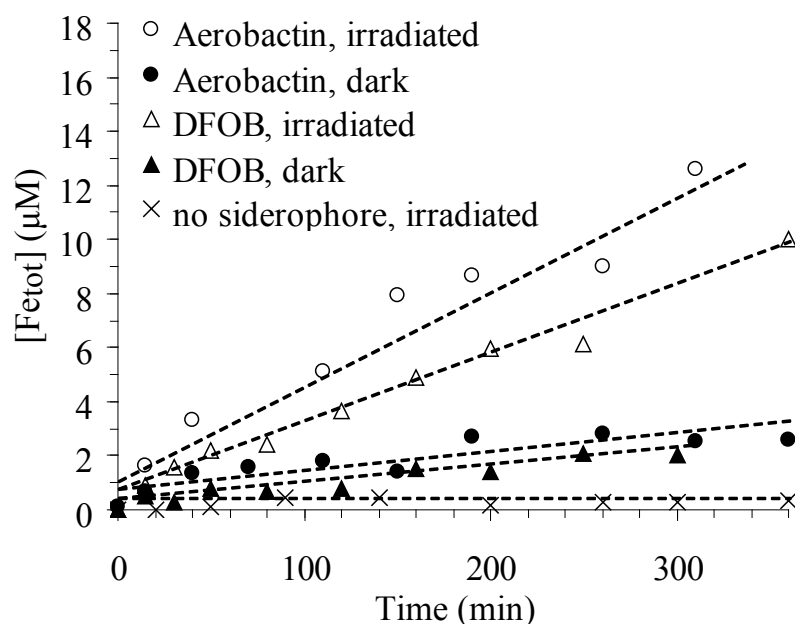


Fig. 4: Dissolution in aerated 0.02 g/L lepidocrocite suspensions in the presence of 45 μM aerobactin or DFOB. Suspensions were either irradiated with $I_0 = 55 \text{ W/m}^2$ (blue actinic light source with a spectral range between 300 - 460 nm) or kept in the dark. Lepidocrocite suspensions (deaerated) were also irradiated in the absence of siderophores. $T = 32 \text{ }^\circ\text{C}$, pH 6, electrolyte = 0.01 M KClO_4 , $[\text{Fe}_{\text{tot}}]$ = total dissolved iron measured by ICP-MS.

under deaerated, irradiated conditions, appreciable dissolution rates were observed in the presence of oxalate only. Photodissolution of lepidocrocite under aerated conditions was greatly enhanced by DFOB when oxalate also was present. There was no significant difference in photodissolution rates in the two-ligand system under aerated and deaerated conditions.

Results of goethite dissolution experiments are summarized in Table 2 and Fig. 6. The dissolution rates were generally lower than those observed for lepidocrocite under the same conditions. For example, the lepidocrocite dissolution rate in the presence of 80 μM DFOB and 200 μM oxalate in the dark was $6.2 \text{ nmol m}^{-2} \text{ min}^{-1}$, and hence more than an order of magnitude higher than the corresponding dissolution rate for goethite ($0.1 \text{ nmol m}^{-2} \text{ min}^{-1}$). Furthermore, no thermal- or photodissolution of goethite was observed in the presence of either DFOB or oxalate on the time scale of the experiments. Only for goethite suspensions containing both DFOB and oxalate, dissolution rates were increased upon irradiation and dissolution rates were smaller in aerated than in deaerated suspensions (Fig. 6). As mentioned above, oxygen had no effect on light-induced dissolution rates of lepidocrocite in the presence of both DFOB and oxalate (Fig. 5).

Table 1: Dissolution rates in irradiated lepidocrocite suspensions at pH 6 in the presence of DFOB and/or oxalate (0.02 g/L lepidocrocite, electrolyte = 0.01 M KClO_4 ; $T = 25\text{ }^\circ\text{C}$, $I_0 = 1200\text{ W/m}^2$).

[DFOB] (μM)	[Oxalate] (μM)	Deaerated	Dissolution rate ($\text{nmol m}^{-2}\text{ min}^{-1}$)
-	-	No	n.d.
-	-	Yes	n.d.
80	-	No	5.4
80	-	Yes	7.3
-	200	No	Small, non linear
-	200	Yes	11.8
80	200	No	~ 24.3
80	200	Yes	~ 24.3

n.d.: no detectable increase in iron concentrations over the course of the dissolution experiment

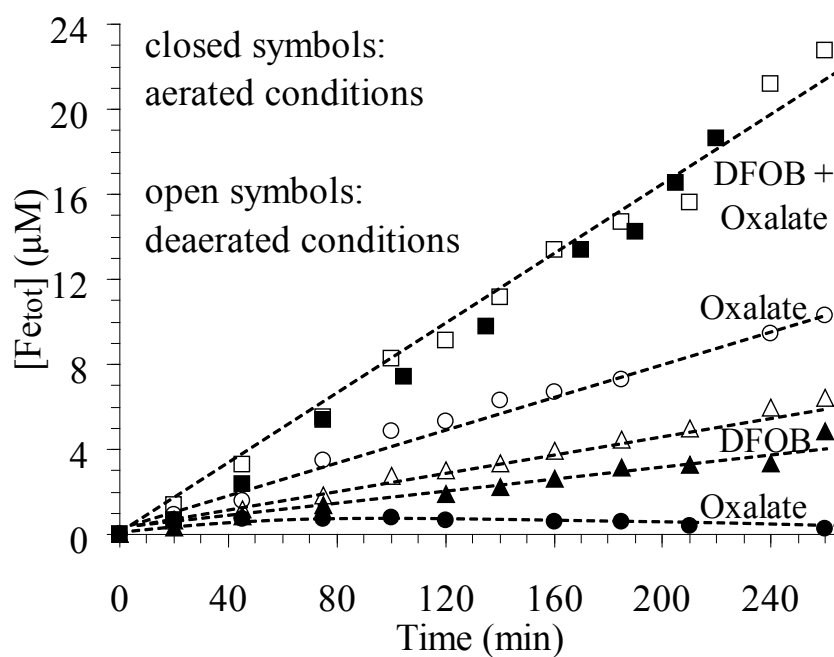


Fig. 5: Dissolution in irradiated 0.02 g/L lepidocrocite suspensions in the presence/absence of 80 μM DFOB / 200 μM oxalate. $I_0 = 1200\text{ W/m}^2$ (xenon lamp with a spectral range between 300 - 800 nm), $T = 25\text{ }^\circ\text{C}$, pH 6, electrolyte = 0.01 M KClO_4 . Closed symbols stand for aerated suspensions, open symbols for deaerated suspensions. $[\text{Fe}_{\text{tot}}]$ = total dissolved iron measured by ICP-MS.

Table 2: Dissolution rates in irradiated goethite suspensions at pH 6 in the presence of DFOB and/or oxalate (0.08 g/L goethite, electrolyte = 0.01 M KClO₄, T = 25 °C, I₀ = 1200 W/m²).

[DFOB] (μM)	[Oxalate] (μM)	Deaerated	Dissolution rate (nmol m ⁻² min ⁻¹)
80	-	No	n.d.
80	-	Yes	n.d.
-	200	No	n.d.
-	200	Yes	n.d.
80	200	No	0.59
80	200	Yes	2.9

n.d.: no detectable increase in iron concentrations over the course of the dissolution experiment

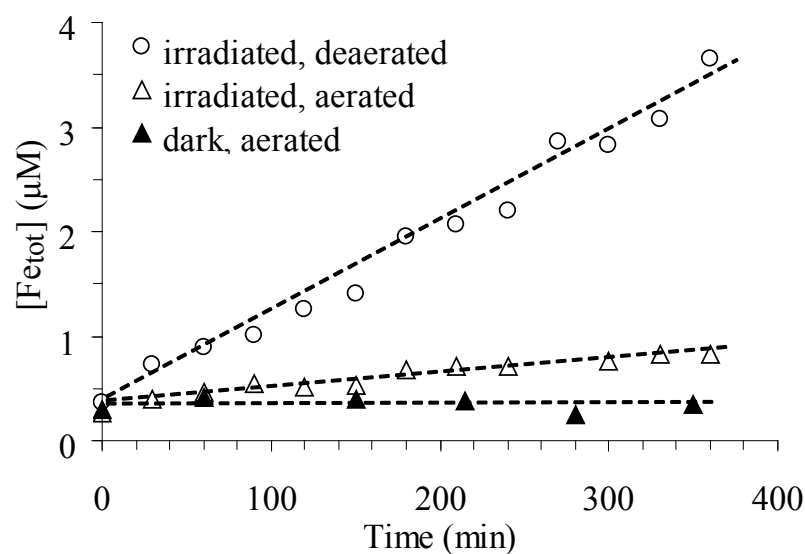


Fig. 6: Dissolution in 0.08 g/L goethite suspensions in the presence of 80 μM DFOB and 200 μM oxalate under different conditions. I₀ = 1200 W/m² (xenon lamp with a spectral range between 300 - 800 nm), T = 25 °C, pH 6, electrolyte = 0.01 M KClO₄. Suspensions were kept first for 17 hours in the dark to circumvent fast dissolution during irradiation experiments. After this time span, total dissolved iron concentrations as measured by ICP-MS were 0.3-0.4 μM.

3.4 Non-steady-state experiments with lepidocrocite and goethite in the two-ligand system DFOB/oxalate

To investigate whether kinetically labile surface sites (e.g., photoproducted Fe(II), or freshly formed iron oxide phases) accumulate at the mineral surface in the presence of oxalate, we conducted non-steady-state experiments. Deaerated or aerated lepidocrocite and goethite suspensions were first exposed to oxalate for a few hours, before adding a spike of DFOB. In Fig. 7A – C the dissolutions kinetics in non-steady-state experiments is compared to that in the steady-state experiments, in which DFOB and oxalate were added simultaneously to lepidocrocite or goethite suspensions. As soon as DFOB was added to irradiated, lepidocrocite (aerated) and goethite (deaerated) suspensions, containing oxalate (at 70 min and 200 min, respectively), the dissolution rate equaled that of the corresponding steady-state experiment (Fig. 7A, B). Hence, on the time scale of this experiment we observed no accumulation of kinetically labile surface sites in irradiated suspensions at pH 6.

Goethite suspensions were first conditioned in the dark for 17 h with oxalate and oxalate/DFOB in non-steady-state and steady-state experiments, respectively, before irradiating the suspensions. Within this conditioning period, no detectable thermal dissolution by oxalate took place, whereas thermal dissolution was obvious in the presence of both oxalate and DFOB, resulting in dissolved iron concentrations of 0.3 – 0.4 μM (at 0 min) in deaerated and aerated suspensions (Fig. 7B, C). In irradiated, aerated goethite suspensions (Fig. 7C), the addition of DFOB led to fast initial dissolution which then slowed down to match the steady-state dissolution rate. No photodissolution was observed in aerated goethite suspensions before DFOB was added. The fast release of 0.3-0.4 μM dissolved iron after the addition of DFOB can be rationalized in terms of thermal formation of kinetically labile surface iron by oxalate during the conditioning phase and the efficient detachment after the addition of DFOB at 200 min.

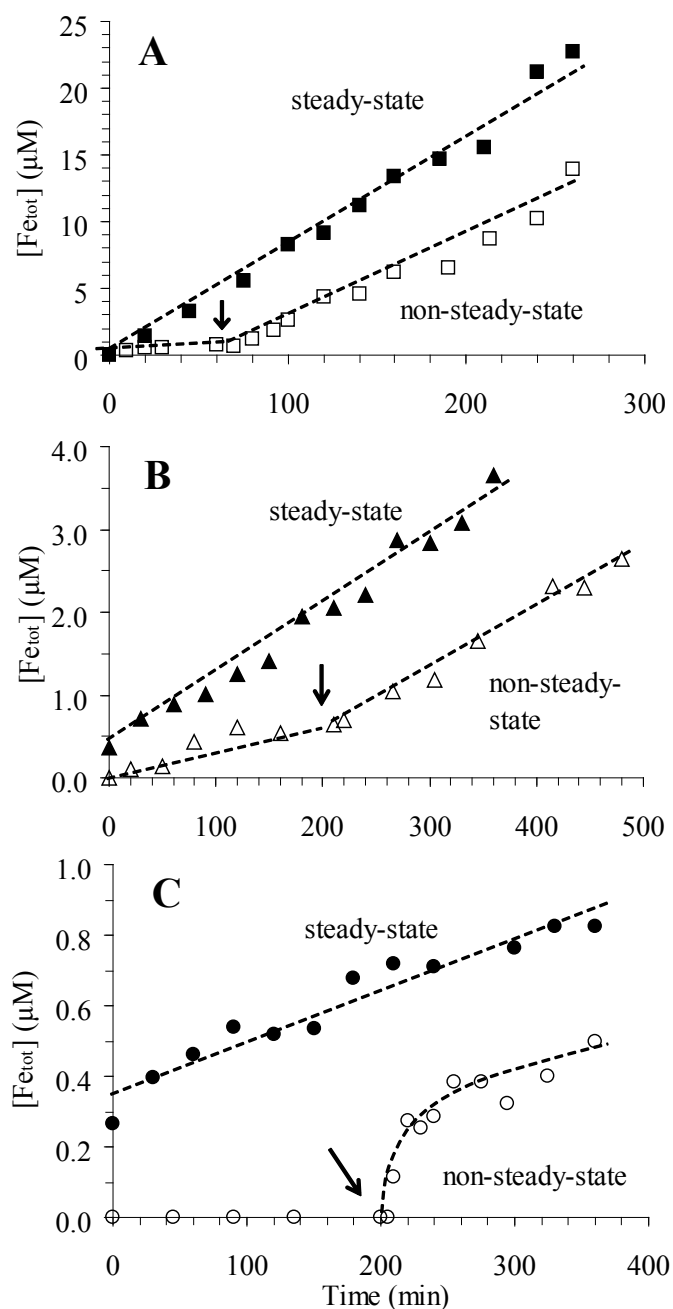


Fig. 7: Comparison of steady-state dissolution and non-steady-state dissolution in irradiated 0.02 g/L lepidocrocite suspensions (A) and 0.08 g/L goethite suspensions (B and C). In steady-state experiments 80 μM DFOB and 200 μM oxalate were added simultaneously to the iron oxide suspensions, whereas in non-steady-state experiments, oxalate was first left to react with the iron oxides, before DFOB was added (at 70 min and 200 min for lepidocrocite and goethite suspensions, respectively). (A) aerated and irradiated lepidocrocite suspensions; (B) deaerated and irradiated goethite suspensions; (C) aerated and irradiated goethite suspensions. $T = 25\text{ }^\circ\text{C}$, $\text{pH } 6$, $I = 1200\text{ W/m}^2$ (Xenon lamp with a spectral range between 300 - 800 nm), electrolyte = 0.01 M KClO_4 . Goethite suspensions were kept first for 17 hours in the dark to circumvent fast dissolution during irradiation experiments. After this conditioning phase, total dissolved iron concentrations as measured by ICP-MS were 0.3-0.4 μM for steady-state experiments and 0 μM for non-steady-state experiments in (B) and (C).

4. Discussion

4.1 Photolysis of Fe(III)-siderophore complexes

We measured UV-visible absorption spectra of Fe(III)-siderophore complexes before and after irradiation in order to investigate the photoreactivity of these complexes. Irradiation of 1:1 Fe(III)-aerobactin solutions at pH 4, 5, and 6.3 led to light-induced peak shifts in the absorption spectra with a final absorption maximum at approximately 430 nm (for pH 6.3 solution, see Fig. 2). These peak shifts clearly indicate the photoreactivity of dissolved Fe(III)-aerobactin complexes. It is likely that the photoreactivity of aerobactin is imparted by the α -hydroxycarboxylate binding group. This suggests that the coordination of Fe(III) by both oxygen atoms of the hydroxyl and carboxyl moieties of the α -hydroxycarboxylate group is a prerequisite for photolysis to occur. We hypothesize that photolysis of the Fe(III)-aerobactin complex is likely to result in the destruction of the α -hydroxycarboxylate group and the formation of a 3-ketoglutarate residue in analogy to the structurally similar petrobactin (see Fig. 1) [42]. The changes in absorption spectra of the Fe(III)-aerobactin complex therefore reflect the loss of iron coordination by the α -hydroxycarboxylate group. This interpretation is supported by similar spectral changes due to pH shifts and hence changes of the coordination sphere of Fe(III)-aerobactin complexes. Harris et al. [65] have observed UV-visible absorption spectra of Fe(III)-aerobactin complexes as a function of pH and concluded that pH dependent shifts are due to changes in the coordination of iron by the citrate moiety. Raising solution pH from 3.5 to 6 increases the fraction of $[\text{Fe}^{3+}(\text{aerobactin}^{6-})]^{3-}$, in which Fe(III) is coordinated by both hydroxamate binding groups as well as the hydroxyl and carboxyl moieties of the α -hydroxycarboxylate group. According to speciation calculations, the fraction of this species constitutes 16 %, 74 % and 97 % at pH 4.0, pH 5.0 and pH 6.0, respectively, in 1:1 Fe(III)-aerobactin solutions ($I = 0.1$ M). Thermodynamic data for the speciation calculation are listed in Table 3. A linear relationship between the pH-dependent fraction of $[\text{Fe}^{3+}(\text{aerobactin}^{6-})]^{3-}$ and the observed absorption peak maximum is found in non-irradiated 1:1 Fe(III)-aerobactin solutions (Fig. 8). At pH 3.5 the absorption peak maximum lies at approximately 430 nm, whereas at pH 6 the peak maximum occurs at 395 nm. Irradiation of 1:1 Fe(III)-aerobactin solutions with pH > 3.5 leads to a peak shift to 430 nm, indicating photodegradation of the citrate moiety in the photoreactive species $[\text{Fe}^{3+}(\text{aerobactin}^{6-})]^{3-}$ and hence loss of one binding group.

We have not observed changes in the UV-visible spectra of Fe(III)-DFOB complexes due to irradiation. This is consistent with previous reports on the photostability of

Fe(III)-DFOB complexes [46].

Table 3: Thermodynamic stability constants at 25 °C and infinite dilution

Reaction	Log K_{298}^a
$\text{Aerobactin}^{5-} + \text{H}^+ = \text{HAerobactin}^{4-}$	10.51
$\text{Aerobactin}^{5-} + 2\text{H}^+ = \text{H}_2\text{Aerobactin}^{3-}$	20.30
$\text{Aerobactin}^{5-} + 3\text{H}^+ = \text{H}_3\text{Aerobactin}^{2-}$	25.25
$\text{Aerobactin}^{5-} + 4\text{H}^+ = \text{H}_4\text{Aerobactin}^-$	29.16
$\text{Aerobactin}^{5-} + 5\text{H}^+ = \text{H}_5\text{Aerobactin}$	32.49
$\text{Aerobactin}^{5-} + \text{Fe}^{3+} = \text{FeH}_{-1}\text{Aerobactin}^{3-} + \text{H}^+$	20.67
$\text{Aerobactin}^{5-} + \text{Fe}^{3+} = \text{FeAerobactin}^{2-}$	25.72
$\text{Aerobactin}^{5-} + \text{Fe}^{3+} + \text{H}^+ = \text{FeHAerobactin}^-$	29.75
$\text{Aerobactin}^{5-} + \text{Fe}^{3+} + 2\text{H}^+ = \text{FeH}_2\text{Aerobactin}$	33.06
$\text{Aerobactin}^{5-} + \text{Fe}^{3+} + 3\text{H}^+ = \text{FeH}_3\text{Aerobactin}^+$	35.46
$\text{Fe}^{3+} + \text{OH}^- = \text{FeOH}^{2+}$	11.81
$\text{Fe}^{3+} + 2\text{OH}^- = \text{Fe}(\text{OH})_2^+$	23.4
$\text{Fe}^{3+} + 3\text{OH}^- = \text{Fe}(\text{OH})_3(\text{aq})$	30.2
$\text{Fe}^{3+} + 4\text{OH}^- = \text{Fe}(\text{OH})_4^-$	34.4
$2\text{Fe}^{3+} + 2\text{OH}^- = \text{Fe}_2(\text{OH})_2^{4+}$	25.14
$3\text{Fe}^{3+} + 4\text{OH}^- = \text{Fe}_3(\text{OH})_4^{5+}$	49.7

$\text{FeH}_{-1}\text{Aerobactin}^{3-}$ is the photoreactive species $[\text{Fe}^{3+}(\text{aerobactin}^{6-})]^{3-}$

^a values are taken from Martell et al. (2001) and corrected to zero ionic strength using the Davies equation.

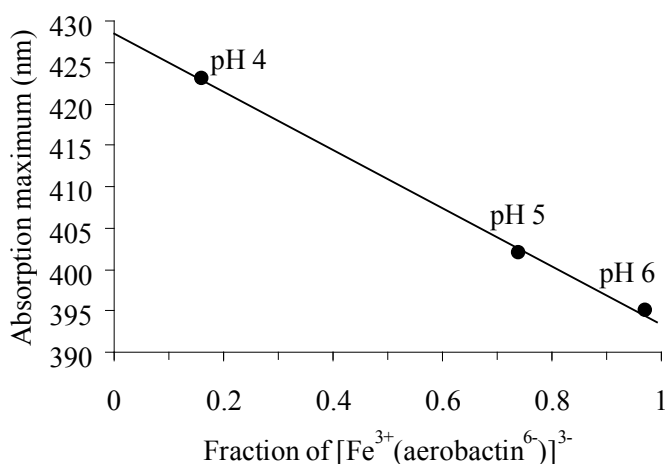
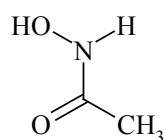


Fig. 8: Observed absorption maxima of non-irradiated solutions of 1:1 Fe(III)-aerobactin complexes (45 μM) at different pH vs. the calculated fraction of the $[\text{Fe}^{3+}(\text{aerobactin}^{6-})]^{3-}$ species. The program CHEAQS vers. L19 was used for speciation calculations [74].

4.2 Thermal and photodissolution of lepidocrocite by DFOB and aerobactin

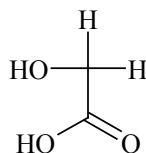
The rate of siderophore-controlled iron oxide dissolution is influenced by the configuration and bonding of Fe-siderophore surface complexes. Similar rate constants of ligand-promoted dissolution of goethite in the presence of the trihydroxamate siderophore DFOB or monohydroxamate aHA (acetohydroxamic acid, see Fig. 9) have been reported [66]. These authors have therefore concluded that only one hydroxamate group of DFOB participates in the formation of a bidentate mononuclear surface complex on goethite. In the case of aerobactin, the α -hydroxycarboxylate moiety as well as the hydroxamate moieties may participate in surface complex formation. The affinities of these functional groups for inner-sphere coordination of Fe(III) at the mineral surface are not known, but may be assessed from the stability constants of aqueous complexes of analogous compounds [67]. The overall stability constant of a typical 1:1 Fe(III)-monohydroxamate complex is much higher than that of an equivalent 1:1 Fe(III)- α -hydroxycarboxylate complex (Fig. 9). For example, the stability constant of 1:1 Fe(III)-acetohydroxamic acid (monohydroxamate complex) is 8 orders of magnitude higher than that of 1:1 Fe(III)-glycolic acid (α -hydroxycarboxylate complex) [68].

Acetohydroxamic acid aHA



$$\text{Log } K_{\text{FeL}} = 10.95$$

Glycolic acid



$$\text{Log } K_{\text{FeL}} = 2.9$$

Fig. 9: Chemical structures of acetohydroxamic acid and glycolic acid and the stability constants [68] of aqueous 1:1 Fe(III)-ligand complexes at ionic strength $I = 1 \text{ M}$ and $25 \text{ }^\circ\text{C}$.

Therefore, we assume that weaker inner-sphere surface complexes are formed with α -hydroxycarboxylate binding groups than with hydroxamate binding groups and that hydroxamate groups will have a stronger effect on dissolution rates than α -hydroxycarboxylate groups. Such a correlation between ligand affinity and dissolution rates of iron oxides has been observed by Duckworth and Martin [69]. They have studied surface complexation and dissolution of hematite by various dicarboxylic acids at pH 5 and have observed a linear relationship between the ligand-promoted dissolution rate constants and the Langmuir binding constants. Based on above considerations, we

propose surface coordination of aerobactin on iron oxides by a hydroxamate binding group. The hypothesis that the α -hydroxycarboxylate group does not participate in surface complexation is consistent with the observation of equal light-induced and thermal lepidocrocite dissolution rates by DFOB and aerobactin (Fig. 4), despite the different photoreactivity of dissolved Fe(III)-aerobactin and Fe(III)-DFOB complexes. This indicates that both siderophores coordinate surface Fe(III) with the hydroxamate group and not with the α -hydroxycarboxylate group in the case of aerobactin, and that both siderophores do not promote photoreduction of Fe(III) surface sites by a ligand-to-metal charge-transfer mechanism. UV-visible absorption spectra of filtered lepidocrocite suspensions that were irradiated in the presence of aerobactin (Fig. 3) exhibited the same spectral features as photolyzed Fe(III)-aerobactin complexes in solution (Fig. 2), typically having an absorption maximum at 430 nm. Most likely, the transfer of surface iron into solution occurs via the hydroxamate binding group of aerobactin, and once dissolved Fe(III) is fully coordinated, photolysis of the Fe(III)-aerobactin complex occurs.

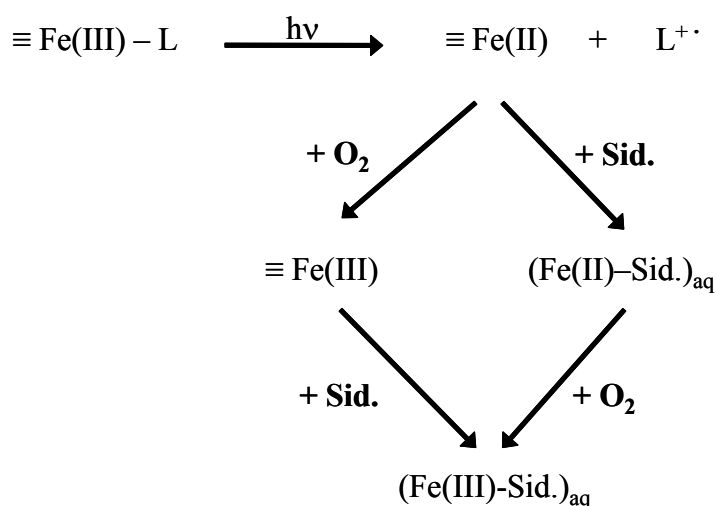
Possible mechanisms of Fe(III) photoreduction at the lepidocrocite surface in the presence of DFOB or aerobactin are photolysis of surface Fe(III)-hydroxo groups or excitation of the $O^{2-} \rightarrow Fe^{3+}$ charge-transfer bands with subsequent migration of the generated photo-electron to the oxide surface. Irrespective of the exact photochemical mechanisms that lead to the formation of surface Fe(II), both DFOB and aerobactin clearly promote the transfer of iron to the solution. This is consistent with the acceleration of the rate determining detachment of Fe(II) in ligand-promoted, reductive dissolution [56].

4.3 Thermal and photodissolution of goethite and lepidocrocite in the two-ligand system DFOB/oxalate

Oxalate is known to form photoreactive surface complexes at goethite and lepidocrocite surfaces and to promote fast photodissolution in the absence of oxygen [8, 53]. In the presence of oxygen and depending on pH, reoxidation of Fe(II) at the mineral surface may outcompete detachment of Fe(II) [8, 9]. In our study, the presence of oxygen reduced the rate of lepidocrocite photodissolution in the presence of oxalate to less than 50 % relative to dissolution rates of deaerated suspensions at pH 6 (Fig. 5 and Table 1). This indicates that fast reoxidation of surface Fe(II) in aerated suspensions outcompetes its slow detachment from the lepidocrocite surface. However, in the presence of both oxalate and DFOB, photodissolution of lepidocrocite was significantly accelerated with similar rates in aerated and deaerated suspensions (Fig. 5). Considering

that DFOB does not act as an electron donor (see discussion above), we conclude that DFOB is an efficient shuttle for the transfer of surface Fe(II) into solution.

The presence of oxygen has a bigger impact on light-induced dissolution of goethite in the presence of DFOB and oxalate (Fig. 6), as compared to lepidocrocite. This can be explained in terms of different thermodynamic stabilities of these two iron oxide phases. With goethite, detachment of reduced iron is likely to be slower than with lepidocrocite, resulting in competitive reoxidation of Fe(II) [8]. These authors have reported that no dissolution took place in irradiated, aerated goethite and hematite suspensions at pH 3. However, as shown in Fig. 6, photodissolution of goethite does take place in aerated suspensions, even at pH 6, if DFOB is added to the system. The likely role of siderophores in the formation of dissolved iron through photoreductive dissolution of iron oxides is shown schematically in Fig. 10.



L = OH, photoreductive ligand

Fig. 10: General mechanism of light-induced dissolution in the presence of siderophores. Following photoexcitation of surface hydroxo complexes or surface ligand complexes and charge transfer, surface Fe(III) is reduced to Fe(II). For simplicity, the $\text{O}^{2-} \rightarrow \text{Fe}^{3+}$ semiconductor charge transfer mechanism is omitted. Detachment of Fe(II) is the rate determining step in the overall photodissolution reaction. A competing reaction is the reoxidation of surface Fe(II). Depending on the thermodynamic stability of the iron oxide, siderophore-promoted detachment may or may not outcompete the surface reoxidation reaction. The dissolution of reoxidized surface Fe(III) is promoted by siderophores in a slow ligand controlled dissolution reaction with similar rates as the dark reaction. In solution Fe(II)-siderophore complexes are oxidized immediately to Fe(III)-siderophore complexes by oxygen.

To investigate, if kinetically labile sites (Fe(II) and reoxidized surface sites) accumulate at irradiated oxide surfaces in the presence of oxalate, non-steady-state dissolution experiments were performed. Goethite and lepidocrocite suspensions were irradiated in the presence of oxalate before adding the siderophore DFOB (Fig. 7A-C). The accumulation of labile surface sites is expected to result in a fast non-steady-state dissolution reaction after the addition of the siderophore. Accumulation and fast non-steady-state release of labile Fe(III) surface sites have been observed previously in thermal dissolution experiments involving oxalate and DFOB [70]. Furthermore, a labilizing effect of light on the dissolution of colloidal iron oxides by unknown organic chromophores in seawater has been observed by Wells et al. [58]. We did not observe such a light-induced labilization of surface sites on goethite and lepidocrocite in the presence of oxalate. The sudden increase in dissolved iron, which occurred upon addition of DFOB to an aerated and irradiated goethite / oxalate suspension (Fig. 7C) is most likely due to the labilizing effect of oxalate during the conditioning phase in the dark (17 h). The thermal formation of about 0.3-0.4 μM kinetically labile surface iron by oxalate is consistent with the results by Reichard et al [70].

5. Conclusions

Considering that the deposition of atmospheric aerosols to ocean waters may provide a significant source of iron in the form of solid oxides, photodissolution processes may be important for increasing the bioavailability of iron to the marine biota. According to our laboratory study, siderophores, including a non-photoreductive siderophore, greatly accelerate light-induced dissolution of crystalline iron oxides. Addition of a second organic ligand, acting as the electron donor, further accelerates the dissolution process. This synergistic effect of siderophores and photoreductive ligands may be an important process in iron solubilization in iron deficient marine surface waters, where photoreductive ligands as well as siderophores are present [37, 41, 54, 71, 72].

6. References

- [1] Martin, J. H. and Fitzwater, S. E. **1988**. Iron-deficiency limits phytoplankton growth in the northeast Pacific Subarctic. *Nature* 331: 341-343.
- [2] Martin, J. H., Coale, K. H., Johnson, K. S., Fitzwater, S. E., Gordon, R. M., Tanner, S. J., Hunter, C. N., Elrod, V. A., Nowicki, J. L., Coley, T. L., Barber, R. T., Lindley, S., Watson, A. J., Vanscoy, K., Law, C. S., Liddicoat, M. I., Ling, R., Stanton, T., Stockel, J., Collins, C., Anderson, A., Bidigare, R., Ondrusek, M., Latasa, M., Millero, F. J., Lee, K., Yao, W., Zhang, J. Z., Friederich, G., Sakamoto, C., Chavez, F., Buck, K., Kolber, Z., Greene, R., Falkowski, P., Chisholm, S. W., Hoge, F., Swift, R., Yungel, J., Turner, S., Nightingale, P., Hatton, A., Liss, P. and Tindale, N. W. **1994**. Testing the iron hypothesis in ecosystems of the equatorial Pacific-Ocean. *Nature* 371: 123-129.
- [3] Martin, J. H., Gordon, R. M., Fitzwater, S. and Broenkow, W. W. **1989**. Vertex - phytoplankton iron studies in the Gulf of Alaska. *Deep-Sea Res.* 36: 649-&.
- [4] Faust, B. C. and Hoffmann, M. R. **1986**. Photoinduced reductive dissolution of α -Fe₂O₃ by bisulfite. *Environ. Sci. Technol.* 20: 943-948.
- [5] Pehkonen, S. O., Siefert, R., Erel, Y., Webb, S. and Hoffmann, M. R. **1993**. Photoreduction of iron oxyhydroxides in the presence of important atmospheric organic compounds. *Environ. Sci. Technol.* 27: 2056-2062.
- [6] Zhu, X., Prospero, J. M., Savoie, D. L., Millero, F. J., Zika, R. G. and Saltzman, E. S. **1993**. Photoreduction of iron(III) in marine mineral aerosol solutions. *J. Geophys. Res.* 98: 9039-9046.
- [7] Siefert, R. L., Pehkonen, S. O., Erel, Y. and Hoffmann, M. R. **1994**. Iron photochemistry of aqueous suspensions of ambient aerosol with added organic acids. *Geochim. Cosmochim. Acta* 58: 3271-3279.
- [8] Sulzberger, B. and Laubscher, H. **1995**. Reactivity of various types of iron(III) (hydr)oxides towards light-induced dissolution. *Mar. Chem.* 50: 103-115.
- [9] Sulzberger, B. and Laubscher, H. (1995). Photochemical reductive dissolution of lepidocrocite. Effect of pH. In: *Aquatic Chemistry: Interfacial and Interspecies Processes*. C. P. Huang, C. R. O'Melia and J. J. Morgan, Eds. American Chemical Society, Washington, DC: 279-290.
- [10] Johansen, A. M., Siefert, R. L. and Hoffmann, M. R. **2000**. Chemical composition of aerosols collected over the tropical North Atlantic Ocean. *J. Geophys. Res.* 105: 15277-15312.
- [11] Millero, F. J., Sotolongo, S. and Izaguirre, M. **1987**. The oxidation-kinetics of

- Fe(II) in seawater. *Geochim. Cosmochim. Acta* 51: 793-801.
- [12] Wells, M. L., Zorkin, N. G. and Lewis, A. G. **1983**. The role of colloid chemistry in providing a source of iron to phytoplankton. *J. Mar. Res.* 41: 731-746.
- [13] Finden, D. A. S., Tipping, E., Jaworski, G. H. M. and Reynolds, C. S. **1984**. Light-induced reduction of natural iron(III) oxide and its relevance to phytoplankton. *Nature* 309: 783-784.
- [14] Rich, H. W. and Morel, F. M. M. **1990**. Availability of well-defined iron colloids to the marine diatom *Thalassiosira weissflogii*. *Limnol. Oceanogr.* 35: 652-662.
- [15] Liu, X. W. and Millero, F. J. **2002**. The solubility of iron in seawater. *Mar. Chem.* 77: 43-54.
- [16] Anderson, M. A. and Morel, F. M. M. **1982**. The influence of aqueous iron chemistry on the uptake of iron by the coastal diatom *Thalassiosira weissflogii*. *Limnol. Oceanogr.* 27: 789-813.
- [17] Jones, G. J., Palenik, B. P. and Morel, F. M. M. **1987**. Trace-metal reduction by phytoplankton: the role of plasmalemma redox enzymes. *J. Phycol.* 23: 237-244.
- [18] Soria-Dengg, S. and Horstmann, U. **1995**. Ferrioxamine-B and ferrioxamine-E as iron sources for the marine diatom *Phaeodactylum tricornutum*. *Mar. Ecol., Prog. Ser.* 127: 269-277.
- [19] Hutchins, D. A., Witter, A. E., Butler, A. and Luther, G. W. **1999**. Competition among marine phytoplankton for different chelated iron species. *Nature* 400: 858-861.
- [20] Maldonado, M. T. and Price, N. M. **1999**. Utilization of iron bound to strong organic ligands by plankton communities in the subarctic Pacific Ocean. *Deep-Sea Res.* 46: 2447-2473.
- [21] Maldonado, M. T. and Price, N. M. **2001**. Reduction and transport of organically bound iron by *Thalassiosira oceanica* (Bacillariophyceae). *J. Phycol.* 37: 298-309.
- [22] Weger, H. G. **1999**. Ferric and cupric reductase activities in the green alga *Chlamydomonas reinhardtii*: experiments using iron-limited chemostats. *Planta* 207: 377-384.
- [23] Winkelmann, G. **1991**. *Handbook of microbial iron chelates*. CRC Press: Boca Raton, Florida.
- [24] Gonye, E. R. and Carpenter, E. J. **1974**. Production of iron-binding compounds by marine microorganisms. *Limnol. Oceanogr.* 19: 840-842.
- [25] Reid, R. T. and Butler, A. **1991**. Investigation of the mechanism of iron acquisition by the marine bacterium *Alteromonas luteoviolaceus*: Characterization of

- siderophore production. *Limnol. Oceanogr.* 36: 1783-1792.
- [26] Haygood, M. G., Holt, P. D. and Butler, A. **1993**. Aerobactin production by a planktonic marine *Vibrio* Sp. *Limnol. Oceanogr.* 38: 1091-1097.
- [27] Wilhelm, S. W. and Trick, C. G. **1994**. Iron-limited growth of cyanobacteria: multiple siderophore production is a common response. *Limnol. Oceanogr.* 39: 1979-1984.
- [28] Tortell, P. D., Maldonado, M. T., Granger, J. and Price, N. M. **1999**. Marine bacteria and biogeochemical cycling of iron in the oceans. *FEMS Microbiol. Ecol.* 29: 1-11.
- [29] Albrecht-Gary, A. M. and Crumbliss, A. L. **1998**. Coordination chemistry of siderophores: Thermodynamics and kinetics of iron chelation and release. *Met. Ions Biol. Syst.* 35: 239-327.
- [30] Hersman, L., Lloyd, T. and Sposito, G. **1995**. Siderophore-promoted dissolution of hematite. *Geochim. Cosmochim. Acta* 59: 3327-3330.
- [31] Yoshida, T., Hayashi, K. and Ohmoto, H. **2002**. Dissolution of iron hydroxides by marine bacterial siderophore. *Chem. Geol.* 184: 1-9.
- [32] Cheah, S. F., Kraemer, S. M., Cervini-Silva, J. and Sposito, G. **2003**. Steady-state dissolution kinetics of goethite in the presence of desferrioxamine B and oxalate ligands: implications for the microbial acquisition of iron. *Chem. Geol.* 198: 63-75.
- [33] Kraemer, S. M. **2004**. Iron oxide dissolution and solubility in the presence of siderophores. *Aquat. Sci.* 66: 3-18.
- [34] Wells, M. L., Price, N. M. and Bruland, K. W. **1994**. Iron limitation and the cyanobacterium *synechococcus* in equatorial Pacific waters. *Limnol. Oceanogr.* 39: 1481-1486.
- [35] Wells, M. L. **1999**. Manipulating iron availability in nearshore waters. *Limnol. Oceanogr.* 44: 1002-1008.
- [36] Rue, E. L. and Bruland, K. W. **1997**. The role of organic complexation on ambient iron chemistry in the equatorial Pacific Ocean and the response of a mesoscale iron addition experiment. *Limnol. Oceanogr.* 42: 901-910.
- [37] Vandenberg, C. M. G. **1995**. Evidence for organic complexation of iron in seawater. *Mar. Chem.* 50: 139-157.
- [38] Wu, J. F. and Luther, G. W. **1995**. Complexation of Fe(III) by natural organic-ligands in the Northwest Atlantic Ocean by a competitive ligand equilibration method and a kinetic approach. *Mar. Chem.* 50: 159-177.
- [39] Witter, A. E., Hutchins, D. A., Butler, A. and Luther, G. W. **2000**. Determination of conditional stability constants and kinetic constants for strong model Fe-

- binding ligands in seawater. *Mar. Chem.* 69: 1-17.
- [40] Powell, R. T. and Donat, J. R. **2001**. Organic complexation and speciation of iron in the South and Equatorial Atlantic. *Deep-Sea Res.* 48: 2877-2893.
- [41] Macrellis, H. M., Trick, C. G., Rue, E. L., Smith, G. and Bruland, K. W. **2001**. Collection and detection of natural iron-binding ligands from seawater. *Mar. Chem.* 76: 175-187.
- [42] Barbeau, K., Zhang, G. P., Live, D. H. and Butler, A. **2002**. Petrobactin, a photoreactive siderophore produced by the oil-degrading marine bacterium *Marinobacter hydrocarbonoclasticus*. *J. Am. Chem. Soc.* 124: 378-379.
- [43] Barbeau, K., Rue, E. L., Bruland, K. W. and Butler, A. **2001**. Photochemical cycling of iron in the surface ocean mediated by microbial iron(III)-binding ligands. *Nature* 413: 409-413.
- [44] Abrahamson, H. B., Rezvani, A. B. and Bruschi, G. J. **1994**. Photochemical and spectroscopic studies of iron(III) with citric acid and other carboxylic acids. *Inorg. Chim. Acta* 226: 117-127.
- [45] Kuma, K., Nakabayashi, S. and Matsunaga, K. **1995**. Photoreduction of Fe(III) by hydroxycarboxylic acids in seawater. *Water Res.* 29: 1559-1569.
- [46] Barbeau, K., Rue, E. L., Trick, C. G., Bruland, K. T. and Butler, A. **2003**. Photochemical reactivity of siderophores produced by marine heterotrophic bacteria and cyanobacteria based on characteristic Fe(III) binding groups. *Limnol. Oceanogr.* 48: 1069-1078.
- [47] Taylor, S. W., Luther, G. W. and Waite, J. H. **1994**. Polarographic and spectrophotometric investigation of iron(III) complexation to 3,4-dihydroxyphenylalanine-containing peptides and proteins from *Mytilus edulis*. *Inorg. Chem.* 33: 5819-5824.
- [48] Welch, K. D., Davis, T. Z. and Aust, S. D. **2002**. Iron autoxidation and free radical generation: effects of buffers, ligands, and chelators. *Arch. Biochem. Biophys.* 397: 360-369.
- [49] Zinder, B., Furrer, G. and Stumm, W. **1986**. The coordination chemistry of weathering: 2. Dissolution of Fe(III) oxides. *Geochim. Cosmochim. Acta* 50: 1861-1869.
- [50] Furrer, G. and Stumm, W. **1986**. The coordination chemistry of weathering: I. Dissolution kinetics of δ -Al₂O₃ and BeO. *Geochim. Cosmochim. Acta* 50: 1847-1860.
- [51] Waite, T. D. and Morel, F. M. M. **1984**. Photoreductive dissolution of colloidal iron-oxide - Effect of citrate. *J. Colloid Interface Sci.* 102: 121-137.
- [52] Litter, M. I. and Blesa, M. A. **1988**. Photodissolution of iron-oxides: 1. Maghemite

- in EDTA solutions. *J. Colloid Interface Sci.* 125: 679-687.
- [53] Siffert, C. and Sulzberger, B. **1991**. Light-induced dissolution of hematite in the presence of oxalate - a case-study. *Langmuir* 7: 1627-1634.
- [54] Sempere, R. and Kawamura, K. **1996**. Low molecular weight dicarboxylic acids and related polar compounds in the remote marine rain samples collected from western Pacific. *Atmos. Environ.* 30: 1609-1619.
- [55] Sempere, R. and Kawamura, K. **2003**. Trans-hemispheric contribution of C₂-C₁₀ α, ω-dicarboxylic acids, and related polar compounds to water-soluble organic carbon in the western Pacific aerosols in relation to photochemical oxidation reactions. *Glob. Biogeochem. Cycles* 17: 1069.
- [56] Banwart, S., Davies, S. and Stumm, W. **1989**. The role of oxalate in accelerating the reductive dissolution of hematite (α-Fe₂O₃) by ascorbate. *Colloid. Surf.* 39: 303-309.
- [57] Stumm, W. and Sulzberger, B. **1992**. The cycling of iron in natural environments: considerations based on laboratory studies of heterogeneous redox processes. *Geochim. Cosmochim. Acta* 56: 3233-3257.
- [58] Wells, M. L. and Mayer, L. M. **1991**. The photoconversion of colloidal iron oxyhydroxides in seawater. *Deep-Sea Res.* 38: 1379-1395.
- [59] Johnson, K. S., Coale, K. H., Elrod, V. A. and Tindale, N. W. **1994**. Iron photochemistry in seawater from the equatorial Pacific. *Mar. Chem.* 46: 319-334.
- [60] Miller, D. M. and Kester, D. R. **1994**. Photochemical iron reduction and iron bioavailability in seawater. *J. Mar. Res.* 52: 325-343.
- [61] Voelker, B. M., Morel, F. M. M. and Sulzberger, B. **1997**. Iron redox cycling in surface waters: Effects of humic substances and light. *Environ. Sci. Technol.* 31: 1004-1011.
- [62] Schwertmann, U. and Cornell, R. M. **1991**. *Iron oxides in the laboratory*. 1st ed.; VCH: Weinheim.
- [63] Brauer, G. **1963**. *Handbuch der präparativen anorganischen Chemie*. Ferd. Enke Verlag: Stuttgart, Germany.
- [64] Bondietti, C. G. (1992). Einfluss ausgewählter Liganden auf die Auflösungskinetik von Lepidokrokit (g-FeOOH). PhD thesis, ETH, Zürich, Switzerland.
- [65] Harris, W. R., Carrano, C. J. and Raymond, K. N. **1979**. Coordination chemistry of microbial iron transport compounds: 16. Isolation, characterization, and formation-constants of ferric aerobactin. *J. Am. Chem. Soc.* 101: 2722-2727.
- [66] Coccozza, C., Tsao, C. C. G., Cheah, S. F., Kraemer, S. M., Raymond, K. N., Miano, T. M. and Sposito, G. **2002**. Temperature dependence of goethite

- dissolution promoted by trihydroxamate siderophores. *Geochim. Cosmochim. Acta* 66: 431-438.
- [67] Stumm, W., Kummert, R. and Sigg, L. **1980**. A ligand-exchange model for the adsorption of inorganic and organic-ligands at hydrous oxide interfaces. *Croat. Chem. Acta* 53: 291-312.
- [68] Martell, A. E., Smith, R. M. and Motekaitis, R. J. **2001**. *NIST Critically Selected Stability Constants of Metal Database.*, NIST: Gaithersburg.
- [69] Duckworth, O. W. and Martin, S. T. **2001**. Surface complexation and dissolution of hematite by C₁-C₆ dicarboxylic acids at pH=5.0. *Geochim. Cosmochim. Acta* 65: 4289-4301.
- [70] Reichard, P. U., Kretzschmar, R. and Kraerner, S. A. **2007**. Rate laws of steady-state and non-steady-state ligand-controlled dissolution of goethite. *Colloids and Surfaces a-Physicochemical and Engineering Aspects* 306: 22-28.
- [71] Kuma, K., Nalabayashi, S., Suzuki, Y., Kudo, I. and Matsunaga, K. **1992**. Photo-reduction of Fe(III) by dissolved organic substances and existence of Fe(II) in seawater during spring blooms. *Mar. Chem.* 37: 15-27.
- [72] Nakabayashi, S., Kudo, I., Kuma, K., Matsunaga, K. and Hasebe, K. **1993**. Trace determination of sugar acids (gluconic acid) in sea-water by liquid-chromatography. *Anal. Chim. Acta* 271: 25-29.
- [73] Bergeron, R. J., Huang, G. F., Smith, R. E., Bharti, N., McManis, J. S. and Butler, A. **2003**. Total synthesis and structure revision of petrobactin. *Tetrahedron* 59: 2007-2014.
- [74] Verweij, W. **1991-2001**. *CHEAQS (a program for calculating chemical equilibria in aquatic systems)*, vers. L19. The Netherlands.

Chapter 2

Photolysis of citrate on the surface of lepidocrocite: An in situ ATR-FTIR study

Paul Borer, Stephan J. Hug, Barbara Sulzberger, Stephan M. Kraemer and Ruben Kretzschmar

Published in Journal of Physical Chemistry C (2007), 111, 10560-10569

Abstract

The photodecomposition of citrate adsorbed to γ -FeOOH (lepidocrocite) was investigated by batch photodissolution experiments and by in situ attenuated total reflection infrared spectroscopy (ATR-FTIR). Batch photodissolution experiments in suspensions of 125 mg/L γ -FeOOH and 100 μ M 14 C radio-labeled citrate revealed that the α -hydroxycarboxylic acid functional group of citrate was selectively photooxidized at pH 4 and pH 6. ATR-FTIR spectra recorded during the irradiation of γ -FeOOH-layers with adsorbed citrate showed that the primary photoproduct of citrate was acetonedicarboxylic acid. In the presence of excess citrate, the adsorbed photoproduct was exchanged in a ligand-exchange reaction indicating that citrate forms stronger surface complexes than acetonedicarboxylic acid. The primary photooxidation reaction was resolved from the subsequent ligand-exchange reaction by the application of a relatively high photon flux (5-10 W/cm², 300-500 nm). Despite consecutive ligand-exchange reactions, the photoconversion of adsorbed citrate to acetonedicarboxylic acid was almost complete at pH 4 within 22 min. At pH 6, only a small photodecomposition was observed. This result was interpreted in terms of (i) different fractions of inner- and outer-sphere citrate surface complexes at pH 4 and pH 6 and (ii) different photoreactivity of different inner-sphere complexes. Furthermore, both batch photodissolution

experiments and ATR-FTIR spectroscopy revealed that adsorbed acetonedicarboxylic acid was further decomposed to acetoacetate at pH 4, but not at pH 6. This study shows that the photooxidation of adsorbed citrate leads to the same products as the photodecomposition of dissolved ferric-citrate complexes. Moreover, it highlights the potential of ATR-FTIR spectroscopy for investigating photoreactions at iron oxide surfaces at the molecular level.

1. Introduction

Photoreductive dissolution of oxide mineral phases by organic ligands and photooxidation of the involved organic ligands are typically studied by batch photoirradiation experiments. A drawback of such experiments is that the numerous underlying processes occurring at the oxide mineral surface cannot be directly investigated. Only a surface sensitive technique such as attenuated total reflection infrared spectroscopy (ATR-FTIR) is capable of providing information on the individual processes at the mineral-water interface. The investigation of photochemical processes at mineral-water interfaces by ATR-FTIR is a relatively new research field. Although ATR-FTIR spectroscopy has been widely used to study adsorption of organic ligands on mineral interfaces, there have been only few studies reporting photochemical processes at such interfaces. The major focus of these recent studies was the investigation of photocatalytic processes at TiO_2 surfaces [1-11]. So far, only two studies have demonstrated the applicability of studying photochemical processes at iron (hydr)oxide surfaces by ATR-FTIR [8, 10]. Compared to TiO_2 , iron(III) (hydr)oxides are perceived as poor photocatalysts for industrial applications, but as ubiquitous natural mineral phases iron(III) (hydr)oxides are known to play a central role in many natural biogeochemical processes. Of particular interest is the photochemical reduction of iron (hydr)oxides in aquatic environments by low molecular weight organic acids. The potential of such organic acids to induce photodissolution of iron oxides and thus to increase the bioavailability of iron in aquatic environments has been reported in many studies [12-19]. The photodecomposition of carboxylic acids at iron (hydr)oxide surfaces and the concomitant photodissolution of the iron (hydr)oxides may proceed by two different mechanisms [20, 21]: (1) As a result of the semiconducting properties of iron (hydr)oxides [22, 23], photoelectrons and photoholes may be generated with the photoholes oxidizing adsorbed organic acids and the photoelectrons reducing surface Fe(III) lattice sites. However, this mechanism may be strongly hampered by the efficient recombination of photo-holes and photo-electrons within the iron oxide bulk [23-26] (in

contrast to TiO_2 phases). (2) The photooxidation of carboxylic acids may also proceed by a light-induced ligand-to-metal charge transfer reaction within the Fe(III)-carboxylic acid surface complexes. On the basis of the available information, it is not possible to unambiguously decide which mechanism dominates the photodecomposition of carboxylic acids at iron oxide surfaces. However, we may assume that photoreductive dissolution of iron (hydr)oxides in the presence of organic acids, for which the photoreactivity of aqueous Fe(III)-complexes have been reported (e.g., oxalic acid, citric acid) [13, 27-29], is likely to proceed by a similar ligand-to-metal charge-transfer reaction at the surface.

In this work, we report the decomposition of citric acid at the surface of γ -FeOOH (lepidocrocite). Citrate is a model compound for polycarboxylic acids that are ubiquitous in atmospheric and surface waters and that rapidly undergo photoredox reactions in the presence of Fe(III) [28]. Citric acid was chosen because the solution photochemistry of Fe(III)-citrate complexes is well known [27, 28] and because it represents the class of α -hydroxycarboxylic acid compounds that are known to induce photodissolution of iron oxides in natural environments even at high pH (e.g., seawater) [13, 19]. In this study, batch photodissolution experiments with lepidocrocite and radio-labeled citrate as well as ATR-FTIR spectroscopy were applied to investigate the photooxidation of citrate at the lepidocrocite surface. An important goal of this work was to show the potential of ATR-FTIR spectroscopy for unraveling the numerous processes that may take place during the photooxidation of organic molecules at iron oxide surfaces. To resolve the initial photooxidation reaction at the surface from other possible parallel and subsequent dark reactions (e.g., desorption of adsorbed photoproducts, ligand-exchange at the surface, etc.), a high photon flux at the mineral-water interface was applied.

2. Experimental section

2.1 Synthesis of lepidocrocite

Lepidocrocite was synthesized by the oxidation of FeCl_2 with NaNO_2 in the presence of hexamethyltetraamine (urotropin) at 60°C for 3 h [30]. To remove excess chloride and oxidation byproducts, the precipitate was washed several times by centrifugation and resuspension in high purity water (Milli-Q, Millipore). The washed precipitate was then freeze-dried and stored at -20°C . X-ray powder diffraction confirmed that the solid powder was pure lepidocrocite and transmission electron microscope images showed aggregates of needle-shaped crystals of 100-200 nm length and 10-20 nm

width. Lepidocrocite synthesized in the presence of urotropin typically results in the formation of such aggregates (see Fig. 4.14c in Cornell and Schwertmann [31]). The specific surface area of 130 m²/g (determined by the Brunauer-Emmet-Teller (BET) method) as well as the point of zero charge (PZC) of 7.4 (determined by the pH titration of lepidocrocite suspensions in various ionic strength media) are close to reported values [32].

2.2 Batch dissolution experiments

Unlabeled and ¹⁴C-labeled citric acid (1,5-¹⁴C-citric acid, specific activity 112 mCi/mmol), 1,3-acetonedicarboxylic acid (3-oxoglutaric acid), and lithium-acetoacetate were obtained from Sigma Aldrich and were used as purchased.

(Photo)dissolution experiments were carried out in a Pyrex glass vessel with a water jacket at 25 ± 1°C. To a solution of 100 μM citric acid spiked with ¹⁴C-labeled citric acid (ratio of labeled / unlabeled citric acid ~ 1/5000), a stock solution of lepidocrocite was added. The resulting solid concentration was 125 mg/L and the ionic strength was 0.01 M (NaClO₄). Dissolution experiments were conducted at pH 4 and pH 6, the pH of the suspensions was maintained by addition of small volumes of HClO₄ and NaOH with a Dosimat (Metrohm). The suspensions were constantly purged with N₂ to ensure oxygen free conditions and were vigorously stirred with a Teflon-coated stirrer. The experiments were conducted in the absence of oxygen to prevent oxidation of Fe(II) and to prevent redox cycling of iron that could considerably complicate the interpretation of the results. After 30 min, the suspensions were either irradiated or left in the dark. The light source was a 1000-W high-pressure xenon lamp (OSRAM) with a spectrum similar to that of sunlight. The bottom window of the pyrex vessel served as a high-pass filter where only light with wavelengths greater than 305 nm passed through. The solution volume was 350 mL and the irradiated area 50 cm². A light intensity of 1250 W/m² inside the vessel was determined by ferrioxalate actinometry. Samples (8 mL) were periodically withdrawn from the reaction vessel and were immediately filtered through 0.025 μm pore size membrane filters (Whatman Schleicher and Schuell). Filtered samples for total iron analysis (ICP-AES, Varian Vista MPX) were acidified with supra-pure nitric acid, and samples for the determination of labeled ¹⁴C-citric acid were acidified with HCl to approximately pH 2.5 and were degassed with N₂ for 5 min. Acidifying and degassing filtered samples prior to determination of ¹⁴C-labeled carbon served to remove ¹⁴C-labeled CO₂ from the filtered solutions. Solution concentrations of ¹⁴C were determined by measuring the β-counts with a scintillation counter (Liquid Scintillation Analyzer 2200CA, Packard).

2.3 Preparation of lepidocrocite thin film layers for ATR-FTIR experiments

The circular diamond ATR crystal surface (12.6 mm²) was coated with approximately 30 µg of lepidocrocite by spreading 2 µl of a sonicated 15 mg/mL lepidocrocite suspension on the ATR crystal surface and gently drying the thin film under a stream of N₂. The thin film was rinsed with high purity water and was dried again. A maximum of 10% of the lepidocrocite film was detached from the ATR surface by this rinsing procedure. Assuming an average layer density of 1000-2000 kg/m³, the height of the more or less homogeneous layer was in the range of 1-2.5 µm. The layer is of similar thickness as the penetration depth of the probing evanescent wave in the ATR-FTIR experiments. Estimations for effective penetration depths for TiO₂/water films have been reported recently [33]. Thin oxide films of the aforementioned thickness facilitate the rapid exchange of adsorbates between solution and oxide surface and thus are ideal for probing the adsorption of adsorbates to the oxide surfaces.

2.4 ATR-FTIR adsorption and photoirradiation experiments

Spectra were recorded on a Bio-Rad FTS 575C instrument equipped with a mercury cadmium telluride (MCT) detector and a horizontal nine reflection diamond ATR unit with KRS-5 optics (SensIR Technologies, Danbury, CT). Scans were taken from 400 to 4000 cm⁻¹ at 2 cm⁻¹ resolution. Data analysis was performed with Matlab (The MathWorks, Inc.).

A 50 mL liquid cell was tightly screwed down to the ATR unit with a silicon O-ring seal between the liquid cell and the ATR unit. The liquid cell was covered with a UV transparent polymethylmethacrylate (PMMA) window (Plexiglas GS 2458, Degussa) to allow UV irradiation from above. Light from a 103 W high-pressure mercury lamp (HBO 103W/2, OSRAM) was passed through a glass filter (cutoff wavelength 300 nm) and was focused by a quartz lens onto the ATR crystal/oxide layer/water interface inside the liquid cell. The filtered light spectrum of a high-pressure HBO lamp consisted of non-overlapping spectral bands at 312, 334, 365 (strong), 404, 435, 546, and 578 nm. The light intensity of the focused beam (covering the surface area of the ATR crystal) was measured by ferrioxalate actinometry. 300 µL of a vigorously stirred 0.2 M ferrioxalate solution was irradiated with the focused light beam in time steps of 1 s for a total of 7 s. As only light below 500 nm was (totally) absorbed by the 0.2 M ferrioxalate solution with a path length of ~6 mm, the calculated light intensity of 5-10 W/cm² refers only to the wavelength range 300-500 nm. This wavelength range is ideal to study photochemical processes of iron(III) complexes with carboxylic or α-hydroxycarboxylic acids. Iron complexes with these ligands generally do not absorb

light above 500 nm and ligand-to-metal charge-transfer transitions are also not expected above 500 nm.

For the ATR-FTIR photoirradiation experiments, an oxide layer was formed on the ATR crystal and ~50 mL of high-purity water adjusted to an ionic strength of 0.01 M with NaCl was added to the liquid cell. NaCl was used as an ionic strength adjuster, because chloride anions (adsorbed or in solution) have no characteristic IR vibration bands in the wavenumber range studied that could mask or overlap characteristic IR bands of adsorbed citrate (in contrast to oxo-anions like ClO_4^-). The presence of NaCl had no measurable effect on the results of the photoirradiation experiments with adsorbed citrate. The solutions in the liquid cell were purged with high-purity N_2 gas to exclude the formation of carbonates by sorption of CO_2 from air and to stir the solution. After purging the solution above the oxide layer with N_2 for 45 min, a background spectrum of the water-solid interface was measured (51 co-added scans). Then a small volume of an organic acid stock solution (citrate, acetonedicarboxylic acid) was added to reach a concentration of 200 μM , and the pH was adjusted with HCl or NaOH to the desired value. Absorbance spectra measured against the background spectrum were recorded, and it was found that after 30-40 min adsorption of the investigated organic acids to lepidocrocite reached a stable maximum. Subsequently, the mineral-water interface was irradiated and absorbance spectra were recorded in time-steps of 1 min (51 co-added scans per spectrum). The relatively high-intensity irradiation setup (no IR-Filter was used) lead to a temperature increase in the liquid cell of not more than 7 $^\circ\text{C}$ (from initially 25 $^\circ\text{C}$) within the irradiation time of 22 min. A consequence of the heat generation was a negative baseline drift that leveled off during prolonged irradiation and a development of a vibration band that was associated with the bending mode of water at $\sim 1638\text{ cm}^{-1}$. It was therefore necessary to conduct reference irradiation experiments in the absence of organic acids. The reference spectra, in the following called “heat-spectra” were subtracted from the absorbance spectra recorded in the presence of organic acids. Generally the subtraction method worked very well, so that the baseline drift could be corrected without the need of applying a scaling factor.

3. Results and discussion

3.1 Batch photoirradiation experiments with ^{14}C -labeled citrate

Dark and irradiated experiments were conducted with suspensions of 125 mg/L lepidocrocite and 100 μM ^{14}C -labeled citric acid at pH 4 and pH 6. Only the two terminal carboxylic acid groups of citrate were ^{14}C -labeled, not the carboxyl moiety of the α -hydroxycarboxylic acid functional group. In Fig. 1a,b, the results of the dark and irradiated batch dissolution experiments are shown.

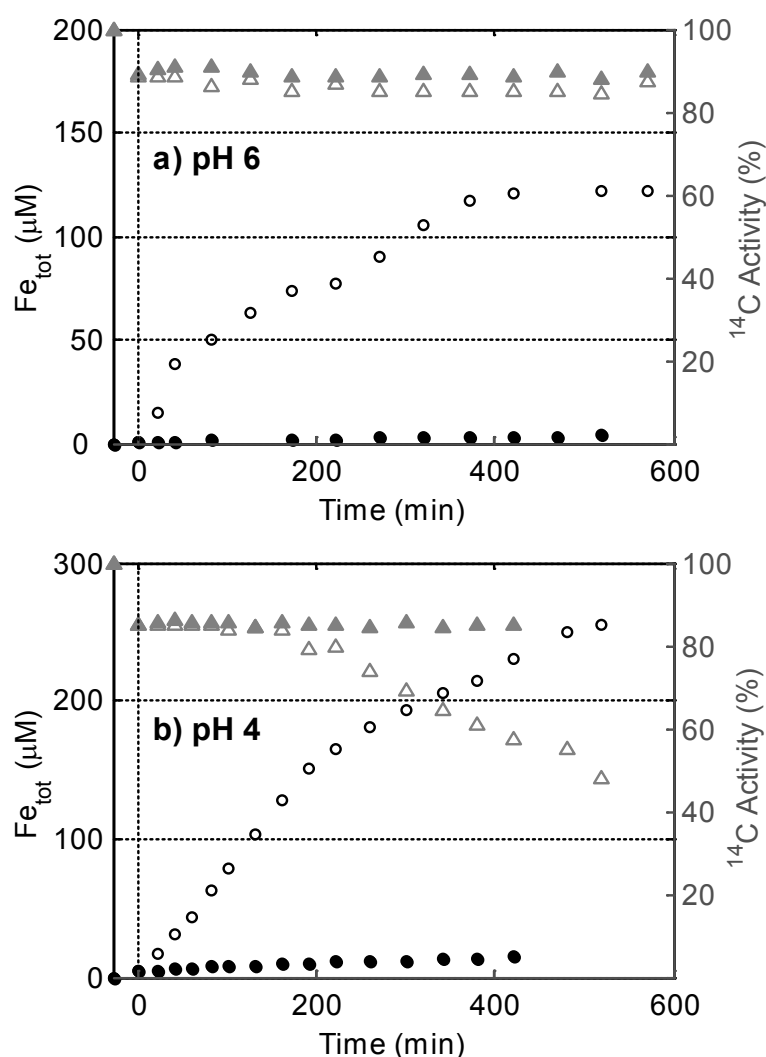


Fig. 1: (Photo)dissolution experiments in 0.125 g/L lepidocrocite suspensions in the presence of 100 μM citric acid under oxygen-free conditions at pH 6 (a) and pH 4 (b). Total iron (circles) was measured by ICP-AES and ^{14}C activities (triangles) were measured by liquid scintillation of filtered samples. Suspensions were kept in the dark (filled symbols) or were irradiated (empty symbols). Adsorption of citrate to the oxide surface was observed in the 30 min previous to irradiation starting at 0 min. Experimental conditions: ionic strength $I = 0.01 \text{ M}$ (NaClO_4), $T = 25 \text{ }^\circ\text{C}$, irradiance = 1250 W/m^2 (simulated sunlight).

For the dark experiments, where citrate was not photooxidized, total dissolved citrate was determined by measuring the ^{14}C activity in the filtered samples normalized to the initial activity before lepidocrocite was added (at -30 min). 30 min after the addition of lepidocrocite, the dissolved citrate concentration (filled triangles) decreased to $\sim 89\%$ and 85% at pH 6 and pH 4, respectively. This decrease is consistent with adsorption of citrate to the surface of lepidocrocite. During the dark experiments, adsorption of citrate was complete after 30 min and no further significant change in the ^{14}C signal was observed thereafter.

The adsorption of citrate to the surface and the formation of surface Fe(III)-citrate complexes is the prerequisite for ligand promoted dissolution of lepidocrocite in the dark and for photoreductive dissolution under irradiation. Thermal dissolution of lepidocrocite (dark experiments) at pH 6 and pH 4 resulted in the solubilization of 3.3 and 14.5 μM Fe(III), respectively, within 420 min (Fig. 1a,b, filled circles). In the irradiated (oxygen-free) suspensions, the dissolution rate was greatly enhanced. This enhancement is interpreted in terms of photolysis of surface Fe(III)-citrate complexes and the concomitant release of ferrous iron into the solution. The difference between total dissolved iron in the irradiated (oxygen-free) and in the dark experiments is a measure of the photoreductive dissolution of lepidocrocite. By comparing the dissolution rates, we may assume that the contribution of thermal dissolution to the overall dissolution in irradiated suspensions is negligible. Thus, under irradiation the formation of aqueous Fe(III)-citrate complexes with subsequent ligand-to-metal charge-transfer within the solution complex should not contribute significantly to the overall photooxidation of citrate. At pH 6, the light-enhanced dissolution rate decreased over time and a steady-state concentration of 120 μM total dissolved iron was determined after 400 min in the deaerated suspension. The major finding of the experiments at pH 6 (Fig. 1a) is that the light-enhanced dissolution of lepidocrocite, presumably initiated by a ligand-to-metal charge-transfer reaction within the surface Fe(III)-citrate complex was not accompanied by a decrease in the ^{14}C -signal. Thus, it was the unlabeled α -hydroxycarboxylic group of citrate that was photooxidized at the surface of lepidocrocite. The formation of 120 μM Fe(II) (more than the initial citrate concentration of 100 μM) supports a photoredox reaction in which more than one electron is transferred. It has been shown that the photolysis of solution Fe(III)-ferric complexes leads to the formation of acetonedicarboxylic acid [27, 34, 35] (see Fig. 2). This photoproduct has also been observed in irradiated suspensions containing amorphous iron (hydr)oxides and citrate [36]. Hydroxyl groups in α -position to carboxylic acid groups are known to enhance decarboxylation reactions, because the OH group can be transformed into an aldehyde or ketone group by two consecutive electron-transfer reactions [27] (see Fig. 2). Thus,

a maximum of 200 μM Fe(II) could be formed by the photooxidation of initially 100 μM citrate to acetonedicarboxylic acid. The observation that less than 200 μM Fe(II) (or total iron) was formed at pH 6 is an indication for incomplete release of Fe(II) into the solution or readsorption of aqueous Fe(II). This will be discussed later in detail. Bearing in mind that the ^{14}C activity in the irradiated experiments is a measure of both total dissolved citrate and acetonedicarboxylic acid, the close match of total dissolved ^{14}C activities in the dark and the irradiated experiment at pH 6 indicates a similar adsorption behavior for citrate and acetonedicarboxylic acid. In this case, potential ligand-exchange reactions at the surface between photoproduct acetonedicarboxylic acid and excess citrate would not alter the total amount of adsorbed ligands (and thus not alter the ^{14}C activity in solution).

3.2 Decomposition of the photoproduct

As all β -keto-carboxylic acids, acetonedicarboxylic acid is unstable and is known to decompose in solution to acetoacetic acid and ultimately to acetone by non-oxidative decarboxylation [37] (see Fig. 2).

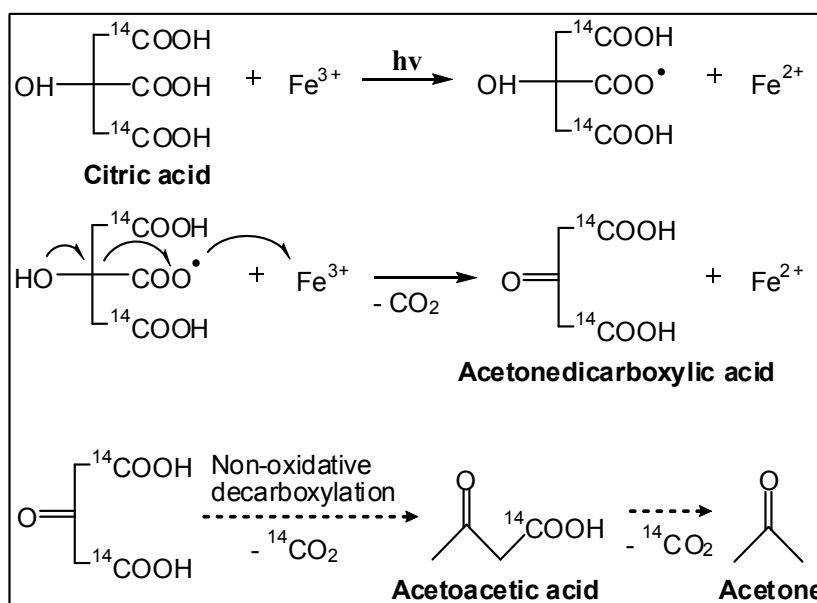


Fig. 2: Photooxidation reaction of Fe(III)-citrate complexes leading to the formation of acetonedicarboxylic acid. As all β -keto-carboxylic acids, acetonedicarboxylic acid is subject to further non-oxidative decarboxylation reactions. The formation of acetoacetic acid and acetone as possible decomposition products of acetonedicarboxylic acid are also shown.

Decarboxylation of acetonedicarboxylic acid would lead to a decrease of the ^{14}C activity in the batch photodissolution experiments, as CO_2 was degassed prior to

activity measurements (see Experimental Section). At pH 6, we observed no decrease of the ^{14}C activity under irradiation (Fig. 1a, empty triangles). At pH 4, however, the situation was different. In the first phase of the irradiated experiment, spanning the first 200 min, the ^{14}C activity in the solution (Fig. 1b, empty triangles) was stable at the same level as the ^{14}C -activity obtained in the dark experiment (fast initial decrease due to adsorption). After 200 min of irradiation, a linear decrease in the ^{14}C activity was observed, indicating slow decomposition of acetonedicarboxylic acid. As reported by Hay et al. [37], the uncatalysed decarboxylation of acetonedicarboxylic acid is at its maximum at pH 3.5 and decreases at lower and higher pH values. In addition, Hay et al. [37] have shown that the decomposition of acetonedicarboxylic acid is catalyzed by divalent metal cations. The presence of higher solution concentrations of Fe(II) at pH 4 may additionally explain why a decrease of the ^{14}C activity was only observed at pH 4. The dissolution curve also gives valuable information about the various decomposition reactions. There is an inflection point in the dissolution curve at approximately 200 min shortly after the onset of acetonedicarboxylic acid decomposition. Moreover, during the course of the irradiated experiment a total of 250 μM Fe was dissolved. This is more than what would be expected by the complete conversion of citrate to acetonedicarboxylic acid by two consecutive electron-transfer reactions (see Fig. 2). The fact that more than 200 μM iron was dissolved indicates that acetonedicarboxylic acid (in addition to decomposition by uncatalysed and metal-catalyzed nonoxidative decarboxylation in solution) must be involved in the photoreductive dissolution of lepidocrocite at longer irradiation times. As a dicarboxylic acid, acetonedicarboxylic acid might contribute to thermal dissolution of lepidocrocite at pH 4, although at a lower rate than citrate. It is also conceivable that acetonedicarboxylic acid is photooxidized at the surface by ligand-to-metal charge transfer or by trapping photoholes formed within the iron oxide bulk. These additional reactions are expected to occur in the late stages of the photodissolution experiments, where acetonedicarboxylic acid accumulates and is less affected by ligand-exchange reactions at the surface of lepidocrocite in the presence of (excess) citrate.

3.3 Readsorption of Fe(II)

In the batch photodissolution experiments, the incomplete release of Fe(II) from the surface of lepidocrocite or the readsorption of Fe(II) to the surface, directly to a surface site or as a ternary surface complex involving citrate or the photoproduct, has to be considered for the interpretation of the dissolution rates. From an experimental perspective, readsorption of Fe(II) cannot be distinguished from an incomplete release

of Fe(II) into the solution. The affinity of oxide surfaces for Fe(II), however, can be assessed by Fe(II) adsorption studies. Recent publications have reported pH edges for the adsorption of Fe(II) to lepidocrocite in the pH range of 5-7 [38, 39]. Thus, at pH 6 (and not at pH 4), photoproduct Fe(II) is likely to readsorb at the surface resulting in smaller solution concentrations. Readsorption of Fe(II) may serve as an explanation for the nonlinear dissolution at pH 6 (Fig. 1a) for which a decrease of the dissolution rate was observed even in the early stages of the photodissolution experiment. Fe(II) complexes of citrate and acetonedicarboxylic acid may also readsorb to the surface, but we expect this interaction to be of minor importance. A simple speciation calculation with a 2-pK constant capacitance model (2-pK CCM) supports this view. The readsorption of Fe(II) to lepidocrocite was calculated with the adsorption reactions and surface stability constants listed in Table 1. The surface site density of lepidocrocite and the capacitance of the double layer were estimated and the computer program Visual Minteq [40] was used for the thermodynamic calculations. One of the unknown parameters in this calculation is the total Fe(II) concentration. As indicated in Fig. 1a, there was no net photodissolution observed at pH 6 after 400 min. Therefore, we may assume that citrate has been fully photooxidized within the first 400 min and that a maximum solution concentration of 200 μM Fe(II) could have been formed. In accordance with the constant capacitance adsorption model, a significant fraction, 72 μM Fe(II) of the 200 μM Fe(II), adsorbs to the surface. The resulting value of 128 μM Fe(II) in solution is in close agreement with the observed concentration of 120 μM Fe(II) (Fig. 1a). Of course, such calculations are very sensitive toward the estimated surface site density of the lepidocrocite phase. From proton and fluoride exchange experiments, Bondietti [32] determined a surface site density of 600-890 $\mu\text{mol/g}$ of lepidocrocite. The lepidocrocite phase used in this study was synthesized by the same urotropin method, and measured BET and PZC values are in very close agreement to those values determined by Bondietti [32]. Therefore, a surface site density of 5 sites/ nm^2 is very reasonable. The effect of citrate on the readsorption of Fe(II) has been neglected in these calculations, because citrate was constantly photooxidized during the photodissolution experiments and the ratio of citrate/Fe(II) strongly decreased on prolonged photolysis. Assuming that the photoproduct of citrate, acetonedicarboxylic acid, forms only weak Fe(II)-complexes, the Fe(II) speciation in solution is dominated by free Fe(II) in the late stages of the photodissolution experiments. Therefore, the loss of Fe(II) to the surface by readsorbing Fe(II)-ligand complexes may be fully neglected. Contrary to this view, Waite and Morel [19] have concluded that readsorption of Fe(II) to lepidocrocite in the presence of citrate at pH 6.5 proceeded in a ligand-like manner, as the Fe(II)-citrate complex. The apparent contradiction can be reconciled when the ratio of citrate/Fe(II)

in their study is considered, which was at least 2 orders of magnitude higher than in this study. Thus in their study, the Fe(II) speciation in solution was dominated by Fe(II)-citrate complexes and loss of Fe(II) from the solution was likely to proceed by the adsorption of Fe(II)-citrate complexes to the lepidocrocite surface.

The surface reactions described in the batch photoirradiation experiments are so far hypothetical, derived from measurements of dissolved species and formulated in analogy to known solution reactions (e.g., photolysis of dissolved Fe(III)-citrate complexes). Surface specific spectroscopic techniques are needed to observe and investigate surface reactions in situ and in real time. In the following sections, we will show that ATR-FTIR is a sensitive and suitable method to follow surface reactions of citrate and its photoproduct on the surface of lepidocrocite in contact with aqueous solutions, and that this technique is able to provide insight that cannot be gained by batch experiments alone.

Table 1: Fe(II) adsorption to lepidocrocite (2-pK constant capacitance model)

Reactions	Log ₁₀ K
$\equiv\text{FeOH} + \text{H}^+ \leftrightarrow \equiv\text{FeOH}_2^+$	6.46 ^a
$\equiv\text{FeOH} \leftrightarrow \equiv\text{FeO}^- + \text{H}^+$	-8.07 ^a
$\equiv\text{FeOH} + \text{Fe}^{2+} \leftrightarrow \equiv\text{FeOFe(II)}^+ + \text{H}^+$	-2.13 ^b
$\equiv\text{FeOH} + \text{Fe}^{2+} + \text{H}_2\text{O} \leftrightarrow \equiv\text{FeOFe(II)OH} + 2\text{H}^+$	-8.53 ^b
Conditions	
- pH 6, ionic strength: 0.01 M	
- surface site density: 5 sites/nm ²	
- total surface sites: 135 μM (125 mg/L, 130 m ² /g)	
- total Fe ²⁺ : 200 μM	
- specific capacitance: 2 F/m ²	

^a From Bondietti [32]. Values determined at 0.4 M ionic strength.

^b From Zhang et al. [39]. Values determined at 0.6 M ionic strength.

3.4 ATR-FTIR photoirradiation experiments

The spectroscopic analysis of photoredox reactions at mineral surfaces can be complicated by various side reactions such as desorption of photoproducts, competitive adsorption of unaltered ligands and photoproducts by ligand-exchange at the surface, and further (photochemical) decomposition of photoproducts. This is especially the case if the time scale of the photolysis reaction and the subsequent processes are similar. By applying a high light flux, photolysis rates may be achieved that are fast compared to the timescales of the consecutive processes. To resolve the initial photooxidation

reaction from the subsequent reactions, the light flux was maximized and the scan time for recording FTIR spectra was minimized. A light flux of 5-10 W/cm² (300-500 nm) and a scan time of 1 min per measured spectra (51 co-added scans per spectra) were used to study the photooxidation of citrate at the surface of lepidocrocite. Under the chosen conditions, only 2 and 4 nmol citrate was adsorbed at the lepidocrocite layer at pH 6 and pH 4, respectively. With the comparatively high light flux of 45-90 $\mu\text{mol photons/min}$ at the lepidocrocite layer, the photooxidation of adsorbed citrate should be observed within minutes. Moreover, the high light flux can compensate for radiation losses by the strong light-absorbing lepidocrocite layer.

During these ATR-FTIR photoirradiation experiments, the concentration of dissolved citrate was expected to decrease only slightly, because of the high ratio of citrate/Fe (200 μM citrate in a total volume of 50 mL in contact with a 30 μg lepidocrocite layer). Thus, the amount of adsorbed citrate was not affected by the slight decrease of dissolved citrate (in contrast to the batch photodissolution experiments, where the ratio of citrate/Fe was much smaller). The pH of the solution was measured before and directly after irradiation and no pH shifts were observed.

3.5 ATR-FTIR spectra of adsorbed citrate and acetonedicarboxylic acid

Prerequisite for ATR-FTIR photoirradiation studies as described above is that the spectra of the reactants and the photoproducts are distinguishable. FTIR spectra of citrate and acetonedicarboxylic acid adsorbed to the lepidocrocite layer at pH 4 and pH 6 were recorded and were used as reference spectra for the photoirradiation experiments. As shown in Fig. 3 for pH 4, these ligands have distinct spectral features in the range of 1200-1470 cm^{-1} , such that the photooxidation of citrate to acetonedicarboxylic acid at the surface of lepidocrocite can directly be followed in the IR spectra.

At pH 6 and even also at pH 4, both citric acid and acetonedicarboxylic acid are adsorbed as the (fully) deprotonated species. This is indicated by a very small contribution of the generally strong C=O stretching vibration of protonated carboxylic groups located above 1700 cm^{-1} . Adsorbed citrate has a broad asymmetric and symmetric carboxyl stretching vibration at 1570 and 1393 cm^{-1} , respectively. In acetonedicarboxylate, the asymmetric carboxyl stretching vibration is also located at 1570 cm^{-1} . However, the assignment of the symmetric carboxyl stretching vibration(s) is ambiguous. The difficulty of interpreting the FTIR spectra of adsorbed acetonedicarboxylic acid arises because it is affected by a keto/enol tautomerism. In aqueous solution, the keto form dominates [37], whereas at the surface of lepidocrocite the enol form of the inner-spherically adsorbed acetonedicarboxylate may be favored, if a stronger binding environment for an Fe(III)

center is provided by the enol functional group. Unlike citrate, where the locations of the symmetric and asymmetric carboxyl stretching vibrations (peak maxima) were only slightly shifted upon adsorption to the surface (spectra of dissolved citrate not shown), a dramatic change occurred in the spectrum of acetonedicarboxylic acid after adsorption. In solution, the fully deprotonated acetonedicarboxylate exhibits a large peak located at 1377 cm^{-1} and a far smaller peak at 1417 cm^{-1} (data not shown). The 1377 cm^{-1} peak can be unambiguously assigned as the symmetric carboxylate stretching vibration and the peak at 1417 cm^{-1} as a typical C-H deformation vibration seen in many aliphatic carboxylic acids. After adsorption of acetonedicarboxylic acid to lepidocrocite, the spectra changes dramatically, with two intense peaks evolving at 1437 and 1379 cm^{-1} . Most likely, this spectral change is the result of the formation of enol-like inner-sphere acetonedicarboxylate complexes. Probably both bands at 1437 and 1379 cm^{-1} belong to different symmetric carboxyl stretching vibrations, but without further *ab initio* calculations this spectral interpretation remains speculative.

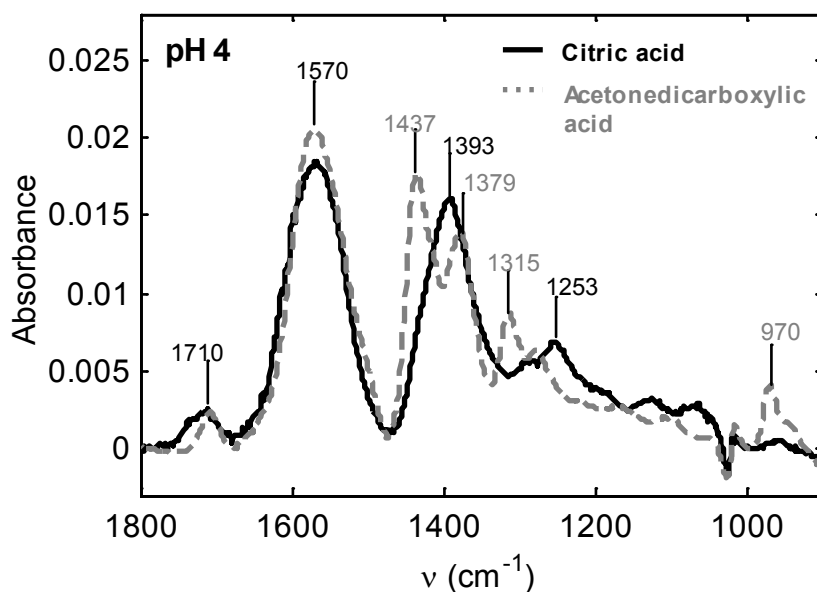


Fig. 3: Spectra of citric acid and acetonedicarboxylic acid adsorbed to lepidocrocite at pH 4. Conditions: [citric acid] = $200\ \mu\text{M}$, [acetonedicarboxylic acid] = $200\ \mu\text{M}$, $I = 0.01\ \text{M}$, $T = 25\ ^\circ\text{C}$.

3.6 Heat generation during ATR-FTIR photoirradiation experiments

In the ATR-FTIR photoirradiation experiments, the recorded spectra were corrected for spectral changes occurring due to heat generation at the mineral-water interface. The exact temperature at the interface could not be measured; however, the temperature of the water column in contact with the oxide layer ($50\ \text{mL}$) increased by not more than $7\ ^\circ\text{C}$ during the experiments. The limited warming resulted in a reproducible decrease

of the baseline over a large spectral region and to an increasing band at 1638 cm^{-1} , where the center of the O-H bending mode of liquid water is located. Fig. 4 shows the spectral changes observed during the irradiation of the lepidocrocite-water interface in the absence of organic ligands at pH 5. The negative band evolving at 1022 cm^{-1} indicates that part of the lepidocrocite layer (less than 10%) detached from the diamond ATR crystal. The overall negative baseline drift and the increase of the water bending mode at 1630 cm^{-1} were also observed when the ATR crystal-water interface (without lepidocrocite) was irradiated. Thus, these spectral changes are completely attributed to the heating of the water solution in contact with the ATR crystal. To compensate for this heat artifact, such series of “heat spectra” were subtracted from the absorbance spectra recorded in the photoirradiation experiments with the organic ligands (see also experimental section).

The effect of the temperature rise during photoirradiation on the adsorption of additional citrate has been neglected in this study. In preceding photoirradiation experiments with apparently non-photoreactive organic acids, we have observed an overall increase of IR band intensities of only 5% to maximum 25%. The gradual increase in the adsorption capacity for citrate can be neglected if the photooxidation of citrate and therefore the depletion of citrate at the mineral-water interface are much faster (as is the case in this photoirradiation setup).

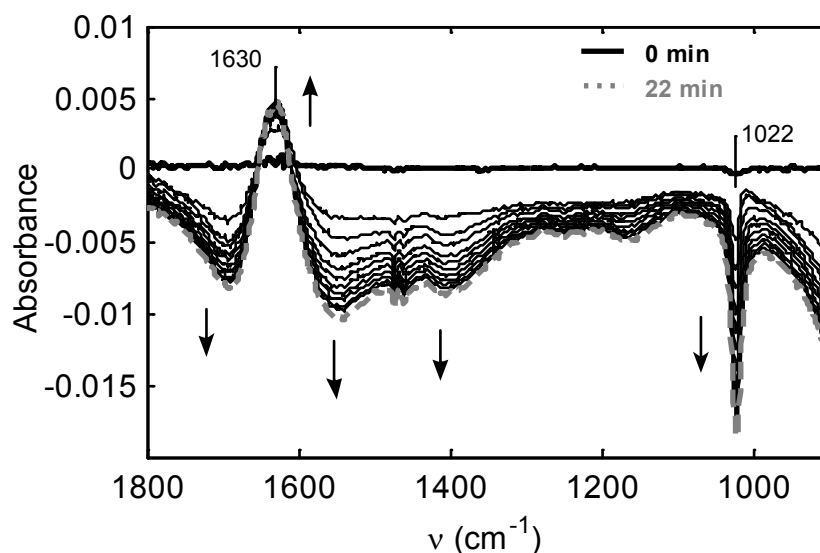


Fig. 4: Photoirradiation of the lepidocrocite-water interface without any organic ligands. Spectra were recorded in time steps of 1 min. For clarity, only every second spectrum is shown. Arrows indicate the direction of spectral changes during irradiation. The spectra recorded before and at the end of irradiation (0 and 22 min) are shown as a bold black line and a bold gray dashed line, respectively. Conditions: pH \sim 5, I = 0.01 M, 5-10 W/cm² (300-500 nm), T = 25-32 °C (solution).

3.7 ATR-FTIR photoirradiation experiment at pH 4

In Fig. 5a,b, the results of the ATR-FTIR photoirradiation experiment at pH 4 are shown. The spectral changes in the sequence of the recorded spectra are indicated by arrows and are consistent with the photooxidation of adsorbed citrate to adsorbed acetonedicarboxylic acid (Fig. 5a). Over the course of the experiment, the decline of citrate peaks at 1570, 1393, and 1253 cm^{-1} was accompanied by the development of acetonedicarboxylic acid peaks at 1437, 1379, and 1315 cm^{-1} (cf. Fig. 3). The development of a negative peak was observed at 1022 cm^{-1} in the wavenumber region of the first δ -OH in-plane vibrations of structural OH groups in lepidocrocite. The negative peak can be explained by dissolution of lepidocrocite, and/or by partial detachment of the oxide layer from the ATR crystal. In Fig. 5b, the fractions of citrate and the evolving acetonedicarboxylic acid were calculated by fitting the sequence of spectra in Fig. 5a with linear combinations of the reference spectra shown in Fig. 3. Deviations in the fitting range of 1200 and 1470 cm^{-1} were less than 0.001 absorbance units. The reference spectrum of citrate in Fig. 3 is identical to the spectrum shown in Fig. 5a before irradiation (at 0 min). Thus, the fraction of citrate can be calculated quantitatively. At the end of the irradiation period, citrate was almost totally oxidized. The reference spectrum of acetonedicarboxylic acid (Fig. 3) was recorded in a separate experiment and represents the maximum surface concentration in equilibrium with initially 200 μM acetonedicarboxylic acid at pH 4. Therefore, the calculated fractions of the evolving acetonedicarboxylic acid in the photoirradiation experiment (where no excess of acetonedicarboxylic acid was present in solution) are less well constrained. Potential parallel and consecutive reactions involved in the heterogeneous photooxidation of citrate that may affect the surface concentrations of citrate and acetonedicarboxylic acid will be presented later.

3.8 ATR-FTIR photoirradiation experiment at pH 6

As shown in Fig. 6, the photooxidation of citrate adsorbed to lepidocrocite at pH 6 occurs at a much lower rate than at pH 4 (Fig. 5a). There is only a small decrease of citrate bands and a small increase of the typical acetonedicarboxylic acid bands. Interestingly, the spectra of adsorbed citrate and acetonedicarboxylic acid are almost identical to the spectra at pH 4, yet the extent of citrate photooxidation at the surface at pH 6 is apparently much smaller. This difference may be attributed to (i) different fractions of inner/outer-sphere complexes at pH 4 and pH 6, and (ii) different inner-sphere complexes at pH 4 and pH 6 exhibiting different photoreactivity.

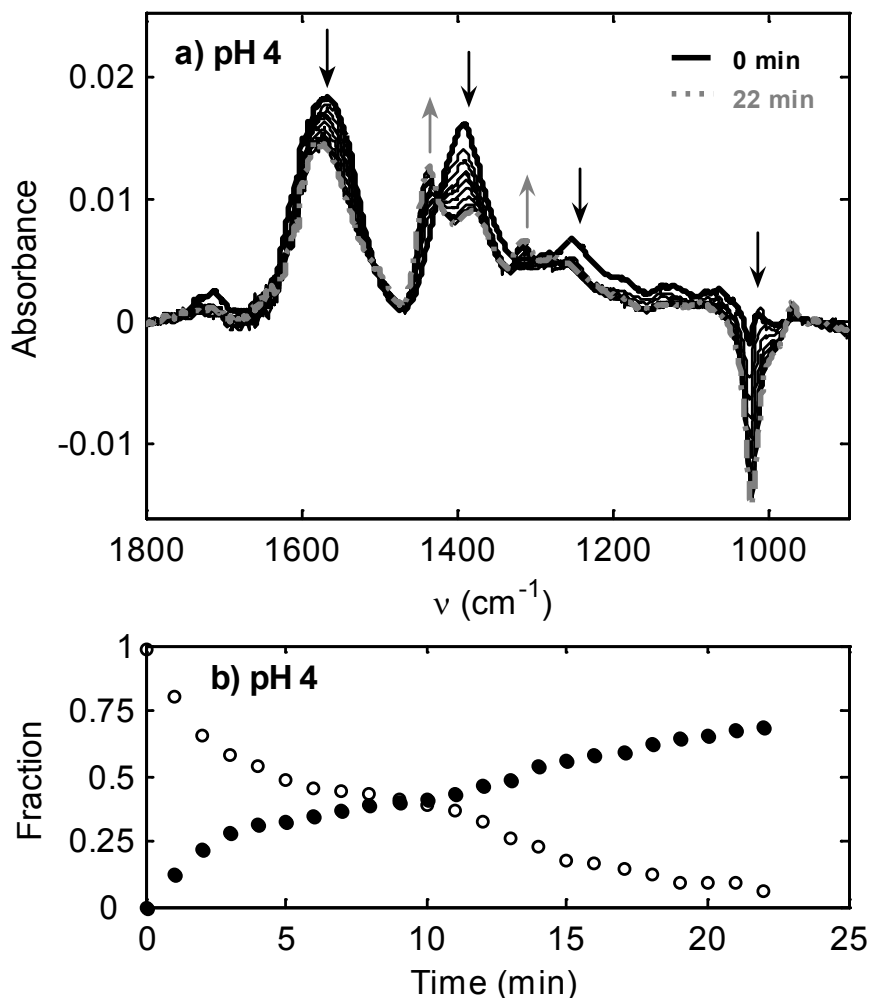


Fig. 5: (a) Photooxidation of citric acid adsorbed to lepidocrocite at pH 4 as a function of time (spectra shown as described in Fig. 4). Conditions: [citric acid] = 200 μM , $I = 0.01 \text{ M}$, 5-10 W/cm^2 (300-500 nm), $T = 25\text{-}32^\circ\text{C}$ (solution). (b) The fractions of adsorbed citric acid and acetonedicarboxylic acid (photoproduct) were calculated by fitting the spectra shown in Fig. 5a with reference spectra of adsorbed citric acid and adsorbed acetonedicarboxylic acid (see Fig. 3).

A higher outer-sphere fraction at pH 6 is expected to result in a lower overall photooxidative conversion of citrate because only inner-spherically adsorbed citrate is able to be photooxidized by ligand-to-metal charge transfer. Indeed, carboxylic acid ligands are expected to have higher fractions of outer-sphere complexes with increasing pH values as demonstrated by a recent ATR-FTIR adsorption study of oxalic acid on goethite [41]. Various inner-sphere complexes with different photoreactivity may also form. Citrate complexes in which only the outer carboxylic groups are coordinated to Fe(III) are expected to be less photoreactive than complexes in which the central α -hydroxycarboxylate group is also coordinated. In a previous study, it was shown that the quantum yield for the photoreduction of dissolved Fe(III) in the presence of citrate

was similar at pH 4 and 6 for certain Fe(III)/citrate ratios [27]. The situation at an iron oxide surface appears to be more complex and a range of different photoreactive citrate complexes may explain part of the differences at pH 4 and 6. Unfortunately, the ATR-FTIR spectra of adsorbed citrate at pH 4 and pH 6 are too similar to the spectrum of fully deprotonated citrate in solution (data not shown) so that no valuable information about different inner-sphere and outer-sphere surface complexes can be gained from the ATR-FTIR spectra alone. The only significant spectral change that occurred upon adsorption to lepidocrocite was a broadening of the asymmetric carboxyl stretching vibrations of citrate.

Interestingly, the initial photooxidation rate of citrate in the batch photodissolution experiments as indicated by the light-enhanced dissolution of lepidocrocite in the first 60 min is very similar at pH 4 and pH 6 (see Fig. 1a,b; empty circles). At first glance, this observation is not consistent with the ATR-FTIR photoirradiation experiments. The apparent contradiction can be reconciled when the ratio of citrate/lepidocrocite in the two different experimental setups is considered. In the batch photodissolution experiments, the initial ratio was 100 μM citrate / 125 mg/L lepidocrocite ($\sim 135 \mu\text{M}$ Fe(III) surface sites), whereas in the ATR-FTIR photoirradiation experiments the initial ratio was 200 μM citrate / 0.6 mg/L lepidocrocite (30 μg lepidocrocite layer in contact with a 50 mL solution, equivalent to $\sim 0.65 \mu\text{M}$ Fe(III) surface sites). Thus, the surface coverage of citrate on lepidocrocite was much lower in the batch photodissolution experiments and we may expect citrate to be adsorbed to a higher extent at reactive surface sites. As a result, the photooxidation rate of adsorbed citrate may be less dependent on the pH in the batch photodissolution experiments (in contrast to the ATR-FTIR photoirradiation experiments where a much lower fraction of total adsorbed citrate is assumed to be adsorbed at reactive surface sites).

3.9 Parallel and consecutive reactions during photoirradiation experiments

The desorption of photoproducted acetonedicarboxylic acid from the surface, ligand-exchange reactions between excess citrate and adsorbed acetonedicarboxylic acid, and decomposition of acetonedicarboxylic acid are reactions that may proceed on a similar time scale as the preceding photolysis reaction of adsorbed citrate. Mass transfer reactions or diffusion processes like adsorption or desorption of single organic acid ligands to oxide phases have been shown to occur on a time scale of minutes to tens of minutes in the same non-vigorously stirred ATR-FTIR setup as used in this study [42]. The applied light flux in the ATR-FTIR photoirradiation experiments was maximized to accelerate the initial photolysis reaction relative to these aforementioned consecutive

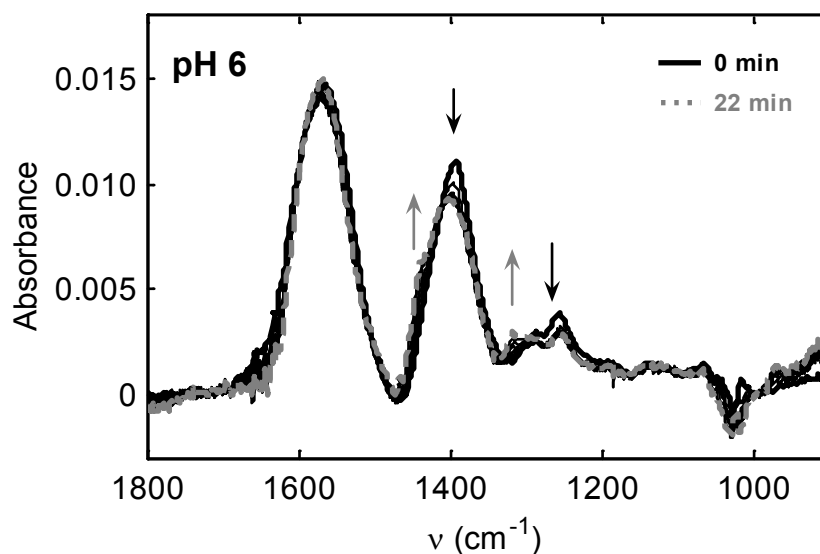


Fig.6: Photooxidation of citric acid adsorbed to lepidocrocite at pH 6 as a function of time (spectra shown as described in Fig. 4). Conditions: [citric acid] = 200 μM , I = 0.01 M, 5-10 W/ cm^2 (300-500 nm), T = 25-32 $^{\circ}\text{C}$ (solution).

reactions. After the first few minutes of illumination, the effects of the consecutive reactions are assumed to grow. Thus, on a longer time scale, the fractions of adsorbed citrate or acetonedicarboxylic acid as calculated in Fig. 5b will be strongly affected by the aforementioned reactions. In the following, the effect of ligand-exchange reactions and the decomposition of the intermediate photoproduct (acetonedicarboxylic acid) will be discussed in detail. A quantitative discussion of these consecutive reactions on the kinetics of citrate photooxidation, however, is beyond the scope of this study.

3.10 Ligand-exchange reactions

In the ATR-FTIR photoirradiation experiments, only adsorbed citrate was photooxidized, while citrate in solution was largely unaffected. The large excess of dissolved citrate may induce ligand-exchange reactions at the surface of lepidocrocite between acetonedicarboxylic acid and citrate. Additional ATR-FTIR experiments were conducted in the dark to investigate the relevance of ligand-exchange. The results are shown in Fig. 7a,b. In a first experiment, a 200 μM citrate solution was equilibrated with a lepidocrocite layer at pH 4 for half an hour, before 200 μM acetonedicarboxylic acid was added (Fig. 7a). The solution above the oxide layer was only gently mixed by constantly purging with N_2 , in the same manner as during illumination. Thus, the kinetics of potential ligand-exchange reactions may be somewhat different in vigorously stirred systems (e.g., batch dissolution experiments). As can be seen in Fig. 7a, adsorbed

citrate is virtually unaffected by the presence of acetonedicarboxylic acid even after 2 h. In Fig. 7b, a 200 μM acetonedicarboxylic acid solution was first equilibrated with the oxide layer before 200 μM citrate was added. Within 2 h, a significant spectral change was observed, consistent with the formation of surface citrate complexes and desorption of acetonedicarboxylic acid. Fig. 8 shows the fractions of adsorbed ligands calculated by fitting the spectral data in Fig. 7b with reference spectra of adsorbed citrate and acetonedicarboxylic acid (Fig. 7a,b at 0 min). Desorption of acetonedicarboxylic acid (filled circles) is initially fast and constantly decreases over the course of the experiment. Approximately 40 and 60% of adsorbed acetonedicarboxylic acid was exchanged at the surface by citrate within 20 min and 2 h, respectively.

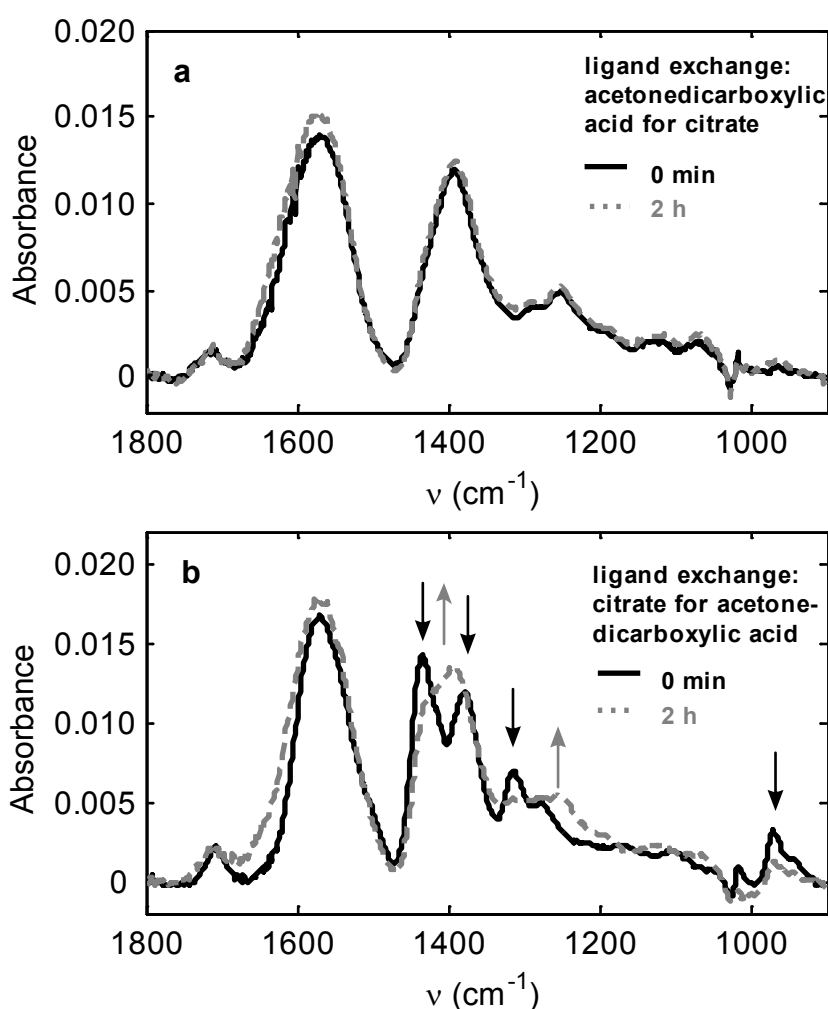


Fig. 7: Ligand-exchange reactions at the surface of lepidocrocite at pH 4. (a) Desorption of citrate in response to the addition of acetonedicarboxylic acid. (b) Desorption of acetonedicarboxylic acid in response to addition of citric acid. Citrate and acetonedicarboxylic acid were equilibrated with the oxide layer for 30 min, before the counter ligand was added. The spectra before the addition of the counter ligand and after 2h of reaction time are shown. Conditions: [citric acid] = 200 μM , [acetonedicarboxylic acid] = 200 μM , $I = 0.01 \text{ M}$, $T = 25 \text{ }^\circ\text{C}$.

The results in Fig. 7a,b lead to the conclusion that citrate forms much stronger surface complexes than acetonedicarboxylic acid at pH 4 and that citrate is able to exchange adsorbed acetonedicarboxylic acid. Very similar results were obtained at pH 6 (data not shown). The calculated fraction of 40 % of acetonedicarboxylic acid that is exchanged by excess citrate within 20 min most likely represents the upper limit of the potential ligand-exchange reaction occurring in the ATR-FTIR photoirradiation experiment at pH 4 (Fig. 5). We conclude that this is the upper limit, because the concentration of citrate at the mineral-water interface is constantly depleted during irradiation, in contrast to the ligand-exchange experiments conducted in the dark.

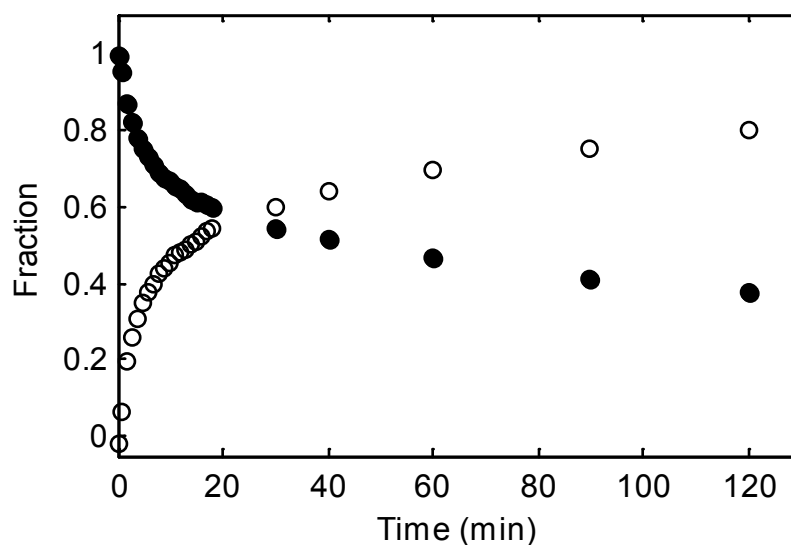


Fig. 8: The fractions of adsorbed acetonedicarboxylic acid (filled circles) and citric acid (empty circles) in the ligand-exchange reaction at pH 4 shown in Fig. 7b (desorption of acetonedicarboxylic acid in response to addition of citric acid).

3.11 Decomposition of the intermediate photoproduct(s)

In the batch photodissolution experiments, the decreasing ^{14}C activity in solution was interpreted as the decomposition of the intermediate photoproduct acetonedicarboxylic acid (Fig. 1b, empty triangles). To investigate if the proposed decomposition of acetonedicarboxylic acid also occurs at the surface of lepidocrocite under irradiation and to determine the reaction products, additional ATR-FTIR experiments were conducted. 50 mL solutions containing 200 μM acetonedicarboxylic acid in equilibrium with a layer of lepidocrocite at pH 4 and 6 were irradiated for 22 min. At pH 6, we observed no decrease of band intensities (data not shown), whereas at pH 4 (Fig. 9) a measurable change occurred. Interestingly, a small overall decrease of band intensities was accompanied by a rather pronounced decrease of the peak located at 1379 cm^{-1} .

These spectral changes are consistent with the conversion of acetonedicarboxylic acid to acetoacetic acid (see also Fig. 2).

As shown in Fig. 10, the IR spectra of adsorbed acetonedicarboxylic acid and adsorbed acetoacetic acid, both β -keto-carboxylic acids, are very similar. Unlike adsorbed acetonedicarboxylic acid, adsorbed acetoacetic acid only exhibits very weak vibrations in the region of 1379 cm^{-1} . Therefore, the only evidence for the conversion of acetonedicarboxylic acid to acetoacetic acid is provided by the observed decrease of the peak intensity at 1379 cm^{-1} .

Hay et al. [37] have shown that the decarboxylation rate of aqueous acetonedicarboxylic acid is strongly pH dependent and that divalent metal ions catalyze the decomposition reaction. The batch photodissolution experiments and the ATR-FTIR experiments (cf. Fig. 1 and 9) both show that the decomposition of acetonedicarboxylic acid at the surface of lepidocrocite is also pH dependent. Decomposition of acetonedicarboxylic acid was observed only at pH 4 under irradiation, indicating that photoexcitation is the driving force. Thermal excitation as an explanation for the decomposition reaction can be excluded because at pH 6 decomposition of acetonedicarboxylic acid was not observed, although the mineral-water interface was also heated up during the course of the photoirradiation experiment.

The decomposition of acetonedicarboxylic acid to acetoacetic acid at pH 4 was not taken into account for the calculation of the fractions of citrate and acetonedicarboxylic acid shown in Fig. 5b. Considering the very similar IR spectra of acetonedicarboxylic acid and acetoacetate, the fractions of these two (photo)products cannot be determined precisely. Furthermore, acetoacetate is a β -keto-acid and is also prone to decarboxylation (see Fig. 2). In this study, acetone as the ultimate decomposition product of citrate has not been considered because it adsorbs very weakly, if at all, to iron oxide surfaces.

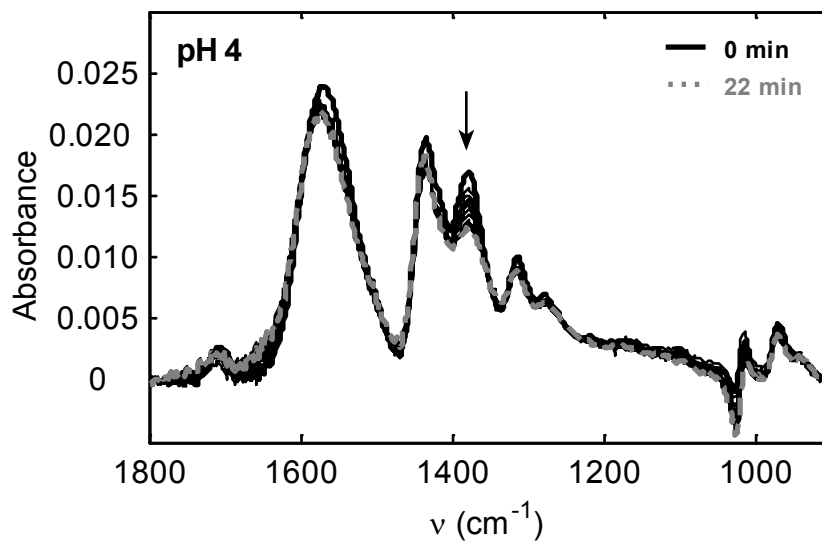


Fig. 9: Light-induced decomposition of acetonedicarboxylic acid adsorbed to lepidocrocite at pH 4 as a function of time (spectra shown as described in Fig. 4). Conditions: [acetonedicarboxylic acid] = 200 μM , I = 0.01 M, 5-10 W/cm^2 (300–500 nm), T = 25-32 $^{\circ}\text{C}$ (solution).

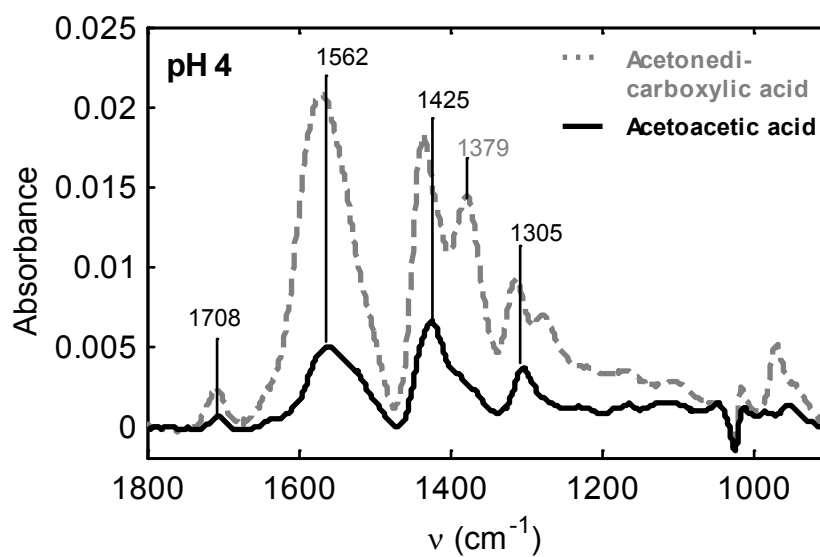


Fig. 10: Spectra of acetonedicarboxylic acid and acetoacetic acid adsorbed to lepidocrocite at pH 4. Note the different solution concentrations: [acetonedicarboxylic acid] = 200 μM , [acetoacetate] = 600 μM , I = 0.01 M, T = 25 $^{\circ}\text{C}$.

4. Conclusions

In this work, we have exemplified that ATR-FTIR spectroscopy combined with UV-visible irradiation is a powerful tool that provides direct evidence of photoredox processes occurring at the mineral-water interface of iron (hydr)oxides. From batch photodissolution experiments conducted in this work, it was concluded that citrate is photooxidized at the surface of lepidocrocite (γ -FeOOH) at pH 4 and pH 6 and that only at pH 4 the proposed photoproduct, acetonedicarboxylic acid, is further decomposed. ATR-FTIR spectroscopy provided key information that led to the identification of acetonedicarboxylic acid as the primary photoproduct and acetoacetic acid as its decomposition product at pH 4. Thus, the photooxidation of citrate at the surface of lepidocrocite follows the same photooxidation route as dissolved Fe(III)-citrate complexes.

With the aid of a high irradiation flux, it was possible to observe the photooxidation of citrate at the surface of lepidocrocite despite subsequent ligand-exchange reactions between the photoproduct acetonedicarboxylic acid and excess citrate from the solution. From additional ligand-exchange experiments, it was concluded that citrate forms much stronger surface complexes than acetonedicarboxylic acid. An upper limit of 40% of acetonedicarboxylic acid exchanged at the surface by excess citrate in the photoirradiation experiments was estimated.

ATR-FTIR spectroscopy has proven to be a valuable tool for investigating the photoreactivity of adsorbed ligands formed at different conditions. In contrast to the almost complete photooxidation of citrate at the surface of lepidocrocite at pH 4 within the measurement period (22 min), photooxidation of citrate at pH 6 was apparently much smaller. It was concluded, that either less inner-sphere surface complexes or less reactive inner-sphere complexes were formed at pH 6. This latter point emphasizes the importance of understanding the reactivity of adsorbed ligands in terms of the surface coordination.

5. References

- [1] Dolamic, I. and Buergi, T. **2006**. Photoassisted decomposition of malonic acid on TiO₂ studied by in situ attenuated total reflection infrared spectroscopy. *J. Phys. Chem. B* 110: 14898-14904.
- [2] Mendive, C. B., Bredow, T., Blesa, M. A. and Bahnemann, D. W. **2006**. ATR-FTIR measurements and quantum chemical calculations concerning the

- adsorption and photoreaction of oxalic acid on TiO₂. *Phys. Chem. Chem. Phys.* 8: 3232-3247.
- [3] Araujo, P. Z., Mendive, C. B., García Rodenas, L. A., Morando, P. J., Regazzoni, A. E., Blesa, M. A. and Bahnemann, D. W. **2005**. FT-IR-ATR as a tool to probe photocatalytic interfaces. *Colloids Surf., A* 265: 73-80.
- [4] Kiwi, J. and Nadtochenko, V. **2005**. Evidence for the mechanism of photocatalytic degradation of the bacterial wall membrane at the TiO₂ interface by ATR-FTIR and laser kinetic spectroscopy. *Langmuir* 21: 4631-4641.
- [5] Lana-Villareal, T., Rodes, A., Pérez, J. M. and Gómez, R. **2005**. A spectroscopic and electrochemical approach to the study of the interaction and photoinduced electron transfer between catechol and anatase nanoparticles in aqueous solution. *J. Am. Chem. Soc.* 127: 12601-12611.
- [6] Mendive, C. B., Bahnemann, D. W. and Blesa, M. A. **2005**. Microscopic characterization of the photocatalytic oxidation of oxalic acid adsorbed onto TiO₂ by FTIR-ATR. *Catal. Today* 101: 237-244.
- [7] Warren, D. S. and McQuillan, A. J. **2004**. Influence of adsorbed water on phonon and UV-induced IR absorptions of TiO₂ photocatalytic particle films. *J. Phys. Chem. B* 108: 19373-19379.
- [8] Borda, M. J., Strongin, D. R. and Schoonen, M. A. **2003**. A novel vertical attenuated total reflectance photochemical flow-through reaction cell for Fourier transform infrared spectroscopy. *Spectrochim. Acta, Part A* 59: 1103-1106.
- [9] Ekström, N. G. and Mcquillan, A. J. **1999**. In situ infrared spectroscopy of glyoxylic acid adsorption and photocatalysis on TiO₂ in aqueous solution. *J. Phys. Chem. B* 103: 10562-10565.
- [10] Kesselman-Truttman, J. M. and Hug, S. J. **1999**. Photodegradation of 4,4'-bis(2-sulfostyryl)biphenyl (DSBP) on metal oxides followed by in situ ATR-FTIR spectroscopy. *Environ. Sci. Technol.* 33: 3171-3176.
- [11] Awatani, T. and Mcquillan, A. J. **1998**. Adsorbed thiosulfate intermediate of cadmium sulfide aqueous photocorrosion detected and characterized by in situ infrared spectroscopy. *J. Phys. Chem. B* 102: 4110-4113.
- [12] Borer, P. M., Sulzberger, B., Reichard, P. and Kraemer, S. M. **2005**. Effect of siderophores on the light-induced dissolution of colloidal iron(III)(hydr)oxides. *Mar. Chem.* 93: 179-193.
- [13] Kuma, K., Nakabayashi, S. and Matsunaga, K. **1995**. Photoreduction of Fe(III) by hydroxycarboxylic acids in seawater. *Water Res.* 29: 1559-1569.
- [14] Sulzberger, B. and Laubscher, H. **1995**. Reactivity of various types of iron(III) (hydr)oxides towards light-induced dissolution. *Mar. Chem.* 50: 103-115.

-
- [15] Miller, D. M. and Kester, D. R. **1994**. Photochemical iron reduction and iron bioavailability in seawater. *J. Mar. Res.* 52: 325-343.
- [16] Goldberg, M. C., Cunningham, K. M. and Weiner, E. R. **1993**. Aquatic photolysis: photolytic redox reactions between goethite and adsorbed organic acid in aqueous solutions. *J. Photochem. Photobiol.* 73: 105-120.
- [17] Kuma, K., Nalabayashi, S., Suzuki, Y., Kudo, I. and Matsunaga, K. **1992**. Photo-reduction of Fe(III) by dissolved organic substances and existence of Fe(II) in seawater during spring blooms. *Mar. Chem.* 37: 15-27.
- [18] Wells, M. L. and Mayer, L. M. **1991**. The photoconversion of colloidal iron oxyhydroxides in seawater. *Deep-Sea Res.* 38: 1379-1395.
- [19] Waite, T. D. and Morel, F. M. M. **1984**. Photoreductive dissolution of colloidal iron-oxide - Effect of citrate. *J. Colloid Interface Sci.* 102: 121-137.
- [20] Waite, T. D. **1990**. Photo-redox processes at the mineral-water interface. *Rev. Mineral.* 23: 559-603.
- [21] Siffert, C. and Sulzberger, B. **1991**. Light-induced dissolution of hematite in the presence of oxalate - a case-study. *Langmuir* 7: 1627-1634.
- [22] Sherman, D. M. **2005**. Electronic structures of iron(III) and manganese(IV) (hydr)oxide minerals: Thermodynamics of photochemical reductive dissolution in aquatic environments. *Geochim. Cosmochim. Acta* 69: 3249-3255.
- [23] Leland, J. K. and Bard, A. J. **1987**. Photochemistry of colloidal semiconducting iron oxide polymorphs. *J. Phys. Chem.* 91: 5076-5083.
- [24] Lindgren, T., Wang, H., Beermann, N., Vayssieres, L., Hagfeldt, A. and Lindquist, S. **2002**. Aqueous photoelectrochemistry of hematite nanorod array. *Sol. Energ. Mater. Sol. Cells* 71: 231-243.
- [25] Cherepy, N. J., Liston, D. B., Lovejoy, J. A., Deng, H. and Zhang, J. Z. **1998**. Ultrafast studies of photoexcited electron dynamics in γ - and α -Fe₂O₃ semiconductor nanoparticles. *J. Phys. Chem. B* 102: 770-776.
- [26] Björkstén, U., Moser, J. and Grätzel, M. **1994**. Photoelectrochemical studies on nanocrystalline hematite films. *Chem. Mater.* 6: 858-863.
- [27] Abrahamson, H. B., Rezvani, A. B. and Bruscmiller, G. J. **1994**. Photochemical and spectroscopic studies of iron(III) with citric acid and other carboxylic acids. *Inorg. Chim. Acta* 226: 117-127.
- [28] Faust, B. C. and Zepp, R. G. **1993**. Photochemistry of aqueous iron(III)-polycarboxylate complexes: roles in the chemistry of atmospheric and surface waters. *Environ. Sci. Technol.* 27: 2517-2522.
- [29] Balzani, V. and Carassiti, V. **1970**. *Photochemistry of coordination compounds*. Academic Press: London.

- [30] Brauer, G. **1963**. *Handbuch der präparativen anorganischen Chemie*. Ferd. Enke Verlag: Stuttgart, Germany.
- [31] Cornell, R. M. and Schwertmann, U. **2003**. *The Iron Oxides: Structure, Properties, Reactions, Occurrences and Uses*. 2 ed.; Wiley-VCH: Weinheim, Germany.
- [32] Bondietti, C. G. (1992). Einfluss ausgewählter Liganden auf die Auflösungskinetik von Lepidokrokit (γ -FeOOH). PhD thesis, ETH, Zürich, Switzerland.
- [33] Hug, S. J. and Sulzberger, B. **1994**. In-situ Fourier-transform infrared spectroscopic evidence for the formation of several different surface complexes of oxalate on TiO_2 in the aqueous-phase. *Langmuir* 10: 3587-3597.
- [34] Bennet, J. H., Lee, E. H., Krizek, D. T., Olsen, R. A. and Brown, J. C. **1982**. Photochemical reduction of iron. II. Plant related factors. *J. Plant Nutr.* 5: 335-344.
- [35] Frahn, J. L. **1958**. The photochemical decomposition of the citrate-ferric iron complex: A study of the reaction products by paper ionophoresis. *Aust. J. Chem.* 11: 399-405.
- [36] Hug, S. J., Canonica, L., Wegelin, M., Gechter, D. and Von Gunten, U. **2001**. Solar oxidation and removal of arsenic at circumneutral pH in iron containing waters. *Environ. Sci. Technol.* 35: 2114-2121.
- [37] Hay, R. W. and Leong, K. N. **1971**. Uncatalysed and metal-ion catalysed decarboxylation of 3-oxoglutaric acid: model for an enzyme system. *J. Chem. Soc. A* 3639-3647.
- [38] Silvester, E., Charlet, L., Tournassat, C., Gehin, A., Greneche, J. M. and Liger, E. **2005**. Redox potential measurements and Mössbauer spectrometry of Fe^{II} adsorbed onto Fe^{III} (oxyhydr)oxides. *Geochim. Cosmochim. Acta* 69: 4801-4815.
- [39] Zhang, Y., Charlet, L. and Schindler, P. W. **1992**. Adsorption of protons, $\text{Fe}(\text{II})$ and $\text{Al}(\text{III})$ on lepidocrocite (γ -FeOOH). *Colloid. Surf.* 63: 259-268.
- [40] Gustafsson, J. P. **2004**. *Visual MINTEQ*, vers. 2.30. KTH (Royal Institute of Technology), Sweden.
- [41] Persson, P. and Axe, K. **2005**. Adsorption of oxalate and malonate at the water-goethite interface: molecular surface speciation from IR spectroscopy. *Geochim. Cosmochim. Acta* 69: 541-552.
- [42] Hug, S. J. and Bahnemann, D. **2006**. Infrared spectra of oxalate, malonate and succinate adsorbed on the aqueous surface of rutile, anatase and lepidocrocite measured with in situ ATR-FTIR. *J. Electron Spectrosc. Relat. Phenom.* 150: 208-219.

Chapter 3

ATR-FTIR spectroscopic study of the adsorption of desferrioxamine B and aerobactin to the surface of lepidocrocite (γ -FeOOH)

Paul Borer, Stephan J. Hug, Barbara Sulzberger, Stephan M. Kraemer,
and Ruben Kretzschmar

Prepared for publication in Geochimica et Cosmochimica Acta

Abstract

The adsorption of two model siderophores, desferrioxamine B (DFOB) and aerobactin, to lepidocrocite (γ -FeOOH) was investigated by attenuated total reflection infrared spectroscopy (ATR-FTIR). The spectra of adsorbed DFOB indicated that two to three hydroxamic acid groups of adsorbed DFOB are deprotonated in the pH range from 4.0 - 8.2. Deprotonation of hydroxamic acid groups of adsorbed DFOB at pH values well below the first acid dissociation constant of solution DFOB species ($\text{pK}_a = 8.3$) and well below the point of zero charge of lepidocrocite ($\text{pH}_{\text{PZC}} = 7.4$) suggested that the surface speciation at the lower end of this pH range (pH 4) is dominated by a surface DFOB species with inner-sphere coordination of two to three hydroxamic acids groups to the surface. Maximum adsorption of DFOB occurred at approximately pH 8.6, close to the first pK_a value of the hydroxamic acid groups, and decreased at lower and higher pH values.

The spectra of adsorbed aerobactin in the pH range 3 to 9 indicated at least three different surface species. Due to the small spectral contributions of the hydroxamic acid groups of aerobactin, the interactions of these functional groups with the surface could not be resolved. At high pH, the spectral similarity of adsorbed aerobactin with free aerobactin deprotonated at the carboxylic acid groups indicated outer-sphere

complexation of the carboxylate groups. With decreasing pH, a significant peak shift of the asymmetric carboxylate stretch vibration was observed. This finding suggested that the (lateral) carboxylic acid groups are coordinated to the surface either as inner-sphere complexes or as outer-sphere complexes that are strongly stabilized at the surface by hydrogen bonding at low pH. Additional ATR-FTIR experiments coupled with UV-Vis irradiation could not provide conclusive information on the surface coordination of the photochemically reactive α -hydroxycarboxylic acid group.

1. Introduction

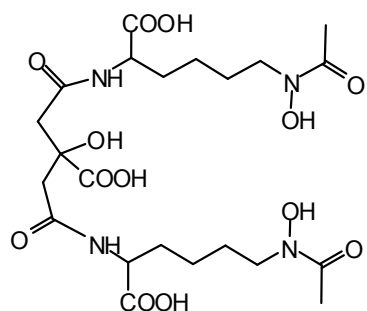
In recent years, an increasing number of studies have addressed the role of siderophores in mineral weathering and nutrient iron cycling [1-6]. The adsorption and coordination of siderophores to the surface of iron bearing minerals such as iron(III) (hydr)oxides are important key parameters determining the dissolution of these phases, particularly in the absence of additional organic matter or ligands. In this regard, recent studies have shown that siderophore-promoted dissolution of goethite is surface-controlled, as indicated by the strong correlation between dissolution rates and the surface concentration of adsorbed siderophores [7-9]. Siderophores are multidentate ligands with metal binding groups including hydroxamate and catecholate groups, and less commonly α -hydroxycarboxylate and carboxylate groups [10]. Recent studies showed that siderophores with α -hydroxycarboxylic acid groups form Fe(III)-complexes in solution that are susceptible to direct photolysis under simulated or natural sunlight, leading to the oxidation of the metal binding group and to the reduction of the coordinated Fe(III) atom [11]. In contrast, hydroxamate and catecholate groups coordinated to Fe(III) in hexadentate siderophore complexes are not affected by light-induced intra-molecular redox reactions [12].

To date, only a small number of studies have provided spectroscopic information on the interaction of siderophores with iron (hydr)oxides or other mineral surfaces. Often, the interaction of smaller analog compounds with oxide surfaces has been studied by spectroscopic techniques [13, 14]. Other research groups have investigated the interactions of siderophores with Fe(III) in solution as a proxy for possible interactions at iron (hydr)oxide surfaces by X-ray and IR spectroscopic techniques [15-17].

Attenuated total reflection infrared spectroscopy (ATR-FTIR) is a promising spectroscopic technique to study the interactions of siderophores at mineral oxides surfaces. However, the size and the complexity of siderophores complicate the analysis and interpretation of vibration data. It has been shown by ATR-FTIR that pyoverdine -

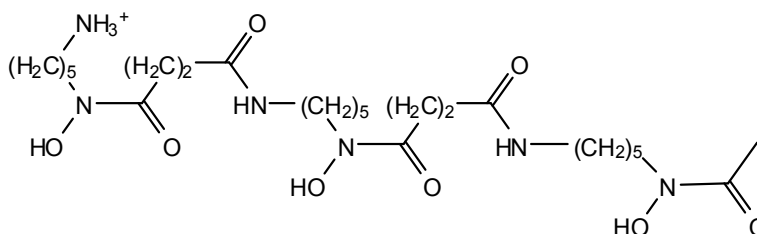
a mixed catecholate and hydroxamate siderophore – forms covalent bonds between the catecholate groups and TiO_2 or Fe_2O_3 particle films [18, 19]. By the use of grazing-angle specular-reflection FTIR, it was shown that parabactin – a catecholate siderophore – forms a surface complex on aluminum oxide [20]. Recently, a thermo-IR spectroscopic study [21] provided some insight into the interactions of desferrioxamine B (DFOB), a trihydroxamate siderophore, with Ca-montmorillonite (clay mineral). ATR-FTIR spectroscopy has also been used to study dissolution processes of goethite in situ in the presence of oxalic acid and DFOB [22]. The development of chemical force microscopy has also promoted the investigations of siderophore-surface interactions [23, 24].

In this study, we investigated the adsorption of DFOB and aerobactin to lepidocrocite ($\gamma\text{-FeOOH}$) by ATR-FTIR spectroscopy. Lepidocrocite is an iron(III) (hydr)oxide mineral that is found in hydromorphic soils, aquatic environments, and iron ore deposits. This iron(III) (hydr)oxide mineral is well suited for ATR-FTIR studies because of its high surface area, resulting in spectroscopically measurable surface concentrations of adsorbed DFOB and aerobactin. The investigated siderophores are similar in size, but differ (partly) in their metal binding groups as well as in their overall charge (Fig. 1).



aerobactin

$\text{H}_5(\text{aerobactin})$; pK_a values: - carboxylic acid: 3.11, 3.48, 4.31
- hydroxamic acid: 8.93, 9.44



desferrioxamine B

$\text{H}_3(\text{HDFOB})$; pK_a values: - hydroxamic acid: 8.32, 8.96, 9.55
- amine group: 10.79

Fig. 1: Chemical structures of the fully protonated siderophores desferrioxamine B (DFOB) and aerobactin and reported pK_a values of the functional acid groups at 0.1 M ionic strength [28, 31]

The presence of a photochemically reactive iron binding group (α -hydroxycarboxylic acid group) [25, 26] and the presence of two lateral carboxylic acid groups in aerobactin represent the major differences compared to DFOB that may influence their reactivity at the surface of lepidocrocite. In addition, aerobactin has only two hydroxamic acid functional groups in comparison to the trihydroxamate siderophore DFOB.

Even though the ligand and iron oxide concentrations used in this laboratory study likely do not reflect natural conditions, information on the coordination of siderophores may help to understand the reactivity of these compounds towards dissolution of iron bearing minerals in terrestrial and aquatic environments.

2. Materials and methods

2.1 Samples

Iron-free aerobactin ($C_{22}H_{32}O_{12}N_4$, lyophilized, from EMC microcollections in Tübingen, Germany) was used as received. Desferrioxamine B (DFOB) was received as the methanesulfonate salt ($[C_{25}H_{46}N_5O_8NH_3^+(CH_3SO_3)^-]$, Sigma Aldrich) and was converted to the chloride salt by using an anion exchange resin. A column packed with 70 g of chloride anion resin (AG 1-X2, Biorad) was preconditioned with 0.1 M HCl and rinsed thoroughly with high purity water (18.2 M Ω cm) until the pH of the effluent was neutral. Then a 150 mL solution of 0.04 M DFOB was passed twice through the column during 5 hours in the dark. The resulting effluent was immediately freeze dried and stored at -20 °C and was further analyzed for residual methanesulfonate by ion chromatography (Metrohm ion chromatograph with a Metrosep A Supp 5-150 column, effluent: 3.2 mM Na_2CO_3 , 1 mM $NaHCO_3$, retention time: 4.2 minutes). Samples were either directly analyzed for methanesulfonate or were first oxidized by UV irradiation in an acidic hydrogen peroxide solution (in Quartz glass tubes) prior to the measurement of sulfate (resulting from the oxidation of methanesulfonate, retention time: 13.9 minutes). Neither methanesulfonate nor sulfate was detected by ion chromatography.

The concentrations of aerobactin and DFOB (chloride salt) stock solutions were measured by total organic carbon analysis with a Shimadzu 5000A TOC analyzer (TOC standards from Fluka).

The synthesis and characterization of lepidocrocite used in this study has been presented elsewhere [27]. A specific surface area of 130 m²/g was measured by multipoint N₂-BET analysis and the point of zero charge (pH_{PZC} = 7.4) was determined by acid-base titrations in different ionic strength media.

2.2 ATR-FTIR spectra of solution species

Spectra were recorded on a Bio-Rad FTS 575C instrument equipped with a mercury cadmium telluride (MCT) detector and a horizontal nine reflection diamond ATR unit with KRS-5 optics (SensIR Technologies, Danbury, CT). Scans were taken from 400 to 4000 cm^{-1} with 2 cm^{-1} resolution. Data analysis was performed with Matlab (The Math Works, Inc.).

Absorbance spectra of aqueous solutions of 50 mM DFOB and 50 mM aerobactin, respectively, were measured against a background spectrum of high purity water (128 co-added scans). Solution pH was varied between 3 and 12 by small additions of concentrated HCl or NaOH. DFOB solutions were analyzed in a 5 mL liquid cell mounted above the ATR-crystal. Because we only had a very small quantity of aerobactin available, we minimized the consumption of aerobactin by spreading 100 μL of a 50 mM aerobactin stock solution over the surface of the ATR crystal. The pH of the solution was changed by transferring the solution into an Eppendorf vial and adding minute amounts of concentrated HCl and NaOH before bringing the solution back onto the ATR crystal. Solution pH was measured with a micro-electrode (Metrohm 6.0224.100 with saturated KCl as internal electrolyte, shaft diameter 3 mm). Dilution by addition of HCl or NaOH amounted to less than 10 % and was not accounted for in the analysis of the spectra.

Spectra of aqueous 1:1 complexes of Fe(III)-DFOB and Fe(III)-aerobactin at pH 6 were recorded as well. Fe(III)-DFOB (50 mM) was prepared by mixing a stock solution of $\text{FeCl}_3 \cdot 6\text{H}_2\text{O}$ with a stock solution of DFOB and adjusting to pH 6. A pure stock solution of 1:1 Fe(III)-aerobactin complexes at neutral pH could not be synthesized in this way and would have required subsequent purification by HPLC. However, due to the limited amount of available aerobactin a purification step was not feasible. Instead, freshly synthesized and carefully washed hydrous ferric oxide was added in excess to a stock solution of approximately 50 mM aerobactin (100 μL volume) in an Eppendorf vial and was left to react for one week in the dark. The solution was heated up to 50 $^\circ\text{C}$ for few hours each day to speed up the dissolution process. During the reaction time, the pH was gradually adjusted with small volumes of concentrated NaOH to pH 6. The suspension was subsequently centrifuged and the supernatant was filtered through a 0.45 μm filter (Millipore, SJHV004NS). The final stock solution was characterized by UV-Vis spectroscopy, total organic carbon and total iron analysis. It consisted of approximately 16 mM free aerobactin and 14 mM 1:1 Fe(III)-aerobactin complexes.

2.3 ATR-FTIR spectra of adsorbed species

The circular diamond ATR crystal (diameter 4 mm) was coated with a thin film of lepidocrocite by spreading 2 μL of a 30 g/L lepidocrocite suspension over the crystal and drying the film under a gentle stream of N_2 . Only a small fraction of the film detached from the ATR crystal during the rinsing procedure with high purity water. Then, a 5 mL liquid cell (polypropylene beaker) was tightly pressed onto to the ATR unit with a silicon O-ring seal between the liquid cell and the ATR unit. The liquid cell was covered with a PMMA window (Plexiglas) through which a pH electrode and tubes for N_2 purge gas and for the addition of HCl and NaOH were inserted. The solutions in the liquid cell were purged with high purity N_2 gas to stir the solution and to reduce the input of CO_2 from air and the concomitant adsorption of carbonate. The ionic strength was adjusted to 0.01 M with NaCl. After purging the solution above the oxide layer with N_2 for 45 minutes, a background spectrum of the water-solid interface at pH \sim 5 was measured (128 co-added scans). Then, concentrated stock solutions of DFOB or aerobactin were added to a final solution concentration of 400 μM . The pH of the solution was adjusted with small additions of HCl or NaOH.

Absorbance spectra of adsorbed DFOB or aerobactin (128 co-added scans) were measured against the background spectrum (solid-water interface without any ligands). Measurements were all carried out in the dark. Adsorption of DFOB and aerobactin did not increase measurably after a reaction time of \sim 30 min. During the pH edge adsorption experiments, dissolution of lepidocrocite in the presence of the siderophores occurred, but less than 2 μM Fe(III)-siderophore complexes in solution formed in total during the experiments. Total dissolved iron was measured by UV-visible absorption of the solution at 430 nm for Fe(III)-DFOB complexes and by inductively coupled plasma optical emission spectroscopy (ICP-OES) for Fe(III)-aerobactin complexes, respectively.

By using this ATR-FTIR setup with low amounts of lepidocrocite (thin film) and rather high siderophore concentrations (400 μM), we could ensure that (i) the solution above the oxide film was sufficiently well buffered (no significant pH shifts during experiments), (ii) the formation of Fe(III)-DFOB or Fe(III)-aerobactin complexes due to dissolution of lepidocrocite did not lead to a significant decrease in the solution concentration of uncomplexed DFOB or aerobactin, and (iii) high ratios of free ligand concentrations to solution concentrations of Fe(III)-complexes minimized spectral contributions from possible readsorption of Fe(III)-aerobactin or Fe(III)-DFOB complexes [9].

2.4 ATR-FTIR photoirradiation experiments

An ATR-FTIR setup coupled with UV-Vis irradiation was used to investigate the photoreactivity of adsorbed siderophores at the surface of lepidocrocite [27]. Spectra of adsorbed DFOB and aerobactin were measured at pH 8 and pH 4, respectively, as described above. For the photoirradiation experiments, the 5 mL liquid cell was covered with an UV-transparent PMMA window (Plexiglas GS 2458, Röhm, Germany) to allow UV irradiation from above. Light from a 103 W high pressure mercury lamp (HBO 103W/2, OSRAM) was passed through a glass filter (cut-off wavelength 300 nm) and focused by a quartz glass lens onto the ATR crystal/oxide layer/water interface inside the liquid cell. The filtered light spectrum of the high pressure HBO lamp consisted of non-overlapping spectral bands at 312, 334, 365 (strong), 404, 435, 546, and 578 nm. The light intensity of the focused beam was approximately 5-10 W/cm² (300 nm – 500 nm wavelength range) [27].

Under irradiation, spectra were recorded in time-steps of 1 minute (51 co-added scans per spectrum). The solution above the oxide layer was gently purged during the irradiation period. It was necessary to perform background spectra of the irradiated mineral-water interface in the absence of the siderophores to correct for spectral artifacts occurring due to the heat generation that accompanied the intense irradiation [27]. The temperature of the solution in the 5 mL liquid cell above the oxide layer increased from 25 °C to 40 °C within 9 minutes of irradiation. The pH of the solution was measured after the irradiation period at room temperature and no pH shifts were observed.

3. Results and discussion

3.1 IR spectra of DFOB in aqueous solutions

The spectra of aqueous DFOB at 20 different pH values (pH 3.5 to 12) were analyzed by applying singular value decomposition (SVD) and oblique rotation with a matrix expressing the protonation equilibria of different DFOB species with known pK_a values (see Fig. 1, pK_a values at 0.1 M ionic strength [28]). The SVD procedure is described elsewhere [29]. The different component spectra of aqueous DFOB are shown in Fig. 2. We have adopted a notation in which the proton of the amine group is written within brackets. For example, (HDFOB)²⁻ is a species which is still protonated at the amine group (pK_a = 10.79 [28]), but where the hydroxamic functional groups are deprotonated (pK_a values: 8.32, 8.96, 9.55 [28]). According to SVD, the experimental data set could be fitted with four different SVD-components to within 0.0005 absorbance units

(close to spectral noise), indicating the presence of four spectral distinct species. The application of oblique rotation with known pK_a values resulted in 5 spectra of differently protonated species, where the spectra of DFOB³⁻ (totally deprotonated) and (HDFOB)²⁻ (protonated at the primary amine group) were very similar (Fig. 2). Thus, the protonation or deprotonation of the primary amine group in solution did not result in noticeable spectral changes. The spectra of aqueous DFOB are in agreement with published spectra [17], except that the intense bands of methanesulfonate at 1185 cm⁻¹ and 1049 cm⁻¹ (Fig. S1 in the Supporting Information) are absent (methanesulfonate in the purchased desferrioxamine B salt was exchanged by chloride in this study). The most important band positions and vibrational modes of DFOB as assigned by Edwards et al. (2005) are listed in Table 1. Fig. 2 illustrates that the spectra and the spectral changes with pH were dominated by vibrations of the hydroxamic acid functional groups. The deprotonation of the hydroxamic acid groups was accompanied by a decrease of the 1605 cm⁻¹ band and a concomitant increase of a band at 1578 cm⁻¹. The 1605 cm⁻¹ band is assigned to the oxime related amide I vibration ($\nu_{C=O}$ stretch vibration of the hydroxamic carbonyls), which is downshifted to 1578 cm⁻¹ upon deprotonation [17]. The major potential energy contributions to the absorption bands at 1605 cm⁻¹ and 1578 cm⁻¹ originate from vibrations within the hydroxamic acid groups, with a predominant contribution from the oxime $\nu_{C=O}$ stretch [17]. The amide I band ($\nu_{C=O}$ stretch) of the amide carbonyls located at 1620 cm⁻¹ was not affected by pH change. The amide II band of the amide groups (coupling of δ_{N-H} bend and ν_{C-N} stretch [30]) is located at approximately 1540 to 1561 cm⁻¹. For the protonated DFOB species, H₃(HDFOB)⁺, Edwards et al. (2005) have assigned bands located at 1470, 1444 and 1426 cm⁻¹ to δ_{NOH} bend and ν_{C-N} stretch (oxime), δ_{NH} deformation (primary amine) and δ_{CCN} bend vibrations, respectively. Except for the δ_{NH} deformation vibration (primary amine), the bands assigned to the above vibrational modes were well resolved in the measured spectrum of H₃(HDFOB)⁺ (cf. Table 1 and Fig. 2). With the disappearance of the δ_{NOH} bend vibrational mode (~1469 cm⁻¹) upon deprotonation of the hydroxamic acids, a distinct band located at 1472 cm⁻¹ evolved. Without published ab initio calculations of vibrational modes and frequencies of deprotonated DFOB species, we can only tentatively assign the 1472 cm⁻¹ band to hydroxamate related vibrations (e.g. ν_{C-N} stretch of the hydroxamate group). Deprotonated DFOB species also exhibited a distinct peak at 1149 cm⁻¹, which may be assigned to a ν_{N-O} stretch. This band was not observed by FTIR spectroscopy by Edwards et al. (2005), probably due to the masking effect of the strong methanesulfonate bands, but a resonance Raman spectrum of Fe(III)-DFOB revealed a peak located at 1209 cm⁻¹ that was unambiguously assigned to the ν_{N-O} stretch vibration [17].

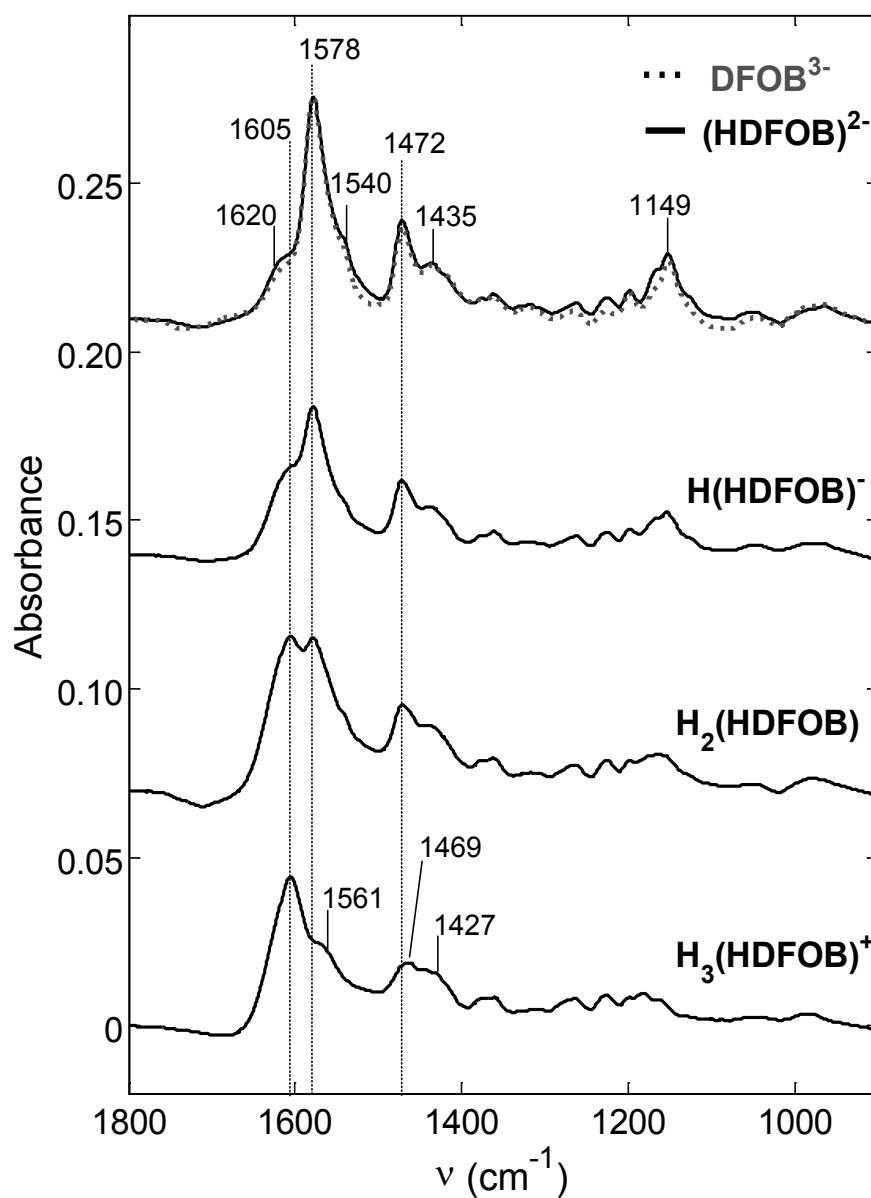


Fig. 2: Aqueous component spectra of DFOB (50 mM). The spectra of totally deprotonated DFOB^{3-} (gray dashed line) and amine-protonated $(\text{HDFOB})^{2-}$ (black line) are overlaid.

Table 1: Experimental vibrational modes for DFOB species.

Assignment ^a	H ₃ (HDFOB) ⁺	DFOB ³⁻	Fe(III)-DFOB pH 6	Adsorbed DFOB pH 4.0 - 8.2
$\nu_{\text{C=O}}$ (amide)	1620	1620	1626	1625
$\nu_{\text{C=O}}$ (oxime)	1605	1578	1578	1578
δ_{NH} rock (amide) $\nu_{\text{C-N}}$ (amide)	1561	1540	n.r. ^b	n.r. ^b
δ_{NOH} bend ^d $\nu_{\text{C-N}}$ (oxime)	1469 ^d			
Hydroxamate related vibrations ^e		1472 ^e	1455 ^e	1463 ^e
δ_{NH} (amine)	n.r. ^b (1444 ^e)			
δ_{CCN} bend	1427			
$\nu_{\text{N-O}}$		1149 ^f		

^a Assignments of aqueous DFOB species according to Edwards et al. (2005). rock = rocking mode, bend = bending mode. ^b n.r. = not resolved in this study. ^c From Edwards et al. (2005). ^d The δ_{NOH} bend is lost upon deprotonation of the hydroxamic acids. ^e Due to the absence of ab initio calculations of vibrational modes of the Fe(III)-DFOB complex and deprotonated DFOB species, we tentatively relate these bands to vibrations of the Fe(III)-coordinating or free hydroxamate groups. ^f This band was not observed by IR spectroscopy by Edwards et al. (2005), probably due to masking by methanesulfonate bands, but a band assigned to $\nu_{\text{N-O}}$ was observed at 1209 cm⁻¹ by Raman spectroscopy [17].

3.2 IR spectra of aerobactin in aqueous solutions

Due to the limited amount of available aerobactin, only a small set of spectra was recorded in aqueous solution (9 spectra from pH 2.75 to 10.43). SVD analysis of these spectra revealed that a minimum of three SVD-components were required to fit all important peaks to within a residual of 0.0005 absorbance units. To illustrate spectral changes occurring due to deprotonation of the carboxylic acid groups (pK_a values: 3.11, 3.48, 4.31 at 0.1 M ionic strength [31]) and hydroxamic acid groups (pK_a values: 8.93, 9.44 [31]), spectra of the following species are shown in Fig. 3: H₅(aerobactin) (fully protonated, pH 2.75), H₂(aerobactin)³⁻ (carboxylic acid groups deprotonated, pH 6.52), and aerobactin⁵⁻ (carboxylic and hydroxamic acid groups deprotonated, pH 10.43). In addition, difference spectra of these species are presented in Fig. 4. Peak positions and band assignments of aerobactin solution species are listed in Table 2. In the fully protonated species the $\nu_{\text{C=O}}$ stretch vibrations of the carboxylic groups (1720 cm⁻¹), amide groups (1650 cm⁻¹) and oxime groups (1605 cm⁻¹) were clearly resolved. The bands located at 1553 cm⁻¹, 1458 cm⁻¹ and 1238 cm⁻¹ are assigned to δ_{NH} rock (amide), δ_{NOH} bend vibration, and $\nu_{\text{C-OH}}$ stretch ($\delta_{\text{C-OH}}$ bend) vibrations, respectively. Deprotonation

of the carboxylic groups resulted in a decrease of the 1720 cm^{-1} and 1238 cm^{-1} bands and in the development of bands at 1578 cm^{-1} (ν_{COO^-} asymmetric stretch vibration) and 1404 cm^{-1} (ν_{COO^-} symmetric stretch vibration) (see Fig. 3 and 4). Upon deprotonation of the hydroxamic acid groups, the oxime related $\nu_{\text{C=O}}$ vibration at 1605 cm^{-1} was downshifted to 1578 cm^{-1} (Fig. 4). The formation of the band located at 1474 cm^{-1} is tentatively assigned to vibrations of the hydroxamate groups, consistent with the band at 1472 cm^{-1} of deprotonated DFOB. Fig. 4 shows furthermore that the intensities of carboxylate vibrations were much larger than the intensities of hydroxamate vibrations. This masking effect introduces some difficulties in the interpretation of spectral data of aerobactin adsorbed to metal oxide surfaces.

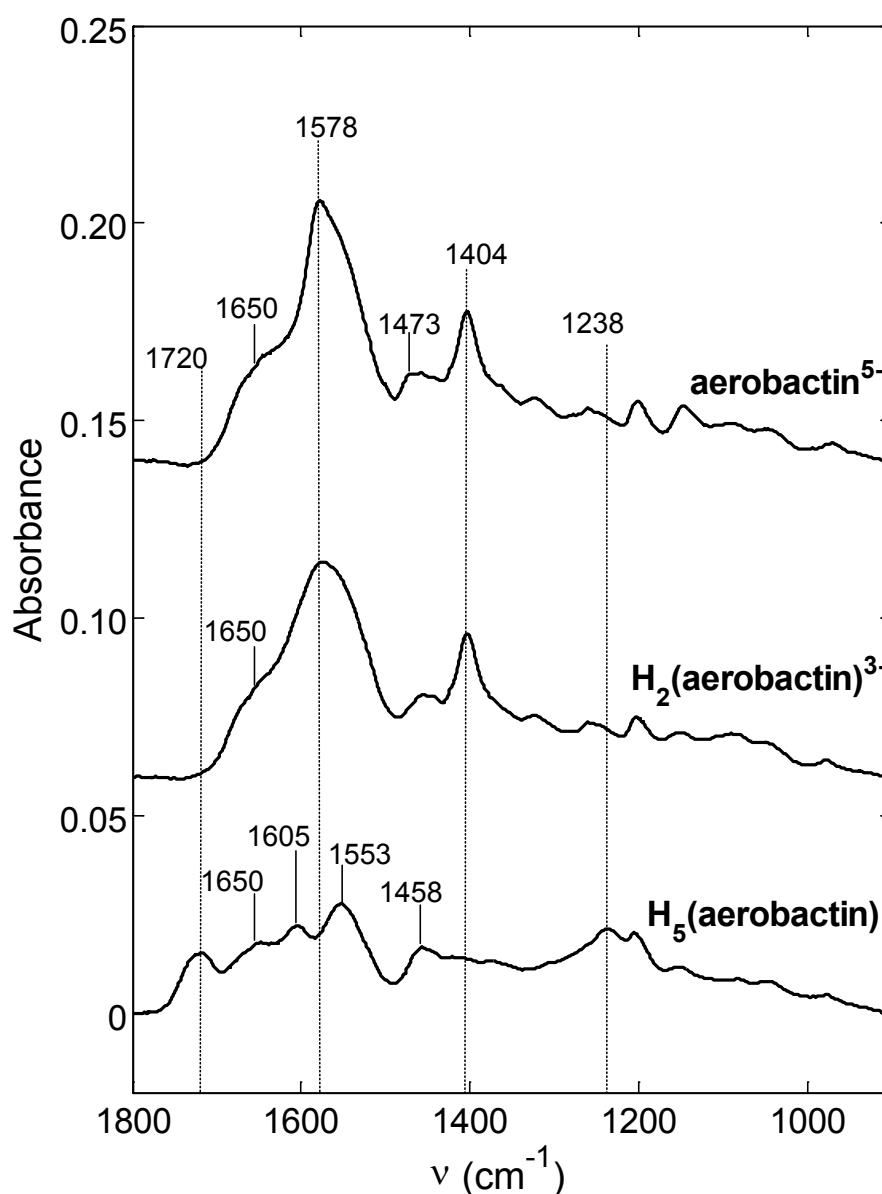


Fig. 3: Aqueous component spectra of aerobactin (50 mM): $\text{H}_5(\text{aerobactin})$ (fully protonated, pH 2.75), $\text{H}_2(\text{aerobactin})^{3-}$ (carboxylic acid functional groups deprotonated, pH 6.52), aerobactin^{5-} (totally deprotonated, pH 10.43).

Table 2: Experimental vibrational modes for aerobactin species in solution.

Assignment ^a	Fully protonated H ₅ (aerobactin)	Fully deprotonated aerobactin ⁵⁻
$\nu_{\text{C=O}}$ (carboxylic acid)	1723	-
$\nu_{\text{C=O}}$ (amide)	1650	1650
$\nu_{\text{C=O}}$ (oxime)	1605	1578
ν_{COO} . as	-	1578
δ_{NH} rock (amide)	1553	1535
δ_{NOH} bend ^b	1458	-
$\nu_{\text{C-N}}$ (oxime)		
Hydroxamate related vibrations	-	1473 ^c
ν_{COO} . sy	-	1404
$\nu_{\text{C-OH}}$, $\delta_{\text{C-OH}}$	1238	-

^a Assignments according to this study. as = asymmetric, sy = symmetric. ^b The δ_{NOH} bend disappears upon deprotonation of the hydroxamic acids. ^c This band evolves upon deprotonation of hydroxamic acid groups and can be assigned to hydroxamate related vibrational modes.

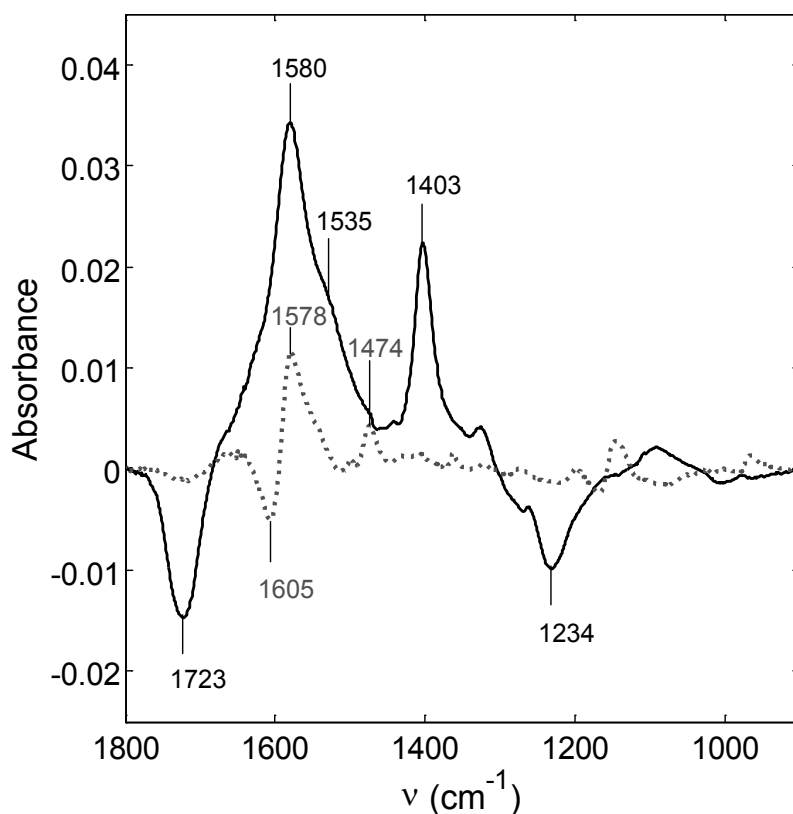


Fig. 4: Difference spectra of aqueous aerobactin species shown in Fig. 3. Black solid line: difference spectrum associated with deprotonation of the carboxylic acid functional groups. Gray dashed line: difference spectrum associated with deprotonation of the hydroxamic acid functional groups.

A comparison of the spectra of DFOB and aerobactin shows the effect of substituents on the band frequencies of corresponding vibrational modes. The chemical environment of the hydroxamic acids in DFOB and aerobactin is very similar (alkyl chains). Accordingly, the frequencies of hydroxamate (or hydroxamic acid) related vibrational modes of DFOB and aerobactin were almost identical (cf. Table 1 and 2). On the other hand, the frequencies of amide associated vibrational modes were significantly different, and this may be related to adjacent carboxylic acid groups present in aerobactin. The amide $\nu_{\text{C=O}}$ stretch vibration was 30 cm^{-1} higher than the equivalent band in DFOB. Furthermore, there was a slight shift of the amide δ_{NH} rock vibration towards lower frequencies.

3.3 IR spectra of aqueous Fe(III)-DFOB and Fe(III)-aerobactin complexes

The spectrum of aqueous Fe(III)-DFOB at pH 6 is presented in Fig. 5. This spectrum is in agreement with the Fe(III)-DFOB spectrum measured by Edwards et al. (2005), except that in this study the resolved amide $\nu_{\text{C=O}}$ vibration (1620 cm^{-1}) was less intense. This spectral region is strongly affected by vibrational modes of solvent water, hence the subtraction of the background water spectrum has to be performed carefully (e.g., the ionic strength of the background spectrum must have exactly the same ionic strength as the probe solution). Compared to fully deprotonated DFOB solution species (Fig. 2 and Table 1), the amide $\nu_{\text{C=O}}$ band of the Fe(III)-DFOB solution complex was apparently shifted by 6 cm^{-1} towards higher energy (1626 cm^{-1}). The coordination of hydroxamate groups to Fe(III) did not lead to a shift in the oxime $\nu_{\text{C=O}}$ stretch band (1578 cm^{-1}). However, a rather intense band at 1455 cm^{-1} emerged upon coordination of hydroxamate groups to Fe(III). Similarly, vibration bands appeared upon deprotonation of hydroxamic acid groups of aqueous DFOB and aerobactin at 1472 and 1474 cm^{-1} , respectively (cf. Fig. 2 and 4). We assigned these bands to vibrations of Fe(III)-coordinating or free hydroxamate groups. A downshift in frequency of this vibrational mode, as observed for the Fe(III)-DFOB solution complex, may tentatively be used to determine the coordination of hydroxamic acids to Fe(III) sites at the surface of iron(III) (hydr)oxides.

The spectral analysis of Fe(III)-aerobactin at pH 6 (Fig. S2 in the Supporting Information) was hampered by the presence of free aerobactin (16 mM free aerobactin versus 14 mM 1:1 Fe(III)-aerobactin complexes). At pH 6, the carboxylic acid groups are deprotonated irrespective of complexation with Fe(III). On the other hand, the hydroxamic acid groups of free aerobactin are protonated at pH 6, thus the measured Fe(III)-aerobactin spectrum (Fig. S2 in the Supporting Information) has a noticeable

contribution of oxime $\nu_{\text{C=O}}$ vibrations at 1605 cm^{-1} . For this reason, the apparent oxime $\nu_{\text{C=O}}$ vibration was at slightly higher energy (1582 cm^{-1}) than what might be expected for deprotonated or Fe(III)-coordinating hydroxamic groups (1578 cm^{-1}).

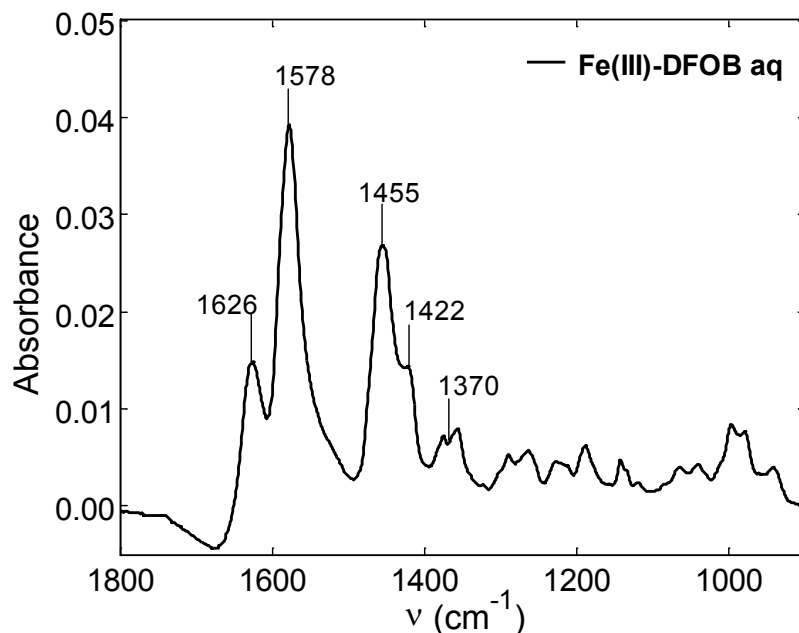


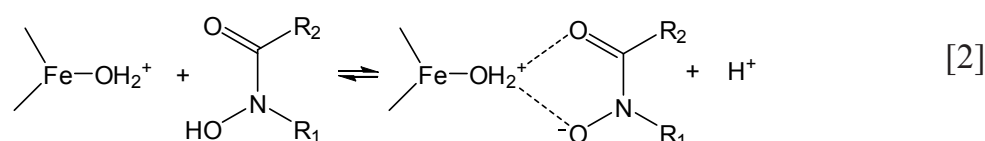
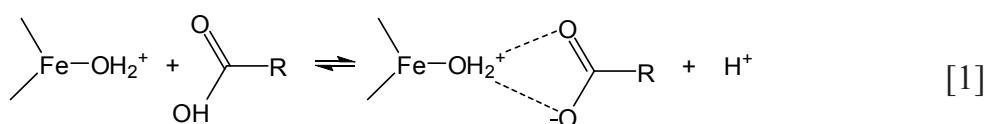
Fig. 5: Spectrum of the aqueous Fe(III)-DFOB complex (50 mM) at pH 6.

3.4 Assessment of surface interactions of siderophore functional groups

This section gives a brief background for the discussion of the spectra of adsorbed DFOB and aerobactin in the following sections. As generally accepted, formation of inner-sphere surface complexes with new bonds between ligand atoms and surface metal atoms (surface sites) lead to distinct spectral changes compared to the spectra of ligands in solution. In contrast, formation of outer-sphere complexes by purely electrostatic forces leaving solvent shells around surface and ligands intact, does not lead to distinct spectral changes. However, strong hydrogen-bonding can complicate spectral interpretations. Formation of outer-sphere surface complexes with strong hydrogen bonds is accompanied by a partial loss of the ligand solvent shell, and can lead to shifts in the vibrational modes of coordinating functional groups [32]. Hydrogen bonds are usually weak (with exceptions) and depend on contributions from electrostatic interactions (acid/base), polarization effects (hard/soft), and van der Waals interactions [33]. Hydrogen bonds may gain in strength if strong electrostatic interactions are involved (ionic hydrogen bonds). Noren and Persson (2007) recently reported that acetate, benzoate and cyclohexanoate adsorb to goethite by hydrogen bonding

interactions in the acidic pH range, based on spectral differences observed in both H₂O and D₂O. These authors proposed that shifts in the ν_{COO} symmetric and asymmetric stretch vibrations that have formerly been interpreted as consequences of inner-sphere coordination, may also occur upon hydrogen bonding. Thus, the distinction between outer-sphere hydrogen bonded carboxylates and inner-sphere complexes based on spectral shifts may not always be unambiguous [32]. On the other hand, distinct shifts are generally observed for ligands for which inner-sphere complexation is expected and energetically favorable, e.g. by formation of ring chelate structures at the surface, such as the five-membered ring chelate structure for oxalate [34].

Inner-sphere coordination of organic acids to mineral oxide surfaces is associated with an increase in acidity [35, 36]. Likewise, we may assume an increase in acidity upon hydrogen-bonding interactions of acid functional groups to the surface resulting in the stabilization of the deprotonated acid groups at the surface. Equation 1 illustrates the possible adsorption mode of a carboxylic acid to a positively charged iron (hydr) oxide surface by formation of a hydrogen bonded outer-sphere carboxylate complex. The situation for hydroxamic acids might be quite similar (equation 2). However, hydroxamic acids have significantly higher acid dissociation constants ($\text{pK}_a > 8.3$) than carboxylic acids ($\text{pK}_a < 5$ for small aliphatic monocarboxylic acids; see also Fig. 1 for pK_a values of the carboxylic acid groups of aerobactin). Thus, we may reasonably assume that the adsorption of hydroxamic acid groups by strong ionic hydrogen bonding interactions can be neglected in the acidic pH range. With increasing pH, both surface sites of lepidocrocite ($\text{pH}_{\text{PZC}} = 7.4$) and the hydroxamic acid functional groups ($\text{pK}_a > 8.3$) gradually deprotonate and the extent and strength of potential hydrogen bonding interactions may vary as a function of pH. In contrast to monocarboxylic acids, hydroxamic acids are able to form stable five-membered ring chelates at the surface of a mineral oxide [13, 14]. Thus, we may predict that hydroxamic acid groups tend to form inner-sphere surface complexes in the acidic pH range and that such surface complexes presumably also form at higher pH.



In this study, we have not attempted to investigate potential hydrogen interactions of hydroxamic acid groups with the surface of lepidocrocite. In comparison to simple monocarboxylates, the investigation of such interactions for complex molecules such as siderophores is probably far more difficult and has not been undertaken so far.

3.5 IR spectra of DFOB adsorbed to lepidocrocite

Fig. 6 shows spectra of DFOB adsorbed to lepidocrocite from an aqueous solution of 400 μM (0.01 M ionic strength) as a function of solution pH. The upper panel shows spectra measured in the pH range 4.0 - 8.2. SVD analysis of the spectra revealed that one SVD-component is sufficient to reproduce the spectral data in this pH range. The maximum residuals between the reproduced and the original spectra were less than 0.001 absorbance units. Residuals contained spectral features at 1470 and 1350 cm^{-1} assigned to desorption of adsorbed carbonate, which could not completely be removed prior to addition of DFOB (even by degassing with N_2 at pH 4 for an hour). Spectral bands increased with increasing pH, consistent with measured pH-dependent surface concentrations of DFOB in batch adsorption experiments conducted in our companion study [9]. Although the spectra in the pH range 4.0 to 8.2 are very similar, we cannot conclusively deduce the number of potentially different surface complexes from the SVD analysis. Possibly, several types of surface complexes with very similar spectra are present.

At solution pH where aqueous DFOB species are fully protonated (e.g. below pH 6.5), spectra of adsorbed DFOB not only resembled the aqueous Fe(III)-DFOB complex (cf. Fig. 5) but also the solution species $\text{H}(\text{HDFOB})^-$ and $(\text{HDFOB})^{2-}$ (cf. Fig 2), where two or three hydroxamic acid groups are deprotonated, respectively. The strong intensity of the oxime $\nu_{\text{C=O}}$ stretch bands located at 1578 cm^{-1} and the rather weak spectral contributions of oxime $\nu_{\text{C=O}}$ stretch bands at 1605 cm^{-1} at the lower end of this pH range (e.g. pH 4) indicated that two to three hydroxamic acid groups within each adsorbed DFOB molecule are deprotonated. In comparison to deprotonated solution species, there were some differences in the spectra of adsorbed DFOB. Apart from the broader oxime $\nu_{\text{C=O}}$ stretch band of adsorbed DFOB at 1578 cm^{-1} , the band assigned to vibrational modes of deprotonated hydroxamic acids was downshifted to 1463 cm^{-1} relative to the corresponding vibrations at 1472 cm^{-1} of deprotonated aqueous DFOB species, towards the position of the corresponding 1455 cm^{-1} band of the aqueous Fe(III)-DFOB complex. Due to the lack of ab initio calculations of vibrational modes of the Fe(III)-DFOB solution complex and possible surface complexes of DFOB at iron(III) (hydr)oxide surfaces or clusters, we can only propose that the rather intense

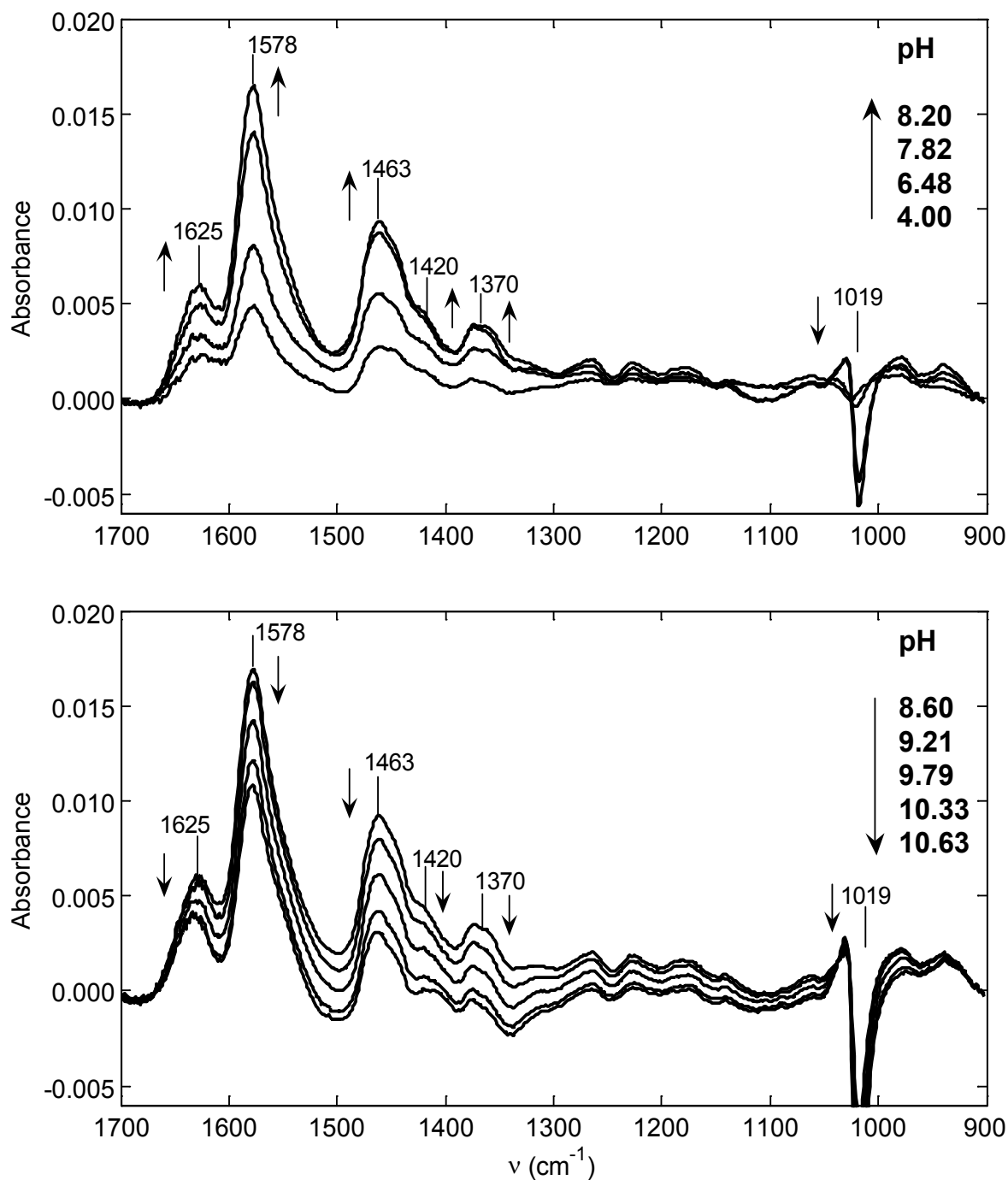


Fig. 6: Spectra of DFOB adsorbed to lepidocrocite from aqueous solutions of DFOB (400 μ M, $I = 0.01$ M). The direction of pH adjustment and the trend of concomitant spectral changes are indicated by arrows.

band at 1463 cm^{-1} is due to vibrations localized at Fe(III)-coordinated hydroxamate groups at the surface.

The observed deprotonation of two to three hydroxamic acid groups of adsorbed DFOB at acidic pH (e.g. pH 4) well below the pK_a values of hydroxamic acid groups and also well below the point of zero charge of lepidocrocite ($\text{pH}_{\text{PZC}} = 7.4$) strongly indicates

inner-sphere coordination of these groups at the surface. With a gradual increase of the pH towards pH 8.2, we cannot rule out the possibility that hydroxamic acid groups coordinate to the surface as deprotonated outer-sphere surface complexes with (ionic) hydrogen bonding interactions to the surface of lepidocrocite. However, the formation of inner-sphere surface complexes may even prevail in a higher pH range, considering that hydroxamic acids - unlike monocarboxylic acids – are able to form stable five-membered chelate rings with Fe(III) [13, 14].

In a recent study it was proposed that in the case of goethite only one hydroxamic group of DFOB coordinates to the surface, based on the analysis of temperature dependent dissolution rate coefficients [37]. However, the distance between hydroxamic acid groups in DFOB (assuming a linear structure) is approximately 9 Å, which allows the possibility that each hydroxamic acid coordinates separately to surface Fe(III) sites (distance of adjacent Fe sites at the goethite surface: 3.01-3.46 Å) [38]. From the spectral data we cannot deduce the spatial geometry of an adsorbed DFOB molecule at the surface of lepidocrocite, e.g., if the suggested inner-sphere coordination of two to three hydroxamate groups of adsorbed DFOB at low pH involves one or more surface Fe(III) sites. However, formation of a surface complex with all three hydroxamate groups coordinated to a single surface site is very unlikely due to steric hindrance at the surface.

Based on a recent adsorption study of acetohydroxamic acid on goethite [38], where it was concluded that surface complexes of acetohydroxamic acid have no charge and where surface concentrations did not change between pH 4 and 8, we assumed that the surface complex of DFOB on lepidocrocite is positively charged in this pH range due to the protonated primary amine group (pK_a : 10.79 [28]). Additional information on the type of surface complexes of DFOB formed on lepidocrocite is provided by batch adsorption and dissolution experiments in our companion study [9]. In the batch adsorption experiments, the increase of surface concentrations of DFOB with increasing pH towards pH 8 at 0.01 M ionic strength was explained by a decrease of repulsive electrostatic interactions between positively charged surface complexes of DFOB (due to the charged amine group) and the surface towards and above the point of zero charge of lepidocrocite ($pH_{pzc} = 7.4$). Hydrogen bonding interactions between negatively charged surface sites and the positively charged amine group with increasing pH towards pH 8 was also assumed to contribute to the free energy of adsorption of DFOB. In line with a reduction of repulsive electrostatic interactions, we observed an increase in surface concentrations of DFOB at pH 3 with an increase in ionic strength (0.2 M NaClO₄) [9].

The results of the batch dissolution experiments suggested that the surface speciation

in terms of dissolution-active surface complexes was rather constant from pH 3 to 8, in support of the spectral interpretation that inner-sphere surface complexation of hydroxamic acid groups of DFOB is dominant in this pH region [9].

Increasing the solution pH above 8.6 resulted in a decrease of the concentration of adsorbed DFOB as shown by decreasing spectral intensities of all absorption bands (lower panel of Fig. 6). The negative peak at $\sim 1020\text{ cm}^{-1}$ can be clearly assigned to δ_{OH} in-plane vibrations of structural OH groups of lepidocrocite (cf. Fig. S3 in the Supporting Information). A negative peak may arise as a result of dissolution [39] or in this study most likely as a result of destabilization and partial detachment of lepidocrocite particles from the ATR crystal at higher pH [27]. In the lower panel of Fig. 6, a loss of maximal 6 % of lepidocrocite was estimated. The partial loss of lepidocrocite may result in a loss of adsorbed DFOB in the penetration depth of the IR evanescent wave. However, the larger decrease of the intensity of absorption bands of up to $\sim 30\%$ is consistent with desorption of DFOB from the lepidocrocite surface. In contrast to the pH range 4.0 to 8.2, SVD analysis of the spectra measured above pH 8.6 revealed that one SVD-component is not sufficient to reproduce the spectral data. Two components were required to fit the spectral data to within 0.0003 absorbance units. Here we assume that the surface speciation varies with pH and that more than one surface complex is present. With an increase in pH, we observed a larger decrease of the spectral intensity at 1605 cm^{-1} than at 1578 cm^{-1} (oxime $\nu_{\text{C=O}}$ stretch bands of protonated or deprotonated hydroxamic acid functional groups, respectively), which points towards deprotonation of residual non-deprotonated hydroxamic acid functional groups of adsorbed DFOB (pK_{a} values of hydroxamic acid groups in solution lie within 8.3 and 9.55).

The spectra in Fig. 6 show that adsorption of DFOB to lepidocrocite was maximal at approximately pH 8.6 and decreased at lower and higher pH values. This study complements experimental adsorption studies of DFOB onto iron (hydr)oxides [8, 9, 37, 40] by extending the pH range to higher pH values that have not been considered so far.

3.6 IR spectra of aerobactin adsorbed to lepidocrocite

Fig. 7 shows spectra of aerobactin adsorbed to lepidocrocite in the pH range 3 to 9. The negative peaks observed at 1480 cm^{-1} and 1350 cm^{-1} originate from residual adsorbed carbonate (asymmetric and symmetric $\nu_{\text{C=O}}$ stretch) which gradually desorbed from the surface along with a decrease in solution pH and a concomitant increase in aerobactin adsorption. According to the SVD analysis of the spectral range not significantly affected by the interference of carbonate, three SVD-components were

required to fit the experimental spectra to within a residual of 0.0005 absorbance units. We conclude that at least three different surface complexes were present, differing in the protonation state and/or type of surface coordination of the hydroxamic and carboxylic acid groups. Since spectral changes occurring due to deprotonation of the hydroxamic acid groups in aerobactin as illustrated in Fig. 4 were comparatively small, we can only speculate on the protonation state of the adsorbed hydroxamic acid groups and thus on the type of their coordination to the surface.

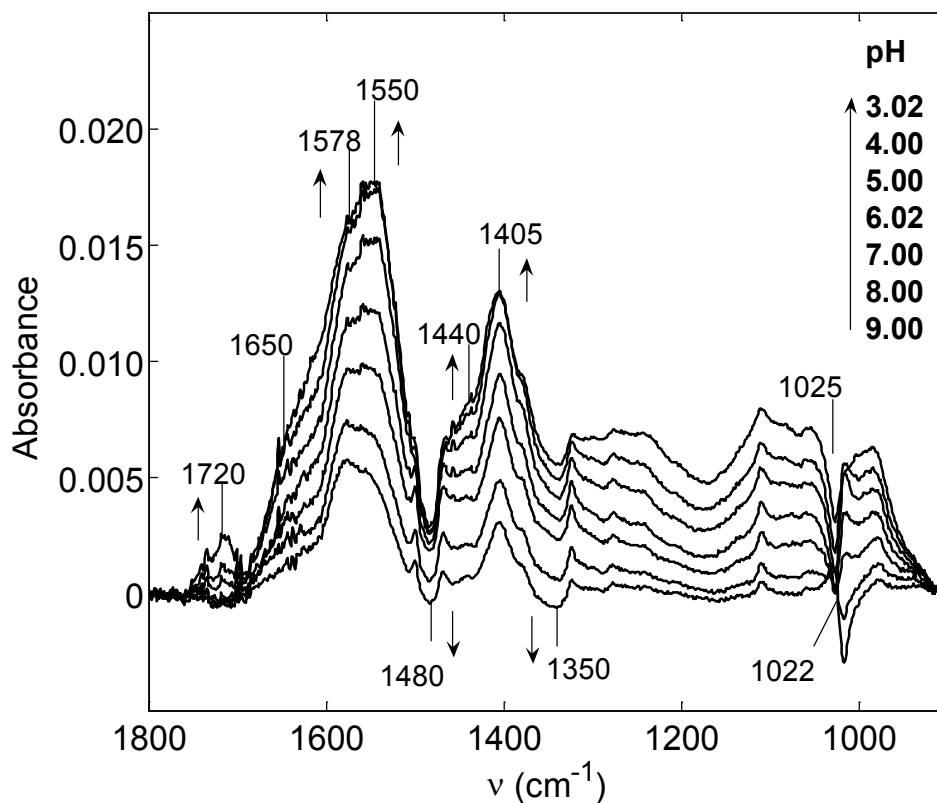


Fig. 7: Spectra of aerobactin adsorbed to lepidocrocite from aqueous solutions of aerobactin (400 μ M, $I = 0.01$ M). The direction of pH adjustment and the trend of concomitant spectral changes are indicated by arrows.

The increase of surface concentrations of aerobactin with decreasing solution pH points to significant interactions of the carboxylic acid groups of aerobactin at the surface. This adsorption behavior is typical for adsorption of carboxylic acids to iron (hydr)oxide surfaces, where maximum adsorption is observed close to the pK_a values of the acids [41-43]. At the highest pH values, the spectra of adsorbed aerobactin resembled the spectra of solution analogs with deprotonated carboxylic acid groups (cf. Fig. 3), suggesting that these groups are not likely not involved in inner-sphere surface complexation at high pH. At the lowest pH values, the emerging peak at 1720 cm⁻¹

points to a partial protonation of adsorbed carboxylate groups. With decreasing pH, the spectra showed a significant downshift of the asymmetric ν_{COO^-} stretch vibrations of aerobactin to 1550 cm^{-1} as compared to deprotonated aerobactin in solution (1578 cm^{-1}) and a slightly higher frequency of the symmetric ν_{COO^-} stretch vibration (increase by 2 cm^{-1}). This feature is consistent with a chelating mode of inner-sphere adsorbed carboxylate groups [44], but spectral shifts due to outer-sphere complexation by strong ionic hydrogen bonding interactions are also conceivable [32]. The available spectroscopic data does not provide the means to distinguish between vibrational bands of the lateral carboxylic groups and the central α -hydroxycarboxylic acid group. In our companion study [9], we observed significant adsorption of the dissolved hexadentate Fe(III)-aerobactin complex to the surface of lepidocrocite at pH 6. Assuming, that the hexadentate structure of Fe(III)-aerobactin is preserved at the surface, the only free functional groups to interact with the surface are the lateral carboxylic groups. Based on the findings of a spectroscopic investigation on the adsorption of α -amino acids to goethite [45], the amine moiety adjacent to the lateral carboxylate group may also interact with the surface by forming a five-membered chelate ring with the lateral carboxylate group. The high affinity of Fe(III)-aerobactin complexes for the surface of lepidocrocite as observed in batch adsorption experiments [9] is likely explained in terms of strong specific interactions by the lateral carboxylate and the adjacent amine group.

The spectra of adsorbed aerobactin presented in this study provide limited but valuable information on the coordination of carboxylate groups of aerobactin to the surface. However, we can only speculate on surface structures of aerobactin, e.g., we cannot say how many iron-binding groups and Fe(III) surface sites are involved in the binding of aerobactin to the surface.

3.7 Photoirradiation of adsorbed DFOB and adsorbed aerobactin

Recent studies have shown that irradiation of the hexadentate Fe(III)-aerobactin complex in solution at circumneutral pH leads to the oxidation of the coordinating α -hydroxycarboxylic acid group and to the reduction of the Fe(III) center [25, 26]. The oxidation of the α -hydroxycarboxylic acid group leads to the formation of an enol functional group. In conjunction with a neighboring amide carbonyl group, the resulting β -ketoenolate functional group retains the hexadentate structure of the original Fe(III)-complex [26]. In-situ ATR-FTIR experiments coupled with UV-Vis irradiation were performed to investigate whether the α -hydroxycarboxylic acid of aerobactin is coordinated to the surface such that photolysis of this group and concomitant reduction

of the coordinated surface Fe(III) site is feasible. The experimental setup has been recently developed to study photoredox reactions of citrate adsorbed to lepidocrocite [27], where it was shown that the α -hydroxycarboxylic acid group of citrate is selectively photooxidized at the surface of lepidocrocite and that the terminal carboxylic acid groups are not directly involved in the photoreductive dissolution of lepidocrocite. Recent studies have shown that Fe(III)-DFOB complexes are not photochemically reactive in solution [12, 25]. Here, in-situ photoirradiation experiments were also performed in the presence of DFOB to provide reference spectra of a siderophore containing no carboxylic acid functional groups.

Fig. 8 shows the spectra of adsorbed DFOB at pH 8 and of adsorbed aerobactin at pH 4 before and immediately after 9 minutes of intense UV-A irradiation. An overall increase of vibrational bands was observed in both cases, caused by a temperature increase of the solution in the reaction cell (5 mL) from 25 °C to 40 °C during irradiation. The adsorption of DFOB and aerobactin to lepidocrocite increased by approximately 14 % and 10 %, respectively, as calculated by the increase of the most intense vibrational bands. These observations are in accordance with recent experimental findings which showed that surface concentrations of DFOB on goethite increased by 6 % and 22 % from 25 °C to 40 °C and 55 °C, respectively [37].

In contrast to the substantiated photolysis of citrate on lepidocrocite [27], we have no spectroscopic indication that the α -hydroxycarboxylic acid functional group of aerobactin is photolyzed at the surface. No distinct bands emerged or disappeared during irradiation. It is possible that no distinct spectral changes occurred, because the vibration spectra of aerobactin and the potential photoproduct are too similar. Additional photoirradiation experiments with aqueous Fe(III)-aerobactin complexes at pH 6 showed that under irradiation a strong electronic transition band at 260 nm emerged (data not presented), which is characteristic for the Fe(III)-aerobactin photoproduct [26]. This electronic transition is linked to the strong delocalization of π -electrons in the Fe(III)-coordinated ketoenolate functional group of the photoproduct complex - similar to Fe(III)(acac)₃ complexes [46]. In contrast, the IR spectra of the photoproduct showed no conclusive changes in spectral bands as compared to Fe(III)-aerobactin (data not presented). Therefore we conclude that photolysis of the α -hydroxycarboxylic acid group in aerobactin adsorbed at the surface of lepidocrocite cannot be investigated reliably by in-situ ATR-FTIR spectroscopy.

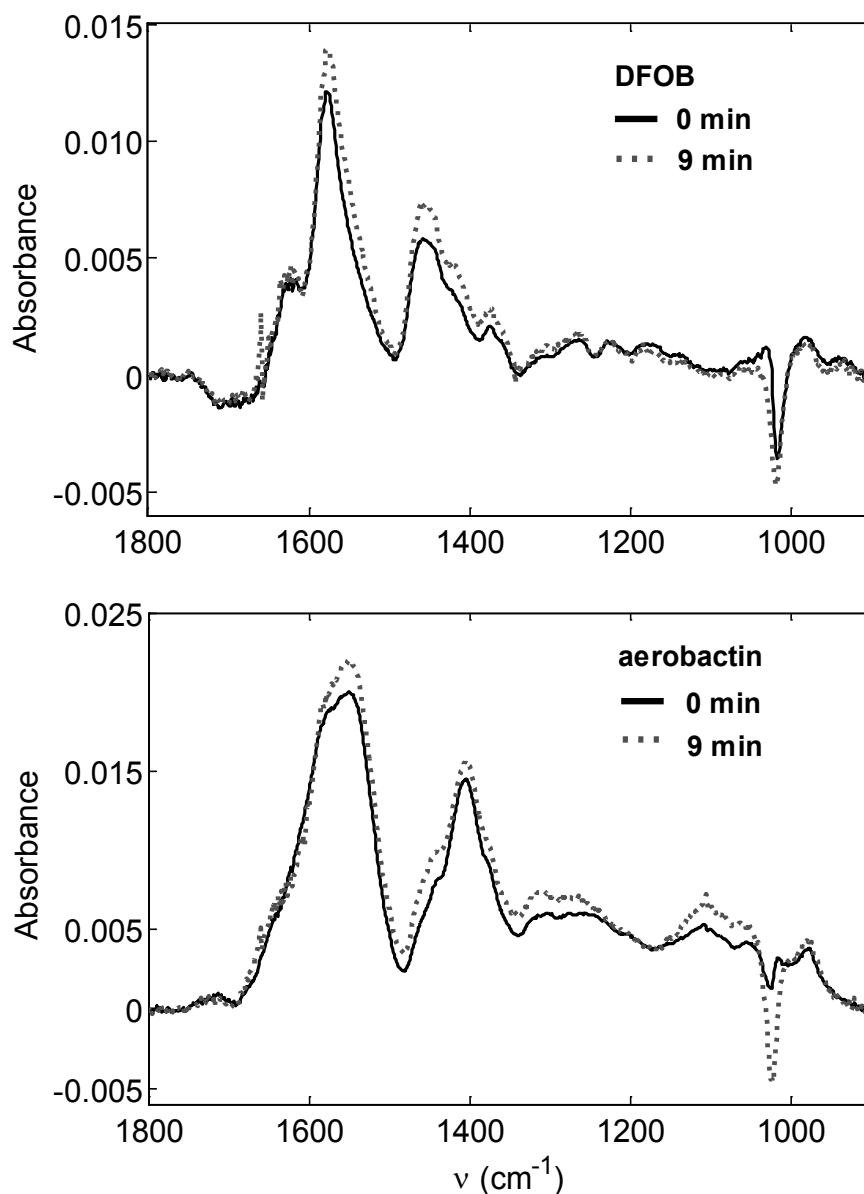


Fig. 8: Spectra of DFOB (pH 8) and aerobactin (pH 4) adsorbed to lepidocrocite (400 μM , $I=0.01\text{ M}$) before irradiation (solid black lines) and after 9 minutes of irradiation (gray dashed lines). Irradiance = 5 -10 W/cm^2 (300 - 500 nm).

4. Summary and conclusions

The spectroscopic data of DFOB adsorbed to lepidocrocite indicated that two to three hydroxamic acid groups within each adsorbed DFOB molecule were deprotonated in the pH range 4.0 to 8.2. Based on the high proton affinity of hydroxamic acid groups and the ability of hydroxamic acid groups to form energetically favorable five-membered Fe(III)-chelate rings, we propose that the dominant surface complex at the lower end

of this pH range (pH 4) involves inner-sphere coordination of two to three hydroxamic acid groups to the surface of lepidocrocite. From the spectroscopic data, we can neither conclusively deduce the number of potential surface species nor can we deduce the number of involved surface Fe(III) sites. With increasing pH, the surface speciation may also involve outer-sphere coordination with hydrogen bonding interactions. However, the results of dissolution experiments performed in our companion study indicate that the surface speciation between pH 3 and 8 in terms of dissolution-active surface species is not pH-dependent [9]. Thus, inner-sphere coordination of hydroxamic acids is likely predominant in this pH range. Surface concentrations of adsorbed DFOB were maximal at pH 8.6 and decreased at both higher and lower pH. At pH > 8.6, the spectroscopic data suggested that the surface speciation is affected by the deprotonation of residual non-deprotonated hydroxamic acid functional groups of adsorbed DFOB.

The investigation of the surface coordination of aerobactin was complicated by the fact that the vibration bands of the hydroxamic acid groups were masked by the much stronger bands of the carboxylic and α -hydroxycarboxylic acid groups. Due to the rather small spectral intensities of Fe(III)-coordinating and free hydroxamate bands the interactions of the hydroxamic acid groups in aerobactin with the surface of lepidocrocite could not be resolved. According to the SVD analysis of the spectral data of adsorbed aerobactin, at least three surface complexes were present between pH 3 and 9. At high pH, the spectra of adsorbed aerobactin strongly resembled solution analogs with deprotonated carboxylic acid groups, indicating outer-sphere complexation of the carboxylic acid groups. At low pH, a significant shift in the asymmetric ν_{COO^-} stretch vibration was observed, which is indicative of either inner-sphere complexation of carboxylic acid groups or outer-sphere complexation to the surface by strong ionic hydrogen bonding. Further evidence of the strong interactions of the lateral carboxylic acid groups (conceivably in combination with the adjacent amine groups) with the surface is provided in our companion study [9], where significant adsorption of the solution Fe(III)-aerobactin complexes to the surface at pH 6 was observed. However, we have no direct spectroscopic substantiation for the coordination of α -hydroxycarboxylic acid group that would indicate that this group participates in photodissolution of lepidocrocite by a surface photoredox reaction.

5. References

- [1] Yoshida, T., Hayashi, K. and Ohmoto, H. **2002**. Dissolution of iron hydroxides by marine bacterial siderophore. *Chem. Geol.* 184: 1-9.
- [2] Kraemer, S. M. **2004**. Iron oxide dissolution and solubility in the presence of siderophores. *Aquat. Sci.* 66: 3-18.
- [3] Kraemer, S. M., Butler, A., Borer, P. and Cervini-Silva, J. **2005**. Siderophores and the dissolution of iron-bearing minerals in marine systems. *Rev. Mineral. Geochem.* 59: 53-84.
- [4] Liermann, L. J., Kalinowski, B. E., Brantley, S. L. and Ferry, J. G. **2000**. Role of bacterial siderophores in dissolution of hornblende. *Geochim. Cosmochim. Acta* 64: 587-602.
- [5] Kraemer, S. M., Crowley, D. E. and Kretzschmar, R. **2006**. Geochemical aspects of phytosiderophore-promoted iron acquisition by plants. *Adv. Agron.* 91: 1-46.
- [6] Hersman, L., Lloyd, T. and Sposito, G. **1995**. Siderophore-promoted dissolution of hematite. *Geochim. Cosmochim. Acta* 59: 3327-3330.
- [7] Reichard, P. U., Kraemer, S. M., Frazier, S. W. and Kretzschmar, R. **2005**. Goethite dissolution in the presence of phytosiderophores: Rates, mechanisms, and the synergistic effect of oxalate. *Plant Soil* 276: 115-132.
- [8] Cheah, S. F., Kraemer, S. M., Cervini-Silva, J. and Sposito, G. **2003**. Steady-state dissolution kinetics of goethite in the presence of desferrioxamine B and oxalate ligands: implications for the microbial acquisition of iron. *Chem. Geol.* 198: 63-75.
- [9] Borer, P., Hug, S. J., Sulzberger, B., Kraemer, S. M. and Kretzschmar, R. **submitted**. Photodissolution of lepidocrocite (γ -FeOOH) in the presence of desferrioxamine B and aerobactin. *Geochim. Cosmochim. Acta*.
- [10] Winkelmann, G. **1991**. *Handbook of microbial iron chelates*. CRC Press: Boca Raton, Florida.
- [11] Barbeau, K. **2006**. Photochemistry of organic iron(III) complexing ligands in oceanic systems. *Photochem. Photobiol.* 82: 1505-1516.
- [12] Barbeau, K., Rue, E. L., Trick, C. G., Bruland, K. T. and Butler, A. **2003**. Photochemical reactivity of siderophores produced by marine heterotrophic bacteria and cyanobacteria based on characteristic Fe(III) binding groups. *Limnol. Oceanogr.* 48: 1069-1078.
- [13] Yang, J., Bremer, P. J., Lamont, I. L. and McQuillan, A. J. **2006**. Infrared spectroscopic studies of siderophore-related hydroxamic acid ligands adsorbed on titanium dioxide. *Langmuir* 22: 10109-10117.

-
- [14] Holmen, B. A., Tejedor-Tejedor, M. I. and Casey, W. H. **1997**. Hydroxamate complexes in solution and at the goethite-water interface: A cylindrical internal reflection Fourier transform infrared spectroscopy study. *Langmuir* 13: 2197-2206.
- [15] Edwards, D. C. and Myneni, S. C. B. **2005**. Hard and soft X-ray absorption spectroscopic investigation of aqueous Fe(III)-hydroxamate siderophore complexes. *J. Phys. Chem. A* 109: 10249-10256.
- [16] Edwards, D. C. and Myneni, S. C. B. **2006**. Near edge x-ray absorption fine structure spectroscopy of bacterial hydroxamate siderophores in aqueous solutions. *J. Phys. Chem. A* 110: 11809-11818.
- [17] Edwards, D. C., Nielsen, S. B., Jarzecki, A. A., Spiro, T. G. and Myneni, S. C. B. **2005**. Experimental and theoretical vibrational spectroscopy studies of acetohydroxamic acid and desferrioxamine B in aqueous solution: Effects of pH and iron complexation. *Geochim. Cosmochim. Acta* 69: 3237-3248.
- [18] McWhirter, M. J., Bremer, P. J., Lamont, I. L. and McQuillan, A. J. **2003**. Siderophore-mediated covalent bonding to metal (oxide) surfaces during biofilm initiation by *Pseudomonas aeruginosa* bacteria. *Langmuir* 19: 3575-3577.
- [19] Upritchard, H. G., Yang, J., Bremer, P. J., Lamont, I. L. and McQuillan, A. J. **2007**. Adsorption to metal oxides of the *Pseudomonas aeruginosa* siderophore pyoverdine and implications for bacterial biofilm formation on metals. *Langmuir* 23: 7189-7195.
- [20] Hansen, D. C., McCafferty, E., Lins, C. W. and Fitzpatrick, J. J. **1995**. An FT-IR investigation of parabactin adsorbed onto aluminum. *Appl. Surf. Sci.* 84: 85-90.
- [21] Siebner-Freibach, H., Hadar, Y., Yariv, S., Lapides, I. and Chen, Y. **2006**. Thermospectroscopic study of the adsorption mechanism of the hydroxamic siderophore ferrioxamine B by calcium montmorillonite. *J. Agric. Food Chem.* 54: 1399-1408.
- [22] Loring, J. S., Simanova, A. A. and Persson, P. **2008**. Highly mobile iron pool from a dissolution-readsorption process. *Langmuir* 24: 7054-7057.
- [23] Kendall, T. A. and Hochella, M. F. **2003**. Measurement and interpretation of molecular-level forces of interaction between the siderophore azotobactin and mineral surfaces. *Geochim. Cosmochim. Acta* 67: 3537-3546.
- [24] Kendall, T. A., Hochella, M. F. and Becker, U. **2005**. Computational modeling of azotobactin-goethite/diaspore interactions: applications to molecular force measurements and siderophore-mineral reactivity. *Chem. Geol.* 216: 17-35.
- [25] Borer, P. M., Sulzberger, B., Reichard, P. and Kraemer, S. M. **2005**. Effect of siderophores on the light-induced dissolution of colloidal iron(III)(hydr)oxides.

- Mar. Chem.* 93: 179-193.
- [26] Kuepper, F. C., Carrano, C. J., Kuhn, J. U. and Butler, A. **2006**. Photoreactivity of iron(III)-aerobactin: Photoproduct structure and iron(III) coordination. *Inorg. Chem.* 45: 6028-6033.
- [27] Borer, P., Hug, S. J., Sulzberger, B., Kraemer, S. M. and Kretzschmar, R. **2007**. Photolysis of citrate on the surface of lepidocrocite: An in situ attenuated total reflection infrared spectroscopy study. *J. Phys. Chem. C* 111: 10560-10569.
- [28] Smith, R. M., Martell, A.E., Motekaitis, R.J. **2001**. *NIST standard reference database 46*, vers. version 6.0. Gaithersburg, MD, USA.
- [29] Hug, S. J. and Sulzberger, B. **1994**. In-situ Fourier-transform infrared spectroscopic evidence for the formation of several different surface complexes of oxalate on TiO₂ in the aqueous-phase. *Langmuir* 10: 3587-3597.
- [30] Nightingale, R. E. and Wagner, E. L. **1954**. The vibrational spectra and structure of solid hydroxylamine and deuterio-hydroxylamine. *J. Chem. Phys.* 22: 203-208.
- [31] Harris, W. R., Carrano, C. J. and Raymond, K. N. **1979**. Coordination chemistry of microbial iron transport compounds:16. Isolation, characterization, and formation-constants of ferric aerobactin. *J. Am. Chem. Soc.* 101: 2722-2727.
- [32] Norén, K. and Persson, P. **2007**. Adsorption of monocarboxylates at the water/goethite interface: The importance of hydrogen bonding. *Geochim. Cosmochim. Acta* 71: 5717-5730.
- [33] Parthasarathi, R. and Subramanian, V. (2006). Characterization of hydrogen bonding: From van der Waals interactions to covalency: Unified picture of hydrogen bonding based on electron density topography analysis. In: *Hydrogen Bonding - New Insights*. S. J. Grabowski, Ed. Springer, Dordrecht: 1-50.
- [34] Persson, P. and Axe, K. **2005**. Adsorption of oxalate and malonate at the water-goethite interface: molecular surface speciation from IR spectroscopy. *Geochim. Cosmochim. Acta* 69: 541-552.
- [35] Kummert, R. and Stumm, W. **1980**. The surface complexation of organic-acids on hydrous γ -Al₂O₃. *J. Colloid Interface Sci.* 75: 373-385.
- [36] Cornell, R. M. and Schwertmann, U. **2003**. *The Iron Oxides: Structure, Properties, Reactions, Occurrences and Uses*. 2 ed.; Wiley-VCH: Weinheim, Germany.
- [37] Coccozza, C., Tsao, C. C. G., Cheah, S. F., Kraemer, S. M., Raymond, K. N., Miano, T. M. and Sposito, G. **2002**. Temperature dependence of goethite dissolution promoted by trihydroxamate siderophores. *Geochim. Cosmochim. Acta* 66: 431-438.

- [38] Holmen, B. A. and Casey, W. H. **1996**. Hydroxamate ligands, surface chemistry, and the mechanism of ligand-promoted dissolution of goethite [α -FeOOH(s)]. *Geochim. Cosmochim. Acta* 60: 4403-4416.
- [39] Hug, S. J. and Bahnemann, D. **2006**. Infrared spectra of oxalate, malonate and succinate adsorbed on the aqueous surface of rutile, anatase and lepidocrocite measured with in situ ATR-FTIR. *J. Electron Spectrosc. Relat. Phenom.* 150: 208-219.
- [40] Kraemer, S. M., Cheah, S. F., Zapf, R., Xu, J. D., Raymond, K. N. and Sposito, G. **1999**. Effect of hydroxamate siderophores on Fe release and Pb(II) adsorption by goethite. *Geochim. Cosmochim. Acta* 63: 3003-3008.
- [41] Filius, J. D., Hiemstra, T. and Van Riemsdijk, W. H. **1997**. Adsorption of small weak organic acids on goethite: Modeling of mechanisms. *J. Colloid Interface Sci.* 195: 368-380.
- [42] Stumm, W., Kummert, R. and Sigg, L. **1980**. A ligand-exchange model for the adsorption of inorganic and organic-ligands at hydrous oxide interfaces. *Croat. Chem. Acta* 53: 291-312.
- [43] Horanyi, G. **2002**. Specific adsorption of simple organic acids on metal(hydr) oxides: A radiotracer approach. *J. Colloid Interface Sci.* 254: 214-221.
- [44] Deacon, G. B., Huber, F. and Phillips, R. J. **1985**. Diagnosis of the nature of carboxylate coordination from the direction of shifts of carbon oxygen stretching frequencies. *Inorg. Chim. Acta* 104: 41-45.
- [45] Noren, K., Loring, J. S. and Persson, P. **2008**. Adsorption of alpha amino acids at the water/goethite interface. *J. Colloid Interface Sci.* 319: 416-428.
- [46] Barnum, D. W. **1961**. Electronic absorption spectra of acetyl-acetonato complexes - 1. Complexes with trivalent transition metal ions. *J. Inorg. Nucl. Chem.* 21: 221-237.

Supporting Information

Chapter 3

Table of contents

IR Spectra of DFOB-methanesulfonate and methanesulfonate	94
IR spectra of the aqueous Fe(III)-aerobactin complex	94
IR spectra of dry lepidocrocite	95

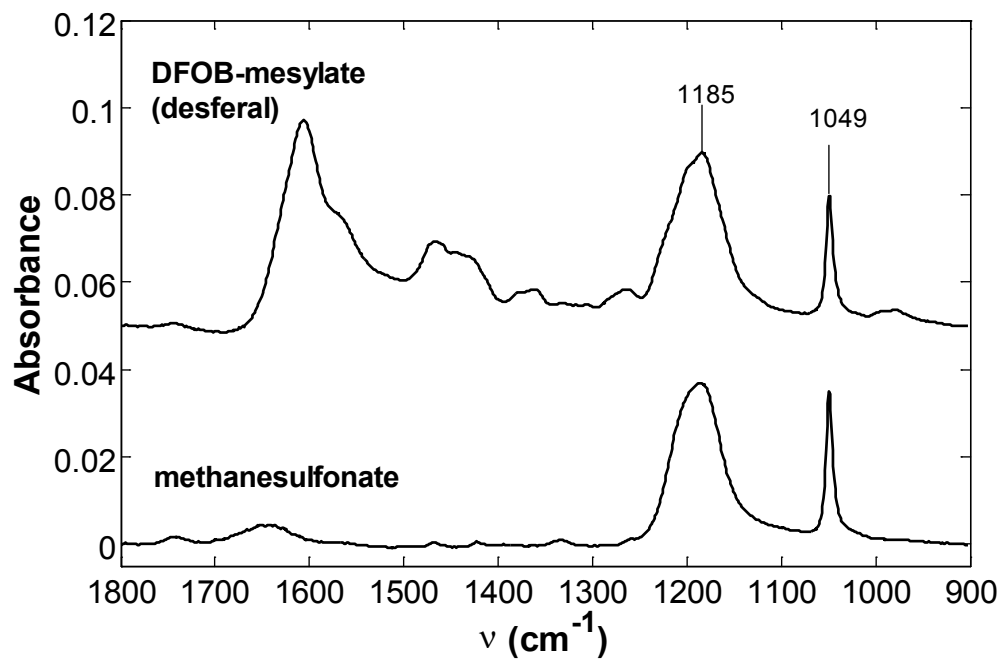


Fig. S1: IR spectra of solutions containing either the mesylate form of desferrioxamine B (50 mM) at pH 5.5 or methanesulfonate (50 mM) at pH 4.0.

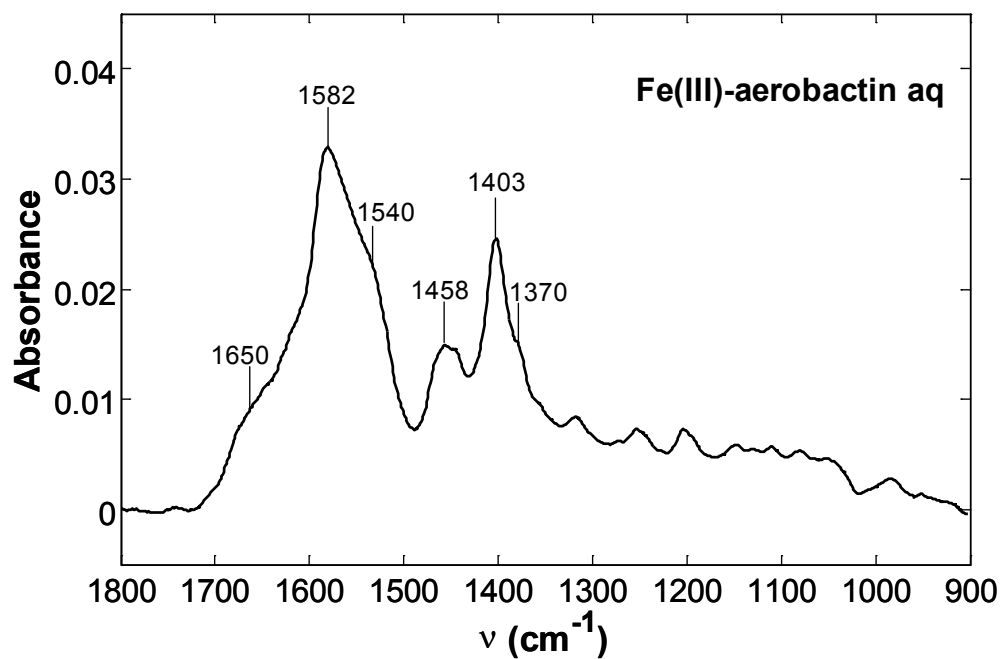


Fig. S2: IR spectrum of a solution containing 14 mM of Fe(III)-aerobactin complexes and 16 mM of free aerobactin at pH 6.

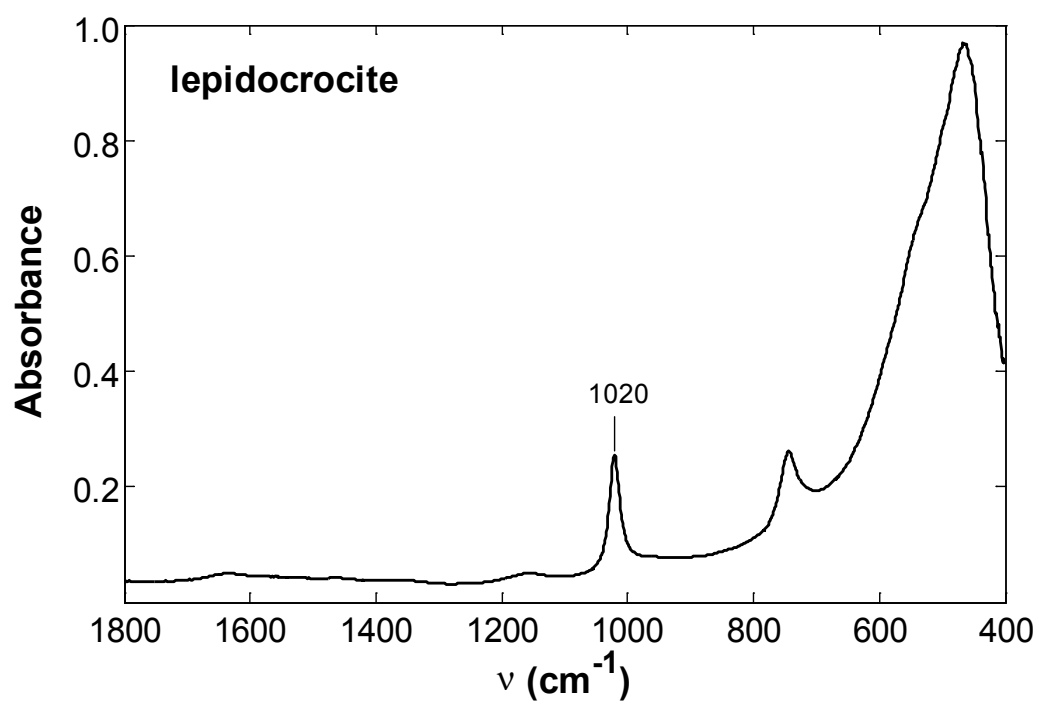


Fig. S3: IR spectra of a dry lepidocrocite film

Chapter 4

Photodissolution of lepidocrocite (γ -FeOOH) in the presence of desferrioxamine B and aerobactin

Paul Borer, Stephan M. Kraemer, Barbara Sulzberger, Stephan J. Hug,
and Ruben Kretzschmar

Prepared for publication in Geochimica et Cosmochimica Acta

Abstract

Batch adsorption and dissolution experiments with lepidocrocite (γ -FeOOH) and two model siderophores, desferrioxamine B (DFOB) and aerobactin, were performed between pH 3 and 8 in the dark and under irradiation with UV-visible light. The increase in surface concentrations of adsorbed DFOB with increasing pH was explained in terms of electrostatic interactions between the protonated and charged terminal amine group of DFOB surface complexes and the charged lepidocrocite surface. The adsorption of aerobactin was consistent with the typical anion-like adsorption behavior of low molecular weight organic acids and indicated that the adsorption properties are strongly determined by the carboxylic acid groups. The adsorption experiments revealed furthermore that the Fe(III)-DFOB solution complex has a very low affinity for the surface, in contrast to Fe(III)-aerobactin solution complexes. In accordance with a surface-controlled mechanism of ligand-promoted dissolution, we found a linear correlation between dissolution rates of lepidocrocite and the surface concentrations of adsorbed DFOB. In the dark, 6- to 8-fold lower dissolution rate coefficients were determined for aerobactin in comparison to DFOB, indicating that less dissolution-reactive surface complexes of aerobactin were formed at the surface of lepidocrocite. These results suggest that aerobactin forms surface complexes where only a fraction of the functional groups binds in a dissolution-active coordination-mode in addition to the formation of a higher degree of multinuclear surface complexes, resulting in slower detachment kinetics of the surface metal complexes. For both DFOB and aerobactin, dissolution rate coefficients increased significantly under irradiation with UV-visible light. This increase was interpreted in terms of light-induced reduction of surface Fe(III),

primarily by intrinsic photochemical processes of the lepidocrocite bulk phase, based on the observed photoreductive dissolution in the absence of organic ligands between pH 3 and 6. We hypothesize that the α -hydroxycarboxylate group of aerobactin may form a surface complex with surface Fe(III) and may additionally promote photoreductive dissolution by a ligand-to-metal charge-transfer (LMCT) reaction, similar to citrate. However, LMCT reactions involving the α -hydroxycarboxylate group of aerobactin are rather ineffective, based on the comparison of dissolution rate coefficients determined in the presence of aerobactin and citrate in irradiated lepidocrocite suspensions.

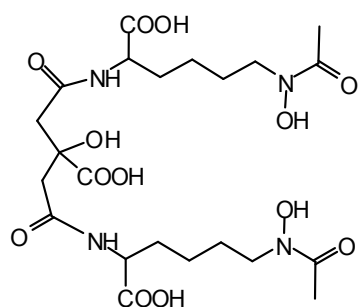
1. Introduction

Dissolution of iron (hydr)oxides and other iron-bearing minerals by siderophores is a key step in an important biological iron acquisition mechanism in terrestrial and aquatic systems with low iron bioavailability [1-5]. An example for large scale ecosystems where primary productivity is limited by the low bioavailability of iron are the so-called high-nutrient low-chlorophyll (HNLC) ocean areas. In the photic zone of these ocean areas, siderophores may promote iron oxide dissolution by shifting the iron solubility and by promoting surface-controlled dissolution mechanisms [1]. Borer et al. (2005) have shown that photoreductive dissolution of iron oxides in the presence of siderophores may provide an efficient means to increase the bioavailability of iron to marine bacteria and potentially to marine phytoplankton.

Recent investigations of siderophore-promoted dissolution of iron(III) (hydr)oxides in pure iron(III) (hydr)oxide/siderophore systems have shown that dissolution rates are linearly correlated with surface concentrations of adsorbed siderophores [6, 7]. These observations suggest that dissolution of iron(III) (hydr)oxides in the presence of siderophores is promoted by the formation of surface siderophore complexes and that the rate determining step is the detachment of the surface Fe(III)-complex. Thus, dissolution of iron(III) (hydr)oxides in the presence of siderophores can be described by a rate expression for ligand-promoted dissolution as proposed by Furrer and Stumm (1986). In the rate expression of equation 1, the overall dissolution rate R is described as the sum of the rate of siderophore-promoted dissolution, which is related to the surface concentration of adsorbed siderophores by the dissolution rate coefficient k [8], and the rate of proton-promoted dissolution R_H .

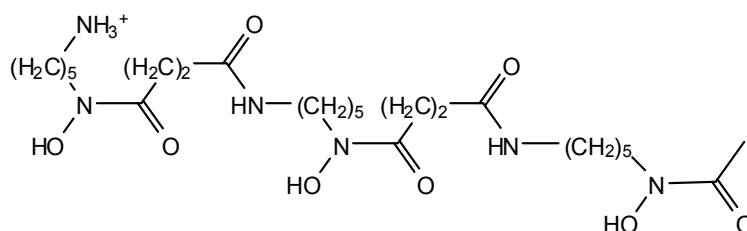
$$R = k * [\text{siderophore}]_{\text{adsorbed}} + R_H \quad [1]$$

The aim of this study was to investigate the thermal and photoreductive dissolution of lepidocrocite (γ -FeOOH) in the presence of the model siderophores desferrioxamine B (DFOB) and aerobactin (Fig. 1) and to investigate the dissolution reactivity of these siderophores based on a comparison of determined dissolution rate coefficients. DFOB and aerobactin are structurally different siderophores and may interact very differently with the surface of lepidocrocite. DFOB contains three metal binding groups (hydroxamic acid functional groups), whereas aerobactin has five metal-binding groups (two hydroxamic acids, one α -hydroxycarboxylic acid group and two lateral carboxylic acid groups). Aerobactin is a particularly interesting siderophore as it contains a photoreactive iron-binding group (α -hydroxycarboxylic acid). Recent studies have shown that solution Fe(III)-aerobactin complexes undergo a light-induced redox reaction, leading to the reduction of Fe(III) and oxidation of the α -hydroxycarboxylic acid group [9, 10]. To investigate whether the α -hydroxycarboxylic acid group is coordinated and photolyzed at the surface, we conducted dissolution experiments under irradiation with UV-visible light (300–460 nm). To assess the role of the α -hydroxycarboxylic acid group in the light-induced dissolution of lepidocrocite, we compared the dissolution reactivity of aerobactin with citrate, which also contains an α -hydroxycarboxylic acid group.



aerobactin

H_5 (aerobactin); pK_a values: - carboxylic acid: 3.11, 3.48, 4.31
- hydroxamic acid: 8.93, 9.44



desferrioxamine B

H_3 (HDFOB); pK_a values: - hydroxamic acid: 8.32, 8.96, 9.55
- amine group: 10.79

Fig. 1: Chemical structures of desferrioxamine B (DFOB) and aerobactin and pK_a values of the functional groups at 0.01 M ionic strength [14, 18].

2. Experimental section

2.1 Samples

Iron-free aerobactin ($C_{22}H_{32}O_{12}N_4$, lyophilized, from EMC microcollections in Tübingen, Germany) was used as received. Desferrioxamine B (DFOB) was received as the methanesulfonate salt ($[C_{25}H_{46}N_5O_8NH_3^+(CH_3SO_3)^-]$, Sigma Aldrich) and was converted to the chloride salt by using an anion exchange resin [11]. Stock solutions of DFOB and aerobactin were either stored at $-20\text{ }^\circ\text{C}$ or freshly prepared. Siderophore concentrations in the stock solutions were determined by total organic carbon measurements (Shimadzu 5000A). Unlabeled and ^{14}C -labeled citrate (1,5- ^{14}C -citric acid, specific activity of 110 mCi/mmol) were obtained from Sigma Aldrich and used as received.

The synthesis and characterization of lepidocrocite used in this study has been reported elsewhere [12]. A specific surface area of $130\text{ m}^2/\text{g}$ was determined by multipoint N_2 -BET analysis and the point of zero charge ($\text{pH}_{\text{pZC}} = 7.4$) was determined by acid-base titration at different ionic strengths. Acid-base titration data were measured by a standard procedure [13] with an initial solid concentration of 16.66 g/L in solutions with 0.01, 0.03, 0.1 and 0.3 M NaClO_4 (Fig. S1 in the Supporting Information).

2.2 Adsorption of siderophores

Adsorption experiments with DFOB and aerobactin were conducted between pH 3 and 8 in 0.01 M NaClO_4 background electrolyte. In addition, some adsorption experiments were conducted at 0.2 M NaClO_4 . Adsorption of DFOB to lepidocrocite was determined in suspensions containing typically 1.5 g/L solid and initial DFOB concentrations of 0-200 μM . The solid concentration for adsorption experiments with aerobactin was varied between 0.2 and 1.5 g/L . Due to the limited amount of aerobactin available, only two points on each aerobactin adsorption isotherm were measured. Initial aerobactin concentrations were chosen to enable a linear interpolation of the amount of aerobactin adsorbed at a solution concentration of 30 μM .

Adsorption experiments were conducted in a temperature-controlled laboratory at $22 \pm 1\text{ }^\circ\text{C}$ in the dark. All glassware used for the adsorption experiments was acid washed and heated for three hours at $500\text{ }^\circ\text{C}$ in a muffle furnace. Lepidocrocite stock suspensions were freshly prepared in 500 mL glass bottles (Schott, Mainz, Germany) at the appropriate ionic strength and stirred by magnetic stir bars. The stock suspensions for the adsorption experiments were constantly purged with high purity N_2 gas to circumvent the input of CO_2 from air and adsorption of carbonate species. The pH of

the stock suspensions was constantly measured and adjusted during the adsorption experiments by small additions of HClO_4 and NaOH . Aliquots of the lepidocrocite stock suspension were transferred to 10 mL glass vials. These suspensions were also purged with high purity N_2 gas and were stirred vigorously. Small volumes of stock solutions of DFOB and aerobactin were added to the lepidocrocite suspension. Within 1 min after addition of DFOB or aerobactin, the pH of the suspension was adjusted to the desired value by addition of HClO_4 or NaOH . During the short reaction time of 15 min, the pH could be maintained within ± 0.05 pH units. The reaction time was optimized such that fast dissolution of lepidocrocite occurring during the adsorption experiments resulted in dissolved Fe(III) concentrations of less than 10 % of the initial free ligand concentrations. The adsorption isotherms were corrected for the decrease of free (uncomplexed) ligand concentrations in solution by formation of dissolved Fe(III)-siderophore complexes due to dissolution of lepidocrocite. After the short reaction time, the suspensions were filtered through $0.025 \mu\text{m}$ nitrocellulose filters (NC 03, Whatman). The solution concentrations of free siderophores and Fe(III)-siderophore complexes in the filtrates were determined by measuring total iron concentrations by ICP-OES and total dissolved carbon by TOC analysis (Shimadzu 5000A). The nitrocellulose filter membranes used in these adsorption experiments were preconditioned by a washing procedure with high purity water at max. 60°C . By exchanging the water solution at least 10 times (two-day procedure), the extent of carbon leakage from the filter membrane filtration could be diminished. Filtration of 5-10 mL high purity water through a preconditioned filter led to a carbon content in the filtrate of less than 1 mg/L C. In each adsorption experiment at least 5 blanks (filtered lepidocrocite suspension without any ligands) were measured to account for carbon leakage by the filter membranes. The ligand concentrations in the filtrates, as determined by total organic carbon analysis, were corrected for carbon leakages of the filter membranes. The standard error of the mean carbon content in the blanks was maximum 10 %. A maximum error of 10 % was also estimated for the measurements of total organic carbon in filtered samples of the adsorption experiments. Filtered samples from the adsorption experiments as well as unfiltered DFOB and aerobactin reference samples were acidified with HCl (suprapure, 1% v/v, Fluka) and diluted to a maximum carbon concentration of 5 mg/L C. The concentrations of adsorbed DFOB or aerobactin were determined by calculating the difference between ligand concentrations in the filtrates and the concentration of appropriate ligand reference solutions. Due to the formation of dissolved Fe(III)-siderophore complexes during the adsorption experiments, the solution concentrations of free (uncomplexed) ligands were calculated by subtracting the measured concentrations of dissolved Fe(III)-ligands (measurement of total dissolved iron by ICP-OES) from

the concentrations of total dissolved ligands (free ligand and Fe(III)-ligand complexes) as determined by TOC analysis.

2.3 Readsorption of Fe(III)-siderophore complexes

In order to quantify the readsorption of Fe(III)-siderophore complexes during dissolution of lepidocrocite, adsorption experiments with 1:1 Fe(III)-complexes of DFOB and aerobactin were performed in 0.01 M background electrolyte (NaClO_4). A 60 μM stock solution of 1:1 Fe(III)-DFOB complexes was prepared by mixing a stock solution of $\text{FeCl}_3 \cdot 6\text{H}_2\text{O}$ with a stock solution of DFOB. The pH of the resulting stock solution was adjusted to neutral pH with NaOH and it was analyzed by UV-visible spectrometry (Fe(III)-DFOB complexes, extinction coefficient of $\sim 2600 \text{ M}^{-1} \text{ cm}^{-1}$ at 430 nm), ICP-OES (total iron concentration) and TOC analysis (total ligand concentration). Comparison of the three analysis methods served to check (within the detection limits of the analytical methods) that only 1:1 complexes and no free ligands or an excess of Fe(III) were present in the stock solution.

A pure stock solution of 1:1 Fe(III)-aerobactin complexes at neutral pH could not be synthesized in this way and would have required subsequent purification by HPLC. However, due to the limited amount of available aerobactin a purification step was not feasible. Instead, approximately 65 μM aerobactin was added to a lepidocrocite suspension of 100 mg/L at pH 5 and was left to react for 10 days in the dark. Thereafter, the solution was filtered and was analyzed for total ligand concentrations and total iron concentrations by TOC and ICP-OES analysis. The presence of 1:1 Fe(III)-aerobactin complexes was supported by the analysis of measured UV-visible absorption spectra [14]. Due to the loss of aerobactin in suspension by adsorption to lepidocrocite, additional aerobactin was added to the filtered stock solution (pH 6). The final stock solution contained 43 μM free aerobactin and 21 μM 1:1 Fe(III)-aerobactin complexes (at pH 6). The stock solution was stored in the dark at 4 °C and used within a few days.

Adsorption experiments were performed by adding 2.5 mL of the Fe(III)-siderophore stock solutions to 2.5 mL of lepidocrocite suspensions of pre-adjusted pH (suspensions were constantly purged with high purity N_2 gas throughout the experiments). The pH of the suspensions was varied between pH 3 and 8. The concentration of Fe(III)-DFOB complexes in these adsorption experiments was 30 μM and the solid concentration was 1.5 g/L. The suspensions were vigorously stirred during the reaction time of 20 min. The pH of the suspension was constantly measured and only negligible pH shifts were observed ($\Delta\text{pH} = \pm 0.1$) so that no additional pH adjustments were necessary. The solid concentration for the Fe(III)-aerobactin adsorption experiments was varied

between 0.2 g/L and 1.0 g/L (pH dependent). The concentration of aerobactin and 1:1 Fe(III)-aerobactin complexes was 21.5 μM and 10.5 μM , respectively. During these experiments, the pH was not maintained at a constant value by addition of HClO_4 or NaOH . pH shifts observed during these experiments decreased with longer equilibration times. The maximum pH shift over the entire reaction time was $\Delta\text{pH} = + 0.6$, observed at higher pH.

2.4 (Photo)dissolution experiments

To investigate photodissolution of lepidocrocite in suspensions of small volumes, we used a custom-built photoirradiation setup which consisted of a flow-through water-bath with a Quartz glass window on each side facing towards a fluorescent lamp (Philipps TL-D 15W/05 or TL-DK 30W/05). Inside the water bath, a cuvette holder (made of Plexiglas) was placed, in which up to eleven cuvettes of 4.5 mL volume were inserted. UV-transparent PMMA cuvettes (Semadeni) with excellent transmission down to 300 nm were used for the (photo)dissolution experiments. The flow-through water-bath was placed on a Variomag multipoint stirrer and the suspensions in the cuvettes were stirred by mini Teflon-coated stir bars. Under irradiation, the temperature of the suspensions in the cuvettes was maintained at $25 \pm 2^\circ\text{C}$. An incident light intensity at the surface of the cuvettes of 70 W/m^2 was determined by 0.1 M ferrioxalate actinometry [15]. The spectrum of light emitted by the fluorescent lamps ranged from 300 nm to 460 nm with maximum emission at 365 nm.

Dissolution experiments were conducted with suspensions of 25 mg/L lepidocrocite in the presence or absence of 30 μM DFOB or 30 μM aerobactin. Lepidocrocite suspensions were freshly prepared in high-purity water (Milli-Q, Millipore) for each experiment. Experiments were performed in the dark and under irradiation between pH 3 and 8. In contrast to the adsorption experiments, the suspensions for the dissolution experiments in the presence of DFOB or aerobactin were not purged with N_2 . The background electrolyte in the suspensions was either 0.01 or 0.2 M NaClO_4 . The pH of the suspensions in the cuvettes was measured periodically with a pH electrode (Metrohm 6.0234.100) and was maintained within 0.05 pH units by addition of small amounts of HClO_4 and NaOH . At regular time intervals, cuvettes were removed from the photoirradiation setup and the suspensions were filtered through 0.025 μm nitrocellulose filters (Whatman). The filtrate was diluted with high purity water, acidified with HNO_3 (suprapure, 1% v/v, Fluka) and subsequently measured for total dissolved iron by ICP-OES (Varian Vista MPX). For photodissolution experiments conducted in the absence of siderophores, filtered samples were also analyzed for dissolved Fe(II) by a modified

ferrozine method [16].

To investigate if readsorption of Fe(III)-aerobactin complexes and Fe-aerobactin photoproducts formed in solution [10] affects dissolution rates of lepidocrocite, additional photodissolution experiments were conducted in the presence/absence of initial concentrations of Fe(III)-aerobactin complexes at pH 6. These photodissolution experiments were performed with 25 mg/L lepidocrocite suspensions in 0.01 M background electrolyte (NaClO_4) in the presence of either 21.5 μM aerobactin plus 10.5 μM Fe(III)-aerobactin complexes or in the presence of 22 μM aerobactin only. Total dissolved iron in the filtered suspensions was measured by ICP-OES.

2.5 Adsorption and dissolution experiments with citrate

A photodissolution experiment with a 25 mg/L lepidocrocite suspension in the presence of 30 μM citrate was performed at pH 4 and 0.01 M ionic strength (NaClO_4). The photoirradiation setup used for this experiment is described elsewhere [12]. The suspension in the reaction vessel was constantly purged with high-purity N_2 gas. Samples for total iron analysis were filtered, acidified and measured by ICP-OES as in the photodissolution experiments described above. Citrate adsorption experiments were performed according to the same procedures as for the siderophore adsorption experiments. A constant spike of ^{14}C -labeled citrate with different total concentrations of unlabeled citrate was added to 0.4 or 0.8 g/L lepidocrocite suspensions at pH 4. The reaction time was kept rather short (15 min) to minimize dissolution of lepidocrocite leading to the formation of Fe(III)-citrate complexes in solution. The free dissolved citrate concentrations in the filtrates were corrected for the presence of Fe(III)-citrate complexes. Adsorbed citrate concentrations were determined by the loss of ^{14}C activity of ^{14}C -labeled citrate in solution with a scintillation counter (Liquid Scintillation Analyzer 2200CA, Packard).

3. Results and discussion

3.1 Adsorption of DFOB and aerobactin to lepidocrocite

Fig. 2A shows adsorption isotherms of DFOB determined between pH 3 and pH 8 at 0.01 M ionic strength. The adsorption isotherms show that DFOB has a high affinity for the surface at low surface coverage. Adsorption of DFOB increased with increasing pH (see also Fig. 3), particularly above pH 6. Surface concentrations of adsorbed DFOB (normalized to the surface area) were approximately three times higher on

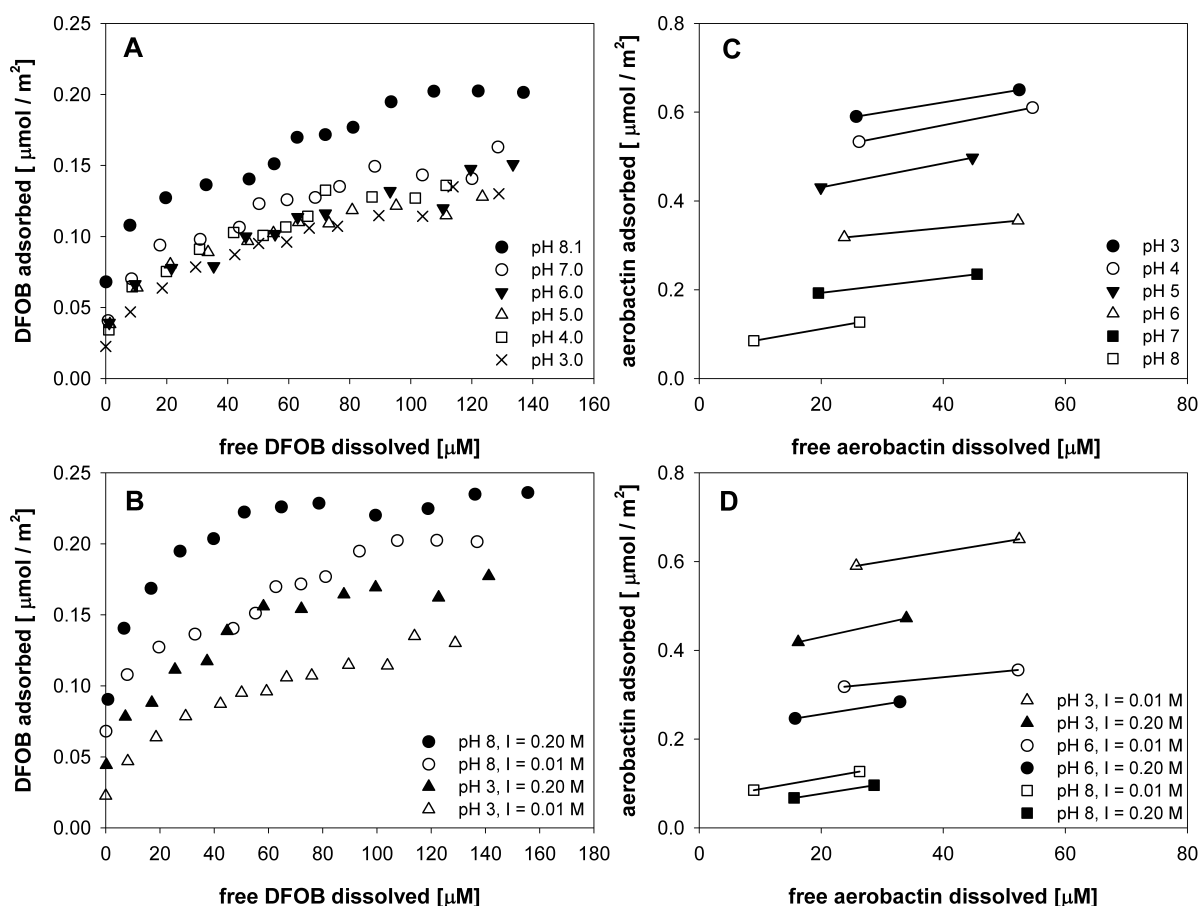


Fig. 2: Adsorption isotherms of DFOB (A) or aerobactin (C) as a function of pH at constant ionic strength ($I = 0.01 \text{ M NaClO}_4$). The effect of ionic strength on the adsorption isotherms of DFOB (B) or aerobactin (D) is illustrated for selected pH. The equilibration time was 15 min.

lepidocrocite than on goethite, where surface concentrations between $0.04\text{--}0.07 \mu\text{mol}/\text{m}^2$ have been reported ($150 \mu\text{M}$ DFOB, 13 g/L goethite, $I = 0.01 \text{ M NaClO}_4$, pH 3-9) [17].

In a companion ATR-FTIR spectroscopic study, we investigated the adsorption of DFOB and aerobactin to lepidocrocite at the molecular level [11]. According to this study, we concluded that DFOB adsorbs to the surface of lepidocrocite predominantly by inner-sphere complexation of two to three hydroxamic acid groups to surface Fe(III) sites at acidic pH values (pH 4). With increasing pH towards the point of zero charge of lepidocrocite ($\text{pH}_{\text{PZC}} = 7.4$) and towards the pK_a values of the hydroxamic acid functional groups (pK_a : 8.32, 8.96, 9.55 [18]), we could not provide conclusive information on the surface speciation of adsorbed DFOB in terms of inner- or outer-sphere complexation of the hydroxamic acid groups based on the spectroscopic data alone [11]. However, the ability of hydroxamic acids to form stable five-membered chelate rings with Fe(III)

[19, 20] suggests that in the experimental pH range (3-8) inner-sphere complexation of hydroxamic acid groups of DFOB is significant.

Recent adsorption experiments with acetohydroxamic acid on goethite indicated that hydroxamate surface complexes have no charge [21]. Surface concentrations of adsorbed acetohydroxamic acid were constant pH between pH 4 and 8, which stands in contrast to the pH-dependent increase of surface concentrations of adsorbed DFOB in this study (Fig. 3). Based on the study by Holmen and Casey (1996), we assume that the DFOB surface complex is positively charged in the experimental pH range (3-8), due to the protonated terminal amine group (pK_a : 10.79 [18]). Increasing surface concentrations of DFOB towards and above the point of zero charge of lepidocrocite ($pH_{pZC} = 7.4$) can be explained by a decrease of repulsive electrostatic interactions of the positively charged amine group of DFOB with the (positively) charged surface. With an increase in negatively charged surface sites near and above the point of zero charge, positive electrostatic interactions and/or hydrogen bonding of the positively charged amine group with negatively charged surface sites may also influence the adsorption of DFOB. In our ATR-FTIR spectroscopic study [11], adsorption of DFOB to lepidocrocite was investigated in a broader pH range (pH 4-10.6). Maximum adsorption was observed at approximately pH 8.6 above which surface concentrations of DFOB decreased again. These observations are consistent with anion-like adsorption of weak acids, where maximum adsorption is observed near the pK_a values of the acid functional groups [22].

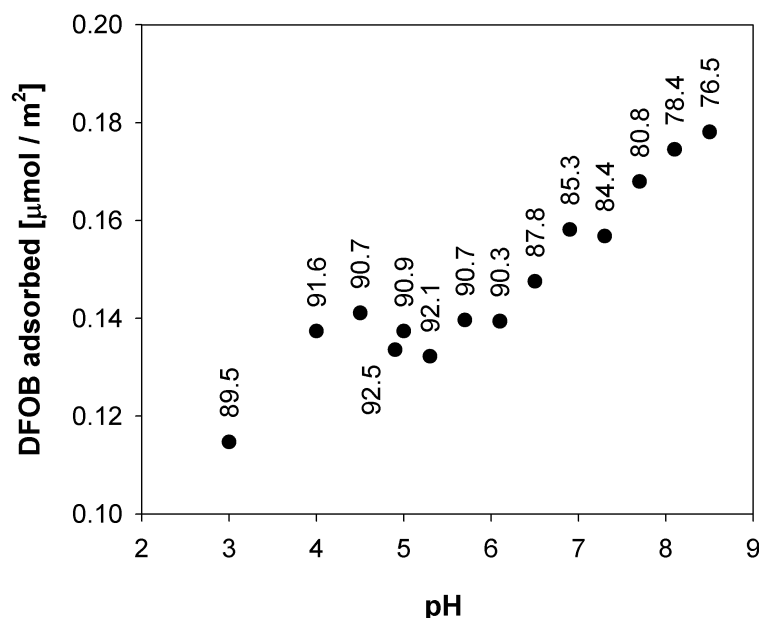


Fig. 3: DFOB adsorption as a function of pH at 0.01 M ionic strength (NaClO_4). Initial DFOB concentration: 125 μM , 1.5 g/L lepidocrocite, reaction time: 15 minutes. The labels show the resulting solution concentrations of free (uncomplexed) DFOB after the reaction time. Error estimates of the surface concentrations are within 10 %.

Fig. 2C shows surface concentrations of aerobactin determined for two different total ligand concentrations as a function of pH. Adsorption of aerobactin decreased with increasing pH, consistent with anion-like adsorption of carboxylic acids [22-24]. This observation indicates that the adsorption properties of aerobactin are strongly determined by the carboxylic acid groups. Surface interactions with the carboxylic acid groups apparently result in a higher affinity of aerobactin for the surface compared to DFOB, based on the comparison of surface concentrations under equivalent conditions (cf. Fig. 2A and C). The formation of surface complexes of aerobactin was also investigated by ATR-FTIR spectroscopy [11]. The ATR-FTIR spectra suggested that the carboxylic acid groups tend to form outer-sphere complexes at the surface at higher pH, and that inner-sphere complexes of the carboxylic acid groups and/or outer-sphere complexes with hydrogen-bonding interactions form at low pH [11]. However, the surface interactions of the hydroxamic acid groups in aerobactin could not be resolved by ATR-FTIR spectroscopy, due to the exceedingly small spectral contributions of hydroxamate related vibration bands. The ATR-FTIR spectra of adsorbed DFOB and aerobactin were measured at much higher ligand-to-solid ratios than in the batch adsorption experiments in this study. Nonetheless, the surface-normalized concentrations of adsorbed DFOB and aerobactin are similar to the surface concentrations in the batch adsorption and dissolution experiments conducted in this study. This is due to the high affinity adsorption of siderophores to the surface of lepidocrocite where an adsorption maximum is already reached at low ligand-to-solid ratios (cf. DFOB adsorption isotherm in Fig. 2B).

3.2 Effect of ionic strength on the adsorption of DFOB and aerobactin

Fig. 2B shows DFOB adsorption isotherms at pH 3 and 8, measured each at 0.01 and 0.20 M ionic strength. A significant increase of surface concentrations of DFOB was observed at higher ionic strength at both pH values. In contrast, surface concentrations of aerobactin at pH 3, 6 and 8 were reduced at higher ionic strength (Fig. 2D).

The increase of DFOB surface concentrations at pH 3 with increasing ionic strength is consistent with a reduction of repulsive electrostatic interactions of positively charged surface complexes of DFOB (due to the protonated terminal amine group) with the positively charged lepidocrocite surface. A similar effect at pH 8 is more difficult to interpret as both the net charge of the lepidocrocite surface and the protonation state of hydroxamic acid groups (aqueous DFOB: $pK_a > 8.3$) change in this pH range.

The observed decrease of surface concentrations of aerobactin at higher ionic strength is interpreted by a decrease of the concentration of weakly bound surface complexes. We can only speculate on the coordination environment of iron-binding

groups of such apparently weak surface complexes. The interpretation of adsorption data is particularly complicated in the case of large complex molecules with several metal binding groups which may (independently) coordinate to the mineral surface by purely electrostatic outer-sphere interactions, hydrogen-bonding interactions or by inner-sphere complexation. It has been suggested that ligands stabilized at the surface by strong interactions, e.g. hydrogen-bonding or inner-sphere complexation are not (strongly) affected by changes in the ionic strength [25, 26]. However, ionic strength effects may occur, if the free energy of adsorption is also determined by a significant electrostatic contribution arising from changes of the electrostatic potential at the surface due to a net change in surface charge during adsorption of the ligand [27]. Thus, it remains to be shown in each case how significant the electrostatic contribution to inner- or outer-sphere adsorption is, e.g., by surface complexation modeling.

3.3 Adsorption of aqueous Fe(III)-siderophore complexes

Fig. 4A shows the adsorption of 30 μM Fe(III)-DFOB complexes onto lepidocrocite. The surface concentrations of Fe(III)-DFOB were one to two orders of magnitude smaller than the surface concentrations of DFOB in equilibrium with ~ 30 μM free DFOB in solution (cf. Fig. 2A). Considering that traces of free DFOB present in the stock solutions may result in surface concentrations in the range of the presented values (due to high affinity adsorption at low solution concentrations), the calculated surface concentrations of Fe(III)-DFOB represent an upper limit. The adsorption data suggest that the Fe(III)-DFOB solution complex has a very low affinity (if at all) for adsorption to the surface of lepidocrocite. For Fe(III)-siderophore solution complexes with free (uncomplexed) metal-binding groups the situation might be very different.

Fig. 4B shows the pH-dependent adsorption of 1:1 Fe(III)-aerobactin complexes to lepidocrocite from an initial solution concentration of 10.5 μM Fe(III)-aerobactin complexes and 21.5 μM free (uncomplexed) aerobactin. Except at low pH, the affinity of Fe(III)-aerobactin complexes for the surface can be compared to the affinity of free aerobactin, taking into account the lower initial solution concentrations of Fe(III)-aerobactin complexes. The adsorption data at low pH was not corrected for the formation of additional Fe(III)-aerobactin complexes due to dissolution of lepidocrocite by free aerobactin during the adsorption experiment. Based on known dissolution rates of lepidocrocite in the presence of aerobactin at pH 3 we estimated an increase of only about 1 μM Fe(III)-aerobactin during the adsorption experiment. Therefore, we conclude that the adsorption data presented in Fig. 4B are not significantly biased by the additional formation of Fe(III)-aerobactin complexes at low pH during dissolution.

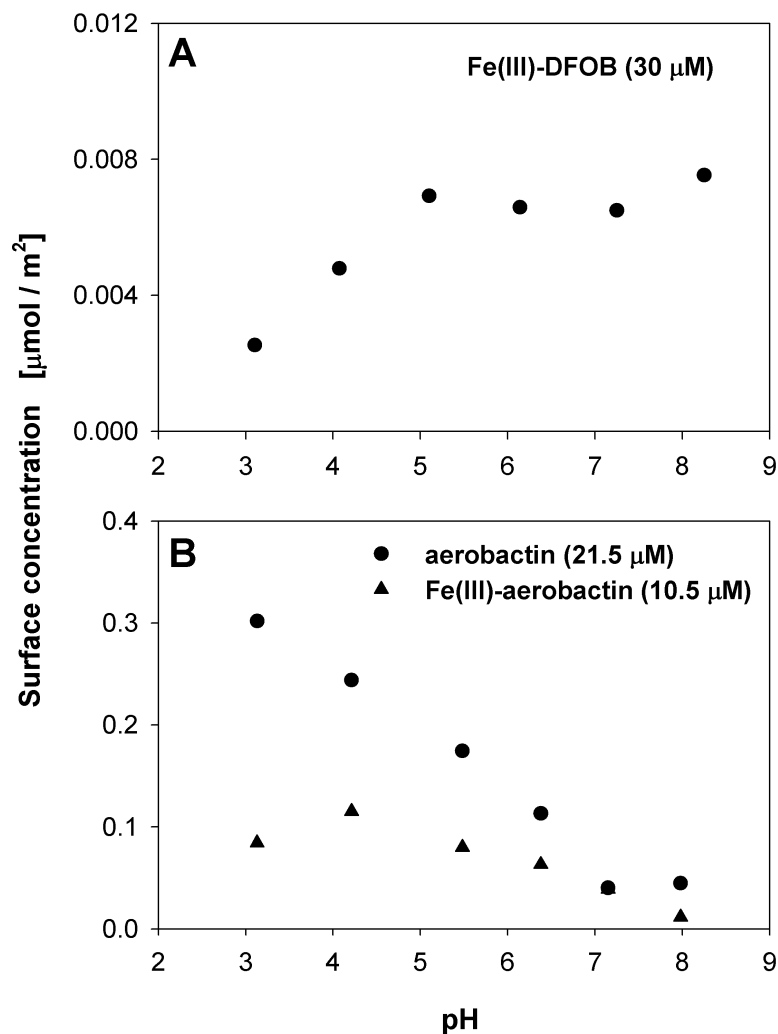


Fig. 4: (A) Adsorption of 30 μM 1:1 Fe(III)-DFOB complexes to lepidocrocite (1.5 g/L) as a function of pH. (B) Adsorption of a stock solution of 10.5 μM Fe(III)-aerobactin complexes and 21.5 μM free aerobactin to lepidocrocite (0.2 - 1 g/L suspensions) as a function of pH. The adsorption of Fe(III)-aerobactin complexes and free aerobactin are shown separately. The ionic strength was 0.01 M (NaClO_4) and equilibration time was 20 min.

For the discussion of the adsorption data of Fe(III)-aerobactin complexes, the solution speciation of Fe(III)-complexes has to be considered. At $\text{pH} > 6$ the solution speciation is dominated by an aqueous Fe(III)-complex in which the central Fe atom is coordinated by two hydroxamate groups (each bidentate) and by the citrate carboxylate and hydroxyl group to form an octahedral coordination sphere [14]. Both lateral carboxylate groups are deprotonated at $\text{pH} > 6$ (pK_a values of 3.11, 3.48) and are at first glance the only free iron-binding groups to interact with the surface, provided that the hexadentate structure of the Fe(III)-aerobactin complex is preserved at the surface of lepidocrocite. However, additional surface interactions might arise from the amine moiety adjacent to the lateral carboxylate functional group (cf. Fig. 1). These moieties form together an α -amino acid

fragment. Based on a recent spectroscopic study, the α -amino acid group may form a surface complex where both the amine and the carboxylate group are coordinated to a surface Fe(III) site by the formation of a five-membered chelate ring [28]. The formation of such five-membered chelate rings at the surface of lepidocrocite might explain the surprisingly high affinity of the Fe(III)-aerobactin solution complexes for the surface of lepidocrocite. The protonation of these lateral carboxylate groups at low pH might affect the extent of the adsorption of solution Fe(III)-aerobactin complexes, as indicated by a slight decrease in surface concentrations below pH 4.

3.4 Proton-promoted (photo)dissolution of lepidocrocite

Proton-promoted dissolution in the absence of siderophores was investigated in freshly prepared lepidocrocite suspensions with a solid concentration of 25 mg/L lepidocrocite at 0.01 M ionic strength (Fig. 5). Dissolution rates are summarized in Table 1. Irradiation of the suspensions with UV-visible light (300 - 460 nm) resulted in a significant increase of the formation of total dissolved Fe. For example, 4.4 μ M total dissolved Fe was formed during 6 hours at pH 3 under irradiation, compared to the corresponding formation of 0.86 μ M total dissolved Fe in the dark (Fig. S2 in Supporting Information). Under irradiation, the dominant redox state of total dissolved Fe at the end of the photodissolution experiments was Fe(II) (Fig. 5). These results substantiate the hypothesis of previous work that Fe(II) can be formed at the surface of lepidocrocite by a semiconducting mechanism in the bulk or directly at the surface (e.g., photolysis of surface Fe(III)-hydroxo groups) and may be released into solution by proton-promoted dissolution, as indicated in Fig. 5, or by ligand-promoted dissolution in the presence of siderophores [10]. These results are in agreement with a previous study in which the formation of Fe(II) was observed in irradiated lepidocrocite suspensions at pH 4 and 0.01 M ionic strength [29]. The ability of some iron (hydr)oxides to form Fe(II) by intrinsic photoreductive mechanisms has been reported in recent years [29-32]. Photoelectrons and photoholes generated in the semiconducting bulk may be scavenged at the surface leading to reduction of surface Fe(III) and oxidation of coordinated water or hydroxyl groups to hydroxyl radicals (\bullet OH). The analog reaction at the surface (photolysis of surface Fe(II)-hydroxo groups) also leads to the formation of Fe(II) and hydroxyl radicals. Subsequent reactions involving hydroxyl radicals (e.g., bimolecular reaction of \bullet OH leading to hydrogen peroxide, H_2O_2) in addition to reoxidation of surface Fe(II) by molecular oxygen (leading to superoxide, O_2^-) may result in considerable amounts of reactive oxygen species (\bullet OH, O_2^-/HO_2 , H_2O_2). We refer to a related study for details of the formation of reactive oxygen species and reoxidation of Fe(II) during photoreductive

dissolution of lepidocrocite in the absence of any organic ligands [33].

Fig. 5 shows furthermore that the formation of total dissolved Fe and Fe(II) decreased with increasing pH. This can be explained by (i) the decreasing susceptibility of lepidocrocite to photoreductive dissolution with increasing pH [34], (ii) Fe(II) re-adsorption to the surface above pH 5 [35], and (iii) oxidative precipitation of Fe(II) in the presence of reactive oxygen species formed during photoreductive dissolution of lepidocrocite [33, 36].

Proton-promoted dissolution at pH 3 was also investigated at higher ionic strength (0.2 M NaClO₄). In the dark and under irradiation, an increase of total dissolved Fe was observed with an increase in ionic strength (see Table 1 or Fig. S2 in Supporting Information) but the formation of Fe(II) was not affected noticeably by the increase in ionic strength. The increase in Fe(III) concentrations can be attributed to the lower activity of dissolved Fe(III) in solution at higher ionic strength.

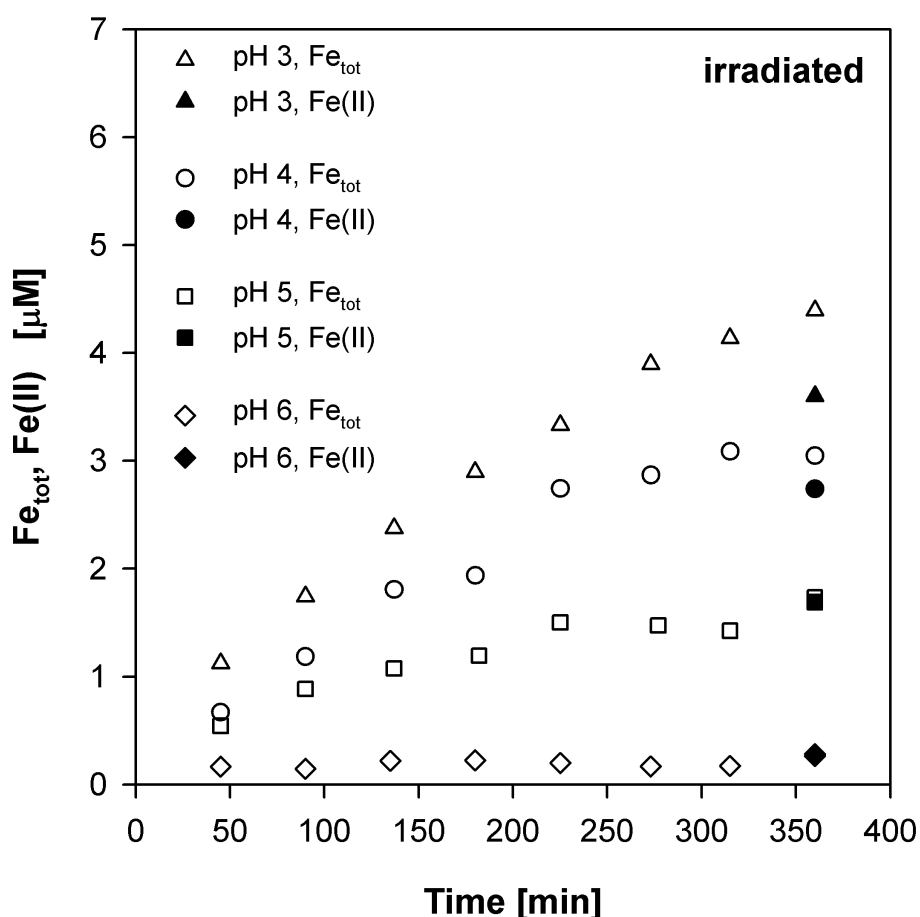


Fig. 5: Dissolution of irradiated lepidocrocite suspensions (25 mg/L) at different pH in the absence of any siderophores. Total dissolved iron of filtered suspensions was measured as well as one sample for Fe(II) at the end of each experiment. Ionic strength = 0.01 M NaClO₄.

3.5 Siderophore-promoted (photo)dissolution of lepidocrocite

Ligand-promoted dissolution of lepidocrocite in the presence of DFOB and aerobactin was observed in the dark and under irradiation (Fig. S3 and S4 in Supporting Information). Subsequent to the fast initial dissolution of lepidocrocite observed in the first 45 min, probably associated with a release of kinetically labile iron from the surface [37-39], dissolution kinetics were in general linear. The only case where non-linear dissolution was observed at longer time scales was in the presence of aerobactin at high dissolved iron concentrations at low pH (≤ 5). Similarly, non-linear dissolution kinetics was observed for proton-promoted dissolution under irradiation (cf. Fig. 5, and Fig. S2 in Supporting Information). Under the assumption that proton-promoted dissolution and siderophore-promoted dissolution are independent dissolution mechanisms (see equation 1) proton-promoted dissolution rates were subtracted from dissolution rates determined in the presence of siderophores. Dissolution rates were calculated from the slopes of linear regression lines of the dissolution data presented in Fig. 5 and in the Supporting Information (Fig. S2, S3, S4) excluding the first 45 min where fast initial dissolution occurred. Rates of lepidocrocite dissolution in the presence of aerobactin under irradiation below pH 5 (non-linear dissolution kinetics) were approximated by the slopes of linear regression lines over the duration of the experiment (45-360 min).

Rates of siderophore-promoted dissolution determined in the dark at 0.01 M ionic strength were correlated with the measured surface concentration of DFOB and aerobactin at the corresponding pH values and ionic strength (Table 1). In the dark, dissolution rates in the presence of DFOB were approximately constant between pH 3 and pH 6 and increased above pH 6 (Table 1). In the presence of aerobactin, dissolution rates determined in the dark decreased with increasing pH (Table 1). For both DFOB and aerobactin, dissolution rates were similarly enhanced under irradiation (Table 1). This is consistent with the results of our previous work at pH 6 [10] where we concluded that siderophores facilitate the detachment of surface Fe(II) formed by irradiation of the photoreactive lepidocrocite phase before reoxidation of surface Fe(II) occurs [10]. Dissolution rates generally increased with decreasing solution pH under irradiation and in the presence of DFOB or aerobactin (Table 1).

Rates of siderophore-promoted dissolution were also determined at higher ionic strength (0.20 M NaClO₄) for selected pH values (Table 1). For DFOB, the dissolution rates determined at different ionic strength in the dark at pH 8 were correlated with the adsorbed concentrations measured at the corresponding ionic strengths. This result suggests that the increase in DFOB surface concentrations at higher ionic strength (Fig. 2B) is correlated with an increase of (dissolution-active) surface complexes. However,

at pH 3, the increase in ionic strength resulted in a higher dissolution rate in the dark than expected by the increase of the concentration of DFOB surface complexes. Aerobactin-promoted dissolution rates at pH 3 and 6 decreased slightly with an increase in ionic strength. The observed decrease is consistent with a decrease of (dissolution-active) surface complexes.

The rates of DFOB- and aerobactin-promoted dissolution under irradiation were not affected by the increase of ionic strength - with the exception of DFOB at pH 3 (Table 1). This result is not consistent with the observed changes of surface concentrations of DFOB or aerobactin. It appears that the interplay of siderophore-promoted dissolution and the intrinsic photochemistry of the lepidocrocite phase is strongly affected by changes in ionic strength.

Table 1: Surface concentrations of DFOB and aerobactin and dissolution rates at different pH and ionic strength

Ionic strength [M]	pH	Surface concentrations ^a [$\mu\text{mol}/\text{m}^2$]		Siderophore-promoted dissolution rates [$\text{nmol}/\text{m}^2/\text{h}$] ^b				Proton-promoted dissolution rates [$\text{nmol}/\text{m}^2/\text{h}$] ^c	
		DFOB	aerobactin	DFOB dark	aerobactin dark	DFOB irradiated	aerobactin irradiated	dark	irradiated
0.01	3	0.075	0.60	79	81	629	387	39	195
0.01	4	0.085	0.54	90	95	379	303	-	147
0.01	5	0.085	0.46	82	55	242	255	-	61
0.01	6	0.085	0.33	79	36	276	232	-	3
0.01	7	0.100	0.21	94	34	266	134	-	-
0.01	8	0.135 ^d	0.14	125	19	285	67	-	-
0.2	3	0.115	0.46	226	67	1004	426	48	209
0.2	6	-	0.28	-	30	-	-	-	-
0.2	8	0.200	0.10	181	-	290	69	-	-

^a Surface concentrations were interpolated for equilibrium solution concentrations of 30 μM (cf. Fig. 2). A maximum error of the surface concentrations of 10 % was estimated. ^b Error estimates for the siderophore-promoted dissolution rates are in the order of 5 % in the presence of DFOB and 10 % in the presence of aerobactin. Error estimates are based on the standard error of the slopes of linear regression lines of the dissolution data. ^c Error estimates for proton-promoted dissolution rates are in the order of 10 %. ^d Measured at pH 8.1.

3.6 Non-linear dissolution kinetics in the presence of aerobactin

At $\text{pH} \leq 5$ and under irradiation, non-linear dissolution kinetics was observed in the presence of aerobactin at high total dissolved iron concentrations. Dissolution rates were approximated by linear regression of the dissolution curves (Fig. S3 in

Supporting Information). Thus, the calculated values in Table 1 represent a lower limit for aerobactin-promoted dissolution over the experimental time frame. Fig. 6 shows a comparison of lepidocrocite dissolution in the presence of DFOB or aerobactin under irradiation at pH 4. At the end of the experiment, the dissolution rates declined in the presence of aerobactin, whereas in the presence of DFOB dissolution kinetics were still linear.

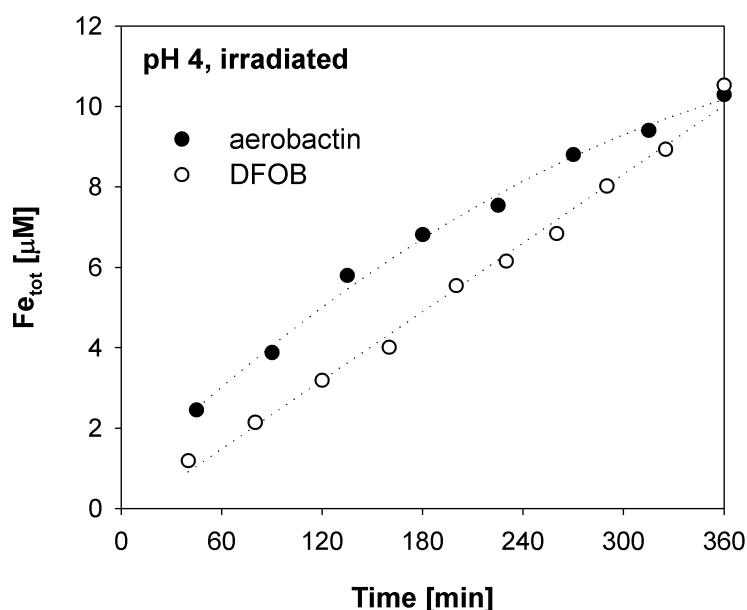


Fig. 6: Dissolution of irradiated lepidocrocite suspensions (25 mg/L) at pH 4 in the presence of DFOB or aerobactin (30 μM). The linear and quadratic regression lines for DFOB and aerobactin are intended to guide the eye. Ionic strength = 0.01 M NaClO_4 .

Non-linear dissolution kinetics were only apparent in dissolution experiments in the presence of aerobactin where high concentrations of total dissolved Fe were measured (e.g., under irradiation and $\text{pH} \leq 5$). This suggests that Fe-aerobactin complexes formed during dissolution were involved in the reduction of overall dissolution rates. We have to consider that dissolved Fe(III)-aerobactin complexes formed during dissolution are susceptible to photolysis under UV-Vis irradiation. Photolysis of Fe(III)-aerobactin complexes in solution involves the oxidation of the coordinated α -hydroxycarboxylate group by a ligand-to-metal electron transfer reaction and yields a Fe(II)-photoproduct complex, which rapidly oxidizes to an Fe(III)-complex in the presence of oxygen [1, 9, 10]. The hexadentate Fe(III)-aerobactin photoproduct is structurally similar to its parent complex and exhibits a similar conditional stability constant and similar pK_a values [9]. As in the case of Fe(III)-aerobactin solution complexes, the lateral carboxylate groups and the adjacent amine groups (α -amino acid moieties) of the Fe(III)-aerobactin

photoproduct are also free to interact with the surface of lepidocrocite. Thus, we may assume that the Fe(III)-aerobactin photoproduct adsorbs equally strong to the surface as Fe(III)-aerobactin (Fig. 4B). Based on the adsorption data presented in Fig. 4B, we estimated that at the end of the photodissolution experiment at pH 4 (Fig. 6) merely 0.4 μM Fe(III)-aerobactin/Fe(III)-photoproduct complexes may readsorb to the surface. Therefore, a loss of iron from solution due to readsorption of Fe(III)-aerobactin or Fe(III)-photoproduct complexes to the surface of lepidocrocite is insufficient to explain the non-linear dissolution kinetics in the presence of aerobactin. Linear extrapolation of the dissolution rate determined by the first 4 data points (Fig. 6; 45 -180 min) suggests that 13 μM total dissolved Fe could have been formed at the end of the experiment. Therefore, dissolution-inhibiting processes must have led to a reduction of total dissolved iron by approximately 3 μM over 5 hours. Such a dissolution-inhibiting effect of Fe-aerobactin/ Fe-photoproduct complexes was observed in a comparative photodissolution experiment at pH 6 in the presence of free aerobactin (21.5 - 22 μM) and in the presence / absence of 10.5 μM Fe(III)-aerobactin complexes (Fig. 7). In the absence of initial Fe(III)-aerobactin complexes, 4 μM total dissolved iron formed within 6 hours. In the presence of added Fe(III)-aerobactin complexes, an increase of only 2 μM total dissolved iron was observed by dissolution of lepidocrocite by free aerobactin.

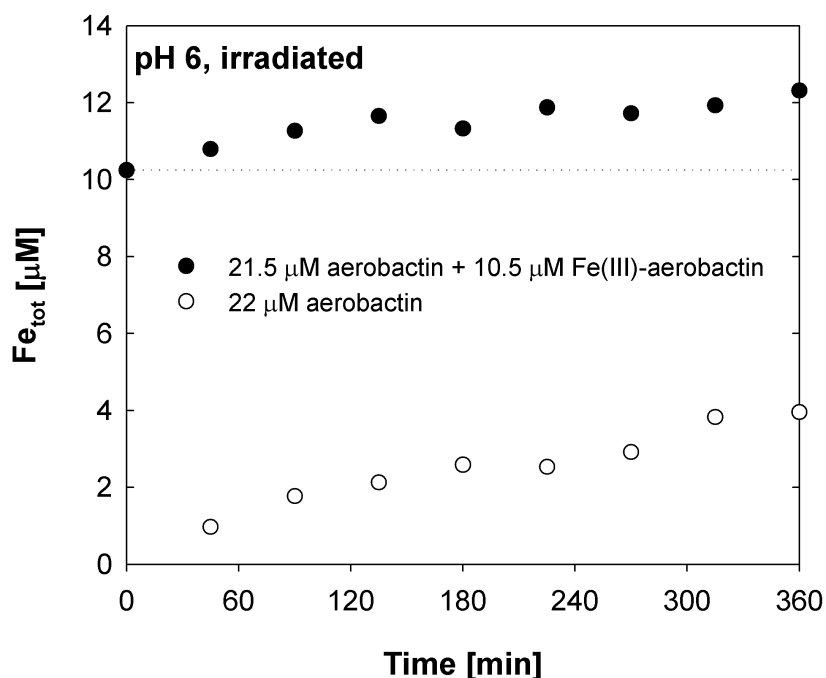


Fig. 7: Dissolution of irradiated lepidocrocite suspensions (25 mg/L) at pH 6 in the presence of 22 μM free aerobactin (empty circles) or in the presence of a mixture of 21.5 μM free aerobactin and 10.5 μM 1:1 Fe(III)-aerobactin complexes (filled circles). Ionic strength = 0.01 M NaClO_4 .

Two different processes may serve as an explanation for this inhibitory effect. It is conceivable that Fe(III)-complexes of aerobactin and its photoproduct form surface complexes (c.f. Fig. 4) that are strong enough to compete with adsorption of free aerobactin and thus are able to reduce overall dissolution rates. In contrast to Fe(III)-aerobactin complexes, it was shown that Fe(III)-DFOB complexes have a very low affinity for the surface (Fig. 4A), hence competitive effects are unlikely to occur in the case of DFOB.

The second inhibitory process is related to the reoxidation of Fe(II) at the mineral surface by reactive oxygen species ($\bullet\text{OH}$, O_2^- , H_2O_2) formed during photoreductive dissolution of lepidocrocite in the presence of aerobactin. Dissolved Fe(II)-siderophore complexes formed upon release of surface Fe(II) into solution are susceptible to rapid reoxidation by molecular oxygen, due to the low redox potentials of the Fe-siderophore complexes [40]. In a recent study, it was demonstrated that oxidation of Fe(II) by O_2 in the presence of DFOB is instantaneous [41]. Reactive oxygen species and O_2 may reoxidize Fe(II) formed at the surface before it is released into solution by proton- or siderophore-promoted dissolution [33]. The oxidation of Fe(II)-DFOB and Fe(II)-aerobactin complexes by molecular oxygen leads to the formation of superoxide (O_2^-), and eventually also to hydrogen peroxide (H_2O_2), e.g., by superoxide dismutation [42]. But an excess production of reactive oxygen species is only possible in the presence of Fe(III)-aerobactin complexes. This is due to the photolysis of Fe(III)-aerobactin solution complexes which leads to the formation of a Fe(II)-photoproduct that is subsequently also oxidized by O_2 in solution to the Fe(III)-photoproduct complex. The conversion of Fe(III)-aerobactin to the Fe(III)-photoproduct complex actually involves a transfer of 2 electrons (oxidation of the α -hydroxycarboxylic acid group to a keto/enol functional group [9]). The formation of 1 mole of the Fe(III)-photoproduct complex potentially leads to the formation of 2 moles of superoxide (O_2^-). Thus, higher concentrations of reactive oxygen species are formed during photodissolution in the presence of aerobactin than in the presence of DFOB. Consequently, more surface Fe(II) can be reoxidized in the presence of aerobactin and dissolution rates may be significantly reduced.

In the absence of siderophores, non-linear dissolution of lepidocrocite over time was also observed under irradiation at low pH (Fig. 5). According to a related study, reactive oxygen species are also formed during photoreductive dissolution of lepidocrocite in the absence of any organic ligands leading to non-linear dissolution kinetics by reoxidation of Fe(II) in solution and at the surface [33].

3.7 The mechanism of siderophore-controlled dissolution in the dark

Given that siderophore-promoted dissolution is controlled by the formation of surface complexes, dissolution rate coefficients can be calculated according to the rate expression for ligand-promoted dissolution in equation 1. In Fig. 8, dissolution rates directly determined in the adsorption experiments in the presence of DFOB (Fig. 2A) were plotted against the experimentally determined surface concentrations of adsorbed DFOB. For each adsorption isotherm measured between pH 5 and 8 a linear dependence of dissolution rates and surface concentrations was observed, in support of a surface-controlled dissolution mechanism. Dissolution rate coefficients calculated for all data points shown in Fig. 8 fall into a fairly narrow range of 0.9 and 1.2 h⁻¹ (cf. Fig. S5 in the Supporting Information), suggesting that the dissolution reactivity of adsorbed DFOB is not pH-dependent.

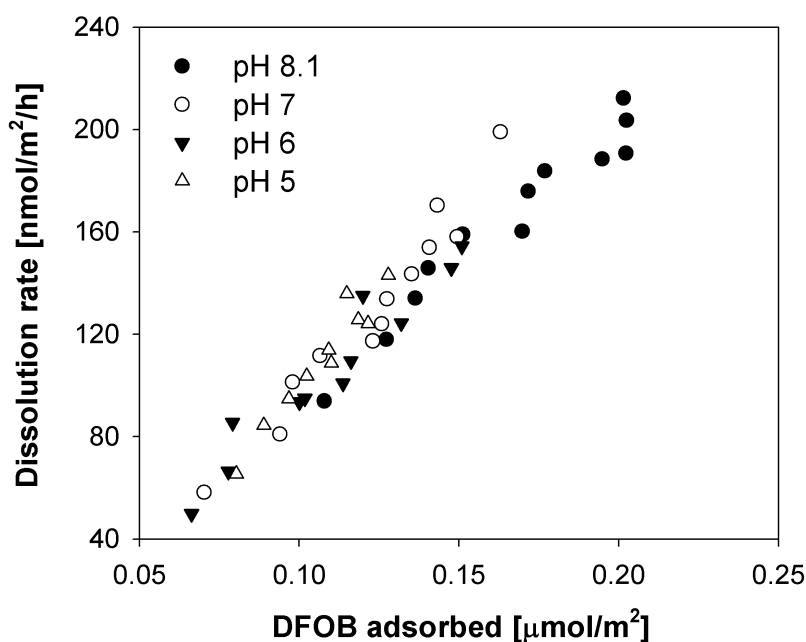


Fig. 8: Observed rates of siderophore-promoted dissolution of lepidocrocite in the adsorption experiments at different pH at 0.01 M ionic strength (cf. Fig. 2A). Dissolution rates are plotted against the surface concentrations of adsorbed DFOB.

At this point, we want to stress that the calculated dissolution rate coefficients are a macroscopic measure of the dissolution reactivity of all adsorbed ligands. Within this macroscopic approach of investigating ligand-promoted dissolution, we can provide no information on the dissolution reactivity of different surface complexes at the molecular level. Considering that siderophores are multidentate ligands, a broad range of surface species with different dissolution reactivity are conceivable. However, by comparing macroscopic dissolution rate coefficients of structurally similar or different

siderophores, we may provide some insights into the reactivity of potentially formed surface complexes.

Apparent dissolution rate coefficients for the (photo)dissolution experiments in the presence of DFOB and aerobactin are listed in Table 2. These rate coefficients were calculated by dividing the dissolution rates listed in Table 1 by estimated surface concentrations of DFOB or aerobactin (also Table 1). For the dissolution experiments conducted in the dark, the results are plotted in Fig. 9. The average rate coefficient of DFOB between pH 3 and 8 in the dark ($0.98 \pm 0.05 \text{ h}^{-1}$) was significantly higher than the average rate coefficient of aerobactin ($0.14 \pm 0.022 \text{ h}^{-1}$) (Fig. 9). The dissolution rate coefficients determined for the dissolution experiments in the presence of DFOB were within the range of rate coefficients determined directly in the adsorption experiments (between 0.9 and 1.2 h^{-1}) (cf. Fig. S5 in Supporting Information). In both data sets, calculated dissolution rate coefficients for DFOB were not pH-dependent and thus indicate that the macroscopic dissolution reactivity of surface complexes of DFOB is not affected by pH changes.

Table 2: Apparent dissolution rate coefficients for siderophore-promoted dissolution

Ionic strength [M]	pH	Apparent rate coefficients [h^{-1}] ^a			
		DFOB dark	aerobactin dark	DFOB irradiated	aerobactin irradiated
0.01	3	1.06	0.13	8.39	0.64 (0.91) ^a
0.01	4	1.06	0.18	4.45	0.56 (0.87) ^a
0.01	5	0.96	0.12	2.85	0.55 (0.85) ^a
0.01	6	0.93	0.11	3.25	0.70
0.01	7	0.94	0.16	2.66	0.64
0.01	8	0.93	0.14	2.11	0.48
0.2	3	1.96	0.15	8.73	0.93 (1.17) ^a
0.2	6	-	0.11	-	-
0.2	8	0.91	-	1.45	0.69

^a Values in parentheses were corrected for non-linear dissolution kinetics. Error estimates for the apparent rate coefficients are 11% for DFOB and 14% for aerobactin.

The scatter in the calculated rate coefficients for aerobactin-promoted dissolution was relatively large and, thus, we may only hypothesize that the reactivity of surface complexes of aerobactin is not affected by a change in pH.

Dissolution rate coefficients in the dark were not affected by a change in ionic strength for DFOB at pH 8 and aerobactin at pH 3 and 6. Under these conditions, we assume that the surface speciation with respect to the proportion of dissolution-active surface complexes is not affected by a change in ionic strength.

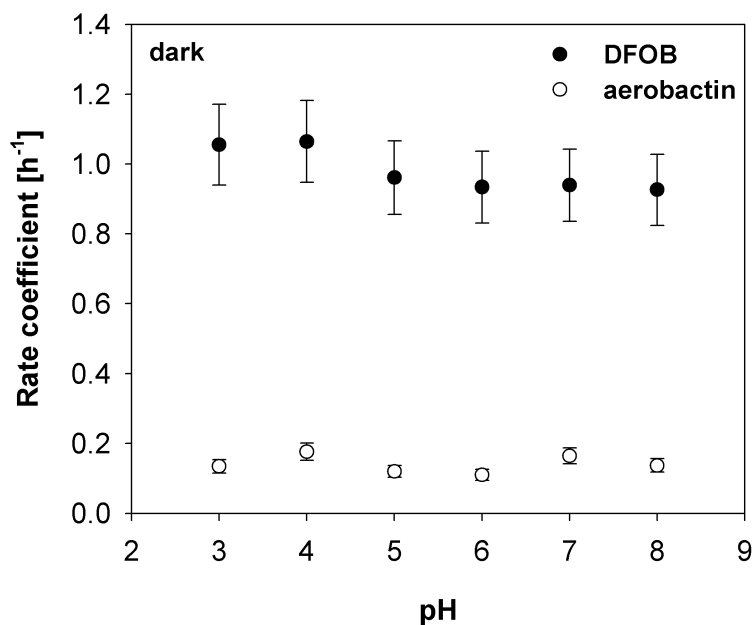


Fig. 9: Apparent dissolution rate coefficients [h^{-1}] determined for DFOB and aerobactin in the dark as a function of pH at 0.01 M ionic strength. The values of the rate coefficients are listed in Table 2. Error estimates for the apparent rate coefficients are 11% for DFOB and 14% for aerobactin.

In combination with the ATR-FTIR spectroscopic investigation of adsorbed DFOB and aerobactin [11], the comparison of rate coefficients determined in the dark provide some insights into the dissolution reactivity of potentially forming surface complexes. The significant difference in the dissolution reactivity can be discussed in the context of suggested reactivity trends of surface complexes of small inorganic/organic ligands formed on oxide/hydroxide phases and oxide clusters [8, 43-49]. These studies suggest that bi- or multidentate ligands which coordinate as mononuclear inner-sphere surface complexes are most efficient in labilizing metal-oxygen bonds at the surface and thus in accelerating the dissolution of the investigated phases. In this context, Ludwig et al. (1995) observed that rate coefficients determined for the dissolution of NiO in the presence of a selected set of aminocarboxylic acids increased with the number of ligating functional groups that may specifically coordinate to a single surface site. Ligands forming monodentate mononuclear inner-sphere surface complexes have been shown to be less effective towards dissolution than ligands forming bi- or multidentate mononuclear surface complexes, as these former ligands conceptually donate less electron density into the coordination sphere of the involved Fe(III) surface site [8, 45]. On the other hand, multidentate ligands which form bi- or multinuclear inner-sphere surface complexes may retard or even inhibit dissolution [45, 46]. This effect has been explained by assuming that the simultaneous removal of bi- or multinuclear surface

complexes from the surface is energetically unfavorable.

In comparison to aerobactin, DFOB forms surface complexes that are apparently very efficient in dissolving lepidocrocite as indicated by the 6- to 8-fold higher dissolution rate coefficients determined in the dark (cf. Fig. 9). From the above discussion, we may assume that the iron-binding groups in DFOB are coordinated at the surface in a manner that significantly accelerates the rate determining detachment of coordinated surface Fe(III) into solution. Due to steric hindrance at the surface, it is likely that mononuclear hexadentate Fe(III)-DFOB complexes do not form on mineral surfaces. Consequently, the most dissolution-active surface complexes potentially formed on lepidocrocite are those with tetradentate mononuclear inner-sphere coordination. Complexes where single hydroxamic acids are coordinated to separate surface Fe(III) sites in mononuclear bidentate inner-sphere coordination are probably less dissolution-active. Furthermore, bidentate binuclear surface complexes of single hydroxamate groups are presumably less reactive than bidentate mononuclear surface complexes. In our companion spectroscopic study of DFOB adsorption to lepidocrocite, we suggested that the predominant surface complex of DFOB at low pH (e.g. pH 4) is characterized by inner-sphere coordination of two to three hydroxamate groups to an unspecified number of surface Fe(III) sites [11]. At higher pH, additional surface interactions such as outer-sphere and/or hydrogen-bonding interactions of hydroxamate groups with Fe(III) surface sites were regarded conceivable. The fact that the dissolution rate coefficients determined in this study were constant over a broad pH range (including acidic pH) (cf. Fig. 9) suggests that the formation of dissolution-active surface complexes, characterized by inner-sphere coordination of hydroxamic acids, dominates the surface speciation also at higher pH.

In the case of aerobactin, the ATR-FTIR spectroscopic investigation could not provide any information on the surface interactions of the two hydroxamic acid functional groups [11]. However, the spectroscopic data indicated an increasing formation of inner-sphere surface complexes of the carboxylate groups with decreasing pH [11]. The carboxylic acid groups interact strongly with the surface, as indicated in this study by the anion-like adsorption typical for carboxylic acids and the higher surface concentrations of aerobactin compared to DFOB (Fig. 2A and C). The adsorption experiments in this study suggest furthermore that the lateral carboxylate groups and conceivably the adjacent amine moieties are responsible for the significant adsorption of Fe(III)-aerobactin complexes to the surface of lepidocrocite. The dissolution of lepidocrocite by aerobactin is determined by the coordination of up to five iron binding groups, all capable of forming dissolution-active surface complexes by the formation of five-membered chelate rings with Fe(III) surface sites (two hydroxamic acid groups, 2 α -amino acid groups and 1 α -hydroxycarboxylic acid group). The significantly smaller

dissolution rate coefficients of aerobactin in comparison to DFOB can be explained by two additive scenarios: (i) aerobactin forms surface complexes where only a small fraction of the functional groups binds in a dissolution-active coordination mode, and (ii) aerobactin forms surface complexes where a higher number of surface Fe(III) sites are coordinated to its iron binding groups, leading to slower detachment kinetics of the higher multinuclear surface complexes.

3.8 The mechanism of photoreductive dissolution

Photoreductive dissolution of lepidocrocite in the absence of siderophores is promoted by the formation of surface Fe(II) by intrinsic photochemical processes of the semiconducting solid, as indicated in this study (cf. Fig. 5). Therefore, dissolution rate coefficients calculated for photoreductive dissolution of lepidocrocite by DFOB and aerobactin do not only depend on the facilitated release of surface Fe(II) by these siderophores but also on the generation of surface Fe(II) unless the detachment of Fe(II) from the surface is rate limiting in all dissolution experiments. However, observations of the dissolution rate coefficients help to identify changes in the photoreductive dissolution mechanism and the rate limiting step. In this context, dissolution rate coefficients for DFOB and aerobactin were determined (Table 2) to investigate if the photoreactive α -hydroxycarboxylate group of aerobactin is coordinated and photolyzed at the surface of lepidocrocite by a light-induced LMCT reaction. Dissolution rates of lepidocrocite in the presence of aerobactin calculated by linear regression of the dissolution curves over the entire time frame (45 – 360 min) underestimate the intrinsic reactivity of adsorbed aerobactin under conditions where non-linear dissolution kinetics were observed ($\text{pH} < 5$). In Table 2, rate coefficients for aerobactin were additionally corrected for non-linear dissolution kinetics by calculating initial dissolution rates linearizing the initial dissolution between 45 and 180 min after the start of the experiment. The values are presented in Table 2 in parentheses. The relative increase in the rate coefficients under irradiation as compared to the dark was higher for aerobactin than for DFOB except at low $\text{pH} (< 5)$. For $\text{pH} \geq 5$, a relative increase in rate coefficients by a factor of 2.3-3.5 and 3.4-7 was observed for DFOB and aerobactin, respectively (Table 2). The absolute values of dissolution rate coefficients in the presence of DFOB were however still significantly greater than the rate coefficients in the presence of aerobactin. The fact that both siderophores promote photoreductive dissolution despite the contrasting photostability of their dissolved Fe(III) complexes indicates that the detachment of Fe(II) from the surface is the rate determining step in the absence of siderophores and that it is accelerated by siderophore-promoted dissolution as suggested by Borer

et al. (2005). A higher relative increase in rate coefficients for aerobactin compared to DFOB suggests that aerobactin does not only promote the detachment of Fe(II) but also its formation by LMCT between coordinated α -hydroxycarboxylate groups of aerobactin and surface sites. The formation of surface Fe(II) by LMCT of surface Fe(III)-aerobactin complexes does not seem to be an effective mechanism compared with the LMCT-induced photodissolution of lepidocrocite by citrate, a model α -hydroxycarboxylate compound. A recent ATR-FTIR and radiotracer study [12] showed that the α -hydroxycarboxylic acid group of citrate is specifically photolyzed at the surface of lepidocrocite leading to considerable amounts of surface Fe(II). In that study, dissolution of lepidocrocite by citrate at pH 4 was measured in the dark and under irradiation in a photoirradiation setup suitable for larger suspension volumes (see experimental section). The ligand-to-solid ratio (125 mg/L lepidocrocite and 100 μ M citrate) was comparable to the corresponding ratio for the dissolution experiments in the presence of aerobactin as presented in this study. Citrate-promoted dissolution rates were 92 and 2900 nmol/m²/h as determined in the initial 160 min in the dark and under irradiation (N₂-purged suspensions), respectively [12]. These rates were divided by a citrate surface concentration of \sim 0.74 μ mol/m² as derived from the adsorption isotherm at pH 4 (Fig. S6 in Supporting Information). The resulting rate coefficients of 0.124 and 3.91 h⁻¹ illustrate that the relative increase in the rate coefficient under irradiation is significant. An additional photodissolution experiment at pH 4 with citrate and with the same ligand-to-solid ratio as applied in this study (25 mg/L lepidocrocite and 30 μ M ligand) was conducted under deaerated conditions (Fig. S7 in Supporting Information). The dissolution rate was 3240 nmol/m²/h, and the surface concentration of citrate was \sim 0.67 μ mol/m² as estimated from the adsorption isotherm (Fig. S6 in Supporting Information). The resulting rate coefficient of 4.83 h⁻¹ was slightly higher than in the published radiotracer study [12]. The much lower rate coefficient for aerobactin-promoted dissolution of lepidocrocite under irradiation (0.87 h⁻¹) suggests that LMCT-induced photodissolution involving the α -hydroxycarboxylate group of aerobactin is not effective. It is conceivable that the release of Fe(II) formed by the photolysis of this functional group is kinetically hindered by the slow desorption of aerobactin which may be coordinated to the surface by several functional groups.

At pH \leq 5, constant rate coefficients were observed under irradiation for aerobactin (\sim 0.88 h⁻¹), whereas the rate coefficients for DFOB drastically increased from pH 5 (2.85 h⁻¹) to pH 3 (8.39 h⁻¹, see Table 2). At low pH, especially in the case of reducing conditions, proton- and ligand-promoted dissolution may not be independent and additive dissolution mechanisms [43]. The increase in DFOB dissolution rate coefficients with decreasing pH is in line with a synergistic interplay of proton- and ligand-promoted

dissolution. We may hypothesize that dissolution of lepidocrocite by aerobactin is not affected by such a synergistic effect, because of the higher surface concentrations of aerobactin and hence a smaller fraction of sites affected by proton-promoted dissolution. At pH 3, the specific surface concentration of aerobactin and DFOB was 0.6 and 0.075 $\mu\text{mol}/\text{m}^2$, respectively. Considering that these siderophores are multidentate ligands, each siderophore molecule may interact with a number of adjacent surface Fe-sites. Thus a significant fraction of the estimated 8 $\mu\text{mol}/\text{m}^2$ surface Fe-sites (based on an average surface site density of 5 sites/ nm^2) is presumably coordinated by aerobactin. In contrast, only a small percentage of surface sites are coordinated by DFOB. Therefore, the effect of proton promoted dissolution is likely smaller in the presence of aerobactin than DFOB.

We may further speculate that the enhanced dissolution under irradiation in the presence of DFOB at $\text{pH} < 5$ is due to the formation of reductive degradation products of DFOB. Hydroxamic acids are known to undergo acid-catalyzed hydrolysis at low pH resulting in carboxylic acid and hydroxylamine compounds [50]. At $\text{pH} < 2$, reduction of dissolved Fe(III) was observed in the presence of DFOB on the time scale of days [51], which is consistent with the formation of reductive hydroxylamine compounds [50]. Reductive dissolution of goethite was also observed at pH 3 in the dark by acid- or surface catalyzed hydrolysis of acetohydroxamic acid [21, 52]. We found no indication that reductive dissolution occurred in the dark in the presence of DFOB (Fig. 9), but we cannot rule out reductive dissolution in irradiated systems, especially if photoreductive carboxylate compounds are formed by acid-catalyzed hydrolysis of DFOB [50].

This study suggests that even at high pH photoreductive dissolution of lepidocrocite in the presence of DFOB is induced by the formation of surface Fe(II) by photochemical mechanisms inherent to the lepidocrocite solid. However, in a companion investigation on the wavelength-dependent photodissolution of lepidocrocite in the presence of DFOB, we found indications for a light-induced reductive effect of adsorbed DFOB at pH 8 [53]. Dissolution rates normalized to the corresponding photon fluxes were higher in the wavelength range 395–435 nm, and decreased at lower and higher wavelengths. This is exactly the wavelength region in which the hexadentate Fe(III)-DFOB solution complex has a strong and broad absorption band. The absorption of light at 430 nm by the solution complex is related to a LMCT transition, but it does not lead to a reduction of the metal center [54]. Absorption spectra of adsorbed species on highly light-absorbing iron(III) (hydr)oxides cannot be measured, but these results indicate that light absorption at 395–435 nm, presumably due to LMCT transitions of inner-sphere surface complexes, is accompanied by an electron transfer to the surface [53]. Further experiments are required to substantiate the potential photoreductive effect of

adsorbed hydroxamic acids on iron(III) (hydr)oxides.

4. Summary and conclusions

Based on the comparison of the pH-dependent adsorption of DFOB on lepidocrocite and acetohydroxamic acid on goethite [21], we suggest that surface complexes of DFOB are positively charged, due to the protonated terminal amine group. Surface concentrations of adsorbed DFOB increased at higher ionic strength (0.2 M NaClO₄) at pH 3, which can be explained by a decrease of repulsive electrostatic interactions of the charged amine group with the charged surface. The anion-like adsorption of aerobactin indicated that the pH-dependent adsorption is strongly determined by interactions of the carboxylic acid groups with the surface. A slight decrease of the surface concentrations of aerobactin at higher ionic strength was interpreted by a decrease of the surface concentrations of weakly bound aerobactin. In order to explain the high affinity of Fe(III)-aerobactin solution complexes for the surface of lepidocrocite, we considered the potential formation of stable five-membered chelate rings at the surface by the joint interaction of the lateral carboxylic acid groups and the adjacent amine groups. In contrast, the adsorption data showed that the Fe(III)-DFOB solution complex has a very low affinity for the surface of lepidocrocite.

We showed exemplarily for DFOB that siderophore-promoted dissolution of lepidocrocite is a surface-controlled process, where dissolution rates are linearly correlated with the surface concentrations of adsorbed siderophores. In the dark, dissolution rate coefficients were significantly higher for DFOB than for aerobactin. This difference was explained by DFOB forming more dissolution-active surface complexes. We assume that aerobactin forms surface complexes where only a small fraction of the available functional groups binds in a dissolution-active coordination mode in addition to the formation of a higher degree of multinuclear surface complexes, resulting in slower detachment kinetics of the surface metal complexes. Future dissolution studies with a greater set of different siderophores are required to substantiate the conclusions drawn in this study.

The constant dissolution rate coefficients for DFOB in the dark suggest that the surface speciation in terms of dissolution-active surface complexes does not change between pH 3 to 8 and that inner-sphere complexation of iron by hydroxamic acid groups dominates the DFOB surface speciation in this entire pH region. This is based on the interpretation of ATR-FTIR spectroscopic data of adsorbed DFOB, where we concluded that the predominant surface complex at low pH (pH 4) involves inner-sphere

coordination of two to three hydroxamic acid groups of DFOB to the surface [11].

Under irradiation, dissolution rates increased both in the presence of DFOB and aerobactin. The observed reduction of dissolution rates over time in the presence of aerobactin at low pH was discussed in terms of the formation of reactive oxygen species during photolysis of dissolved Fe(III)-aerobactin complexes and the re-adsorption of Fe(III)-aerobactin and Fe(III)-photoproduct complexes. In the case of DFOB, the observation of linear dissolution is consistent with the low affinity of Fe(III)-DFOB complexes for the surface and the lack of extensive formation of reactive oxygen-species. The light-induced increase of dissolution rate coefficients was slightly higher for aerobactin than for DFOB at $\text{pH} \geq 5$. We conclude that the light-induced dissolution of lepidocrocite in the presence of aerobactin may be additionally promoted by a photoreductive dissolution mechanism in which the α -hydroxycarboxylate group is photolyzed at the surface in a LMCT reaction. However, based on the comparison with dissolution rate coefficients determined for citrate we suggest that LMCT within surface complexes of aerobactin is not an effective process. In general, the enhancement of dissolution in the presence of both DFOB and aerobactin is attributed to the intrinsic photoreactivity of lepidocrocite.

5. References

- [1] Kraemer, S. M., Butler, A., Borer, P. and Cervini-Silva, J. **2005**. Siderophores and the dissolution of iron-bearing minerals in marine systems. *Rev. Mineral. Geochem.* 59: 53-84.
- [2] Kraemer, S. M., Crowley, D. E. and Kretzschmar, R. **2006**. Geochemical aspects of phytosiderophore-promoted iron acquisition by plants. *Adv. Agron.* 91: 1-46.
- [3] Kraemer, S. M. **2004**. Iron oxide dissolution and solubility in the presence of siderophores. *Aquat. Sci.* 66: 3-18.
- [4] Hersman, L., Lloyd, T. and Sposito, G. **1995**. Siderophore-promoted dissolution of hematite. *Geochim. Cosmochim. Acta* 59: 3327-3330.
- [5] Liermann, L. J., Kalinowski, B. E., Brantley, S. L. and Ferry, J. G. **2000**. Role of bacterial siderophores in dissolution of hornblende. *Geochim. Cosmochim. Acta* 64: 587-602.
- [6] Cheah, S. F., Kraemer, S. M., Cervini-Silva, J. and Sposito, G. **2003**. Steady-state dissolution kinetics of goethite in the presence of desferrioxamine B and oxalate ligands: implications for the microbial acquisition of iron. *Chem. Geol.* 198: 63-75.

-
- [7] Reichard, P. U., Kraemer, S. M., Frazier, S. W. and Kretzschmar, R. **2005**. Goethite dissolution in the presence of phytosiderophores: Rates, mechanisms, and the synergistic effect of oxalate. *Plant Soil* 276: 115-132.
- [8] Furrer, G. and Stumm, W. **1986**. The coordination chemistry of weathering: I. Dissolution kinetics of δ -Al₂O₃ and BeO. *Geochim. Cosmochim. Acta* 50: 1847-1860.
- [9] Kuepper, F. C., Carrano, C. J., Kuhn, J. U. and Butler, A. **2006**. Photoreactivity of iron(III)-aerobactin: Photoproduct structure and iron(III) coordination. *Inorg. Chem.* 45: 6028-6033.
- [10] Borer, P. M., Sulzberger, B., Reichard, P. and Kraemer, S. M. **2005**. Effect of siderophores on the light-induced dissolution of colloidal iron(III)(hydr)oxides. *Mar. Chem.* 93: 179-193.
- [11] Borer, P., Hug, S. J., Sulzberger, B., Kraemer, S. M. and Kretzschmar, R. **submitted**. ATR-FTIR spectroscopic study of the adsorption of desferrioxamine B and aerobactin to the surface of lepidocrocite (γ -FeOOH) *Geochim. Cosmochim. Acta*.
- [12] Borer, P., Hug, S. J., Sulzberger, B., Kraemer, S. M. and Kretzschmar, R. **2007**. Photolysis of citrate on the surface of lepidocrocite: An in situ attenuated total reflection infrared spectroscopy study. *J. Phys. Chem. C* 111: 10560-10569.
- [13] Heidmann, I., Christl, I., Leu, C. and Kretzschmar, R. **2005**. Competitive sorption of protons and metal cations onto kaolinite: experiments and modeling. *J. Colloid Interface Sci.* 282: 270-282.
- [14] Harris, W. R., Carrano, C. J. and Raymond, K. N. **1979**. Coordination chemistry of microbial iron transport compounds: 16. Isolation, characterization, and formation-constants of ferric aerobactin. *J. Am. Chem. Soc.* 101: 2722-2727.
- [15] Parker, C. A. **1968**. *Photoluminescence of solutions, with applications to photochemistry and analytical chemistry*. Elsevier: Amsterdam.
- [16] Voelker, B. M. and Sulzberger, B. **1996**. Effects of fulvic acid on Fe(II) oxidation by hydrogen peroxide. *Environ. Sci. Technol.* 30: 1106-1114.
- [17] Kraemer, S. M., Cheah, S. F., Zapf, R., Xu, J. D., Raymond, K. N. and Sposito, G. **1999**. Effect of hydroxamate siderophores on Fe release and Pb(II) adsorption by goethite. *Geochim. Cosmochim. Acta* 63: 3003-3008.
- [18] Smith, R. M., Martell, A.E., Motekaitis, R.J. **2001**. *NIST standard reference database 46*, vers. version 6.0. Gaithersburg, MD, USA.
- [19] Holmen, B. A., Tejedor-Tejedor, M. I. and Casey, W. H. **1997**. Hydroxamate complexes in solution and at the goethite-water interface: A cylindrical internal reflection Fourier transform infrared spectroscopy study. *Langmuir* 13:

- 2197-2206.
- [20] Yang, J., Bremer, P. J., Lamont, I. L. and McQuillan, A. J. **2006**. Infrared spectroscopic studies of siderophore-related hydroxamic acid ligands adsorbed on titanium dioxide. *Langmuir* 22: 10109-10117.
- [21] Holmen, B. A. and Casey, W. H. **1996**. Hydroxamate ligands, surface chemistry, and the mechanism of ligand-promoted dissolution of goethite [α -FeOOH(s)]. *Geochim. Cosmochim. Acta* 60: 4403-4416.
- [22] Stumm, W., Kummert, R. and Sigg, L. **1980**. A ligand-exchange model for the adsorption of inorganic and organic-ligands at hydrous oxide interfaces. *Croat. Chem. Acta* 53: 291-312.
- [23] Filius, J. D., Hiemstra, T. and Van Riemsdijk, W. H. **1997**. Adsorption of small weak organic acids on goethite: Modeling of mechanisms. *J. Colloid Interface Sci.* 195: 368-380.
- [24] Horanyi, G. **2002**. Specific adsorption of simple organic acids on metal(hydr) oxides: A radiotracer approach. *J. Colloid Interface Sci.* 254: 214-221.
- [25] Hayes, K. F., Papelis, C. and Leckie, J. O. **1988**. Modeling ionic-strength effects on anion adsorption at hydrous oxide solution interfaces. *J. Colloid Interface Sci.* 125: 717-726.
- [26] Johnson, B. B., Sjoberg, S. and Persson, P. **2004**. Surface complexation of mellitic acid to goethite: An attenuated total reflection Fourier transform infrared study. *Langmuir* 20: 823-828.
- [27] Tadanier, C. J. and Eick, M. J. **2002**. Formulating the charge-distribution multisite surface complexation model using FITEQL. *Soil Sci. Soc. Am. J.* 66: 1505-1517.
- [28] Noren, K., Loring, J. S. and Persson, P. **2008**. Adsorption of alpha amino acids at the water/goethite interface. *J. Colloid Interface Sci.* 319: 416-428.
- [29] Waite, T. D. and Morel, F. M. M. **1984**. Photoreductive dissolution of colloidal iron oxides in natural waters. *Environ. Sci. Technol.* 18: 860-868.
- [30] Cunningham, K. M., Goldberg, M. C. and Weiner, E. R. **1988**. Mechanisms for aqueous photolysis of adsorbed benzoate, oxalate and succinate on iron oxyhydroxides (goethite) surfaces. *Environ. Sci. Technol.* 22: 1090-1097.
- [31] Siffert, C. and Sulzberger, B. **1991**. Light-induced dissolution of hematite in the presence of oxalate - a case-study. *Langmuir* 7: 1627-1634.
- [32] Graetzel, M., Kiwi, J., Morrison, C. L., Davidson, R. S. and Tseung, A. C. C. **1985**. Visible-light-induced photodissolution of α -Fe₂O₃ powder in the presence of chloride anions. *J. Chem. Soc., Faraday Trans. 1* 81: 1883-1890.
- [33] Borer, P., Sulzberger, B., Hug, S. J., Kraemer, S. M. and Kretzschmar, R.

- submitted.** Photoreductive dissolution iron(III) (hydr)oxides in the absence of organic ligands: experimental studies and kinetic modeling *Environ. Sci. Technol.*
- [34] Sherman, D. M. **2005.** Electronic structures of iron(III) and manganese(IV) (hydr)oxide minerals: Thermodynamics of photochemical reductive dissolution in aquatic environments. *Geochim. Cosmochim. Acta* 69: 3249-3255.
- [35] Zhang, Y., Charlet, L. and Schindler, P. W. **1992.** Adsorption of protons, Fe(II) and Al(III) on lepidocrocite (γ -FeOOH). *Colloid. Surf.* 63: 259-268.
- [36] Kwan, W. P. and Voelker, B. M. **2002.** Decomposition of hydrogen peroxide and organic compounds in the presence of dissolved iron and ferrihydrite. *Environ. Sci. Technol.* 36: 1467-1476.
- [37] Samson, S. D. and Eggleston, C. M. **1998.** Active sites and the non-steady-state dissolution of hematite. *Environ. Sci. Technol.* 32: 2871-2875.
- [38] Samson, S. D. and Eggleston, C. M. **2000.** The depletion and regeneration of dissolution-active sites at the mineral-water interface: II. Regeneration of active sites on α -Fe₂O₃ at pH 3 and pH 6. *Geochim. Cosmochim. Acta* 64: 3675-3683.
- [39] Eggleston, C. M., Stack, A. G., Rosso, K. M. and Bice, A. M. **2004.** Adatom Fe(III) on the hematite surface: Observation of a key reactive surface species. *Geochemical Transactions* 5: 33-40.
- [40] Boukhalfa, H. and Crumbliss, A. L. **2002.** Chemical aspects of siderophore mediated iron transport. *Biometals* 15: 325-339.
- [41] Welch, K. D., Davis, T. Z. and Aust, S. D. **2002.** Iron autoxidation and free radical generation: effects of buffers, ligands, and chelators. *Arch. Biochem. Biophys.* 397: 360-369.
- [42] Bielski, B. H. J., Cabelli, D. E., Arudi, R. L. and Ross, A. B. **1985.** Reactivity of HO₂/O₂⁻ radicals in aqueous solution. *J. Phys. Chem. Ref. Data* 14: 1041-1100.
- [43] Zinder, B., Furrer, G. and Stumm, W. **1986.** The coordination chemistry of weathering: II. Dissolution of Fe(III) oxides. *Geochim. Cosmochim. Acta* 50: 1861-1869.
- [44] Pokrovsky, O. S., Schott, J. and Castillo, A. **2005.** Kinetics of brucite dissolution at 25°C in the presence of organic and inorganic ligands and divalent metals. *Geochim. Cosmochim. Acta* 69: 905-918.
- [45] Stumm, W. **1997.** Reactivity at the mineral-water interface: Dissolution and inhibition. *Colloid. Surf.* 120: 143-166.
- [46] Bondietti, G., Sinniger, J. and Stumm, W. **1993.** The reactivity of Fe(III) (hydr) oxides - Effects of ligands in inhibiting the dissolution. *Colloid. Surf.* 79: 157-167.

- [47] Amirbahman, A., Gfeller, M. and Furrer, G. **2000**. Kinetics and mechanism of ligand-promoted decomposition of the Keggin Al-13 polymer. *Geochim. Cosmochim. Acta* 64: 911-919.
- [48] Ludwig, C., Casey, W. H. and Rock, P. A. **1995**. Prediction of Ligand-Promoted Dissolution Rates from the Reactivities of Aqueous Complexes. *Nature* 375: 44-47.
- [49] Biber, M. V., Afonso, M. D. and Stumm, W. **1994**. The coordination chemistry of weathering. IV. Inhibition of the dissolution of oxide minerals. *Geochim. Cosmochim. Acta* 58: 1999-2010.
- [50] Ghosh, K. K., Patle, S. K., Sharma, P. and Rajput, S. K. **2003**. A comparison between the acid-catalysed reactions of some dihydroxamic acids, monohydroxamic acids and desferal. *Bull. Chem. Soc. Jpn.* 76: 283-290.
- [51] Solinas, V., Deiana, S., Gessa, C., Pistidda, C. and Rausa, R. **1996**. Reduction of the Fe(III)-desferrioxamine-B complexes by caffeic acid: A reduction mechanism of biochemical significance. *Soil Biol. Biochem.* 28: 649-654.
- [52] Holmen, B. A. and Casey, W. H. **1998**. Hydroxamate ligands, surface chemistry, and the mechanism of ligand-promoted dissolution of goethite [α -FeOOH(s)]. *Geochim. Cosmochim. Acta* 62: 726-726.
- [53] Borer, P., Sulzberger, B., Hug, S. J., Kraemer, S. M. and Kretzschmar, R. **submitted**. Wavelength-dependence of photoreductive dissolution of lepidocrocite (γ -FeOOH) in the absence and presence of the siderophore DFOB. *Environ. Sci. Technol.*
- [54] Barbeau, K., Rue, E. L., Trick, C. G., Bruland, K. T. and Butler, A. **2003**. Photochemical reactivity of siderophores produced by marine heterotrophic bacteria and cyanobacteria based on characteristic Fe(III) binding groups. *Limnol. Oceanogr.* 48: 1069-1078.

Supporting Information

Chapter 4

Table of contents

Acid-base titration of lepidocrocite	132
Dissolution of lepidocrocite in the absence of siderophores	132
Dissolution of lepidocrocite in the presence of siderophores	133
Siderophore-promoted dissolution of lepidocrocite as a function of ionic strength	134
Dissolution rate coefficients determined in the DFOB adsorption experiments	135
Adsorption isotherm of citrate at pH 4	135
Light-induced dissolution of lepidocrocite in the presence of citrate	136
References	136

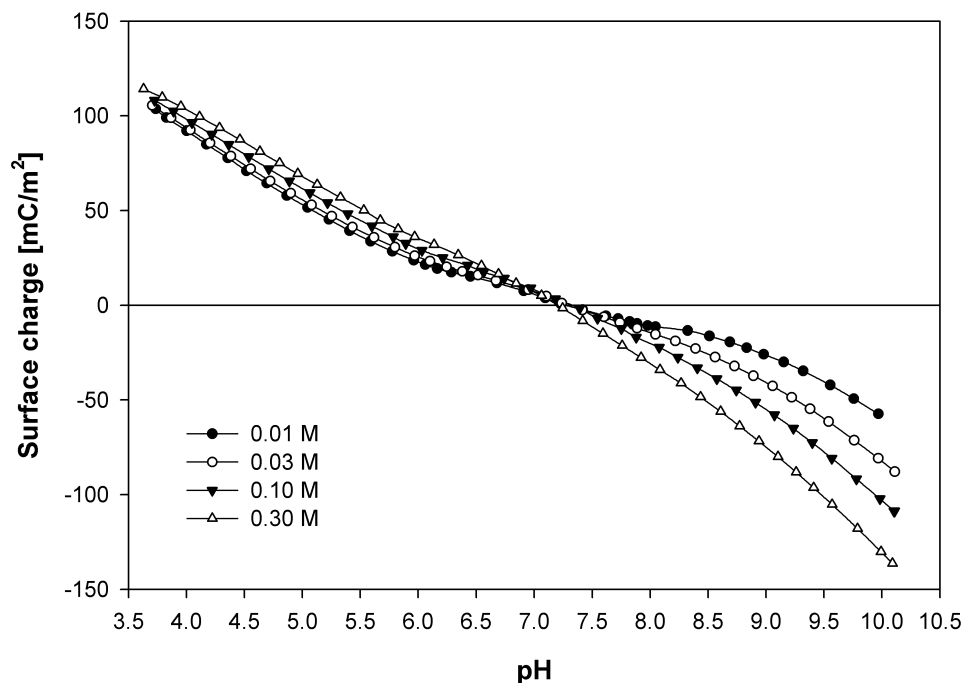


Fig. S1: Surface charge of lepidocrocite as a function of pH at different ionic strengths (NaClO_4). Surface charges were calculated from acid-base titration curves.

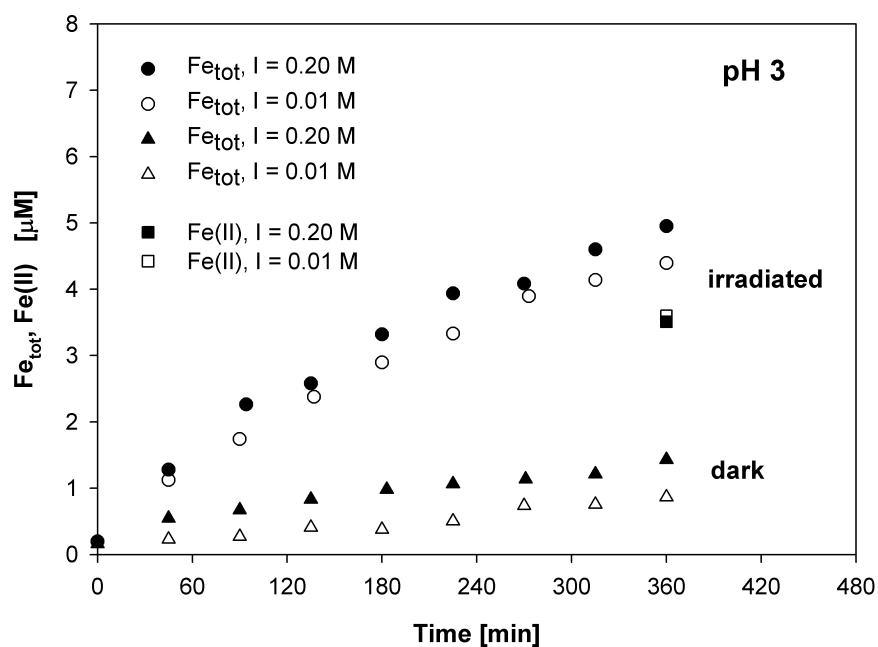


Fig. S2: Dissolution of lepidocrocite (25 mg/L) at pH 3 in the absence of any organic ligands. Dissolution experiments were performed in the dark as well as under irradiation (see experimental section). The ionic strength of the suspensions was adjusted to either 0.01 M or 0.20 M NaClO_4 . For the photodissolution experiments, dissolved Fe(II) was measured as well at the end of each experiment.

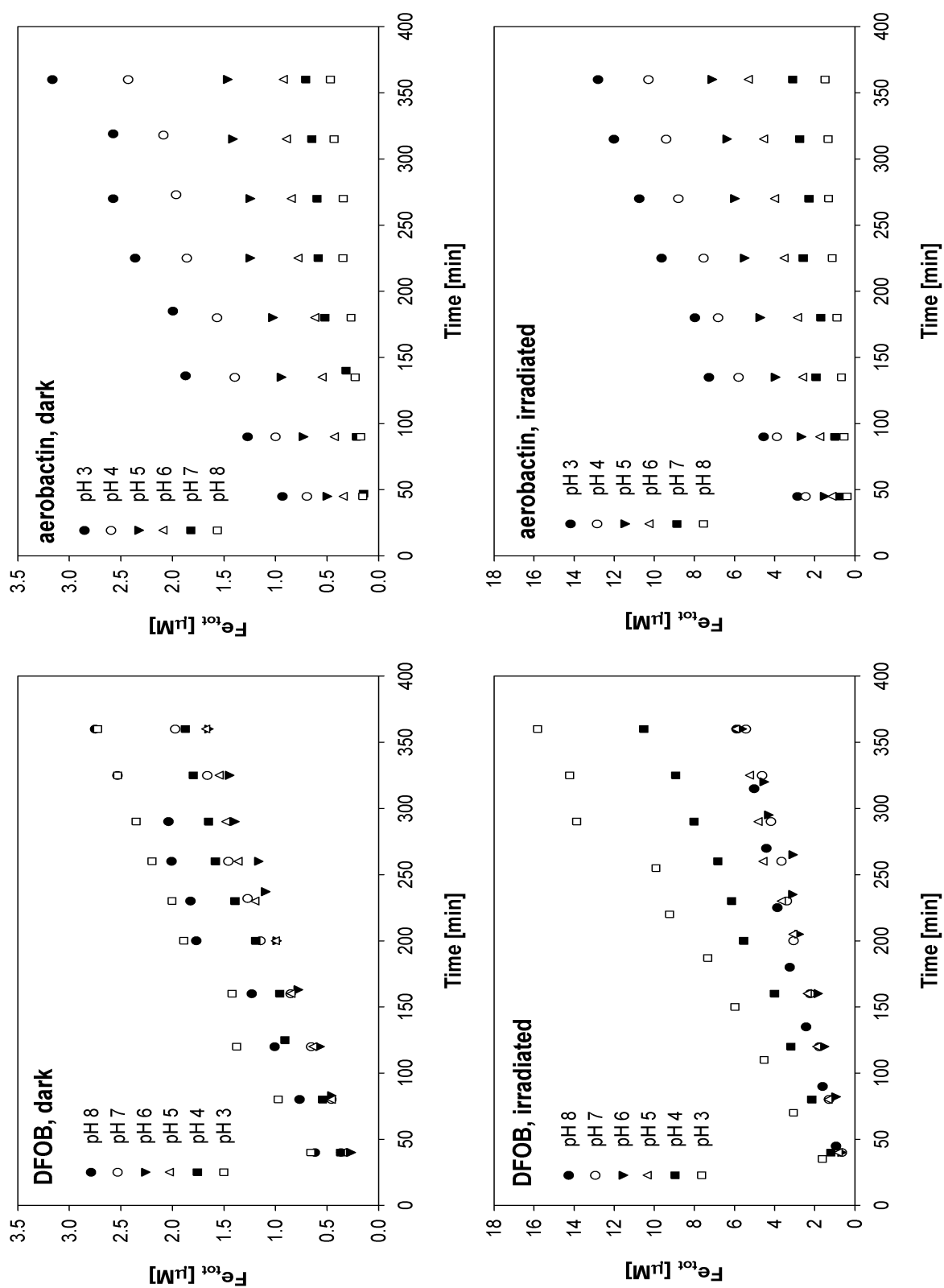


Fig. S3: Dissolution of lepidocrocite (25 mg/L) in the presence of 30 μM DFOB or aerobactin in the dark as well as under irradiation. The pH of the suspensions was varied between pH 3 and pH 8. The ionic strength was 0.01 M (NaClO_4). Total dissolved iron was measured.

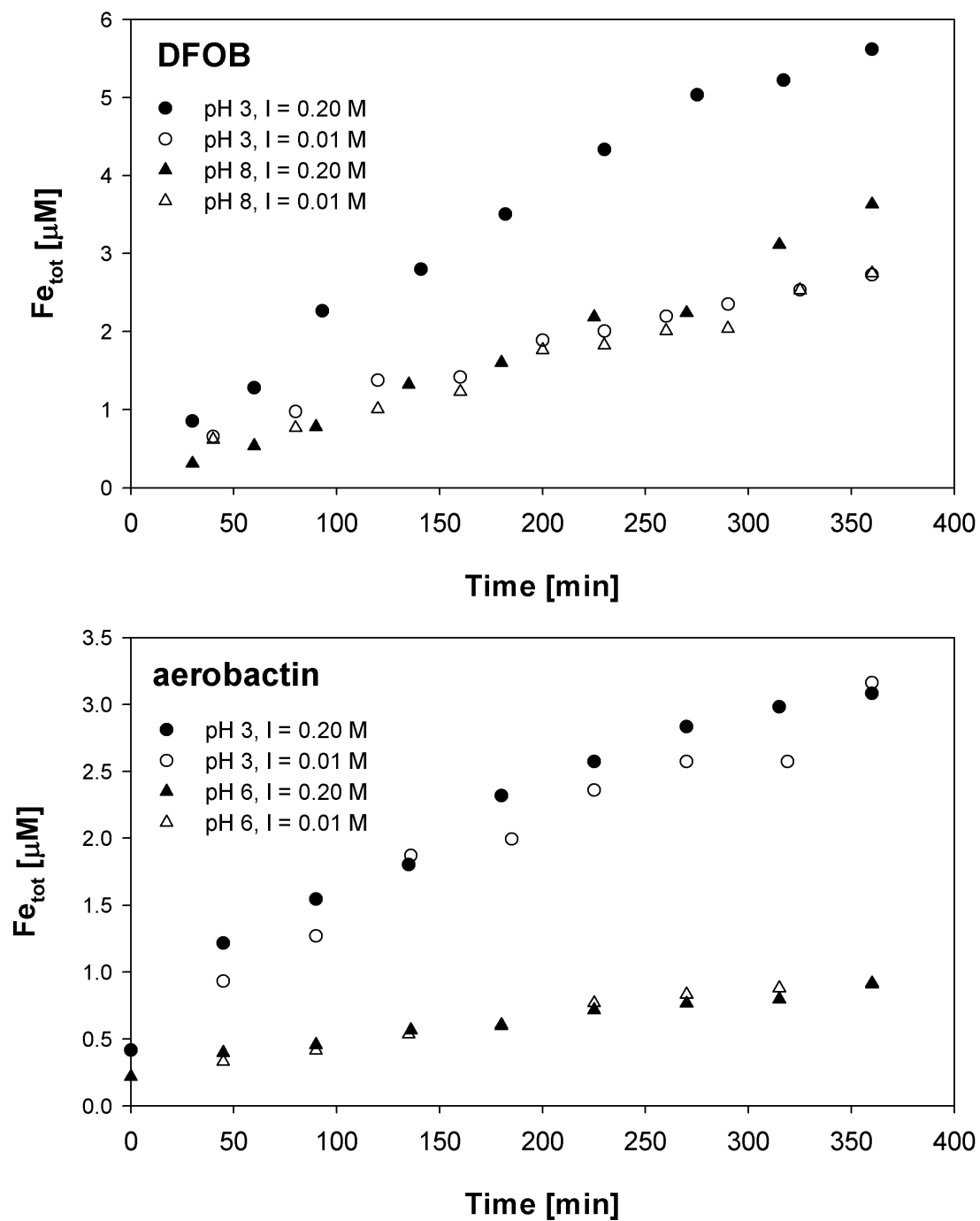


Fig. S4: Dissolution of lepidocrocite (25 mg/L) in the presence of 30 μM DFOB or aerobactin in the dark as a function of pH and ionic strength. Total dissolved iron was measured.

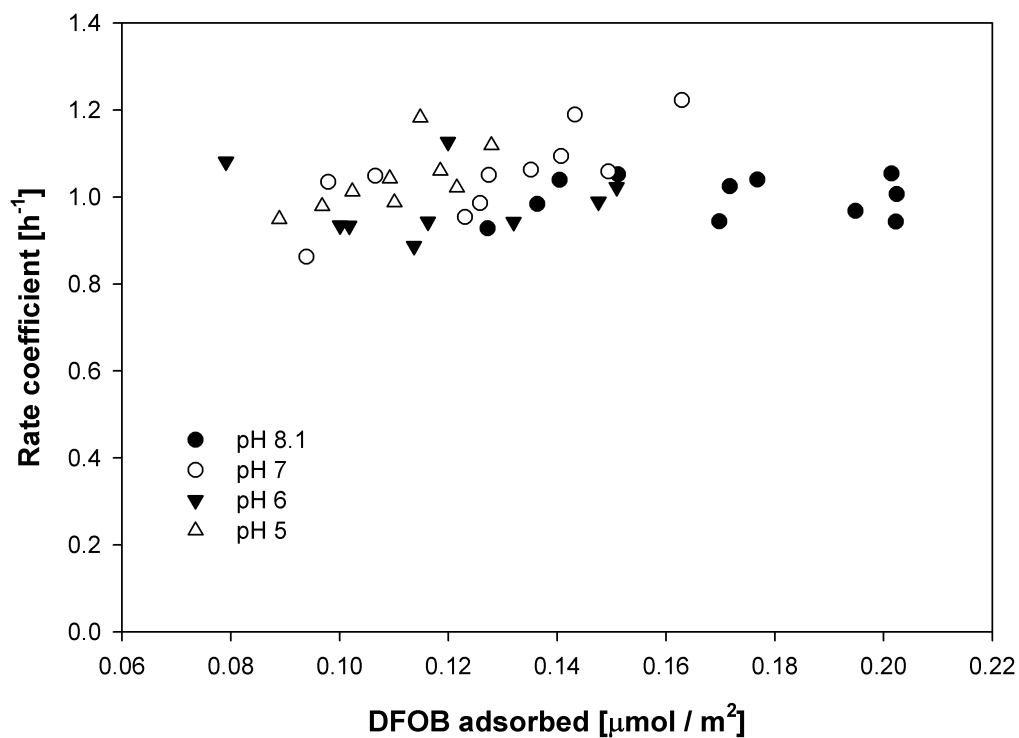


Fig. S5: Dissolution rate coefficients determined for the dissolution of lepidocrocite that occurred during the adsorption experiments between pH 5 and 8.1 (see Fig. 2A). Note that the rate coefficients calculated for these adsorption experiments - where the solid concentration was 1.5 g/L (1 g/L for the adsorption experiment at pH 8.1) - are in agreement to rate coefficients calculated for the dissolution experiments conducted at much higher ligand-to-solid ratios (30 μM DFOB and 25 mg/L lepidocrocite; see Fig S3).

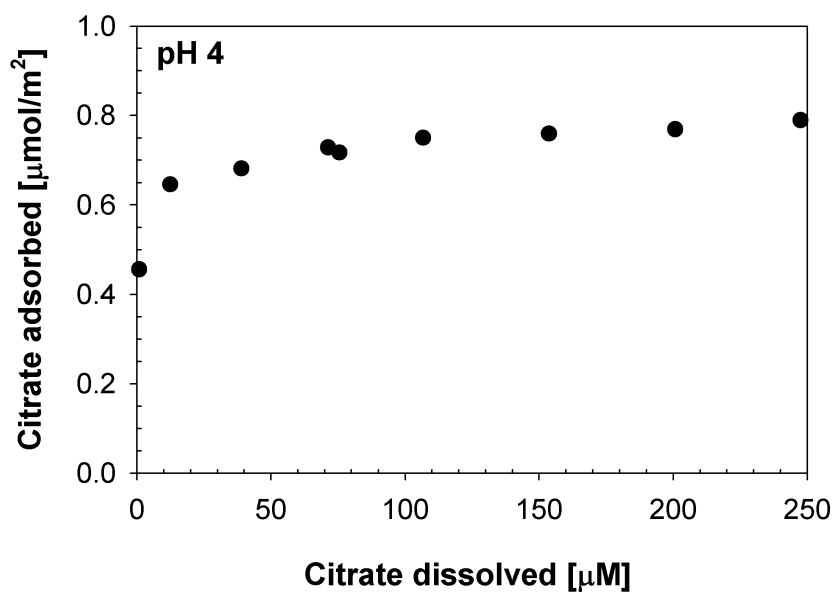


Fig. S6: Adsorption isotherm of citrate at pH 4 and constant ionic strength (0.01 M NaClO₄).

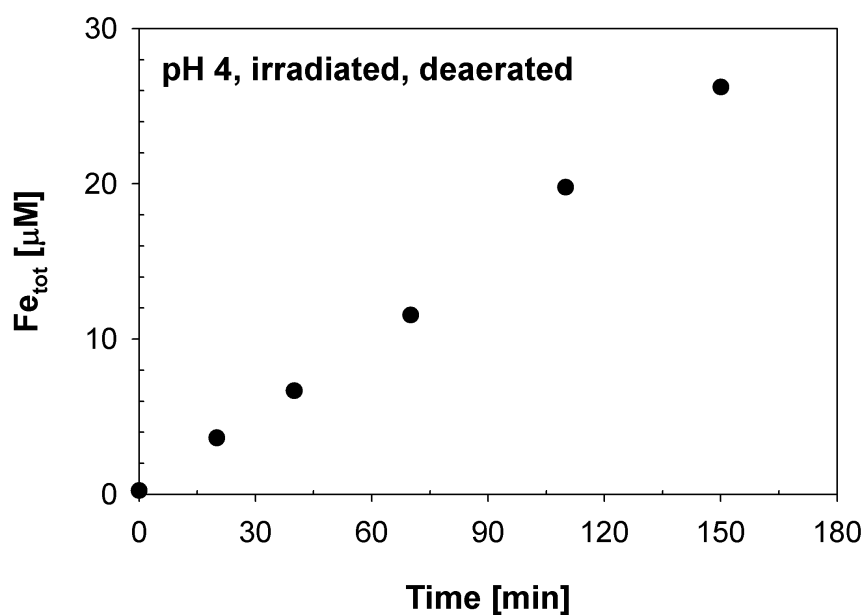


Fig. S7: Photodissolution experiment with a deaerated suspension of 25 mg/L lepidocrocite at pH 4 in the presence of 30 μM citrate. The ionic strength was 0.01 M (NaClO_4). The photo-irradiation setup used for this experiment is described elsewhere [1]. Total dissolved iron was measured in filtered samples.

References

- [1] Borer, P., Hug, S. J., Sulzberger, B., Kraemer, S. M. and Kretzschmar, R. **2007**. Photolysis of citrate on the surface of lepidocrocite: An in situ attenuated total reflection infrared spectroscopy study. *J. Phys. Chem. C* 111: 10560-10569.

Chapter 5

Photoreductive dissolution iron(III) (hydr) oxides in the absence of organic ligands: experimental studies and kinetic modeling

Paul Borer, Barbara Sulzberger, Stephan J. Hug, Stephan M. Kraemer and Ruben Kretzschmar

Prepared for publication in Environmental Science & Technology

Abstract

This study investigated the kinetics of photoreductive dissolution of various iron(III) (hydr)oxide phases (lepidocrocite (γ -FeOOH), ferrihydrite, hydrous ferric oxide) in the absence of organic ligands as a function of pH in deaerated and aerated suspensions. Photoreductive dissolution of lepidocrocite and ferrihydrite was only observed below pH 6. Under oxic conditions, we observed both the formation of aqueous Fe(II) and H₂O₂ during photoreductive dissolution of lepidocrocite and ferrihydrite at pH 3. These experimental findings are consistent with the light-induced reduction of surface Fe(III) at the oxide surface and the concomitant oxidation of coordinated water or hydroxyl groups, leading to surface Fe(II) and •OH radicals and subsequently to H₂O₂. The formation of •OH radicals at the surface was confirmed by photodissolution experiments conducted in the presence of •OH radical scavengers. Kinetic modeling of the experimental data suggested that the relevant pathway for the formation of H₂O₂ is the surface catalyzed reoxidation of surface Fe(II) by molecular oxygen. This study furthermore showed that in the presence of strong iron binding ligands such as siderophores (specifically desferrioxamine B) photoreductive dissolution of lepidocrocite, ferrihydrite and to a lesser extent hydrous ferric oxide may also proceed at seawater pH.

1. Introduction

Photoreductive dissolution of iron(III) (hydr)oxides or iron bearing minerals is an important process in many sunlit surface and atmospheric waters, particularly from the standpoint of iron bioavailability. The conversion of refractory iron phases into labile and bioavailable iron (e.g. dissolved species) may be considerably enhanced by photoreductive mechanisms [1-4]. In general, dissolution of iron(III) (hydr)oxides by (photo)reductive mechanisms is faster than by non-reductive dissolution mechanisms (e.g. proton-promoted or ligand-promoted thermal dissolution) [5, 6].

Photoreductive dissolution of iron(III) (hydr)oxides involves two reaction steps, (i) photoreduction of Fe(III) at the (hydr)oxide surface and (ii) subsequent release of surface-bound Fe(II) into solution. It is well known that organic ligands such as fulvic acids and smaller α -hydroxycarboxylic and carboxylic acids can effectively promote both reaction steps [4, 6-8], but the presence of such ligands is not a prerequisite for photoreductive dissolution. Laboratory studies have shown that photoreductive dissolution of natural or well defined iron(III) (hydr)oxides may also proceed in the absence of organic ligands, although with lower efficiency and only under rather acidic pH [4, 6, 9]. This process may be of importance in sunlit aquatic systems with extremely low dissolved organic carbon content, e.g. in atmospheric waters. It has been proposed that in the absence of organic ligands photoreduction of Fe(III) at the (hydr)oxide surface is enabled by light-induced ligand-to-metal charge-transfer excitations (LMCT) either within the semiconducting bulk or directly at the surface. At the surface, Fe(III)-hydroxo groups may undergo a photoredox reaction where Fe(III) is reduced while the coordinated hydroxyl group is oxidized to a \bullet OH radical [4, 9], akin to the photolysis of dissolved Fe(III)-hydroxo species [10-12]. Additionally, photoholes and photoelectrons generated within the semiconducting bulk may be scavenged at the surface leading to surface Fe(II) and \bullet OH radicals in the absence of organic ligands [9, 13, 14]. Recent studies suggested that this latter process may not be effective due to efficient recombination of photoelectrons and photoholes within the bulk [15, 16].

Photochemically formed Fe(II) and \bullet OH radicals undergo further reactions yielding additional reactive oxygen species (ROS) ($O_2^{\bullet-}/HO_2$, H_2O_2) in the presence of oxygen [17], which in turn may affect the kinetics of photoreductive dissolution [4]. According to recent thermodynamic calculations, photoreductive dissolution of crystalline iron(III) (hydr)oxide phases (hematite, goethite, lepidocrocite) is feasible at low pH in the absence of organic ligands, but cannot be significant at seawater pH, unless the activity of dissolved, uncomplexed Fe^{2+} is drastically reduced by strong complexation by iron binding ligands (e.g., siderophores) [13]. However, a recent study indicated

that photoreductive dissolution of less crystalline Fe(III) (hydr)oxide phases (e.g., amorphous Fe(III) hydroxide) may also occur in the absence of organic ligands at seawater pH [18].

The purpose of this study was to investigate the kinetics of photoreductive dissolution of different iron(III) (hydr)oxide phases (lepidocrocite, ferrihydrite and hydrous ferric oxide) in the absence of organic ligands under various conditions (pH and O₂ content). The focus was on lepidocrocite (γ -FeOOH), a well defined crystalline iron(III) (hydr)oxide, which has been shown to be considerably susceptible to photoreductive dissolution in the absence as well as in the presence of organic ligands [2, 4, 8, 19, 20]. Particular attention was given to the investigation of the formation/decay of reactive oxygen species (ROS) during photoreductive dissolution, particularly at low pH. Iron redox cycling and cycling of ROS at the mineral/water interface during photoreductive dissolution of lepidocrocite at low pH was investigated by kinetic modeling and by experiments in the presence of radical scavengers. In addition, experiments were conducted in the presence of a siderophore (desferrioxamine B) to assess if photoreductive dissolution of different iron(III) (hydr)oxides by intrinsic photoreductive mechanisms is feasible/relevant at higher pH (e.g., in marine waters).

2. Experimental section

2.1 Materials

Desferrioxamine B (DFOB) was purchased as the methanesulfonate salt [$C_{25}H_{46}N_5O_8NH_3^+(CH_3SO_3)^-$] from Sigma-Aldrich and was converted to the chloride salt with an anion exchange resin [21]. All other chemicals were at least reagent grade and were used as received from Sigma-Aldrich (details in Supporting Information). All solutions were prepared in high purity water (Milli-Q, Millipore). All glass- and plasticware were washed with HCl and thoroughly rinsed with high purity water prior to use.

2.2 Synthesis of iron(III) (hydr)oxides

Lepidocrocite (γ -FeOOH) was synthesized by oxidation of FeCl₂ with NaNO₂ in the presence of hexamethylenetetramine at 70 °C [22]. With this procedure, nitrogen- and carbon-containing oxidation by-products were produced, of which traces remained on the surface or within the bulk of the freeze-dried solid, even after extensive washing

(details in Supporting Information). We have used this oxide phase in recently published studies of photoreductive dissolution of lepidocrocite [2, 19]. Reference dissolution experiments with a subsequently synthesized lepidocrocite batch without any contaminants [23], albeit with different morphology, were conducted in order to demonstrate that no artifacts were produced by traces of carbon- and nitrogen-containing by-products. The contamination-free phase was not used as the major lepidocrocite phase in this study, because we observed significant adsorption of lepidocrocite particles from this batch to the walls of the reaction vessel. Photodissolution experiments were also conducted with ferrihydrite and hydrous ferric oxide. Details on the synthesis protocols and characterization of solids used in this study are provided in the Supporting Information.

2.3 Analytical methods

Samples for the determination of dissolved Fe(II) and H₂O₂ were taken from the suspensions and immediately filtered through 0.025 μm pore-size membrane filters (Whatman, Schleicher and Schuell). Dissolved Fe(II) and H₂O₂ were measured by colorimetric methods according to the procedures reported in Voelker and Sulzberger [24]. Filtered samples for total iron analysis were acidified with 1% v/v suprapure nitric acid and were measured with ICP-OES (Vista MPX, Varian). The detection limit for the determination of total iron, Fe(II) and H₂O₂ was ~0.1 μM. Details on the analytical methods are provided in the Supporting Information.

2.4 Experimental procedure

(Photo)dissolution experiments were carried out in a Pyrex glass vessel with a water jacket at 25 ± 1 °C. All experiments were conducted in 10 mM NaClO₄. Suspensions of 25 mg/L lepidocrocite or ferrihydrite were stirred with a Teflon coated stirrer and were pre-equilibrated at ~pH 6 for one hour before adjusting the pH. The pH of the suspensions was measured with a combined glass electrode (Metrohm 6.0253.100) and was automatically adjusted during the experiments with small additions of NaOH or HClO₄ by a dosimat (Metrohm). Deviations of solution pH were within ± 0.02 pH units. For the experiments conducted in the absence of O₂, the suspensions were purged with high purity N₂ gas before and throughout the experiments. The suspensions were irradiated with a solar simulator with a 1000 W high-pressure Xenon light source (OSRAM). The bottom window of the Pyrex vessel served as a high-pass filter so that only light with wavelengths greater than 305 nm penetrated into the vessel (simulated

sunlight). The irradiated area was 56 cm² and the irradiated volume of the suspension was 350 mL. The light intensity of light passing into the reaction vessel was 1340 W/m², as determined by 0.02 M ferrioxalate actinometry [25]. Samples were periodically taken from the suspensions for the analysis of total dissolved Fe, dissolved Fe(II), and H₂O₂. Photodissolution experiments with lepidocrocite also were performed in the presence of the •OH radical scavengers POHPAA (p-hydroxyphenylacetic acid), tert-butanol and benzene. In the case of benzene, additional benzene was added to N₂ purged solutions to account for outgassing during the experiments. In addition, photodissolution experiments with lepidocrocite, ferrihydrite and also hydrous ferric oxide were conducted in the presence of the siderophore desferrioxamine B.

2.5 Kinetic modeling

The formation of Fe(II), Fe(III) and H₂O₂ during the photoirradiation experiments at pH 3 was modeled with ACUCHEM [26] and with global fitting routines in Matlab (The Mathworks Inc.). Known reaction rate constants were taken from the literature. Unknown reaction rate constants were either estimated or varied by the global fitting routine in Matlab such that the sum of normalized square residuals between the model and the data was minimized. The global fitting routine allowed to fit models under different conditions in the same fit (e.g. models with and without oxidation reactions by O₂ in O₂-saturated or O₂-free solutions).

3. Results and discussion

3.1 Photoreductive dissolution of lepidocrocite

Fig. 1 shows the formation of dissolved Fe(II) and total dissolved Fe during irradiation of 25 mg/L lepidocrocite suspensions at different pH in the absence of organic ligands under oxic (Fig. 1A) and anoxic (Fig. 1B) conditions. The experimental results were highly reproducible. Replicate experiments conducted at pH 3 in aerated suspension and at pH 6 in deaerated (N₂-purged) suspension showed that the average difference of total dissolved iron or Fe(II) concentrations at all sampling times was less than 0.15 μM (data not shown). The significant formation of dissolved Fe(II) can only be explained by the light-induced formation of Fe(II) at the surface of lepidocrocite and subsequent release of Fe(II) into solution. At pH 2 and 3, 9.38 and 6.13 μM total dissolved Fe were formed, respectively, after 6 h irradiation of deaerated suspensions, and 86 and 90 % of

total dissolved Fe was present as Fe(II) (Fig. 1A). In comparison, reference dissolution experiments conducted in the dark resulted in 1.8 and 0.65 μM total dissolved Fe and no dissolved Fe(II) after 6 hours at pH 2 and 3, respectively (data not shown). Above pH 4, total Fe and Fe(II) concentrations were almost identical. At pH 2, the presence of O_2 led to significantly smaller Fe(II) solution concentrations as in the absence of O_2 , without lowering the concentration of total dissolved Fe (Fig. 1A, B). These results indicate that Fe(II) is reoxidized by ROS in solution (e.g., H_2O_2). Oxidation of aqueous Fe(II) by O_2 is far too slow at pH 2 ($t_{1/2} \sim \text{years}$ [27]) to explain the observed oxidation.

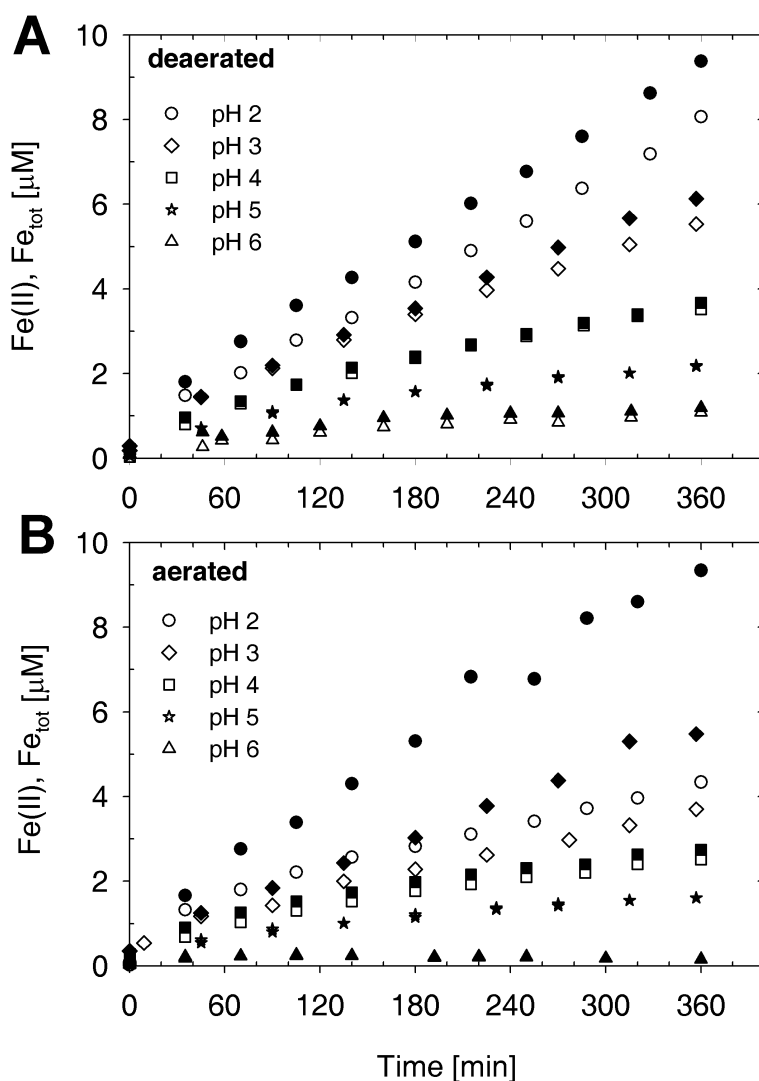


Fig. 1: Photodissolution experiments with suspensions of 25 mg/L lepidocrocite at various pH values at 0.01 M ionic strength (NaClO_4). Total Fe (filled symbols) and Fe(II) (open symbols) were measured in deaerated suspensions (A) and in aerated suspensions (B).

For both aerated and deaerated suspensions, a decrease of Fe(II) and total Fe solution concentrations was observed with increasing pH. This trend is consistent with a decreasing susceptibility of lepidocrocite to photoreductive dissolution with increasing pH, based on recent semiquantitative thermodynamic calculations [13]. Additionally, the formation of dissolved Fe(II) may be lowered by (i) readsorption of Fe(II) to the surface of lepidocrocite above pH 5 [28], and (ii) faster reoxidation of dissolved Fe(II) in solution by oxygen and/or ROS with increasing pH [17], resulting in precipitation of Fe(III) formed in solution at higher pH.

3.2 Formation of reactive oxygen species (ROS)

The photochemically formed Fe(II) and $\bullet\text{OH}$ at the lepidocrocite surface undergo further reactions yielding additional ROS (O_2^- , H_2O_2), particularly in the presence of oxygen [17]. Superoxide (O_2^-) may be formed by oxidation of surface lattice Fe(II) at the surface of lepidocrocite by O_2 and also by oxidation of aqueous Fe(II) by O_2 at higher pH. Dismutation of O_2^- , the bimolecular reaction of $\bullet\text{OH}$, and the oxidation of Fe(II) by O_2^- may lead to considerable amounts of H_2O_2 . To investigate these processes, additional photoirradiation experiments were conducted in which the concentrations of dissolved Fe(II), total dissolved Fe, and H_2O_2 were measured during a 6 h irradiation period and also subsequently in the dark. Fig. 2 shows the experiments performed at pH 3. In the deaerated and aerated suspension, respectively, a maximal H_2O_2 concentration of 370 nM and 1.85 μM was reached after approximately 225 min irradiation. The decay of H_2O_2 occurred before the light source was turned off, indicating a complex interplay of H_2O_2 with Fe(II) and with other ROS. The formation of Fe(II) was smaller in the aerated suspension, which is consistent with reoxidation of Fe(II) by H_2O_2 and by other ROS. Oxidation of Fe(II) by H_2O_2 is also inferred by the decrease of Fe(II) and H_2O_2 concentrations in the dark. An experiment conducted at pH 5 under aerated conditions (Fig. S2 B) showed significantly lower H_2O_2 concentrations as compared to the corresponding experiment at pH 3 (Fig. 2B). This is consistent with faster oxidation of Fe(II) by H_2O_2 and O_2^- at higher pH [17].

The nitrogen- and carbon-contamination of the lepidocrocite phase ($\sim 0.35 \mu\text{M}$ $\text{NO}_3^- + \text{NO}_2^- + \text{NH}_4^+$ and 10 μg carbon in 25 mg/L lepidocrocite suspensions) did not noticeably affect the formation and decay of Fe(II) and H_2O_2 , as indicated by additional photodissolution experiments with an uncontaminated lepidocrocite phase [23]. A comparable formation of Fe(II) and H_2O_2 was observed under irradiation in an aerated suspension at pH 3 (Fig. S3). However, the H_2O_2 concentration did not decline under prolonged irradiation as in the case of the contaminated phase (cf. Fig. 2B),

and precipitation of Fe(III) was observed in the dark after the 6 h irradiation period. The observed differences were reproducible based on replicate experiments (data not shown) and might be explained by taking the distinct morphology of both lepidocrocite phases into account. In contrast to the contamination-free phase, the contaminated phase showed a significant aggregation of lath-like crystals (Supporting Information).

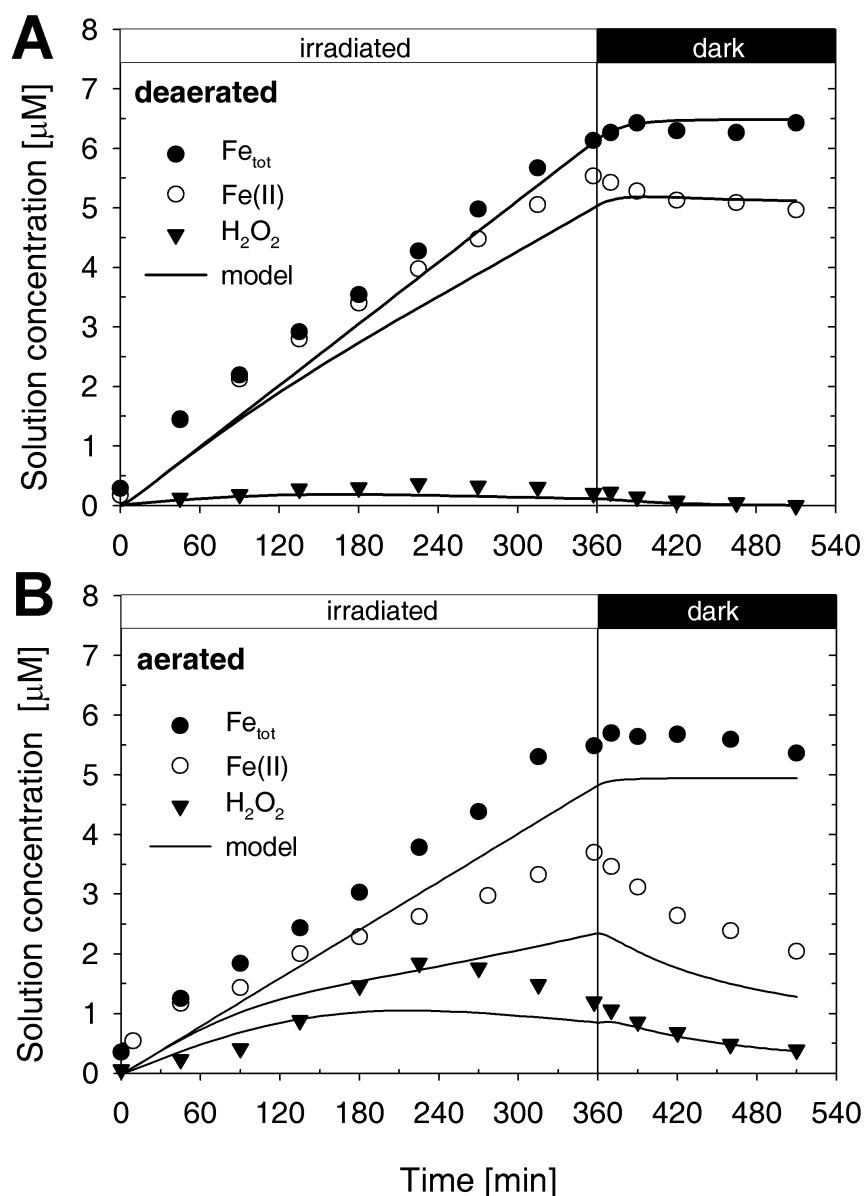


Fig. 2: (Photo-)dissolution experiments with suspensions of 25 mg/L lepidocrocite at pH 3 and 0.01 M ionic strength (NaClO_4). After 360 minutes of irradiation, the light source was turned off. Total dissolved Fe, Fe(II), and H_2O_2 were measured in deaerated suspensions (A) and in aerated suspensions (B). The model results (lines) are also shown.

We assume that the net formation of H_2O_2 is affected by reactions between ROS and Fe(II) during mass transport out of the crystal aggregates. This assumption is corroborated by similar trends in the formation and decay of H_2O_2 for a freeze-dried ferrihydrite batch as presented later in this paper. Similar to lepidocrocite, the batch of freeze-dried ferrihydrite consisted of strongly coagulated particles.

3.3 Kinetic modeling of Fe(II) and ROS formation

A kinetic model was developed to identify key reactions leading to the observed concentrations of dissolved Fe(II) and H_2O_2 at pH 3 during photoreductive dissolution of lepidocrocite and after the light source was turned off (Table 1). The goal of the kinetic modeling was not to provide a complete description of reactions occurring in this complex heterogeneous system, but to identify important reaction pathways by which dissolved Fe(II) and H_2O_2 were formed. For simplicity, it was assumed that surface Fe(II) and $\bullet\text{OH}$ are formed by photolysis of surface Fe(III)-hydroxo groups. Surface and solution reactions of Fe(II), Fe(III) and ROS were modeled with the same set of solution reactions as presented by Kwan and Voelker [17]. Details of the kinetic model are provided in the Supporting Information. Only Fe(II), O_2^- and H_2O_2 formed at the surface were allowed to be released into solution. The release reactions were described by first order reactions, which is a simplification of the probably more complex solid/water mass transfer. It was further assumed that $\bullet\text{OH}$ formed at the surface quickly reacts with other ROS and Fe(II) at the surface, such that release of $\bullet\text{OH}$ into solution can be neglected. Release of Fe(III) into solution was not considered. Since the model was only applied at pH 3, precipitation of Fe(III) in solution was omitted. Rate constants for the release of surface Fe(II), O_2^- and H_2O_2 into solution as well as for the reoxidation of surface Fe(II) by O_2 were fitted (k_1 - k_4). The best fit was achieved by setting the initial value of k_1 to $\sim 10^{-3} \text{ s}^{-1}$ (release of surface Fe(II) into solution), which is equivalent to a half-life of 13 min. The maximal formation rate of dissolved Fe(II) ($4.3 \times 10^{-9} \text{ mol/m}^2/\text{s}$), as calculated by the light-induced formation of surface Fe(II) and its transfer into solution (reactions L1 and RL1 in Table 1), is identical to the Fe(II) formation rates determined during thermal reductive dissolution of different lepidocrocite phases in the presence of excess ascorbic acid [29]

The model results are shown in Fig. 2. The model cannot reproduce the experimental data perfectly, but it does reproduce the observed trends. According to the model, the half-life for the release of H_2O_2 and O_2^-/HO_2 from the lepidocrocite surface was 5 min and 16 min, respectively. The release of H_2O_2 and O_2^-/HO_2 occurs on a similar timescale as the release of surface Fe(II), which suggests that a large fraction of these species

Table 1: Kinetic model and rate constants

	Reactions	rate constants (s⁻¹) or (M⁻¹ s⁻¹)	Ref.
Fe(III) photolysis at the surface			
L1 ^a	$\text{Fe(III)}_{\text{surf}} \rightarrow \text{Fe(II)}_{\text{surf}} + \cdot\text{OH}_{\text{surf}}^?$	5×10^{-4}	Estimated ^c
Fe(II) release into solution			
RL1	$\text{Fe(II)}_{\text{surf}} \rightarrow \text{Fe(II)}$	$k_1 (8.65 \times 10^{-4})$	Fitted
Fe(III) photolysis in solution			
L2 ^a	$\text{Fe(III)} \rightarrow \text{Fe(II)} + \cdot\text{OH}$	1.5×10^{-3}	Estimated ^c
Fe(II) oxidation at the surface			
SO1 ^a	$\text{Fe(II)}_{\text{surf}} + \text{O}_2 \rightarrow \text{Fe(III)}_{\text{surf}} + \text{O}_2^-/\text{HO}_2_{\text{surf}}$	$k_2 (2.70 \times 10^3)$	Fitted
SO2	$\text{Fe(II)}_{\text{surf}} + \text{O}_2^-/\text{HO}_2_{\text{surf}} \rightarrow \text{Fe(III)}_{\text{surf}} + \text{H}_2\text{O}_2_{\text{surf}}$	6.6×10^6	[17] ^b
SO3	$\text{Fe(II)}_{\text{surf}} + \text{H}_2\text{O}_2_{\text{surf}} \rightarrow \text{Fe(III)}_{\text{surf}} + \cdot\text{OH}_{\text{surf}}$	63	[17] ^b
SO4	$\text{Fe(II)}_{\text{surf}} + \cdot\text{OH}_{\text{surf}} \rightarrow \text{Fe(III)}_{\text{surf}}$	3.2×10^8	[17] ^b
Fe(III) reduction at the surface			
SR1	$\text{Fe(III)}_{\text{surf}} + \text{H}_2\text{O}_2_{\text{surf}} \rightarrow \text{Fe(II)}_{\text{surf}} + \text{O}_2^-/\text{HO}_2_{\text{surf}}$	2×10^{-3}	[17] ^b
SR2	$\text{Fe(III)}_{\text{surf}} + \text{O}_2^-/\text{HO}_2_{\text{surf}} \rightarrow \text{Fe(II)}_{\text{surf}} + \text{O}_2$	3.1×10^7	[17] ^b
surface reactions of ROS			
SRC1	$\cdot\text{OH}_{\text{surf}} + \cdot\text{OH}_{\text{surf}} \rightarrow \text{H}_2\text{O}_2_{\text{surf}}$	5.2×10^9	[17] ^b
SRC2	$\cdot\text{OH}_{\text{surf}} + \text{O}_2^-/\text{HO}_2_{\text{surf}} \rightarrow \text{O}_2$	7.1×10^9	[17] ^b
SRC3	$\cdot\text{OH}_{\text{surf}} + \text{H}_2\text{O}_2_{\text{surf}} \rightarrow \text{O}_2^-/\text{HO}_2_{\text{surf}}$	3.3×10^7	[17] ^b
SRC4	$\text{O}_2^-/\text{HO}_2_{\text{surf}} + \text{O}_2^-/\text{HO}_2_{\text{surf}} \rightarrow \text{H}_2\text{O}_2_{\text{surf}}$	2.3×10^6	[17] ^b
ROS release from the surface			
RL2	$\text{H}_2\text{O}_2_{\text{surf}} \rightarrow \text{H}_2\text{O}_2$	$k_3 (2.35 \times 10^{-3})$	Fitted
RL3	$\text{O}_2^-/\text{HO}_2_{\text{surf}} \rightarrow \text{O}_2^-/\text{HO}_2$	$k_4 (7.26 \times 10^{-4})$	Fitted
Fe(II) oxidation in solution			
O1	$\text{Fe(II)} + \text{H}_2\text{O}_2 \rightarrow \text{Fe(III)} + \cdot\text{OH}$	63	[17]
O2	$\text{Fe(II)} + \text{O}_2^-/\text{HO}_2 \rightarrow \text{Fe(III)} + \text{H}_2\text{O}_2$	1.3×10^6	[17]
O3	$\text{Fe(II)} + \cdot\text{OH} \rightarrow \text{Fe(III)}$	3.2×10^8	[17]
Fe(III) reduction in solution			
R1	$\text{Fe(III)} + \text{H}_2\text{O}_2 \rightarrow \text{Fe(II)} + \text{O}_2^-/\text{HO}_2$	2×10^{-3}	[17]
R2	$\text{Fe(III)} + \text{O}_2^-/\text{HO}_2 \rightarrow \text{Fe(II)} + \text{O}_2$	7.8×10^5	[17]
Solution reactions of ROS			
RC1	$\cdot\text{OH} + \cdot\text{OH} \rightarrow \text{H}_2\text{O}_2$	5.2×10^9	[17]
RC2	$\cdot\text{OH} + \text{O}_2^-/\text{HO}_2 \rightarrow \text{O}_2$	7.1×10^9	[17]
RC3	$\cdot\text{OH} + \text{H}_2\text{O}_2 \rightarrow \text{O}_2^-/\text{HO}_2$	3.3×10^7	[17]
RC4	$\text{O}_2^-/\text{HO}_2 + \text{O}_2^-/\text{HO}_2 \rightarrow \text{H}_2\text{O}_2$	2.3×10^6	[17]

^a The rate constants of these reactions are set to zero under conditions where these reactions do not take place (e.g. in the dark or in the absence of O₂). ^b Surface reactions are formulated in analogy to solution reactions as reported by Kwan and Voelker [17]. ^c Details in Supporting Information.

undergo further surface reactions. The model suggests that the most relevant reaction leading to the formation of solution H_2O_2 is the oxidation of lattice Fe(II) by O_2 . The fitted rate constant of $2700 \text{ M}^{-1} \text{ s}^{-1}$ (k_2) is almost three orders of magnitude greater than the rate constant reported for the oxidation of Fe(II) adsorbed on goethite [27]. In analogy to the faster oxidation of aqueous Fe(II) species with an increasing degree of hydrolysis of the Fe^{2+} cation (sequence: Fe^{2+} , FeOH^+ , $\text{Fe}(\text{OH})_2$) [27], we assume that surface lattice Fe(II) of lepidocrocite is more strongly coordinated by lattice oxygen atoms than Fe(II) that is adsorbed on goethite, resulting in the higher stabilization of the Fe(III) redox state and hence in faster reoxidation by O_2 . These arguments apparently do not hold for the oxidation of lattice Fe(II) by H_2O_2 , based on our simplified model, because an increase in the rate constant of 2-3 orders of magnitude for the oxidation of surface Fe(II) by H_2O_2 resulted in a less good agreement between model and data. Except for the release of $\text{O}_2^-/\text{HO}_2^-$ from the surface (rate constant k_4), the fitted parameters (k_1 - k_3) were well constrained (Fig. S4). Apparently, the release $\text{O}_2^-/\text{HO}_2^-$ into solution can be neglected in this reaction scheme (Table 1). Further experimental studies combined with kinetic modeling are required to gain more conclusive insight into the oxidation kinetics of Fe(II) at the mineral/water interface by O_2 and H_2O_2 .

3.4 Effect of radical scavengers and organic ligands on photoreductive dissolution

Fig. 3 shows the effect of $\bullet\text{OH}$ radical scavengers on the photoreductive dissolution of lepidocrocite in deaerated suspensions at pH 5. In comparison to the experiment conducted in the absence of any radical scavengers, the presence of 1 mM tert-butanol or benzene did not significantly change the extent of dissolved Fe(II) formation. However, an increase in total Fe and Fe(II) solution concentrations by a factor of 3 was observed after 6 h irradiation in the presence of 1 mM POHPAA (cf. Fig. 1). POHPAA, which is negatively charged at pH 5 (carboxylate containing compound) interacts more strongly with the positively charged surface of lepidocrocite by electrostatic forces as compared to the neutral compounds tert-butanol and benzene. This interaction results in higher concentrations of POHPAA in the interfacial region where $\bullet\text{OH}$ is formed. These results support the kinetic model according to which $\bullet\text{OH}$ radicals are formed at the surface of lepidocrocite. Hence scavenging of $\bullet\text{OH}$ radicals at the surface diminishes the back reaction of surface Fe(II) and $\bullet\text{OH}$ and thus results in higher solution concentrations of Fe(II). These results furthermore indicate that $\bullet\text{OH}$ formed at the surface does not diffuse into solution and that radical scavengers are only effective if

they interact strongly with the surface. The observation that neutral radical scavengers are less effective in scavenging $\bullet\text{OH}$ radicals formed at a positively charged oxide surface, as compared to negatively charged scavengers, has been reported recently [30]. Photodissolution experiments at pH 5 in the presence of POHPAA are shown in Fig. S5. In the presence of POHPAA, the rates of light-induced dissolved Fe(II) formation were considerably higher in both the deaerated and the aerated suspensions, as compared to the photodissolution experiments in the absence of POHPAA at pH 5 (see Fig. 1).

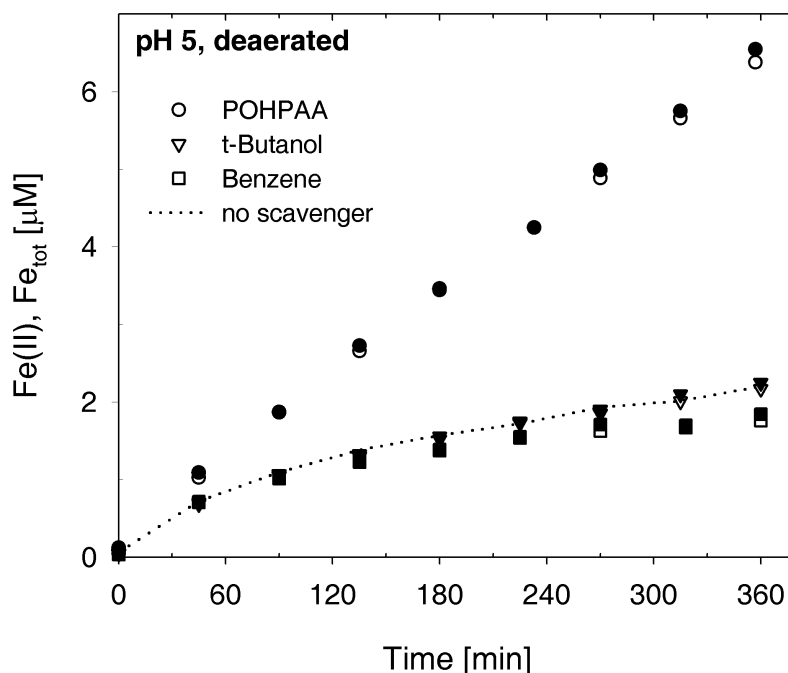


Fig. 3: Photodissolution experiments with deaerated suspensions of 25 mg/L lepidocrocite at pH 5 and at 0.01 M ionic strength (NaClO_4) in the presence of the hydroxyl radical scavengers POHPAA, tert-butanol or benzene (1 mM). Both total dissolved Fe (filled symbols) and dissolved Fe(II) (open symbols) were measured. For comparison, the corresponding experiment in the absence of radical scavengers is included (line; total dissolved Fe concentration) (cf. Fig. 1).

Organic ligands may enhance photoreductive dissolution of iron(III) (hydr)oxides, not only by acting as radical scavengers, but in the case of iron binding ligands also by facilitating the release of surface Fe(II) into solution and by preventing oxidative precipitation of dissolved Fe(II). This is illustrated by photodissolution experiments conducted in the presence of the siderophore DFOB, a strong iron binding ligand which also has radical scavenging properties [31]. Under the same experimental conditions as given in Fig. 3, the dissolution rate of lepidocrocite was twice as high in the presence of 80 μM DFOB as in the presence of 1 mM POHPAA (data with DFOB not shown in Fig. 3). Fig. 4 shows that in the presence of DFOB, dissolution rates at pH 3 and 8

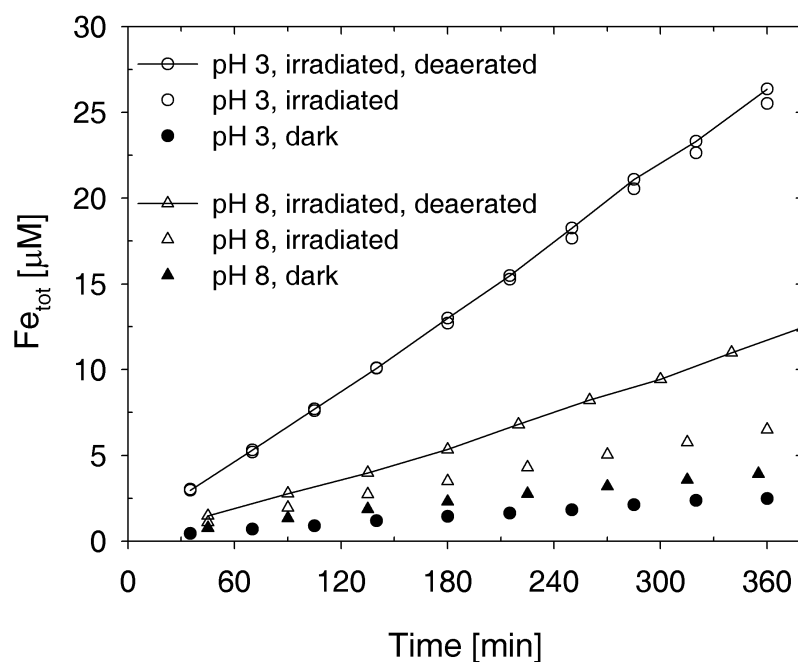


Fig. 4: (Photo-)dissolution experiments with suspensions of 25 mg/L lepidocrocite at pH 3 and pH 8 and 0.01 M ionic strength (NaClO_4) in the presence of 80 μM DFOB. Total dissolved Fe was measured.

increased upon irradiation with simulated sunlight.

At pH 3, the dissolution rate was almost identical in the deaerated and aerated suspensions and was by a factor of 4 higher than in the absence of DFOB (cf. Fig. 1A, deaerated suspension). At pH 8, the presence of oxygen reduced the light-induced formation of dissolved Fe. This result is consistent with faster oxidation kinetics of surface Fe(II) by oxygen and ROS at pH 8 as compared to pH 3. Under oxic conditions where surface Fe(II) is rapidly reoxidized by molecular oxygen and ROS, DFOB may enhance the release of Fe(II) before significant reoxidation occurs and may prevent precipitation of dissolved Fe [2]. According to the thermodynamic predictions of Sherman [13], only sub-femtomolar concentrations of dissolved Fe(II) can be formed by direct photoreductive dissolution of lepidocrocite at pH 8 in the absence of iron-binding ligands. Our results confirm that in the presence of a strong iron binding ligand like DFOB much higher concentrations of total dissolved Fe can form upon photoreductive dissolution of lepidocrocite at pH 8 (cf. Fig. 4). After 6 hours approximately 3 μM total dissolved Fe was formed due to photoreductive dissolution of lepidocrocite in the presence of DFOB under aerated conditions at pH 8, as calculated by the difference in the concentrations of total dissolved Fe in the dark and under irradiation.

3.5 Photoreactivity of other iron (hydr)oxides

Irradiation experiments were conducted with a freeze-dried batch of ferrihydrite and with aged hydrous ferric oxide (see also Supporting Information). Ferrihydrite showed a similar photoreactivity towards photodissolution in organic-free suspensions at pH 3 as lepidocrocite (Fig. 5), despite its larger surface area (330 m²/g). We assume that freeze-drying of ferrihydrite and the resulting coagulation of particles was the cause of the relatively low dissolution rates of ferrihydrite. The dissolution rate of ferrihydrite at pH 3 in the dark was as twice as high as the corresponding dissolution rate of lepidocrocite (Fig. S6). However, unlike lepidocrocite, almost no photoreductive dissolution of ferrihydrite under oxygen-free conditions was observed at pH 6 (Fig. S6). This phenomenon may be attributed to stronger readsorption of Fe(II) at the ferrihydrite surface. In the presence of DFOB, only a slight increase in the dissolution rate of ferrihydrite was observed at pH 8 under irradiation (deaerated suspension) as compared to the corresponding dark experiment (Fig. S7). In contrast, irradiation of lepidocrocite suspensions resulted in a significant increase in the dissolution rate under the same conditions (cf. Fig. 4). Dissolution experiments with aged hydrous ferric oxide (100 μM Fe(III) aged for 5 hours at pH 8) in the presence of 40 μM DFOB at pH 8 were also conducted (Fig. S8). Dissolution in the dark by DFOB, as measured by the formation of dissolved Fe-DFOB complexes, was fast and the dissolution rate was only slightly enhanced under irradiation. Apparently, light has only a weak effect on the dissolution of ferrihydrite and hydrous ferric oxides in the presence of siderophores. In a previous study, we observed that dissolution of goethite at pH 6 under similar conditions was not observed in the presence of DFOB, both in the dark and under irradiation [2].

These results suggest that under conditions where direct photoreductive dissolution of iron(III) (hydr)oxides is thermodynamically feasible, e.g. at low pH or at high pH in the presence of siderophores, the detachment of surface Fe(II) into solution and reoxidation of surface Fe(II) by oxygen and ROS are two key processes determining the extent of photoreductive dissolution. With increasing thermodynamic stability of iron(III) (hydr)oxides, the release of lattice surface Fe(II) into solution may be increasingly outcompeted by reoxidation by oxygen and/or ROS [20]. This is the likely reason why photoreductive dissolution of goethite was not observed at pH 6 even in the presence of DFOB [2]. In the case of lepidocrocite, which is an intermediate phase between thermodynamically more stable iron (hydr)oxide phases (e.g., goethite) and less stable phases (e.g., ferrihydrite), release of surface Fe(II) into solution at pH 8 seems to take place in the presence of DFOB before complete reoxidation occurs. In the case of ferrihydrite and hydrous ferric oxide, thermal dissolution by DFOB is apparently

more important for the overall dissolution, as compared to the small contribution of photoreductive dissolution.

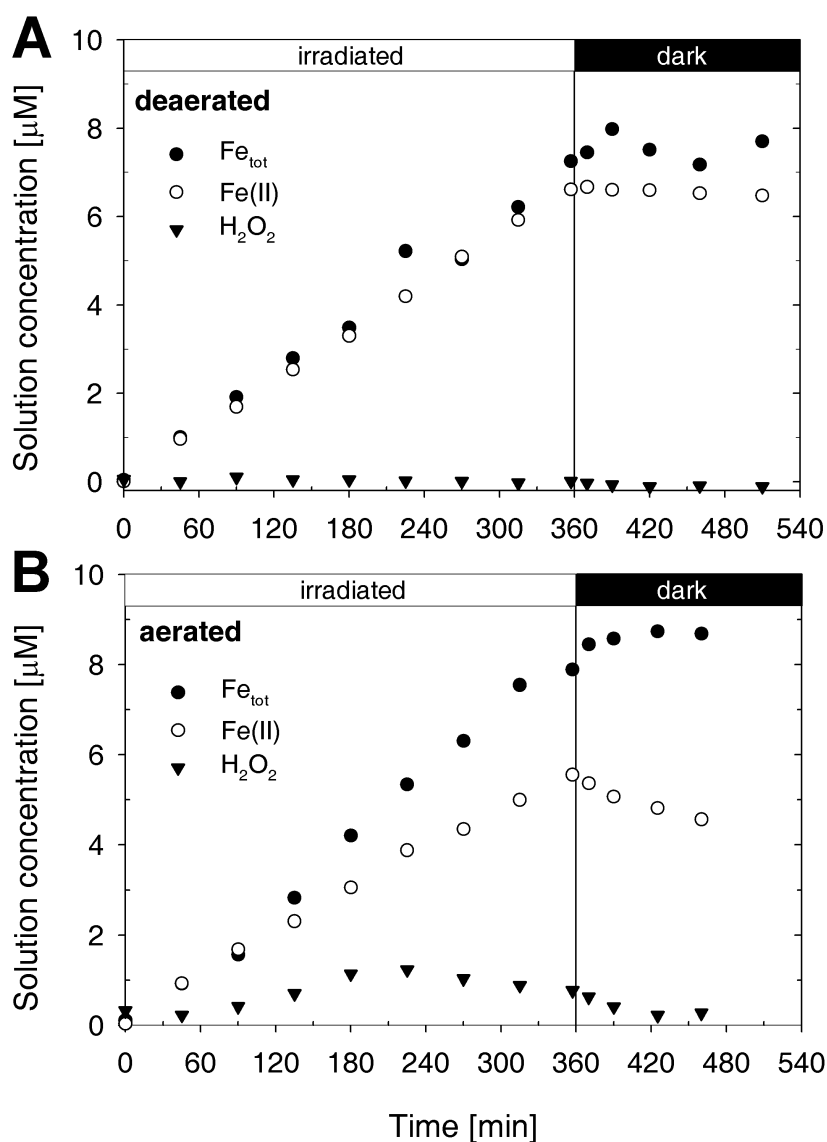


Fig. 5: (Photo-)dissolution experiments with suspensions of 25 mg/L ferrihydrite at pH 3 and 0.01 M ionic strength (NaClO_4). After 360 minutes of irradiation, the light source was turned off. Total dissolved Fe, Fe(II), and H_2O_2 were measured in deaerated suspensions (A) and in aerated suspensions (B).

3.6 Environmental significance

Photolysis of aqueous Fe(III)-hydroxo complexes has been proposed as one of the major sources of $\cdot\text{OH}$ radicals and Fe(II) in low pH atmospheric waters [11]. This study suggests that photoreductive dissolution of colloidal iron in the absence of organic matter also contributes to the formation of dissolved Fe(II) and ROS at low

pH. This process may be of importance in atmospheric waters that exhibit low pH values and low organic carbon content. The atmospheric transport and deposition of iron into open marine systems has been shown to play an important role regarding iron bioavailability [32]. At high pH, i.e. seawater pH, the presence of organic matter seems to be a prerequisite for photoreductive dissolution of Fe(III) (hydr)oxides to occur. Our results show that strong iron binding ligands like siderophores enable photoreductive dissolution of Fe(III) (hydr)oxides even at pH 8, with the strongest effect observed for lepidocrocite, which is an intermediate phase regarding thermodynamic stability. The ability of siderophores like DFOB to shift the thermodynamic feasibility of direct photoreduction of iron(III) (hydr)oxides [13], to facilitate the release of photochemically produced Fe(II) into solution before complete reoxidation by oxygen or ROS occurs, and to prevent Fe(III) precipitation suggests that photoreductive dissolution of colloidal iron may significantly contribute to the generation of dissolved and bioavailable iron even in high pH waters.

4. References

- [1] Johnson, K. S., Coale, K. H., Elrod, V. A. and Tindale, N. W. **1994**. Iron photochemistry in seawater from the equatorial Pacific. *Mar. Chem.* 46: 319-334.
- [2] Borer, P. M., Sulzberger, B., Reichard, P. and Kraemer, S. M. **2005**. Effect of siderophores on the light-induced dissolution of colloidal iron(III)(hydr)oxides. *Mar. Chem.* 93: 179-193.
- [3] Wells, M. L. and Mayer, L. M. **1991**. The photoconversion of colloidal iron oxyhydroxides in seawater. *Deep-Sea Res.* 38: 1379-1395.
- [4] Waite, T. D. and Morel, F. M. M. **1984**. Photoreductive dissolution of colloidal iron oxides in natural waters. *Environ. Sci. Technol.* 18: 860-868.
- [5] Suter, D., Banwart, S. and Stumm, W. **1991**. Dissolution of hydrous iron(III) oxides by reductive mechanisms. *Langmuir* 7: 809-813.
- [6] Siffert, C. and Sulzberger, B. **1991**. Light-induced dissolution of hematite in the presence of oxalate - a case-study. *Langmuir* 7: 1627-1634.
- [7] Kuma, K., Nakabayashi, S. and Matsunaga, K. **1995**. Photoreduction of Fe(III) by hydroxycarboxylic acids in seawater. *Water Res.* 29: 1559-1569.
- [8] Voelker, B. M., Morel, F. M. M. and Sulzberger, B. **1997**. Iron redox cycling in surface waters: Effects of humic substances and light. *Environ. Sci. Technol.* 31: 1004-1011.

- [9] Cunningham, K. M., Goldberg, M. C. and Weiner, E. R. **1988**. Mechanisms for aqueous photolysis of adsorbed benzoate, oxalate and succinate on iron oxyhydroxides (goethite) surfaces. *Environ. Sci. Technol.* 22: 1090-1097.
- [10] Benkelberg, H. J. and Warneck, P. **1995**. Photodecomposition of iron(III) hydroxo and sulfato complexes in aqueous-solution - wavelength dependence of OH and SO_4^- quantum yields. *J. Phys. Chem.* 99: 5214-5221.
- [11] Faust, B. C. and Hoigne, J. **1990**. Photolysis of Fe(III)-hydroxy complexes as sources of OH radicals in clouds, fog and rain. *Atmos. Environ.* 24: 79-89.
- [12] King, D. W., Aldrich, R. A. and Charnecki, S. E. **1993**. Photochemical redox cycling of iron in NaCl solutions. *Mar. Chem.* 44: 105-120.
- [13] Sherman, D. M. **2005**. Electronic structures of iron(III) and manganese(IV) (hydr)oxide minerals: Thermodynamics of photochemical reductive dissolution in aquatic environments. *Geochim. Cosmochim. Acta* 69: 3249-3255.
- [14] Waite, T. D. **1990**. Photo-redox processes at the mineral-water interface. *Rev. Mineral.* 23: 559-603.
- [15] Leland, J. K. and Bard, A. J. **1987**. Photochemistry of colloidal semiconducting iron oxide polymorphs. *J. Phys. Chem.* 91: 5076-5083.
- [16] Cherepy, N. J., Liston, D. B., Lovejoy, J. A., Deng, H. and Zhang, J. Z. **1998**. Ultrafast studies of photoexcited electron dynamics in γ - and α - Fe_2O_3 semiconductor nanoparticles. *J. Phys. Chem. B* 102: 770-776.
- [17] Kwan, W. P. and Voelker, B. M. **2002**. Decomposition of hydrogen peroxide and organic compounds in the presence of dissolved iron and ferrihydrite. *Environ. Sci. Technol.* 36: 1467-1476.
- [18] Rijkenberg, M. J. A. (2005). Photochemistry and organic complexation of iron: interactions in the Southern Ocean. PhD Thesis, University of Groningen.
- [19] Borer, P., Hug, S. J., Sulzberger, B., Kraemer, S. M. and Kretzschmar, R. **2007**. Photolysis of citrate on the surface of lepidocrocite: An in situ attenuated total reflection infrared spectroscopy study. *J. Phys. Chem. C* 111: 10560-10569.
- [20] Sulzberger, B. and Laubscher, H. **1995**. Reactivity of various types of iron(III) (hydr)oxides towards light-induced dissolution. *Mar. Chem.* 50: 103-115.
- [21] Borer, P., Hug, S. J., Sulzberger, B., Kraemer, S. M. and Kretzschmar, R. **submitted**. ATR-FTIR spectroscopic study of the adsorption of desferrioxamine B and aerobactin to the surface of lepidocrocite (γ - FeOOH) *Geochim. Cosmochim. Acta*.
- [22] Brauer, G. **1963**. *Handbuch der präparativen anorganischen Chemie*. Ferd. Enke Verlag: Stuttgart, Germany.
- [23] Schwertmann, U. and Cornell, R. M. **1991**. *Iron oxides in the laboratory*. 1st ed.;

VCH: Weinheim.

- [24] Voelker, B. M. and Sulzberger, B. **1996**. Effects of fulvic acid on Fe(II) oxidation by hydrogen peroxide. *Environ. Sci. Technol.* 30: 1106-1114.
- [25] Parker, C. A. **1968**. *Photoluminescence of solutions, with applications to photochemistry and analytical chemistry*. Elsevier: Amsterdam.
- [26] Braun, W., Herron, J. T. and Kahaner, D. K. **1987**. Acuchem: a computer program for modeling complex chemical reaction systems. *Int. J. Chem. Kinet.* 20: 51-62.
- [27] Wehrli, B. (1990). Redox reactions of metal ions at mineral surfaces. In: *Aquatic chemical kinetics*. Wiley-Interscience, New York: 311-337.
- [28] Zhang, Y., Charlet, L. and Schindler, P. W. **1992**. Adsorption of protons, Fe(II) and Al(III) on lepidocrocite (γ -FeOOH). *Colloid. Surf.* 63: 259-268.
- [29] Larsen, O. and Postma, D. **2001**. Kinetics of reductive bulk dissolution of lepidocrocite, ferrihydrite, and goethite. *Geochim. Cosmochim. Acta* 65: 1367-1379.
- [30] Kwan, W. P. and Voelker, B. M. **2004**. Influence of electrostatics on the oxidation rates of organic compounds in heterogeneous Fenton systems. *Environ. Sci. Technol.* 38: 3425-3431.
- [31] Morehouse, K. M., Flitter, W. D. and Mason, R. P. **1987**. The enzymatic oxidation of Desferal to a nitroxide free-radical. *Febs Lett.* 222: 246-250.
- [32] Cassar, N., Bender, M. L., Barnett, B. A., Fan, S., Moxim, W. J., Levy, H. and Tilbrook, B. **2007**. The Southern Ocean biological response to aeolian iron deposition. *Science* 317: 1067-1070.

Supporting Information

Chapter 5

Table of contents

1. Experimental Section	156
1.1 Synthesis of iron(III) (hydr)oxide phases	156
1.2 Analytical methods	157
1.3 Experimental procedure	158
2. Photoirradiation experiments with lepidocrocite	159
3. Kinetic modeling of Fe(II) and ROS formation	160
4. Photoirradiation experiments with additional iron(III) (hydr)oxides	163
5. References	165

1. Experimental section

1.1 Synthesis of iron(III) (hydr)oxide phases

The major lepidocrocite phase was synthesized by oxidation of FeCl_2 with NaNO_2 in the presence of a hexamethylenetetramine buffer solution at 70 °C (chemicals from Sigma-Aldrich) [1]. By this procedure, nitrogen- and carbon-containing oxidation by-products were produced of which traces remained on the surface or within the bulk of the freeze-dried solid, even after an extensive washing procedure. A total nitrogen content of the freeze-dried solid of 0.075% w/w was measured by CHNS analysis. In addition, the concentrations of NO_2^- , NO_3^- , NH_4^+ and total organic carbon in lepidocrocite suspensions with 0.1 M KCl background electrolyte equilibrated for 6 hours at pH 8 were measured by standard colorimetric methods and total organic carbon analysis, respectively. Suspensions of 25 mg/L lepidocrocite were contaminated by approximately 0.17 μM NO_2^- , 0.11 μM NO_3^- , 0.07 μM NH_4^+ and 10 $\mu\text{g/L}$ organic carbon. The specific surface area of this solid was 130 m^2/g , and the point of zero charge was at pH 7.4 [2, 3].

A second batch of lepidocrocite phase was synthesized from FeCl_2 by a method described by Schwertmann and Cornell [4]. The synthesized solid was washed thoroughly with high purity water until the conductivity of the suspension was minimal (~ 20 $\mu\text{S}/\text{cm}$) and was shock-frozen with liquid nitrogen and subsequently freeze-dried. The freeze-dried lepidocrocite was characterized by XRD, CHNS analysis (for detection of nitrogen contamination) and surface area measurements by multipoint BET analysis (Sorptomatic 1990, Thermo). In contrast to the major lepidocrocite phase used in this study, the second lepidocrocite phase had a smaller surface area (70 m^2/g) and thicker lath-like crystals. TEM images for both lepidocrocite phases are shown in Figure S1.

A batch of 2-line ferrihydrite was synthesized from FeCl_3 according to the protocol described by Schwertmann and Cornell [4]. Synthesized ferrihydrite was washed as described above and freeze-dried. The measured XRD diffraction pattern confirmed that 2-line ferrihydrite was synthesized. A surface area of 330 m^2 was measured by multipoint BET analysis (Sorptomatic 1990, Thermo). The batch of freeze-dried ferrihydrite was stored at -20 °C and was immediately used for photodissolution experiments within three weeks.

Hydrous ferric oxide (HFO) was synthesized by adding a 0.5 mL of a freshly prepared solution of FeCl_3 (70 mM) to the Pyrex vessel (see experimental setup in this study) containing 335 mL of high purity water and constantly adding NaOH to adjust and keep the pH of the suspension at pH 8. The suspension was stirred for 5 hours in the

dark, and thereafter immediately used for (photo-)dissolution experiments. The final concentration of hydrous ferric oxide in the Pyrex vessel (350 mL) was 100 μM .

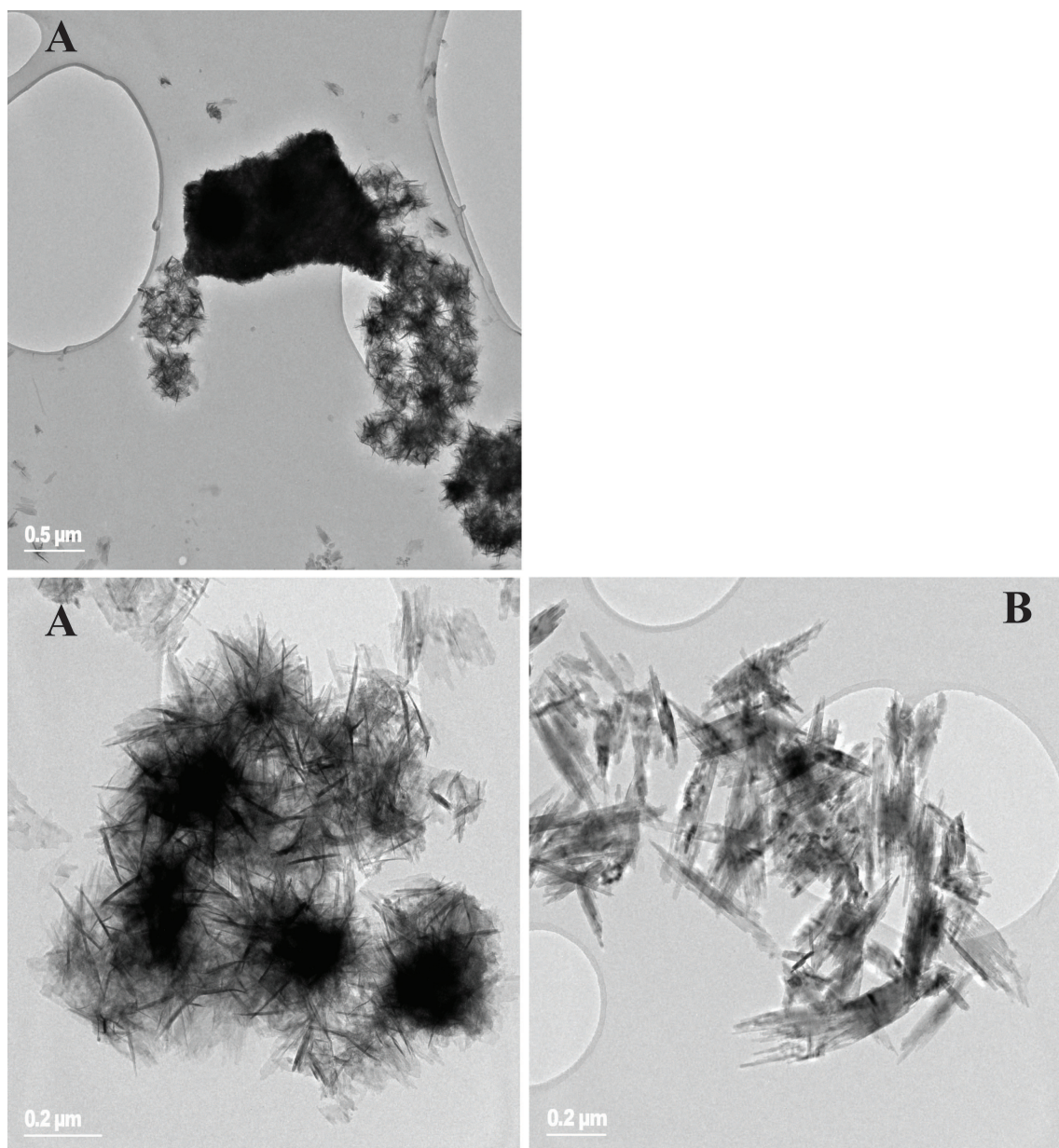


Fig. S1: TEM images of two different lepidocrocite phases. (A) Lepidocrocite synthesized according to Brauer [1]. Crystal aggregates are typically formed by this procedure [5]. (B) Lepidocrocite synthesized according to Schwertmann and Cornell [4].

1.2 Analytical methods

The analytical procedure for measuring H_2O_2 was taken from Voelker and Sulzberger [6] and was slightly modified: 100 μL of a phosphate buffer (0.575 M Na_2HPO_4 / 0.575 M NaH_2PO_4 , from Sigma-Aldrich) and 100 μL of a bipyridine stock solution (10 mM

bipyridine in 1 mM HClO₄, 2,2'-biypridine from Sigma-Aldrich) were premixed in a plastic tube and 1 mL of the filtered sample from the reaction vessel (see experimental setup) was added. Subsequently, 50 µL of a stock solution of EDTA (400 µM Na₂EDTA, from Sigma-Aldrich) was added. Before and after this last step, we followed the procedure for the Fe(II) determination with ferrozine (3-(2-Pyridyl)-5,6-diphenyl-1,2,4-triazine-4',4''-disulfonic acid sodium salt from Sigma-Aldrich) as described by Voelker and Sulzberger [6]. With this schedule, enough time was provided for complete complexation of dissolved Fe(II) and Fe(III) present in the filtered samples that otherwise would interfere with the H₂O₂ measurement. In the next step, 25 µL of a stock solution of DPD (10.4 mM in 10 mM H₂SO₄, 4-Amino-N,N-diethylanilinesulphate from Sigma-Aldrich) and 25 µL of a stock solution of horseradish peroxidase (Type II, 27 units/mL, from Sigma-Aldrich) were added. Both stock solutions were kept on ice during the experiments. After sufficient mixing, the solution was rapidly transferred to a 5 cm micro-cuvette and approximately 50 seconds after the addition of DPD and peroxidase, a UV-visible scan from 700 to 350 nm was measured with a photospectrometer (Cary 1E, Varian). The measured spectra were fitted with reference spectra of Fe(II)-bipyridine (ϵ (522 nm) = 8650 M⁻¹ cm⁻¹) and oxidized DPD (as a proxy for H₂O₂, ϵ (551 nm) = 21500 M⁻¹ cm⁻¹) with a simplex routine in Matlab (The Mathworks Inc.). Dissolved Fe(III) that was present in the µM range in the suspensions and in the filtered solutions did not effect the determination of H₂O₂ by this procedure. Fe(II) determined with bipyridine (H₂O₂ procedure) was in agreement with Fe(II) measured by the ferrozine method. In this paper the latter values are presented.

1.3 Experimental procedure

Photodissolution experiments with lepidocrocite and ferrihydrite were conducted as described in the study. (Photo)dissolution of hydrous ferric oxide (HFO) was investigated only in the presence of desferrioxamine B (DFOB). Hydrous ferric oxide (100 µM Fe) was aged for 5 hours in the Pyrex vessel and 40 µM DFOB was added prior to the start of the experiments. The formation of dissolved Fe-DFOB complexes was used as a proxy to quantify (photo)dissolution of HFO. A UV-Vis absorption spectrum of the suspension (background spectrum) was measured in a 5 cm cuvette prior to the addition of DFOB. During the dissolution experiments, samples were taken from the Pyrex vessel and UV-Vis spectra of the suspension were measured. The background spectrum was subtracted and the absorbance at 430 nm was used to calculate the concentration of Fe(III)-DFOB complexes (ϵ (430 nm) \approx 2600 M⁻¹ cm⁻¹).

2. Photoirradiation experiments with lepidocrocite

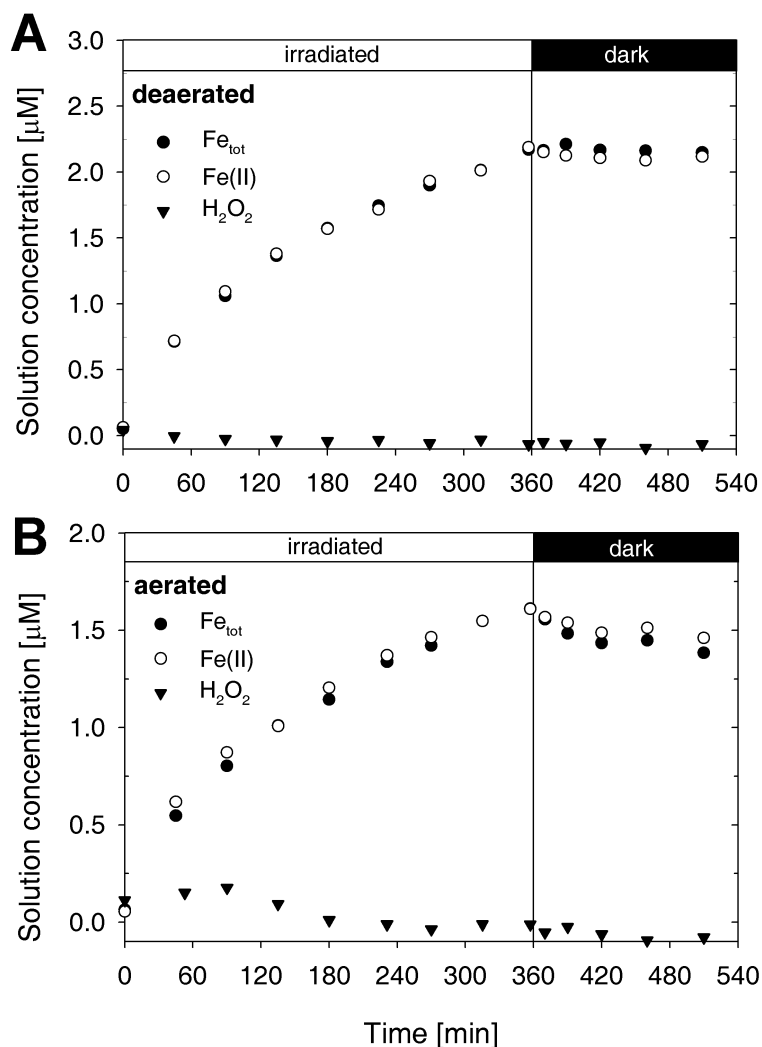


Fig. S2: (Photo-)dissolution experiments with 25 mg/L lepidocrocite (major lepidocrocite phase used in this study) at pH 5 and 0.01 M ionic strength (NaClO_4). After 360 minutes of irradiation, the light source was turned off. Total dissolved Fe, Fe(II) and H_2O_2 were measured in deaerated suspensions (A) and in aerated suspensions (B).

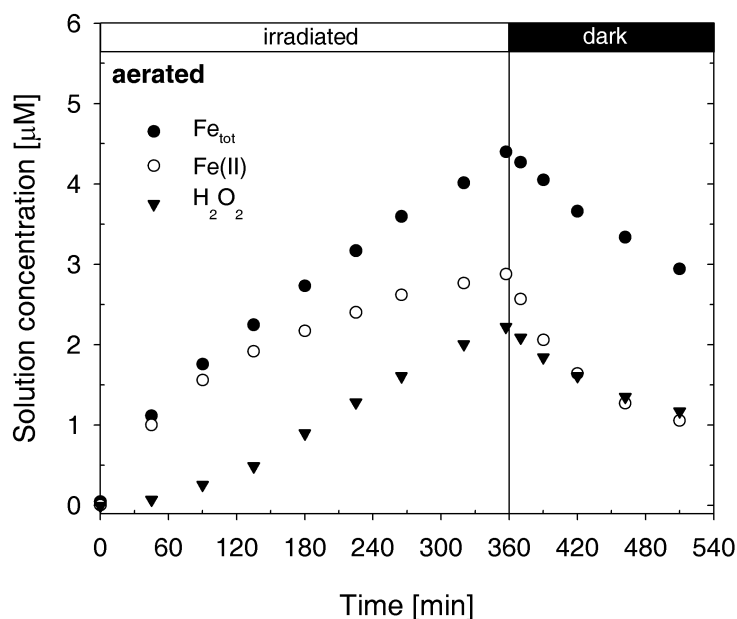


Fig. S3: (Photo-)dissolution experiments with 25 mg/L lepidocrocite (solid synthesized according to Schwertmann and Cornell [4]) at pH 3 and 0.01 M ionic strength (NaClO_4). After 360 minutes of irradiation, the light source was turned off. Total dissolved Fe, Fe(II) and H_2O_2 were measured in an aerated suspension.

3. Kinetic modeling of Fe(II) and ROS formation

The kinetic model of photoreductive dissolution of lepidocrocite in the absence of organic ligands was based on the formation of Fe(II) and $\cdot\text{OH}$ radicals at the surface by photolysis of surface Fe(III)-OH groups. The lepidocrocite surface was modeled with a constant concentration of surface Fe(III) sites ($28 \mu\text{M}$, equivalent to a suspension of 25 mg/L lepidocrocite with a surface area of $130 \text{ m}^2/\text{g}$ and a site density of 5 sites/ nm^2). The concentration of dissolved O_2 under oxygenated conditions was kept constant at $250 \mu\text{M}$. Fe(III) sites located at different crystallographic faces of lepidocrocite may exhibit a broad range of photoreactivity. It was assumed that the average surface Fe(III)-hydroxo group on lepidocrocite is less photoreactive than the solution Fe(III)-hydroxo species $\text{Fe}(\text{OH})^{2+}$. $\text{Fe}(\text{OH})^{2+}$, which accounts for 75% of total aqueous Fe(III) in solution at pH 3, is the most photoreactive Fe(III)-hydroxo species [7, 8]. The more strongly hydrolyzed species $\text{Fe}(\text{OH})_2^+$ which makes up 10 % of total aqueous Fe(III) at pH 3 is assumed to be non-photoreactive [7, 8], although charge-transfer bands for ligand-to-metal charge-transfer have been indicated by semi-empirical calculations [9]. The rate constant of photolysis of aqueous Fe(III) was calculated by assuming

only $\text{Fe}(\text{OH})^{2+}$ being photoreactive. The rate constant of photolysis of $\text{Fe}(\text{OH})^{2+}$ was calculated according to Balmer and Sulzberger [10], by multiplying the absorption spectra of $\text{Fe}(\text{OH})^{2+}$ [11] with the light-flux at the corresponding wavelengths and with interpolated quantum yields for the photolysis reaction [11]. For the photolysis reaction of average surface $\text{Fe}(\text{III})\text{-OH}$ sites, a rate constant was used which was 4 times smaller than the rate constant of photolysis of dissolved $\text{Fe}(\text{OH})^{2+}$. Values for input parameters (k_1 - k_4 , see Table 1) were derived by preliminary model simulations performed with the computer program Kintecus [12].

The goal of the kinetic modeling was not to provide a complete description of this rather complicated heterogeneous system, but to identify important reaction pathways by which dissolved $\text{Fe}(\text{II})$ and H_2O_2 are formed. A major shortcoming of the description is the treatment of a heterogeneous system as a homogeneous system with two compartments, the surface and the solution, where the transport of $\text{Fe}(\text{II})$ and H_2O_2 from the surface into solution is modeled by first order reactions. The surface of lepidocrocite particles and hence the surface sites are treated as homogeneously distributed species in solution space. It was not taken into account that the local concentrations of surface sites and reactive oxygen species formed in the interfacial region are likely higher than described in this model.

The goodness of the model fit for the combined photoirradiation/dark experiments with lepidocrocite at pH 3 was tested by varying each single fitting parameter (k_1 - k_4) while keeping the other parameters at their optimized values. A good fit is achieved when the sum of squared residuals between model and data is small and all the fitting parameters are well constrained. Figure S4 shows that the rate constant for the fitted reactions (list below) are all well constrained, except the release of O_2^- from the surface of lepidocrocite.

rate constant k_1 for reaction: $\text{Fe}(\text{II})_{\text{surf}} \rightarrow \text{Fe}(\text{II})$

rate constant k_2 for reaction: $\text{Fe}(\text{II})_{\text{surf}} + \text{O}_2 \rightarrow \text{Fe}(\text{III})_{\text{surf}} + \text{O}_2^-/\text{HO}_2_{\text{surf}}$

rate constant k_3 for reaction: $\text{H}_2\text{O}_2_{\text{surf}} \rightarrow \text{H}_2\text{O}_2$

rate constant k_4 for reaction: $\text{O}_2^-/\text{HO}_2_{\text{surf}} \rightarrow \text{O}_2^-/\text{HO}_2$

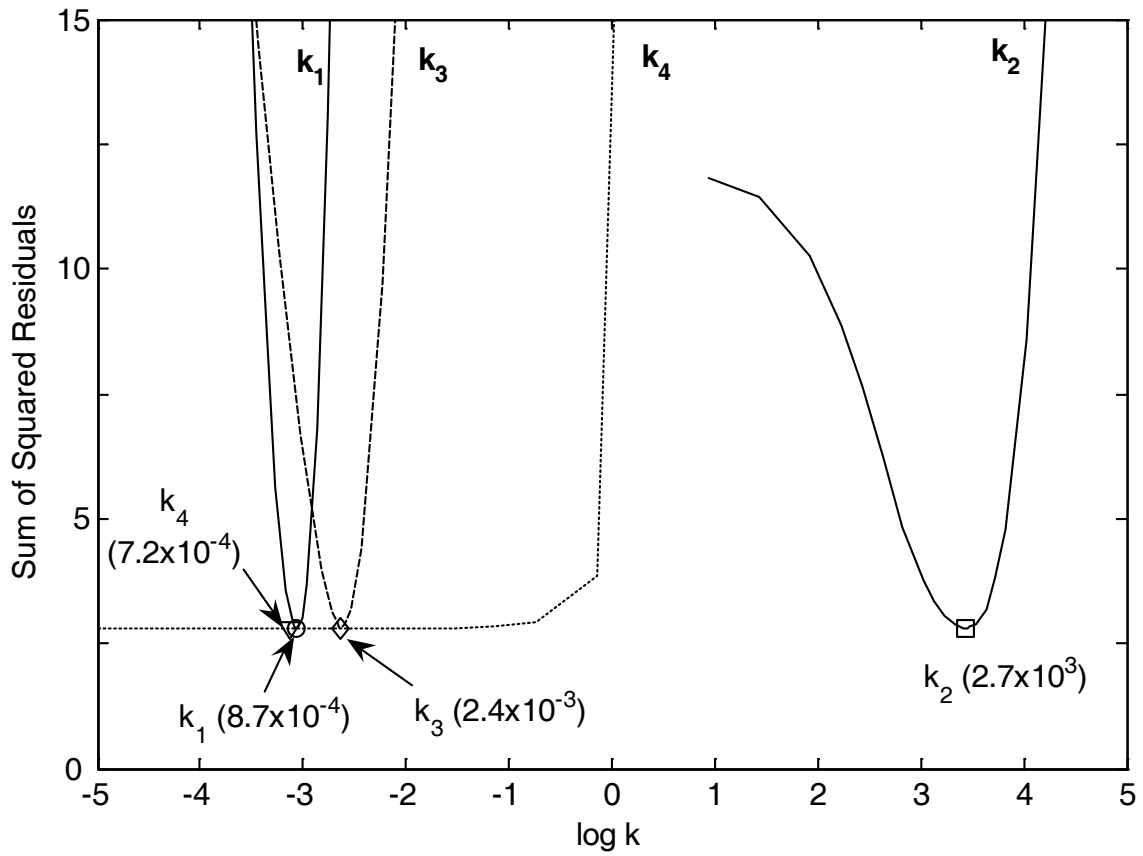


Fig. S4: Sum of squared residuals between model and data as a function of varying each single fitting parameter while keeping the other parameters at their optimized values. The values of k_1 - k_4 correspond to those in Table 1.

4. Photoirradiation experiments with additional iron(III) (hydr) oxides

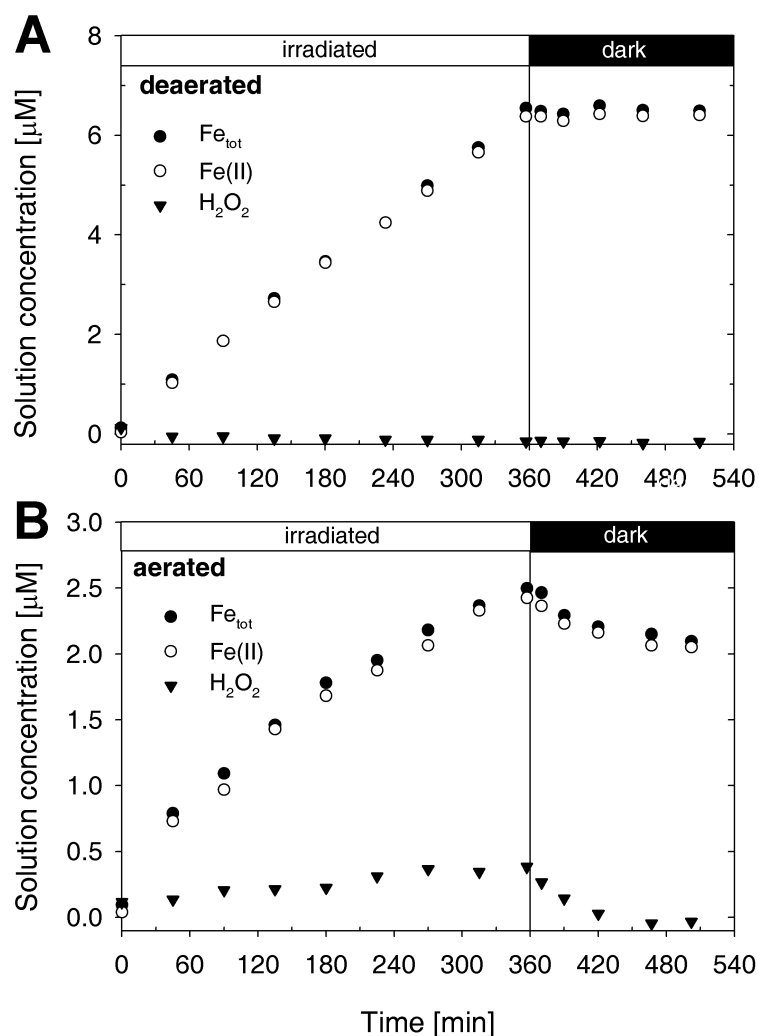


Fig. S5: (Photo-)dissolution experiments with 25 mg/L lepidocrocite in the presence of the $\cdot\text{OH}$ scavenger POHPAA (p-hydroxyphenylacetic acid) at pH 5 and 0.01 M ionic strength (NaClO_4). After 360 minutes of irradiation, the light source was turned off. Total dissolved Fe, Fe(II) and H_2O_2 were measured in deaerated suspensions (A) and in aerated suspensions (B).

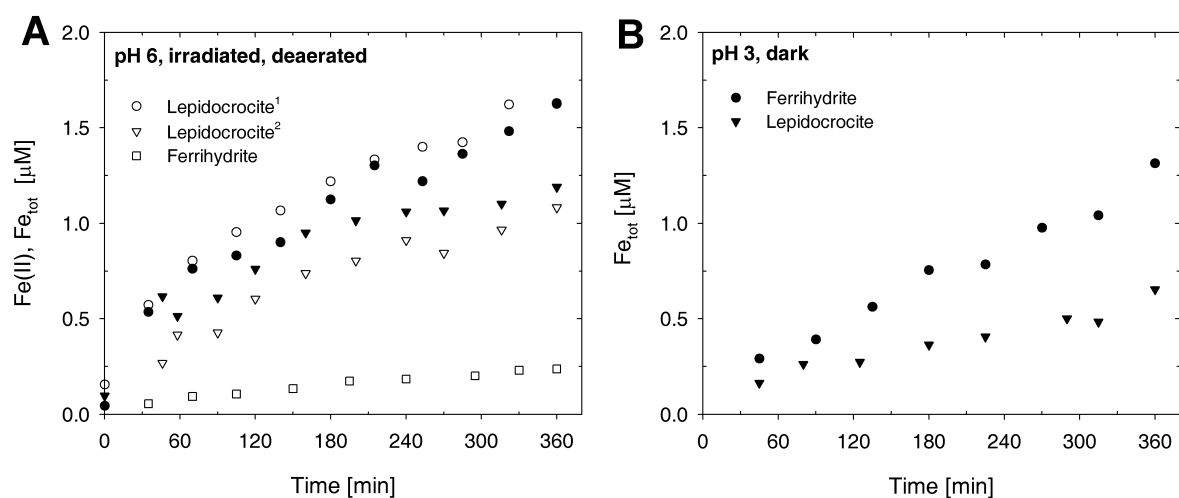


Fig. S6: (A) Photodissolution experiment with 25 mg/L ferrihydrite or lepidocrocite in oxygen-free suspensions at pH 6 and 0.01 M ionic strength ($NaClO_4$). The formation of total dissolved Fe during dissolution of lepidocrocite (lepidocrocite¹: synthesized by the method of Schwertmann and Cornell [4]; lepidocrocite²: major phase used in this study) and ferrihydrite is shown. (B) Dissolution experiment in the dark with 25 mg/L lepidocrocite or ferrihydrite at pH 3 and 0.01 M ionic strength ($NaClO_4$)

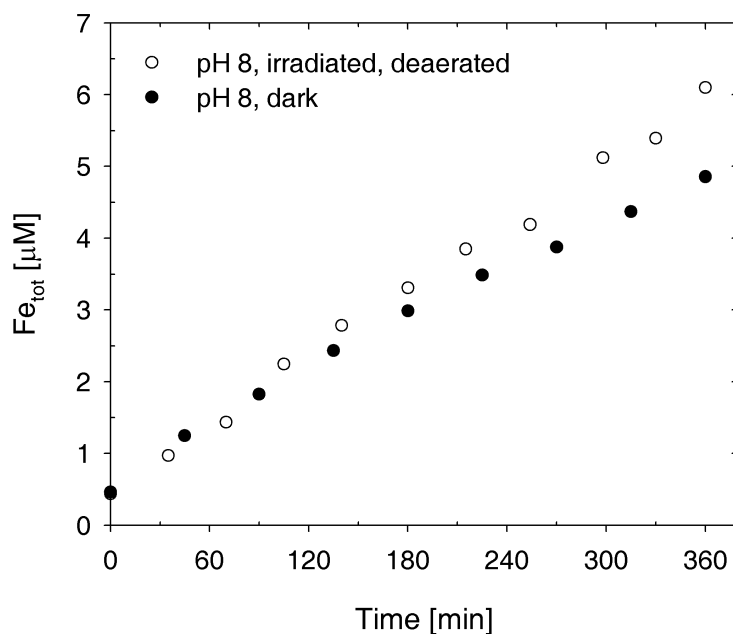


Fig. S7: (Photo-)dissolution experiment with 25 mg/L ferrihydrite in the presence of DFOB at pH 8 and 0.01 M ionic strength ($NaClO_4$). The formation of total dissolved Fe during dissolution of ferrihydrite is shown.

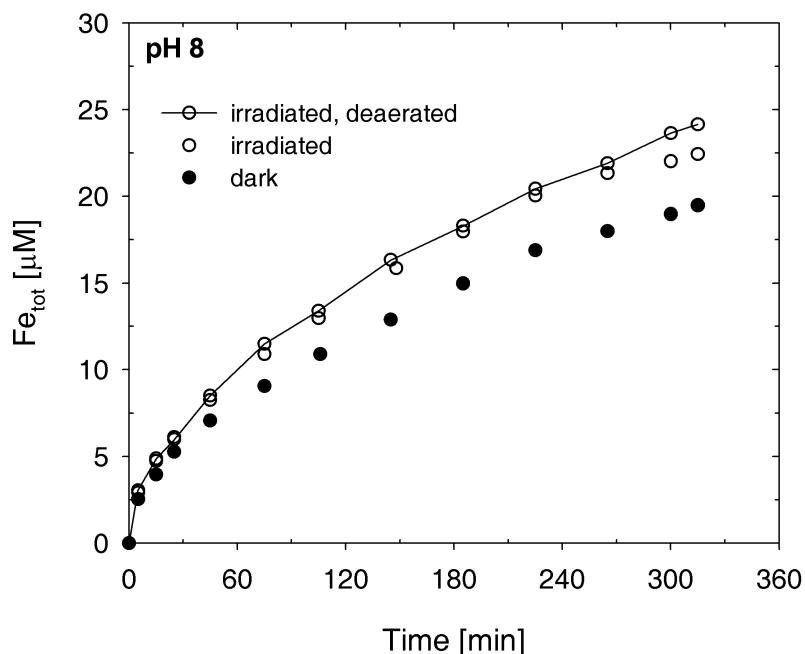


Fig. S8: (Photo-)dissolution experiment with hydrous ferric oxide ($100 \mu M$ Fe) in the presence of $40 \mu M$ DFOB at pH 8 and 0.01 M ionic strength ($NaClO_4$). Total dissolved Fe was calculated from the formation of Fe(III)-DFOB complexes as measured by UV-visible spectrometry.

5. References

- [1] Brauer, G. **1963**. *Handbuch der präparativen anorganischen Chemie*. Ferd. Enke Verlag: Stuttgart, Germany.
- [2] Borer, P., Hug, S. J., Sulzberger, B., Kraemer, S. M. and Kretzschmar, R. **2007**. Photolysis of citrate on the surface of lepidocrocite: An in situ attenuated total reflection infrared spectroscopy study. *J. Phys. Chem. C* 111: 10560-10569.
- [3] Borer, P., Hug, S. J., Sulzberger, B., Kraemer, S. M. and Kretzschmar, R. **submitted**. Photodissolution of lepidocrocite (γ -FeOOH) in the presence of desferrioxamine B and aerobactin. *Geochim. Cosmochim. Acta*.
- [4] Schwertmann, U. and Cornell, R. M. **1991**. *Iron oxides in the laboratory*. 1st ed.; VCH: Weinheim.
- [5] Cornell, R. M. and Schwertmann, U. **2003**. *The Iron Oxides: Structure, Properties, Reactions, Occurrences and Uses*. 2 ed.; Wiley-VCH: Weinheim, Germany.

- [6] Voelker, B. M. and Sulzberger, B. **1996**. Effects of fulvic acid on Fe(II) oxidation by hydrogen peroxide. *Environ. Sci. Technol.* 30: 1106-1114.
- [7] King, D. W., Aldrich, R. A. and Charnecki, S. E. **1993**. Photochemical redox cycling of iron in NaCl solutions. *Mar. Chem.* 44: 105-120.
- [8] Benkelberg, H. J. and Warneck, P. **1995**. Photodecomposition of iron(III) hydroxo and sulfato complexes in aqueous-solution - wavelength dependence of OH and SO₄⁻ quantum yields. *J. Phys. Chem.* 99: 5214-5221.
- [9] Lopes, L., de Laat, J. and Legube, B. **2002**. Charge transfer of iron(III) monomeric and oligomeric aqua hydroxo complexes: Semiempirical investigation into photoactivity. *Inorg. Chem.* 41: 2505-2517.
- [10] Balmer, M. E. and Sulzberger, B. **1999**. Atrazine degradation in irradiated iron oxalate systems: Effects of pH and oxalate. *Environ. Sci. Technol.* 33: 2418-2424.
- [11] Faust, B. C. and Hoigne, J. **1990**. Photolysis of Fe(III)-hydroxy complexes as sources of OH radicals in clouds, fog and rain. *Atmos. Environ.* 24: 79-89.
- [12] Ianni, J. C. **2006**. *Kintecus*, vers. Windows Version 3.90.

Chapter 6

Wavelength-dependence of photoreductive dissolution of lepidocrocite (γ -FeOOH) in the absence and presence of the siderophore DFOB

Paul Borer, Barbara Sulzberger, Stephan J. Hug, Stephan M. Kraemer and Ruben Kretzschmar

Prepared for publication in Environmental Science & Technology

Abstract

Photoreductive dissolution of lepidocrocite (γ -FeOOH) in the presence/absence of the siderophore desferrioxamine B (DFOB) was investigated at different wavelengths. At pH 3 in the absence of DFOB, Fe(II) formation rates normalized to the photon flux increased with decreasing wavelengths below 515 nm, consistent with enhanced Fe(II) formation at lower wavelengths by photolysis of surface Fe(III)-hydroxo groups or by surface scavenging of photoelectrons generated in the semiconducting bulk. In the presence of DFOB at pH 3, photoreductive dissolution rates normalized to the photon flux increased more strongly with decreasing wavelengths below 440 nm. We hypothesize that acid-catalyzed hydrolysis of DFOB generates degradation products that form photoreactive surface complexes leading to an increase in photodissolution rates at low pH. At pH 8 in the presence of DFOB, normalized photodissolution rates had a maximum in the spectral window 395-435 nm and were significantly smaller at lower wavelengths, suggesting that adsorbed DFOB is directly involved in the reduction of surface Fe(III) by a light-induced ligand-to-metal charge-transfer reaction within the surface Fe(III)-DFOB complex. The strong response in the visible light suggests that photoreductive dissolution of iron (hydr)oxides promoted by siderophores with hydroxamic acid groups may occur deep into in the euphotic zone of oceans.

1. Introduction

The presence of dissolved Fe(II) in many surface and atmospheric waters has been related to photoreductive dissolution of Fe(III) (hydr)oxides or other Fe(III)-bearing minerals [1-4]. Particularly in iron-deficient oceanic waters, photoreductive dissolution of such phases may potentially increase the amount of dissolved and bioavailable iron and thus effect the carbon cycle [5, 6]. Photoreductive dissolution of Fe(III) (hydr)oxides can be significantly enhanced in the presence of a variety of organic and inorganic ligands (e.g. carboxylic acids, α -hydroxycarboxylic acids, bisulfite) [7-9], but may also occur, albeit with lower efficiency, in the absence of organic or inorganic ligands other than H₂O or OH⁻ [8, 10-12]. In the latter case, photoreductive dissolution of crystalline Fe(III) (hydr)oxides is proposed to involve O²⁻ \rightarrow Fe³⁺ ligand-to-metal charge-transfer (LMCT) transitions within the semiconducting bulk or directly at the semiconducting oxide surface [10-13]. Charge carriers (photoholes, photoelectrons) formed upon such transitions within the bulk may be scavenged at the surface, leading conceivably to the reduction of surface Fe(III) to Fe(II) and to the oxidation of coordinated water or hydroxyl groups to hydroxyl radicals (\bullet OH) [11, 13, 14]. At the oxide surface, Fe(III)-hydroxo groups may be directly photolyzed by LMCT [10, 11]. This surface reaction is related to the photolysis reaction of solution Fe(III)-hydroxo species (e.g., FeOH²⁺), where the O²⁻ \rightarrow Fe³⁺ LMCT leads to the reduction of Fe(III) and the oxidation of coordinated OH⁻ ligands [15-17]. It has been shown experimentally and with semi-empirical calculations that the excitation energy of the lowest LMCT transitions decreases in the sequence of dissolved Fe³⁺_{aq}, FeOH²⁺, polynuclear Fe(III)-hydroxo complexes (e.g., Fe₂(OH)₂⁴⁺, Fe₃(OH)₄⁵⁺) [16, 17]. LMCT transitions of Fe³⁺_{aq} occur at wavelengths below 300 nm, whereas LMCT transitions of dissolved polynuclear Fe(III)-hydroxo species may occur well into the visible spectrum of light [17].

Iron(III) (hydr)oxides generally absorb light strongly below \sim 600 nm. The onset of adsorption refers to a semiconductor band-gap of \sim 2 eV [18]. Adsorption of light in the visible range has been assigned primarily to exchange-enhanced d-d transitions (Fe(3d) \rightarrow Fe(3d)) [19], which have not been ascribed so far in the literature to contribute to surface photoredox reactions. Iron(III) (hydr)oxides may have O²⁻ \rightarrow Fe³⁺ LMCT transitions also in the visible spectrum of light, in analogy to dissolved polynuclear Fe(III)-hydroxo species. Hence, the visible part of solar radiation may also induce reductive dissolution of Fe(III) (hydr)oxides [13, 17].

While photoreductive dissolution is feasible in the absence of any ligands other than H₂O or OH⁻ at low pH, recent thermodynamic calculations indicated that photoreductive dissolution of crystalline iron(III) (hydr)oxides cannot be significant at seawater pH,

unless the activity of dissolved, uncomplexed Fe^{2+} is drastically reduced by strong complexation by iron binding ligands (e.g., siderophores) [13]. In iron limited marine waters, dissolved iron is strongly bound to organic compounds, that conceivably consist of siderophore-like compounds exuded by marine organisms (e.g. cyano- and heterobacteria) under iron-limiting conditions [20]. In a companion study, we investigated photoreductive dissolution of various iron(III) (hydr)oxides at different pH and in the presence/absence of the trihydroxamate siderophore desferrioxamine B (DFOB). These experiments showed that photoreductive dissolution of lepidocrocite and ferrihydrite in the absence of any ligands at pH 3 results in the formation of dissolved Fe(II) and reactive oxygen species ($\text{ROS} = \bullet\text{OH}, \text{O}_2^-/\text{HO}_2, \text{H}_2\text{O}_2$) [12]. In the presence of DFOB, photoreductive dissolution of lepidocrocite was even observed at pH 8 [12]. DFOB apparently facilitates the release of Fe(II) formed at the surface into solution before (complete) reoxidation of surface Fe(II) by present oxygen or ROS occurs [12]. Based on these findings, we hypothesized that photoreductive dissolution of colloidal Fe(III) in high pH surface waters may be promoted in the presence of siderophores and may contribute to the formation of dissolved and bioavailable iron [6, 12].

The spectral quality of light required to induce photoreductive dissolution of iron(III) (hydr)oxides in the absence of organic ligands at acidic pH or in the presence of strong iron binding ligands like siderophores at higher pH has not been investigated so far. As the penetration of light into natural surface waters is wavelength-dependent [21], information of the spectral quality of light required to induce photoreductive dissolution is important to assess the relevance of such processes. In this study, we specifically studied the wavelength-dependence of photoreductive dissolution of lepidocrocite in the absence and presence of the DFOB. Lepidocrocite has been shown to be particularly susceptible to photoreductive dissolution in the presence of siderophores, in contrast to more thermodynamic stable phases (e.g. goethite) [6, 12, 22]. The results obtained in this work are discussed in the context of laboratory studies which have investigated the wavelength-dependence of photoreductive dissolution of less crystalline iron(III) (hydr)oxides (e.g., ferrihydrite, amorphous ferric hydroxide) in natural surface waters at high pH.

2. Experimental section

2.1 Materials

Desferrioxamine B (DFOB) was purchased as the methanesulfonate salt

$[\text{C}_{25}\text{H}_{46}\text{N}_5\text{O}_8\text{NH}_3^+(\text{CH}_3\text{SO}_3)^-]$ from Sigma Aldrich and was converted to the chloride salt with an anion exchange resin [23]. All other chemicals were at least reagent grade and were used as received. All solutions were prepared in high purity water (Milli-Q, Millipore). All glassware and plastic ware were thoroughly washed with HCl and rinsed with high purity water prior to use.

Lepidocrocite used in this study was characterized previously [12, 24]. The specific surface area was 130 m²/g, and the point of zero charge was at pH 7.4. Further details on the synthesis and characterization (e.g. UV-Visible absorption) of lepidocrocite are provided in the Supporting Information (Fig. S1, S2).

2.2 Analytical methods

Samples for the determination of total dissolved Fe and dissolved Fe(II) were withdrawn from the irradiated lepidocrocite suspensions and were immediately filtered through 0.025 μm pore-size membrane filters (NC 03, Whatman). Dissolved Fe(II) formed during photodissolution of lepidocrocite was measured by photospectrometry in a 5 cm micro-cuvette by a modified Ferrozine method [25]. Filtered samples for total iron analysis were acidified with 1% v/v suprapure nitric acid (Fluka) and were measured by ICP-OES (Vista MPX, Varian). The detection limit for the measurement of dissolved Fe(II) and total dissolved iron was ~0.05 and 0.1 μM, respectively. The concentrations of DFOB stock solutions were measured using a total organic carbon analyzer (Shimadzu 5000A).

2.3 Experimental setup

Two different photoirradiation setups were used to study the wavelength-dependence of lepidocrocite photodissolution (in the following referred to as “Setup I” and “Setup II”). The light source used for both setups consisted of a 1000 W high pressure Xenon lamp (OSRAM).

In Setup I, the light was focused onto the bottom circular window of a Pyrex reaction vessel, which was placed on top of an optical high-pass glass filter that varied the wavelength-range of the light entering the reaction vessel from below. The filters with a diameter of 10 cm and a thickness of 2 mm (Schott Guinchard, Yverdon-les-Bains, Switzerland) exhibited 50 % transmission cut-off edges at the following wavelengths: 305, 395, 435, 475, 515, 550, 590 and 630 nm. Measured transmittance spectra of these filters are provided in Fig. S3 (Supporting Information). The bottom window of the Pyrex vessel itself strongly absorbed light below 305 nm (transmission through the

bottom window $< 0.4\%$ at wavelengths $< 305\text{ nm}$). The reaction volume was 350 mL and the irradiated area was 56 cm^2 . The photon flux penetrating into the reaction vessel was measured by ferrioxalate actinometry [26]. Total light absorption by the actinometer solution (0.05 M ferrioxalate, 350 mL volume, pathlength of 6.2 cm) only occurred at wavelengths $\leq 475\text{ nm}$ (see Fig. S4 in Supporting Information). Since the photon flux could not be measured using ferrioxalate actinometry at wavelengths above 475 nm , the photon flux at higher wavelengths was estimated based on spectral irradiance data provided by the lamp manufacturer and by comparison of measured light fluxes at lower wavelengths with the provided irradiance data. Measured and estimated photon fluxes are provided in the Supporting Information (Table S1, S3). The entire photoirradiation setup and the compartment with the irradiated Pyrex vessel (wrapped in aluminum foil) were covered with a thick black cloth to reduce the amount of diffuse stray light from the Xenon light source. Suspensions of 25 mg/L lepidocrocite were pre-equilibrated at neutral pH in 0.01 M NaClO_4 for about one hour and were vigorously stirred in the Pyrex vessel with a Teflon coated stirrer. The suspensions were purged with N_2 gas and were irradiated at pH 3 and pH 8 in the absence or presence of $80\text{ }\mu\text{M}$ DFOB. The temperature in the Pyrex vessel was maintained at $25 \pm 1\text{ }^\circ\text{C}$ by the aid of a flow-through water jacket around the Pyrex vessel. The pH of the suspensions was constantly measured with a combined glass electrode (Metrohm 6.0253.100) and was automatically adjusted with small additions of NaOH or HClO_4 by a dosimat (Metrohm). Deviations of solution pH were within $\pm 0.02\text{ pH}$ units.

In Setup II, a single grating monochromator (PTI Model 101, Photon Technology International) was placed between the Xenon light source and the sample compartment. The entrance and exit slits were set each to 5 mm in width and 20 mm in height resulting in a bandpass of 20 nm . The sample compartment was equipped with a temperature-controlled 10 mm cuvette holder and a magnetic stirrer. UV-transparent PMMA (polymethylmethacrylate) cuvettes with 10 mm pathlength were used. The sample volume in the cuvettes was 3.5 mL . Analogous to Setup I, 25 mg/L lepidocrocite suspensions were pre-equilibrated at neutral pH in 0.01 M NaClO_4 for one hour prior to the experiment. Dissolution experiments were performed in the presence of $80\text{ }\mu\text{M}$ DFOB at pH 3. In contrast to Setup I, Setup II did not allow for N_2 -purging of the lepidocrocite suspensions. Thus, all dissolution experiments with Setup II were conducted under ambient air. The suspension in the cuvette was stirred with a magnetic Teflon coated stir bar and was irradiated for 6 hours at $25 \pm 1\text{ }^\circ\text{C}$. Subsequently, the suspension was filtered and total dissolved iron in the filtrate was measured by ICP-OES. The pH of the suspension was regularly measured with a combined glass micro-electrode (Metrohm 6.0224.100 with saturated KCl as the internal electrolyte) and was

maintained at pH 3 by the addition of minute volumes of HClO_4 or NaOH. Deviations of solution pH were within ± 0.03 pH units. The entrance slit of the sample compartment was covered with a 305 nm cutoff filter (50% internal transmittance at 305 nm) to reduce stray light at lower wavelengths. Photodissolution experiments under ambient air were conducted with irradiation wavelengths centered at 300, 320, 340, 360, 380, 400, 420, and 440 nm (20 nm bandpass). A reference experiment was conducted with light at 630 nm to assess the rate of thermal dissolution of lepidocrocite by DFOB and the effects of stray light emerging from the monochromator. Measured photon fluxes are provided in the Supporting Information (Table S2).

2.4 Calculation of normalized photoreductive dissolution rates

Photoreductive dissolution rates were determined by the increase in solution Fe(II) in the absence of DFOB and by the light-induced increase in total dissolved iron in the presence of DFOB, respectively, as a function of time. These rates were normalized to the photon fluxes at the corresponding wavelengths. Details of the calculation of normalized photoreductive dissolution rates and of the error estimation are provided in the Supporting Information (Table S1-S3).

3. Results and discussion

3.1 Photoreductive dissolution of lepidocrocite in the absence of organic ligands

Fig. 1 shows the wavelength-dependence of the formation of dissolved Fe(II) during irradiation of a deaerated lepidocrocite suspension (25 mg/L) at pH 3 in the absence of DFOB, as determined with Setup I. The rate of light-induced Fe(II) formation decreased with increasing cut-off wavelengths. Apart from the wavelength-dependence of photoreductive dissolution of lepidocrocite, the processes occurring during photoreductive dissolution at the water/mineral interface (e.g. formation of Fe(II) or ROS) have been investigated in detail in our companion study [12]. The rate of Fe(II) formation determined with the 305 nm cut-off filter was almost identical to the Fe(II) formation rate reported in our companion paper under non-filtered polychromatic light (300-800 nm) [12]. In each experiment shown in Fig. 1, dissolved Fe(III) was also formed due to proton-promoted dissolution. The average concentration of dissolved Fe(III) at 360 min in these experiments was 0.60 ± 0.037 μM (data not shown in Fig. 1). The formation of dissolved Fe(II) induced by the release of Fe(III) from the surface of lepidocrocite

by proton-promoted dissolution and by subsequent photolysis of dissolved Fe(III) is negligible. In our companion study, we used a kinetic model to simulate the formation of dissolved Fe(II) and ROS in irradiated, deaerated lepidocrocite suspensions at pH 3 [12]. According to a simplified version of this model (details in Supporting Information), only about 20 % of dissolved Fe(III) formed by proton-promoted dissolution of lepidocrocite is reduced to Fe(II) under polychromatic irradiation (300-800 nm). Hence, the solution photochemistry accounts for a maximum of 0.16 μM dissolved Fe(II) after 6 h irradiation with polychromatic light, which is slightly less than the corresponding concentration of dissolved Fe(II) formed under filtered light above 630 nm.

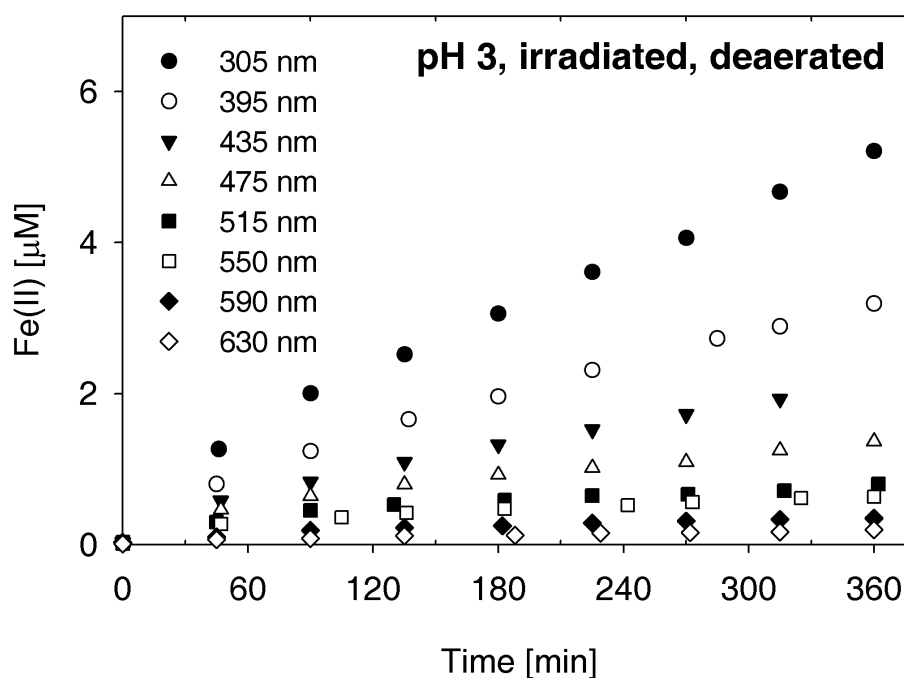


Fig. 1: Photodissolution of lepidocrocite in deaerated organic-free suspensions (25 mg/L lepidocrocite) measured under artificial sunlight filtered by different optical cutoff filters (Setup I). Only dissolved Fe(II) concentrations are shown. Total dissolved Fe concentrations at the end of the experiments (360 min) were on average $0.60 \pm 0.037 \mu\text{M}$ higher than the measured Fe(II) concentrations. The cutoff wavelength of each filter (50 % internal transmittance) is specified in the legend.

Rates of photoreductive dissolution of lepidocrocite were calculated from the slopes of the linearized Fe(II) formation in Fig. 1 between 45 and 360 minutes for the different spectral windows (details in Supporting Information). These rates were normalized to the photon flux in the specific spectral windows (details in Supporting Information, cf. Table S1). Error estimates of the normalized rates are provided in the Supporting

Information. Fig. 2 shows that normalized photoreductive dissolution rates determined at pH 3 in the absence of DFOB decreased with increasing wavelengths of the spectral windows. The illustrated wavelength-dependence of photoreductive dissolution is consistent with diminished surface Fe(II) formation with increasing wavelengths by photolysis of surface Fe(III)-hydroxo groups or by surface scavenging of photoelectrons generated in the semiconducting bulk. As a comparison, reported quantum yields for the solution photolysis reaction $\text{FeOH}^{2+} + h\nu \rightarrow \text{Fe}^{2+} + \bullet\text{OH}$ decrease with increasing wavelengths towards ~ 400 nm, above which FeOH^{2+} does not absorb light [15]. Although normalized rates of photoreductive dissolution of lepidocrocite were small at wavelengths above 515 nm, photoreductive dissolution was observed up to 630 nm (Fig. 2). Photolysis of dissolved Fe(III) species (Fe^{3+} , FeOH^{2+} and $\text{Fe}(\text{OH})_2^+$) cannot explain the formation of dissolved Fe(II) above 515 nm because of the lack of light absorption by all of these species above 515 nm [16, 17]. This result suggests that lepidocrocite has electronic transitions presumably of the type LMCT, which extend into the visible spectrum of light and which lead to photoreductive dissolution of lepidocrocite above 515 nm. Most of the electronic transitions leading to absorption of light by lepidocrocite in this wavelength region, however, are not effective in promoting photoreductive dissolution of lepidocrocite. This is illustrated in Fig. 2 by a comparison of the normalized photoreductive dissolution rates and the average light absorption of lepidocrocite powder (cf. Fig. S1) in each spectral window. Above 475 nm, normalized photoreductive dissolution rates were smaller than expected by the adsorption of light. The absorption of light above 475 nm primarily involves exchange-enhanced ligand field transitions ($\text{Fe}(3d) \rightarrow \text{Fe}(3d)$) [19], which presumably do not lead to photoredox reactions at the surface. Similar results were observed in photoelectrochemical studies with hematite electrodes, where photocurrents were determined under irradiation with light of different wavelengths [27, 28]. In both studies, the photocurrent action spectrum in the visible range did not correspond to the absorption spectrum. This phenomenon was interpreted in terms of a lower charge carrier generation in the visible as compared to the UV range. Nevertheless, small photocurrents were also measured near the absorption edge at ~ 600 nm, in agreement with the photocurrent measurements of hematite by Dare-Edwards et al. [29].

The normalized rate of photoreductive dissolution of lepidocrocite at pH 3 in the wavelength range 305 – 395 nm was about 15 $\mu\text{mol}/\text{einstein}$, which is more than an order of magnitude higher than the normalized rate of Fe(II) formation in irradiated organic-free goethite suspensions (0.5 g/L) at pH 5.5 under otherwise similar conditions [11]. This observation can be explained by (i) less favorable thermodynamics of photoreductive dissolution of iron(III) (hydr)oxides in general with increasing pH [13]

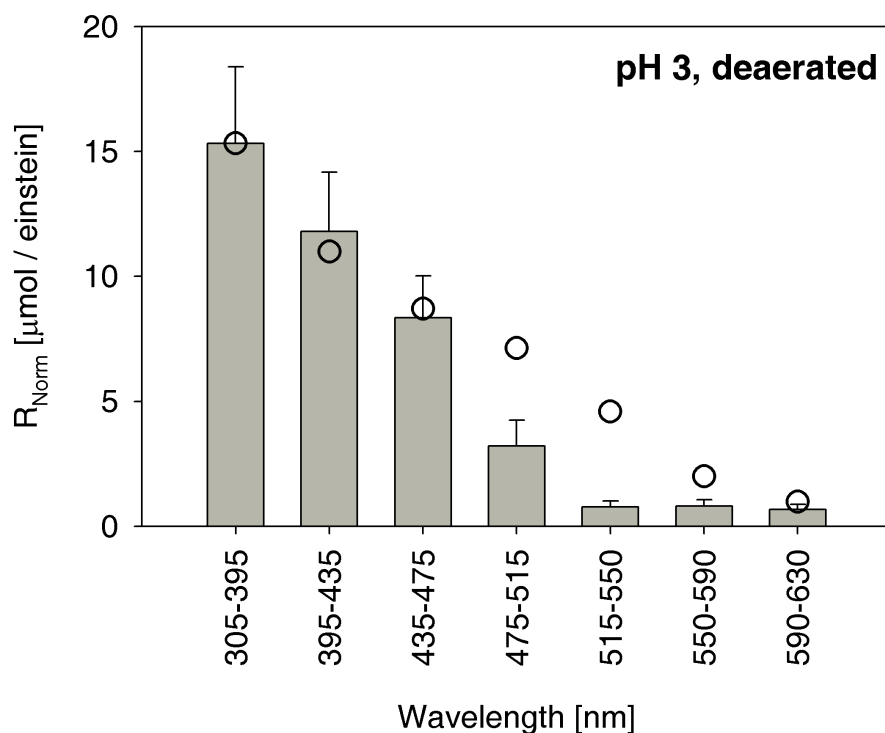


Fig. 2: Fe(II) formation rates normalized to the photon flux in irradiated organic-free suspensions of lepidocrocite determined from the slopes of the Fe(II) formation shown in Fig. 1 (Setup I). The circles designate the average absorption of light by lepidocrocite (arbitrary units) in the spectral windows in Setup I (cf. Fig. S5). The average absorption of lepidocrocite in the different spectral windows is normalized, such that the absorption and the Fe(II) formation rate in the spectral window 305 – 395 nm are equal. Values and error estimates of the normalized Fe(II) formation rates are provided in the Supporting Information (cf. Table S1).

and (ii) slower detachment of potentially formed Fe(II) from the surface of more thermodynamic stable iron(III) (hydr)oxides such as goethite in comparison to lepidocrocite and consequently in enhanced reoxidation of surface Fe(II) by present ROS ($\bullet\text{OH}$, O_2^-/HO_2 , H_2O_2) [12, 22]. We refer to our companion study for details on the formation of ROS and cycling of both iron species and ROS during photoreductive dissolution of iron(III) (hydr)oxides [12].

Due to the reoxidation of surface and dissolved Fe(II) by ROS, we cannot calculate the quantum yield for the photoreduction of Fe(III) at the surface of lepidocrocite based on measured formation rates of dissolved Fe(II) and rates of light absorption. This is the reason why quantum yields for the photolysis of dissolved Fe(III)-hydroxo species are typically determined in the presence of an excess of radical scavengers [15, 16]. However, we may estimate an apparent quantum yield for the formation of surface Fe(II) with the help of the kinetic model that was used in our companion study to

model photoreductive dissolution of lepidocrocite in aerated and deaerated suspensions (25 mg/L) at pH 3 under irradiation with polychromatic light (300-800 nm) [12]. In the kinetic model, a formation rate of surface Fe(II) of 0.014 $\mu\text{M/s}$ was estimated for the given experimental conditions to provide a good fit of the experimental data (formation of dissolved Fe(II) and H_2O_2) [12]. Assuming that only light below 475 nm significantly contributes to the formation of surface Fe(II) by LMCT (cf. Fig. 2) and that approximately only half of the measured photon flux between $\sim 300\text{-}475$ nm (13.2 μM photons/s) was absorbed by lepidocrocite under the experimental conditions in this study (see Supporting Information), we calculated an average apparent quantum yield of ~ 0.002 for the formation of surface Fe(II) in this wavelength region. This value is in the same order of magnitude as the reported quantum yield of 0.007 for the photolysis of the solution species $\text{Fe}_2(\text{OH})_2^{4+}$ at 350 nm [30].

3.2 Photoreductive dissolution of lepidocrocite in the presence of desferrioxamine B

As indicated by recent studies, DFOB can enhance the rate of photoreductive dissolution of lepidocrocite by acting as a shuttle for the transfer of surface Fe(II) into solution and conceivably also by acting as a radical scavenger [31], thus reducing the rate of reoxidation of surface Fe(II) by oxygen or ROS [6, 12]. Fig. 3 shows normalized rates of photoreductive dissolution of lepidocrocite (aerated suspensions) in the presence of 80 μM DFOB at pH 3, as determined with Setup II. Increasing normalized rates of photoreductive dissolution of lepidocrocite with decreasing wavelengths of the incoming light were observed. To compare the results in Fig. 2 and 3 (dissolution experiments performed at pH 3 in the absence/presence of DFOB), we calculated the average normalized rate for photoreductive dissolution of lepidocrocite in the presence of DFOB (Fig. 3) in the spectral ranges 300-400 nm and 400-440 nm. The calculated normalized rate was 7.70 and 2.53 $\mu\text{mol/einstein}$ in the spectral range 300-400 nm and 400-440 nm, respectively. The stronger increase in the normalized rate in the spectral range 300-400 nm with respect to the rate in the spectral range 400-440 nm in the dissolution experiments with DFOB (cf. Fig. 2 and 3) points to an additional mechanism of light-induced reductive dissolution of lepidocrocite. It has been reported that DFOB is able to promote the reduction of dissolved iron in the dark [32]. At pH < 2 thermal reduction of Fe(III) was observed on a time scale of days [32]. This observation is consistent with the formation of carboxyl and hydroxylamine compounds by acid-catalyzed hydrolysis of the hydroxamic acid functional groups [33], and the reduction of Fe(III) by hydroxylamine compounds. In a recent study, it was concluded that reductive

dissolution of goethite at pH 3 in the dark was induced by acid- or surface-catalyzed hydrolysis of acetohydroxamic acid, a monohydroxamic acid compound [34]. If carboxylic acid compounds are formed upon hydrolysis of DFOB at pH 3, dissolution of lepidocrocite may be promoted by photolysis of Fe(III)-carboxylate complexes formed at the surface. Quantum yields of the photolysis of Fe(III)-carboxylate complexes are known to increase strongly with decreasing wavelengths, as reported in the case of EDTA [35]. Thus, the presence of carboxylic acids might explain the stronger increase in the normalized average rate of photoreductive dissolution of lepidocrocite between the wavelength ranges 400-440 and 300-400 nm (see Fig. 3), as compared to the increase in rates between corresponding wavelength ranges in the organic-free experiment (see Fig. 2).

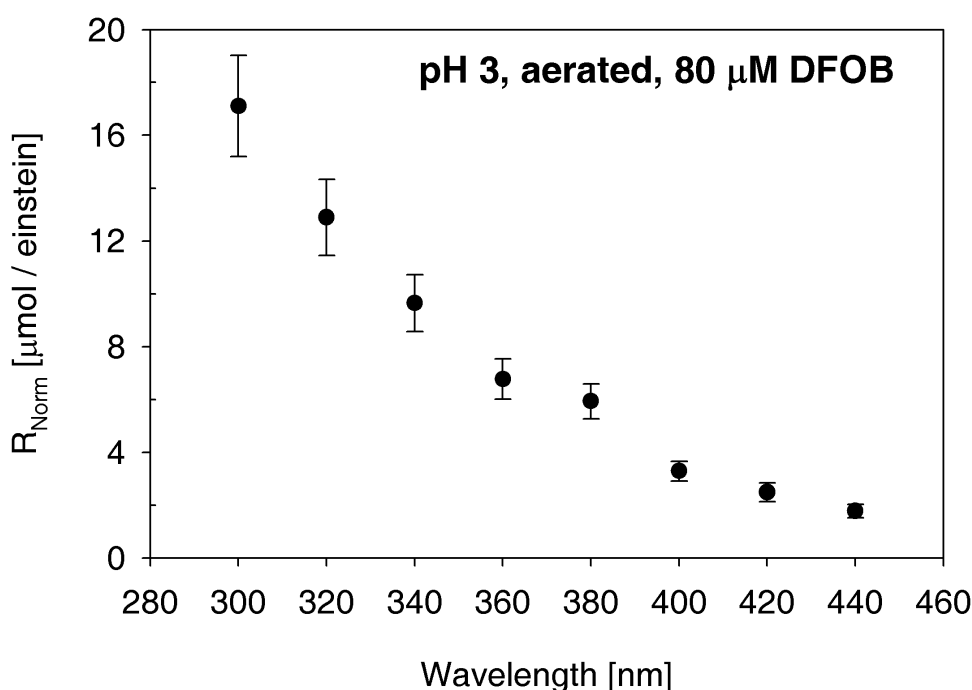


Fig. 3: Photoreductive dissolution rates of lepidocrocite at pH 3 in the presence of 80 μM DFOB normalized to the photon flux determined at different wavelengths (Setup II). The spectral width of the incoming light at each specified wavelength was 20 nm. Values and error estimates of the normalized photoreductive dissolution rates are provided in the Supporting Information (cf. Table S2).

At pH 8, photoreductive dissolution of lepidocrocite in the absence of any ligands other than H_2O or OH^- is thermodynamically unfavorable according to Sherman (2005) and may result merely in the formation of sub-femtomolar concentrations of dissolved Fe(II). Complexation of Fe(II) by strong iron binding ligands such as siderophores may significantly increase the thermodynamic feasibility of photoreductive dissolution of crystalline iron(III) (hydr)oxides [13]. This is confirmed by our companion study, where

light-induced dissolution of lepidocrocite under polychromatic light (300-800 nm) in the presence of DFOB resulted in an increase of total dissolved iron in the range of a few μM within 6 hours under deaerated conditions [12]. In contrast, recent experiments showed that on the same timescale DFOB was not able to dissolve goethite above the detection limit of dissolved iron ($\sim 0.1 \mu\text{M}$) under irradiation (or in the dark) even at lower pH (pH 6) [6]. Photoreductive dissolution was only observed in the additional presence of the photoreductive ligand oxalic acid [6]. This observation suggests that the effect of siderophores in enhancing photoreductive dissolution of iron(III) (hydr)oxides in the absence of additional organic ligands is more important for less thermodynamic stable phase (e.g. ferrihydrite, lepidocrocite) [12].

Fig. 4 shows normalized photoreductive dissolution rates of lepidocrocite at pH 8 in the presence of $80 \mu\text{M}$ DFOB under deaerated conditions (Setup I). A clear change in the spectral response of photoreductive dissolution was observed in comparison with the experiments conducted at pH 3 in the absence of DFOB (cf. Fig. 2 and 4). The highest normalized photoreductive dissolution rate was obtained in the spectral window 395-435 nm. The much smaller normalized rate in the spectral window 305-395 nm indicates that the formation of surface Fe(II) cannot be explained solely by photolysis of surface Fe(III)-hydroxo groups or by surface scavenging of photoelectrons generated in the semiconducting bulk. Surface-coordinated DFOB must be involved directly in the formation of surface Fe(II). We hypothesize that at pH 8, a relevant pathway of photoreductive dissolution of lepidocrocite in the presence of DFOB is a light-induced ligand-to-metal charge-transfer within Fe(III)-DFOB surface complexes. This is an unexpected result considering that the hexadentate Fe(III)-DFOB complex is photostable at non-acidic pH [36]. LMCT excitation of the hexadentate Fe(III)-DFOB complex, leading to a broad absorption band with the maximum at 430 nm, is apparently not accompanied by reduction of the Fe(III) center. The situation might be different at the surface of lepidocrocite, where hexadentate surface complexes cannot be formed with a single surface Fe(III) site due to steric constraints. If the LMCT excitation of the Fe(III)-DFOB surface complex is followed by electron transfer to the coordinated surface Fe(III) site, a nitroxide radical of DFOB is expected to form [31]. Theoretical calculations of charge-transfer transitions of possible surface complexes as well as more sophisticated experimental techniques (e.g., ESR spectroscopy for the detection of nitroxide radicals of DFOB) may help to verify our hypothesis of Fe(III)-DFOB complexes being subject to photolysis.

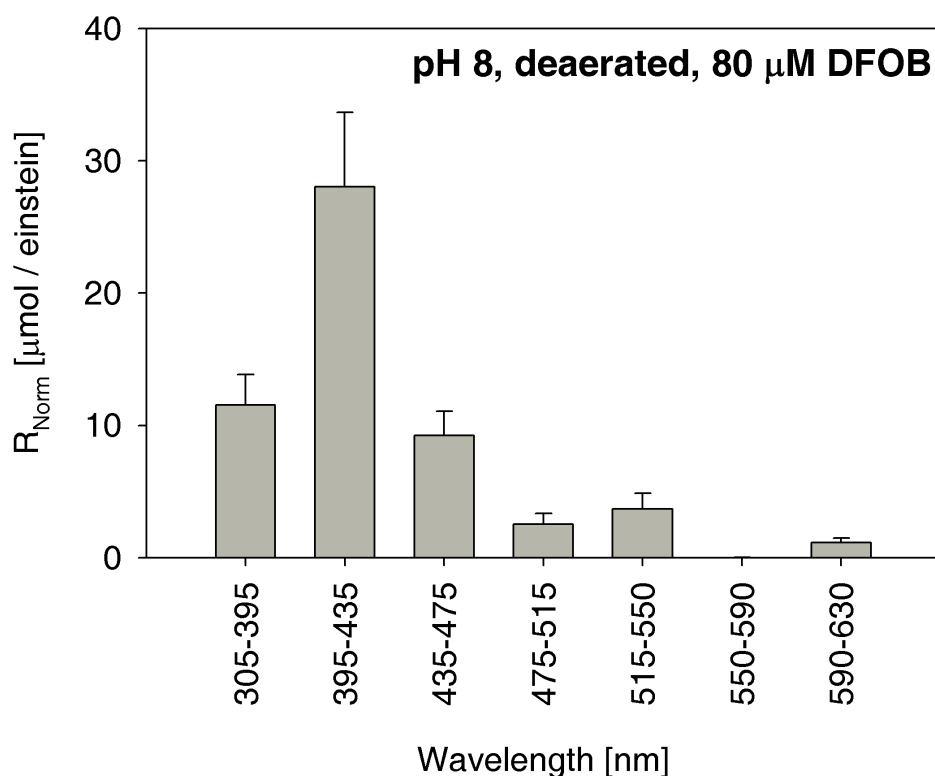


Fig. 4: Photoreductive dissolution rates of lepidocrocite at pH 8 in the presence of 80 μM DFOB normalized to the photon flux determined in different spectral windows (Setup I). Values and error estimates of the normalized photoreductive dissolution rates are provided in the Supporting Information (cf. Table S3).

3.3 Environmental significance

The strong response of photoreductive dissolution of lepidocrocite to irradiation of visible light in the presence of DFOB at pH 8 calls for a comparison of wavelength-dependent dissolution studies in natural surface waters at high pH. Here, we only refer to studies where natural surface waters at high pH have been spiked with iron(III) (hydr) oxides or sufficient Fe(III) to form precipitates of amorphous ferric hydroxides in order to appropriately investigate the wavelength-dependent photoreduction of colloidal Fe(III). Recent photoirradiation experiments with Fe(III)-spiked Southern Ocean water and organic-free artificial seawater indicated that the formed amorphous ferric hydroxides contained a photoreducible fraction of Fe(III) and that the rate of photochemical Fe(II) formation decreased with increasing aging time of the amorphous ferric hydroxides [37, 38]. Rijkenberg and coworkers showed that the rate of Fe(II) photoproduction from such amorphous ferric hydroxides in Southern Ocean water decreased exponentially from 300 nm into the visible range of light [39]. They concluded that although UVB

irradiation was the most effective wavelength region for Fe(II) photoproduction from amorphous ferric hydroxides, the impact of UVB is small due to relatively low fluxes of UVB into the ocean waters [39]. On a depth integrated basis, UVA and visible light accounted for approximately 60% and 30% of the total Fe(II) formation, respectively, in the total irradiated water column [39]. Instead of measuring the formation of dissolved Fe(II) upon irradiation of Fe(III)-spiked seawater, Wells et al. [1] investigated the formation of labile Fe, as determined by extraction with 8-hydroxyquinoline. An increase of labile Fe concentrations was observed in irradiated ferrihydrite-spiked (4 μM) seawater with decreasing wavelengths below 400 nm. The increase in labile Fe was attributed to photoreduction of ferrihydrite by organic chromophores, since pre-irradiation of seawater samples with strong UV light, resulting in the destruction of these chromophores, eliminated the formation of labile iron [1]. In addition, the same technique indicated that goethite is also susceptible to photoreduction in natural seawater at pH 8 [40].

In accordance to our companion study [12], this study showed that dissolved Fe may also be formed by photoreductive dissolution of crystalline iron(III) (hydr)oxides such as lepidocrocite at pH 8 in the presence of siderophores. We observed that photoreductive dissolution of lepidocrocite at pH 8 in the presence of the siderophore DFOB was far more significant in the visible than in the UV range. In comparison to the previous wavelength-dependent studies, the response of photoreductive dissolution to irradiation of light was more strongly shifted towards higher wavelengths (above 400 nm). Since light with wavelengths between 400 and 500 nm has the highest penetration depth in oligotrophic seawaters [21], we hypothesize that photoreductive dissolution of colloidal Fe in the presence of hydroxamate siderophores may occur deep into the irradiated water column of oligotrophic oceanic waters. Further experiments in natural seawater samples with lepidocrocite and other iron(III) (hydr)oxide phases in the presence of lower concentrations of siderophore compounds are required to account for more natural conditions and to corroborate the observed findings in this study.

4. References

- [1] Wells, M. L., Mayer, L. M., Donard, O. F. X., Sierra, M. M. D. and Ackelson, S. G. **1991**. The photolysis of colloidal iron in the oceans. *Nature* 353: 248-250.
- [2] McKnight, D. M., Kimball, B. A. and Bencala, K. E. **1988**. Iron photoreduction and oxidation in an acidic mountain stream. *Science* 240: 637-640.
- [3] Erel, Y., Pehkonen, S. O. and Hoffmann, M. R. **1993**. Redox chemistry of iron in

- fog and stratus clouds. *J. Geophys. Res.* 98: 18423-18434.
- [4] Johnson, K. S., Coale, K. H., Elrod, V. A. and Tindale, N. W. **1994**. Iron photochemistry in seawater from the equatorial Pacific. *Mar. Chem.* 46: 319-334.
- [5] Kraemer, S. M., Butler, A., Borer, P. and Cervini-Silva, J. **2005**. Siderophores and the dissolution of iron-bearing minerals in marine systems. *Rev. Mineral. Geochem.* 59: 53-84.
- [6] Borer, P. M., Sulzberger, B., Reichard, P. and Kraemer, S. M. **2005**. Effect of siderophores on the light-induced dissolution of colloidal iron(III)(hydr)oxides. *Mar. Chem.* 93: 179-193.
- [7] Borer, P., Hug, S. J., Sulzberger, B., Kraemer, S. M. and Kretzschmar, R. **2007**. Photolysis of citrate on the surface of lepidocrocite: An in situ attenuated total reflection infrared spectroscopy study. *J. Phys. Chem. C* 111: 10560-10569.
- [8] Siffert, C. and Sulzberger, B. **1991**. Light-induced dissolution of hematite in the presence of oxalate - a case-study. *Langmuir* 7: 1627-1634.
- [9] Faust, B. C. and Hoffmann, M. R. **1986**. Photoinduced reductive dissolution of α -Fe₂O₃ by bisulfite. *Environ. Sci. Technol.* 20: 943-948.
- [10] Waite, T. D. and Morel, F. M. M. **1984**. Photoreductive dissolution of colloidal iron oxides in natural waters. *Environ. Sci. Technol.* 18: 860-868.
- [11] Cunningham, K. M., Goldberg, M. C. and Weiner, E. R. **1988**. Mechanisms for aqueous photolysis of adsorbed benzoate, oxalate and succinate on iron oxyhydroxides (goethite) surfaces. *Environ. Sci. Technol.* 22: 1090-1097.
- [12] Borer, P., Sulzberger, B., Hug, S. J., Kraemer, S. M. and Kretzschmar, R. **submitted**. Photoreductive dissolution iron(III) (hydr)oxides in the absence of organic ligands: experimental studies and kinetic modeling *Environ. Sci. Technol.*
- [13] Sherman, D. M. **2005**. Electronic structures of iron(III) and manganese(IV) (hydr)oxide minerals: Thermodynamics of photochemical reductive dissolution in aquatic environments. *Geochim. Cosmochim. Acta* 69: 3249-3255.
- [14] Waite, T. D. **1990**. Photo-redox processes at the mineral-water interface. *Rev. Mineral.* 23: 559-603.
- [15] Benkelberg, H. J. and Warneck, P. **1995**. Photodecomposition of iron(III) hydroxo and sulfato complexes in aqueous-solution - wavelength dependence of OH and SO₄⁻ quantum yields. *J. Phys. Chem.* 99: 5214-5221.
- [16] Faust, B. C. and Hoigne, J. **1990**. Photolysis of Fe(III)-hydroxy complexes as sources of OH radicals in clouds, fog and rain. *Atmos. Environ.* 24: 79-89.
- [17] Lopes, L., de Laat, J. and Legube, B. **2002**. Charge transfer of iron(III) monomeric

and oligomeric aqua hydroxo complexes: Semiempirical investigation into photoactivity. *Inorg. Chem.* 41: 2505-2517.

- [18] Leland, J. K. and Bard, A. J. **1987**. Photochemistry of colloidal semiconducting iron oxide polymorphs. *J. Phys. Chem.* 91: 5076-5083.
- [19] Sherman, D. M. and Waite, T. D. **1985**. Electronic-spectra of Fe³⁺ oxides and oxide hydroxides in the near IR to near UV. *Am. Miner.* 70: 1262-1269.
- [20] Witter, A. E., Hutchins, D. A., Butler, A. and Luther, G. W. **2000**. Determination of conditional stability constants and kinetic constants for strong model Fe-binding ligands in seawater. *Mar. Chem.* 69: 1-17.
- [21] Smith, R. C. and Baker, K. S. **1981**. Optical properties of the clearest natural waters (200-800 nm). *Applied Optics* 20: 177-184.
- [22] Sulzberger, B. and Laubscher, H. **1995**. Reactivity of various types of iron(III) (hydr)oxides towards light-induced dissolution. *Mar. Chem.* 50: 103-115.
- [23] Borer, P., Hug, S. J., Sulzberger, B., Kraemer, S. M. and Kretzschmar, R. **submitted**. ATR-FTIR spectroscopic study of the adsorption of desferrioxamine B and aerobactin to the surface of lepidocrocite (γ -FeOOH) *Geochim. Cosmochim. Acta*.
- [24] Borer, P., Hug, S. J., Sulzberger, B., Kraemer, S. M. and Kretzschmar, R. **submitted**. Photodissolution of lepidocrocite (γ -FeOOH) in the presence of desferrioxamine B and aerobactin. *Geochim. Cosmochim. Acta*.
- [25] Voelker, B. M. and Sulzberger, B. **1996**. Effects of fulvic acid on Fe(II) oxidation by hydrogen peroxide. *Environ. Sci. Technol.* 30: 1106-1114.
- [26] Parker, C. A. **1968**. *Photoluminescence of solutions, with applications to photochemistry and analytical chemistry*. Elsevier: Amsterdam.
- [27] Lindgren, T., Wang, H., Beermann, N., Vayssieres, L., Hagfeldt, A. and Lindquist, S. **2002**. Aqueous photoelectrochemistry of hematite nanorod array. *Sol. Energ. Mater. Sol. Cells* 71: 231-243.
- [28] Björkstén, U., Moser, J. and Grätzel, M. **1994**. Photoelectrochemical studies on nanocrystalline hematite films. *Chem. Mater.* 6: 858-863.
- [29] Dare-Edwards, M. P., Goodenough, J. B., Hamnett, A. and Trevellick, P. R. **1983**. Electrochemistry and photoelectrochemistry of iron(III) oxide. *J. Chem. Soc., Faraday Trans. 1* 79: 2027-2041.
- [30] Langford, C. H. and Carey, J. H. **1975**. Charge-transfer photochemistry of hexaquoiron(III) ion, chloropentaaquoiron(III) ion, and μ -dihydroxo dimer explored with tert-butyl alcohol scavenging. *Can. J. Chem.* 53: 2430-2435.
- [31] Morehouse, K. M., Flitter, W. D. and Mason, R. P. **1987**. The enzymatic oxidation of Desferal to a nitroxide free-radical. *Febs Lett.* 222: 246-250.

- [32] Solinas, V., Deiana, S., Gessa, C., Pistidda, C. and Rausa, R. **1996**. Reduction of the Fe(III)-desferrioxamine-B complexes by caffeic acid: A reduction mechanism of biochemical significance. *Soil Biol. Biochem.* 28: 649-654.
- [33] Ghosh, K. K., Patle, S. K., Sharma, P. and Rajput, S. K. **2003**. A comparison between the acid-catalysed reactions of some dihydroxamic acids, monohydroxamic acids and desferal. *Bull. Chem. Soc. Jpn.* 76: 283-290.
- [34] Holmen, B. A. and Casey, W. H. **1996**. Hydroxamate ligands, surface chemistry, and the mechanism of ligand-promoted dissolution of goethite [α -FeOOH(s)]. *Geochim. Cosmochim. Acta* 60: 4403-4416.
- [35] Kari, F. G., Hilger, S. and Canonica, S. **1995**. Determination of the reaction quantum yield for the photochemical degradation of Fe(III)-EDTA - Implications for the environmental fate of EDTA in surface waters. *Environ. Sci. Technol.* 29: 1008-1017.
- [36] Barbeau, K., Rue, E. L., Trick, C. G., Bruland, K. T. and Butler, A. **2003**. Photochemical reactivity of siderophores produced by marine heterotrophic bacteria and cyanobacteria based on characteristic Fe(III) binding groups. *Limnol. Oceanogr.* 48: 1069-1078.
- [37] Rijkenberg, M. J. A., Gerringa, L. J. A., Carolus, V. E., Velzeboer, I. and de Baar, H. J. W. **2006**. Enhancement and inhibition of iron photoreduction by individual ligands in open ocean seawater. *Geochim. Cosmochim. Acta* 70: 2790-2805.
- [38] Rijkenberg, M. J. A. (2005). Photochemistry and organic complexation of iron: interactions in the Southern Ocean. PhD Thesis, University of Groningen.
- [39] Rijkenberg, M. J. A., Gerringa, L. J. A., Neale, P. J., Timmermans, K. R., Buma, A. G. J. and de Baar, H. J. W. **2004**. UVA variability overrules UVB ozone depletion effects on the photoreduction of iron in the Southern Ocean. *Geophys. Res. Lett.* 31.
- [40] Wells, M. L. and Mayer, L. M. **1991**. The photoconversion of colloidal iron oxyhydroxides in seawater. *Deep-Sea Res.* 38: 1379-1395.

Supporting Information

Chapter 6

Table of contents

1. Synthesis and characterization of lepidocrocite	186
1.1. Synthesis of lepidocrocite	186
1.2. UV-Visible spectra of lepidocrocite	186
2. Transmittance spectra of high pass filters used in experimental setup I	189
3. Absorbance of ferrioxalate solutions used for actinometry	190
4. Calculation of normalized photoreductive dissolution rates	190
5. Photodissolution experiment at pH 8 in the presence of DFOB	195
6. Solution photochemistry assessed by a kinetic model	195
7. References	197

1. Synthesis and characterization of lepidocrocite

1.1 Synthesis of lepidocrocite

Lepidocrocite was synthesized by oxidation of FeCl_2 with NaNO_2 in the presence of hexamethylenetetramine at $70\text{ }^\circ\text{C}$ [1]. During synthesis, nitrogen and carbon containing by-products were formed which were not entirely removed during the washing procedure. For 25 mg/L lepidocrocite suspensions, a nitrogen contamination of 0.17, 0.11 and 0.07 μM of NO_2^- -N, NO_3^- -N and NH_4^+ -N, respectively, and a carbon contamination of 10 $\mu\text{g/L}$ was estimated [2]. However, it was demonstrated by reference experiments with a contamination-free lepidocrocite phase that the photoreactivity of lepidocrocite (in terms of dissolved Fe(II) and H_2O_2 formation) was not affected by the traces of these contaminants [2].

1.2 UV-Visible absorption spectra of lepidocrocite

Diffuse reflectance spectra of lepidocrocite powder were measured with an Uvikon 860 spectrophotometer (Kontron Instruments, Zurich, Switzerland) equipped with a 9-cm diameter integrating sphere, and recorded in steps of 1 nm (bandwidth 2 nm) between 275 – 700 nm. The procedure for the determination of absorption coefficients k and scattering coefficients s of lepidocrocite powder is described elsewhere [3]. Different mixtures of lepidocrocite and barium sulfate (Kodak white reflectance standard) were prepared and diffuse reflectance spectra of these mixtures were measured. By using k and s coefficients of barium sulfate (provided in [3]) in the Kubelka-Munk model, absorption coefficients and scattering coefficient for lepidocrocite were calculated (Fig. S1). In addition, UV-visible absorption spectra of aqueous lepidocrocite suspensions were also measured with the same setup, however in the transmission mode. Lepidocrocite suspensions (25 mg/L or 100 mg/L lepidocrocite) in 0.01 M electrolyte (NaClO_4) were transferred into a 1 cm Quartz glass cuvette placed in front of the entrance slit of the integrating sphere of the photospectrometer. Transmittance spectra were measured and corrected for a blank (electrolyte solution). The calculated absorption spectra above ~ 600 nm are not reliable because of the high baseline absorption, due to significant backscattering of incoming light by the oxide particles in the cuvette. These spectra were measured to approximately estimate the fraction of light absorbed in 25 mg/L lepidocrocite suspensions, as used in the photodissolution experiments described below. As shown in Fig. S2, the absorption of light of 25 mg/L lepidocrocite suspensions is small. In the photoirradiation setup with the Pyrex glass vessel, where the pathlength

of light through the suspension was 6.2 cm, ~50% of the incoming light at wavelengths below 400 nm was absorbed by the suspension.

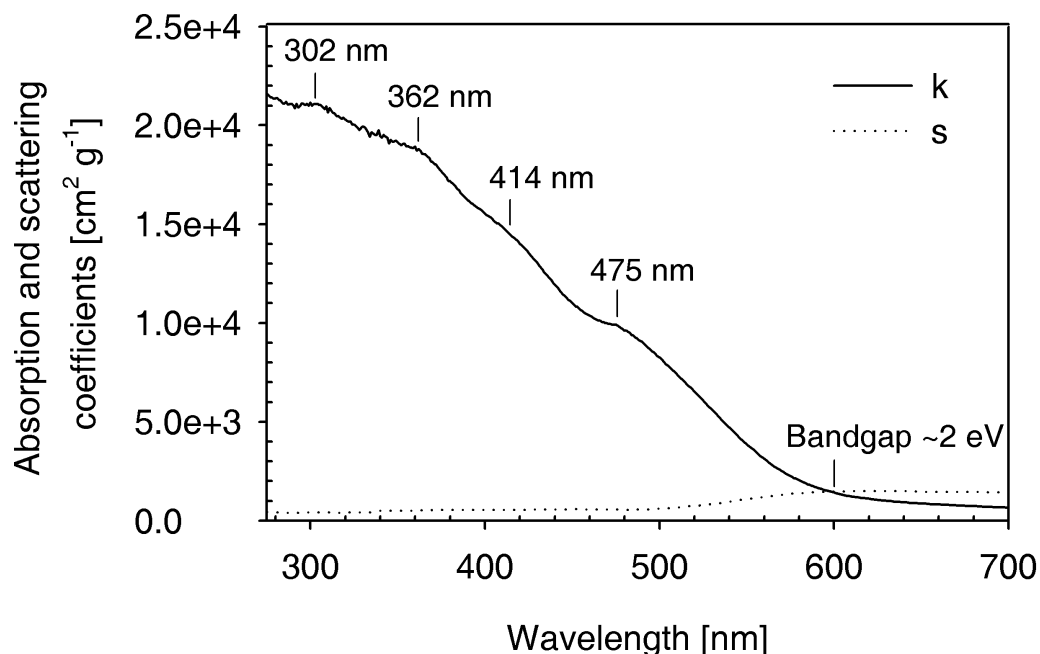


Fig. S1: UV-Vis absorption spectra of lepidocrocite (powder). Absorption (k) and scattering (s) coefficients were measured by diffuse reflectance spectroscopy.

In addition, UV-visible absorption spectra of aqueous lepidocrocite suspensions were also measured with the same setup, however in the transmission mode. Lepidocrocite suspensions (25 mg/L or 100 mg/L lepidocrocite) in 0.01 M electrolyte (NaClO₄) were transferred into a 1 cm Quartzglass cuvette placed in front of the entrance slit of the integrating sphere of the photospectrometer. Transmittance spectra were measured and corrected for a blank (electrolyte solution). The calculated absorption spectra above ~600 nm are not reliable because of the high baseline absorption, which was due to significant backscattering of incoming light by the oxide particles in the cuvette. These spectra were measured to approximately estimate the fraction of light absorbed in 25 mg/L lepidocrocite suspensions, as used in the photodissolution experiments described below. As shown in Fig. S2, the absorption of light of 25 mg/L lepidocrocite suspensions is small. In the photoirradiation setup with the Pyrex glass vessel, where the pathlength of light through the suspension was 6.2 cm, ~50% of the incoming light at wavelengths below 400 nm was absorbed by the suspension.

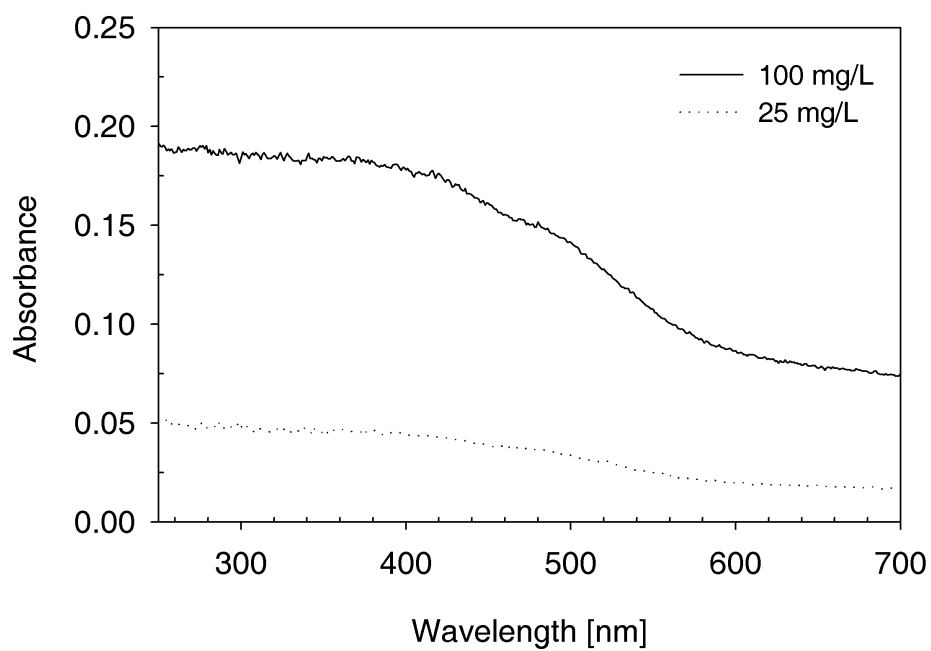


Fig. S2: UV-Vis absorption spectra of aqueous suspensions of lepidocrocite at pH 6 in a 1 cm Quartzglass cuvette.

2. Transmittance spectra of high pass filters used in experimental setup I

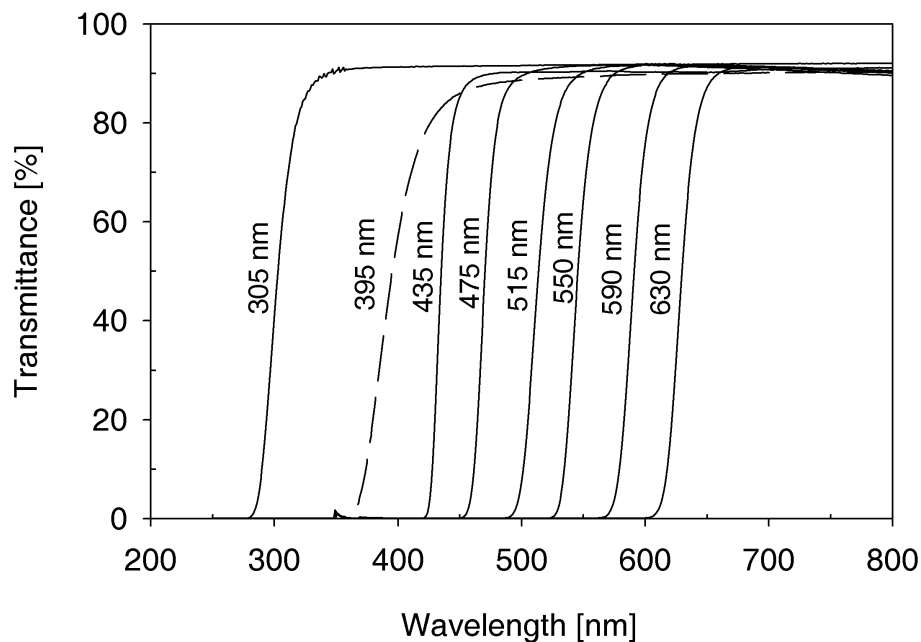


Fig. S3: Transmission spectra of high-pass optical glass filters used in experimental Setup I to determine the wavelength-dependence of lepidocrocite photodissolution. The wavelengths at 50% transmittance (cut-off edges) of each high-pass filter are also indicated in this figure. Filters were purchased from Schott Guinchart, Yverdon-les-Bains, Switzerland. The names of the filters as shown in this figure with increasing wavelengths at 50% transmission are: N-WG305, GG395, GG435, GG475, OG515, OG550, OG590 and RG630.

3. Absorbance of ferrioxalate solutions used for actinometry

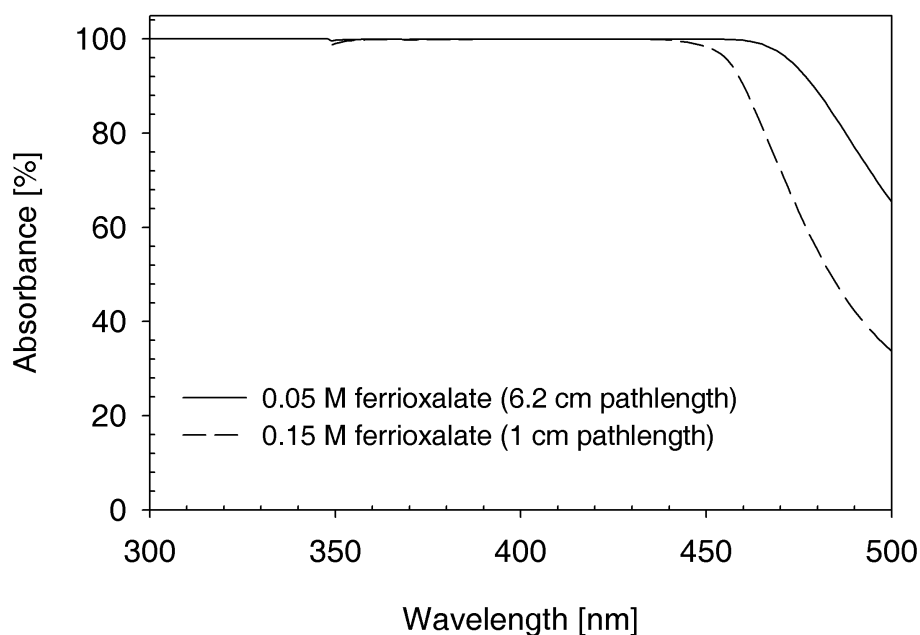


Fig. S4: Absorbance (in %) of the ferrioxalate solution used for the determination of the photon flux in the two photoirradiation setups. For the experimental Setup I (use of high-pass filters), the photon flux at wavelength below 475 nm was determined in the Pyrex vessel containing 350 mL of a 0.05 M ferrioxalate solution (pathlength 6.2 cm). For the experimental Setup II (monochromator-based setup), the photon flux was determined in a UV-transparent cuvette with 1 cm pathlength containing a solution of 0.15 M ferrioxalate.

4. Calculation of normalized photoreductive dissolution rates

In the monochromator setup (Setup II), dissolution rates and photon fluxes were determined directly by dissolution experiments and chemical actinometry under irradiation of light with narrow bandpass spectral windows (20 nm bandwidth). In the presence of DFOB at pH 3, photoreductive dissolution rates were calculated as the difference of the formation rates of total dissolved iron determined under irradiation and in the dark (cf. Fig. 2 and Table S2). The corresponding thermal (dark) dissolution rate was determined under irradiation of light at 630 nm, where photoreductive dissolution was not expected to occur. In doing so, we were able to take into account the effect of stray light (white light) emerging from the monochromator that may lead to systematically too high photoreductive dissolution rates at all investigated wavelengths.

In the case of the experimental setup with optical high-pass filters (Setup I), dissolution rates and photon fluxes were determined under irradiation with high-pass

filtered light (cf. Fig. S3). In order to relate photoreductive dissolution rates and photon fluxes to (narrow) bandpass spectral ranges instead of high-pass spectral ranges (Fig. S3), we calculated the difference in dissolution rates and photon fluxes determined with different high-pass filters. The following example illustrates this procedure: The rate of photoreductive dissolution of lepidocrocite in the spectral range 305-395 nm was calculated by subtracting the rate determined under irradiation of filtered light with the 395 nm high-pass filter from the rate determined under irradiation of filtered light with the 305 nm high-pass filter. The specific photon flux in the spectral range 305-395 nm was calculated accordingly. Fig. S5 shows the resulting spectral windows, as defined by the difference in transmission curves (cf. Fig. S3) of two high-pass filters with cut-off edges next to each other (e.g. 305-395 nm). Not included in Fig. S3 is the reduction of transmission by the Pyrex glass window of the reaction vessel. In the absence or presence of DFOB, photoreductive dissolution rates were calculated by differences in the formation of dissolved Fe(II) (cf. Fig. 2 and Table S1) or total dissolved iron (cf. Fig. S6 and Table S3), respectively. Fe(II) formation rates were calculated without including the first ~45 min, where fast initial dissolution occurred (cf. Fig. 2).

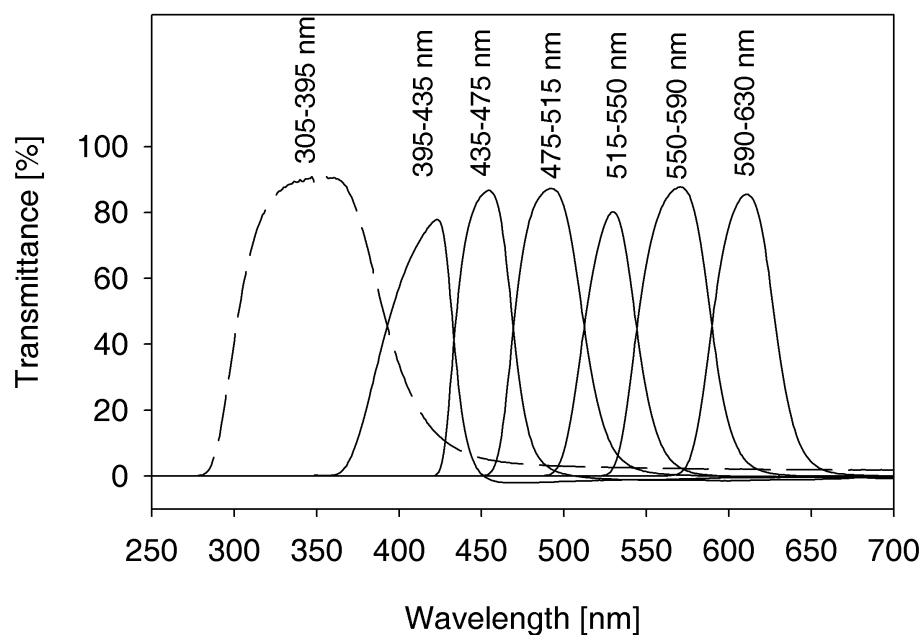


Fig. S5: Spectral windows defined by difference in transmittance of two high-pass filters with cut-off edges next to each other (cf. Fig. S3). The labels are related to the 50 % internal transmittance of each specified high-pass filter.

Photon fluxes in the monochromator based setup (Setup II) were determined by ferrioxalate actinometry. The spectral window with the highest wavelength applied in the monochromator-based setup was 440 ± 10 nm, hence enabling the measurement

of the photon flux by ferrioxalate actinometry. Photon fluxes in the experimental setup with high-pass filters (Setup I) were measured either by ferrioxalate actinometry for wavelengths < 475 nm or were estimated on the basis of spectral emission data of the light source for wavelengths > 475 nm. Spectral emission data were provided by the lamp manufacturer.

Photoreductive dissolution rates were normalized to the flux of incoming light. Measured photon fluxes and photoreductive dissolution rates obtained in both setups as well as photoreductive dissolution rates normalized to the corresponding photon fluxes are listed in Tables S1 to S3. The total error of these normalized rates as calculated by error propagation of estimated relative errors associated with the measurement of dissolution rates and light fluxes are also included in Tables S1 to S3. Error estimates of the photoreductive dissolution rates and photon fluxes are based on measured deviations of rates and fluxes determined in a small number of replicate experiments.

Table S1: Calculation of normalized photoreductive dissolution rates for the dissolution experiments conducted at pH 3 in the absence of DFOB with the experimental Setup I (use of high-pass filters) (cf. Fig. 1 and 2)

Wave-length ^a	Photon flux ^b	Photo-reductive dissolution rate ^c	Normalized photoreductive dissolution rates	Estimated error of single dissolution rates	Estimated error of single light flux measurements	2 x total error ^d
[nm]	[$\mu\text{einstein/s}$]	[$\mu\text{M/s}$]	[$\mu\text{mol/einstein}$]			[$\mu\text{mol/einstein}$]
305 -395	5.16 (1.2)	5.97E-05	15.32	10%	10%	3.06
395 – 435	3.52 (1.04)	9.88E-05	11.81	10%	10%	2.36
435 – 475	4.47 (0.98)	4.13E-05	8.36	10%	10%	1.67
475 – 515	7.03 ^e	1.80E-05	3.23	10%	20%	1.02
515 – 550	5.32 ^e	1.97E-05	0.78	10%	20%	0.25
550 – 590	8.18 ^e	2.91E-07	0.81	10%	20%	0.26
590 – 630	8.17 ^e	9.30E-06	0.68	10%	20%	0.21

^a Spectral window of incoming light as determined by the difference in transmittance (50%) of two optical high-pass filters (see Fig. S5). ^b The photon flux in the spectral windows was calculated as described above. Below 475 nm, light fluxes were determined by 0.15 M ferrioxalate actinometry with average quantum yields estimated for the spectral range (values in parentheses). Above 475 nm, the photon fluxes were estimated on the basis of spectral emission data provided by the lamp manufacturer and by comparison of photon fluxes determined at lower wavelengths by ferrioxalate actinometry. ^c Photoreductive dissolution rates were calculated as described above. ^d The total error of the normalized photoreductive dissolution rates was calculated by error propagation, by including estimated errors of single dissolution rates and of single light flux measurements. ^e Estimated values.

Table S2: Calculation of normalized photoreductive dissolution rates for the dissolution experiments conducted at pH 3 in the presence of DFOB with the experimental Setup II (monochromator-based setup) (cf. Fig. 3)

Wave-length ^a	Photon flux ^b	Photo-reductive dissolution rates ^c	Normalized photoreductive dissolution rates	Estimated error of dissolution rates	Estimated error of light flux measurements	2 x total error ^e
[nm]	[$\mu\text{einstein/s}$]	[$\mu\text{M/s}$]	[$\mu\text{mol/einstein}$]			[$\mu\text{mol/einstein}$]
300 nm	1.86 (1.22)	3.19E-05	17.11	10%	5%	1.91
320 nm	3.74 (1.21)	4.82E-05	12.89	10%	5%	1.44
340 nm	4.71 (1.20)	4.56E-05	9.65	10%	5%	1.08
360 nm	5.64 (1.18)	3.82E-05	6.77	10%	5%	0.76
380 nm	6.42 (1.15)	3.81E-05	5.94	10%	5%	0.66
400 nm	6.81 (1.12)	2.24E-05	3.29	10%	5%	0.37
420 nm	6.97 (1.06)	1.74E-05	2.49	10%	10%	0.35
440 nm	6.54 (1.01)	1.17E-05	1.78	10%	10%	0.25
		Thermal dissolution rate ^d				
		[$\mu\text{M/s}$]				
630 nm		1.81E-04				

^a Wavelengths with maximum emission in the spectral region of incoming light (20 nm bandpass).

^b Photon fluxes were determined with 0.15 M ferrioxalate actinometry. The values in parentheses are quantum yields used for the determination of photon fluxes by ferrioxalate actinometry. These quantum yields were interpolated from recommended values [4]. ^c Photoreductive dissolution rates were calculated as described above. ^d The ‘thermal’ dissolution rate was determined under irradiation of light at 630 nm where photoreductive dissolution of lepidocrocite was not expected to occur. The reason for not conducting this reference experiment in the dark was to take into account the effect of stray light (white light) emerging from the monochromator, which may lead to systematically too high photoreductive dissolution rates at all wavelengths. ^e The total error of the normalized photoreductive dissolution rates was calculated by error propagation, by including estimated errors of the dissolution rates and of the light flux measurements.

Table S3: Calculation of normalized photoreductive dissolution rates for the dissolution experiments conducted at pH 8 in the presence of DFOB with the experimental Setup I (use of high-pass filters) (cf. Fig. 4 and Fig. S6)

Wave-length ^a	Photon flux ^b	Photo-reductive dissolution rate ^c	Normalized photoreductive dissolution rates	Estimated error of single dissolution rates	Estimated error of single light flux measurements	2 x total error ^d
[nm]	[μ einstein/s]	[μ M/s]	[μ mol/einstein]			[μ mol/einstein]
305 -395	5.16 (1.2)	5.97E-05	11.56	10%	10%	2.31
395 – 435	3.52 (1.04)	9.88E-05	28.05	10%	10%	5.61
435 – 475	4.47 (0.98)	4.13E-05	9.22	10%	10%	1.84
475 – 515	7.03 ^e	1.80E-05	2.56	10%	20%	0.81
515 – 550	5.32 ^e	1.97E-05	3.70	10%	20%	1.17
550 – 590	8.18 ^e	2.91E-07	0.04	10%	20%	0.01
590 – 630	8.17 ^e	9.30E-06	1.14	10%	20%	0.36

^a Spectral window of incoming light as determined by the difference in transmittance (50%) of two optical high-pass filters (see Fig S5). ^b The photon flux in the spectral windows was calculated as described above. Below 475 nm, light fluxes were determined by 0.15 M ferrioxalate actinometry with average quantum yields estimated for the spectral range (values in parentheses). Above 475 nm, the photon fluxes were estimated on the basis of spectral emission data provided by the lamp manufacturer and by the comparison of photon fluxes determined at lower wavelengths by ferrioxalate actinometry. ^c Photoreductive dissolution rates were calculated as described above. ^d The total error of the normalized photoreductive dissolution rates was calculated by error propagation, by including estimated errors of single dissolution rates and of single light flux measurements. ^e Estimated values.

5. Photodissolution experiment at pH 8 in the presence of DFOB

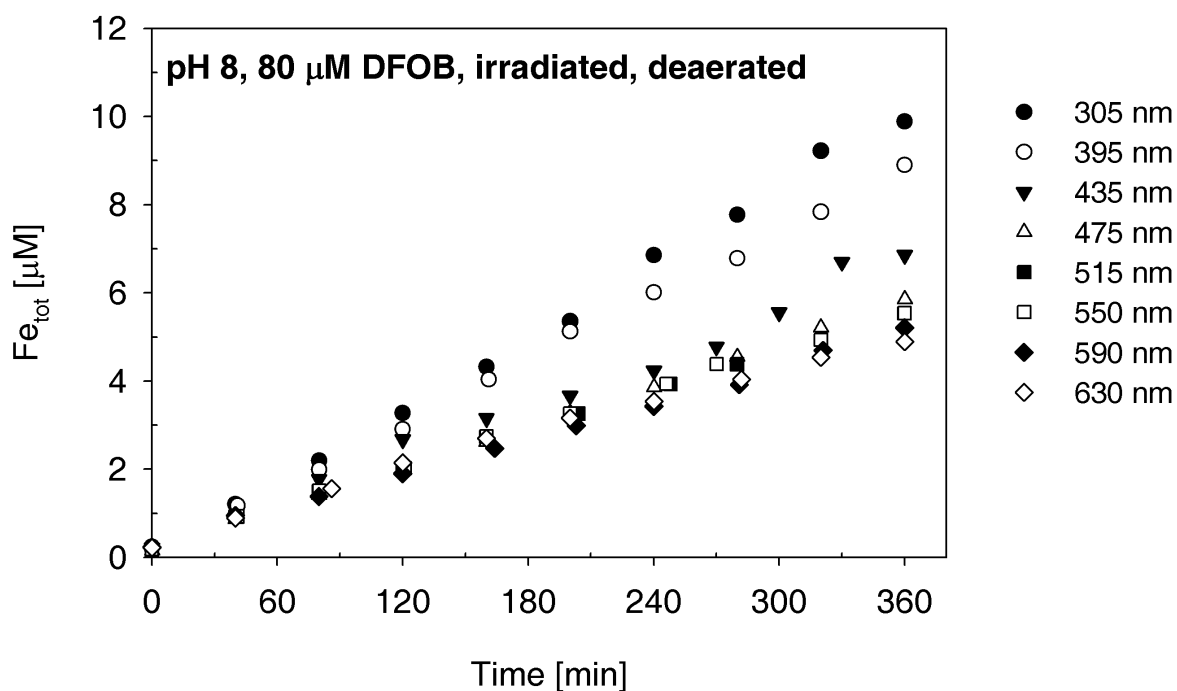


Fig. S6: Wavelength-dependence of photodissolution with 25 mg/L lepidocrocite suspensions at pH 8 in the presence of 80 μM DFOB (0.01 M NaClO_4) as determined with the experimental Setup I (use of high-pass filters). Total dissolved iron was measured. Dissolution rates determined by the slopes of the time-dependent formation of total dissolved iron are listed in Table S3.

6. Solution photochemistry assessed by a kinetic model

With the kinetic model described below, we estimated the concentration of dissolved Fe(II) that may form during photolysis of dissolved Fe(III) at pH 3, whereby the formation of dissolved Fe(III) was modeled by the release of lattice Fe(III) from the surface of lepidocrocite by a proton-promoted dissolution mechanism (cf. reaction RL1 in Table S4). In the model, we adjusted the rate constant of Fe(III) release into solution (reaction RL1), such that 0.8 μM dissolved Fe is formed during proton-promoted dissolution of lepidocrocite (25 mg/L suspension with a surface Fe(III) concentration of 28 μM) within 6 hours at pH 3 under irradiation with polychromatic light (300-800 nm). The formation of 0.8 μM total dissolved Fe is based on experimental results of proton-promoted dissolution of lepidocrocite (25 mg/L) at pH 3 in the dark [5]. According to the model below, only 20 % of the total dissolved Fe is reduced to Fe(II). Thus, only 0.16 μM dissolved Fe(II) is formed after 6 hours of irradiation with polychromatic light (300-800 nm). Depending on the spectral range of light applied in

both experimental setups (I and II), the extent of dissolved Fe(II) formation may be greatly diminished in comparison with the estimated formation under polychromatic light.

Table S4: Kinetic model ^a and rate constants

	Reactions	rate constants (s ⁻¹) or (M ⁻¹ s ⁻¹)	Ref.
	Fe(III) release into solution		
RL1	Fe(III) _{surf} → Fe(III)	1.3 × 10 ⁻⁶	Estimated ^b
	Fe(III) photolysis in solution		
L2 ^a	Fe(III) → Fe(II) + ·OH	1.5 × 10 ⁻³	[2]
	Fe(II) oxidation in solution		
O1	Fe(II) + H ₂ O ₂ → Fe(III) + ·OH	63	[6]
O2	Fe(II) + O ₂ ⁻ /HO ₂ → Fe(III) + H ₂ O ₂	1.3 × 10 ⁶	[6]
O3	Fe(II) + ·OH → Fe(III)	3.2 × 10 ⁸	[6]
	Fe(III) reduction in solution		
	Fe(III) + H ₂ O ₂ → Fe(II) + O ₂ ⁻ /HO ₂	2 × 10 ⁻³	[6]
	Fe(III) + O ₂ ⁻ /HO ₂ → Fe(II) + O ₂	7.8 × 10 ⁵	[6]
	Solution reactions of ROS		
RC1	·OH + ·OH → H ₂ O ₂	5.2 × 10 ⁹	[6]
RC2	·OH + O ₂ ⁻ /HO ₂ → O ₂	7.1 × 10 ⁹	[6]
RC3	·OH + H ₂ O ₂ → O ₂ ⁻ /HO ₂	3.3 × 10 ⁷	[6]
RC4	O ₂ ⁻ /HO ₂ + O ₂ ⁻ /HO ₂ → H ₂ O ₂	2.3 × 10 ⁶	[6]

^a Model simulations were performed with the software program Kintecus [7]. ^b This rate constant was chosen such that the release of surface Fe(III) from a constant pool of 28 μM surface Fe(III) (estimated for a 25 mg/L suspension [2]) results in the formation of approximately 0.8 μM Fe(III) in 6 hours at pH 3 in the dark.

7. References

- [1] Brauer, G. **1963**. *Handbuch der präparativen anorganischen Chemie*. Ferd. Enke Verlag: Stuttgart, Germany.
- [2] Borer, P., Sulzberger, B., Hug, S. J., Kraemer, S. M. and Kretzschmar, R. **submitted**. Photoreductive dissolution iron(III) (hydr)oxides in the absence of organic ligands: experimental studies and kinetic modeling *Environ. Sci. Technol.*
- [3] Ciani, A., Goss, K. U. and Schwarzenbach, R. P. **2005**. Light penetration in soil and particulate minerals. *Eur. J. Soil Sci.* 56: 561-574.
- [4] Faust, B. C. and Hoigne, J. **1990**. Photolysis of Fe(III)-hydroxy complexes as sources of OH radicals in clouds, fog and rain. *Atmos. Environ.* 24: 79-89.
- [5] Borer, P., Hug, S. J., Sulzberger, B., Kraemer, S. M. and Kretzschmar, R. **submitted**. Photodissolution of lepidocrocite (γ -FeOOH) in the presence of desferrioxamine B and aerobactin. *Geochim. Cosmochim. Acta*.
- [6] Kwan, W. P. and Voelker, B. M. **2002**. Decomposition of hydrogen peroxide and organic compounds in the presence of dissolved iron and ferrihydrite. *Environ. Sci. Technol.* 36: 1467-1476.
- [7] Ianni, J. C. **2006**. *Kintecus*, vers. Windows Version 3.90.

Chapter 7

Conclusions and Outlook

1. Siderophore-promoted dissolution iron(III) hydroxide phases

The results presented in this thesis demonstrate that the two siderophores, aerobactin and DFOB, interact with different iron(III) (hydr)oxides by promoting dissolution of these phases. The interactions of these siderophores with the surface of lepidocrocite were investigated at the molecular level by ATR-FTIR spectroscopy (chapter 3). This investigation revealed that DFOB interacts predominantly with the surface at acidic pH by inner-sphere complexation of two to three hydroxamic acid groups. Due to steric hindrance at the surface of lepidocrocite, DFOB cannot form hexadentate mononuclear surface complexes. Thus, surface complexes of DFOB may exhibit a distinct photoreactive behavior as compared to the photostable hexadentate Fe(III)-DFOB complex in solution. In chapter 6, the results of the wavelength-dependent dissolution experiments indicated that DFOB is directly involved in the photoreductive dissolution of lepidocrocite. We suggested that DFOB forms photoreactive surface complexes which are photolyzed in a ligand-to-metal charge-transfer reaction under irradiation of visible light.

It has been recently assumed that siderophores carrying α -hydroxycarboxylic acid functional groups may promote photoreductive dissolution of iron(III) (hydr)oxide phases under irradiation of sunlight [1]. In chapter 1, we demonstrated that solution Fe(III)-complexes of aerobactin are photolysed at pH 6 under irradiation of actinic light (300-460 nm). At the surface of lepidocrocite, we concluded that photolysis of the α -hydroxycarboxylic acid group in surface Fe(III)-aerobactin complexes may occur (chapter 4), but that this reaction is rather ineffective as compared to the surface photolysis of citrate, a small polycarboxylate compound with an α -hydroxycarboxylic acid group. In chapter 2, we showed by radiotracer experiments and by ATR-FTIR spectroscopy that the α -hydroxycarboxylic acid group in citrate is specifically photooxidized at the surface of lepidocrocite.

In comparison to the trihydroxamate siderophore DFOB, the higher number of potentially iron binding groups in aerobactin made it rather difficult to provide conclusive spectroscopic insights into the coordination of aerobactin functional groups

to the surface of lepidocrocite. We concluded that the carboxylate groups coordinate to the surface by inner-sphere complexation to an increasing degree with decreasing pH (chapter 3). However, we could not distinguish between the surface coordination of the carboxylic acid groups or the α -hydroxycarboxylic acid. The interaction of the carboxylic acid groups in aerobactin to the surface was supported by batch adsorption experiments with Fe(III)-aerobactin complexes, where substantial adsorption of Fe(III)-aerobactin complexes was observed and where the lateral carboxylic acid groups were able to interact with the surface. A drawback in the spectroscopic investigation of adsorbed aerobactin were the weak spectral contributions of the hydroxamate groups, which made it impossible to determine the coordination of hydroxamic acid groups in aerobactin at the surface of lepidocrocite (chapter 3).

Complementary to the spectroscopic investigation of siderophore interactions at the surface of lepidocrocite, we conducted a macroscopic study where we related dissolution rates of lepidocrocite in the presence of DFOB and aerobactin to experimentally determined surface concentrations of these siderophores (chapter 4). Dissolution rate constants for DFOB- and aerobactin-promoted dissolution of lepidocrocite were determined according to the rate law of ligand-promoted dissolution [2]. In general, rate constants for DFOB-promoted dissolution were significantly higher than for aerobactin-promoted dissolution of lepidocrocite. These results indicated that DFOB is very efficient in promoting dissolution and that aerobactin forms less dissolution-active surface complexes in comparison to DFOB.

Even in the absence of organic ligands, we observed photoreductive dissolution of lepidocrocite below pH 6 (chapter 4). The formation of dissolved Fe(II) was attributed to a semiconductor mechanism in the bulk of lepidocrocite or directly at the surface leading to the reduction of surface Fe(III) sites and subsequent release of Fe(II) into solution. In the presence of DFOB and aerobactin, dissolution of lepidocrocite was similarly enhanced under irradiation of artificial sunlight. The major conclusion of this thesis is that the light-induced enhancement of dissolution of lepidocrocite and other iron(hydr)oxides (cf. chapter 5) can be attributed to the photochemical properties of the iron(III) (hydr)oxide phases and also to the photoreactivity of surface complexes formed by DFOB and aerobactin. As indicated in chapter 6 and in chapter 4, surface complexes formed by both hydroxamic acids and α -hydroxycarboxylic acids are likely involved in a ligand-to-metal charge-transfer reaction leading to the formation of Fe(II) and the subsequent facilitated release of Fe(II) into solution.

In chapter 5 and 6, we investigated in detail the processes leading to the formation of dissolved Fe(II) during irradiation of lepidocrocite suspensions in the absence of organic ligands. It was observed that dissolved Fe(II) and H_2O_2 were formed during

irradiation and that Fe(II) was rapidly reoxidized by H_2O_2 after the light source was turned off. A kinetic model based on the photolysis of surface Fe(III)-hydroxo groups was developed to simulate the processes leading to the formation of dissolved Fe(II) and H_2O_2 . According to the model, the most relevant reaction leading to the formation of solution H_2O_2 was the oxidation of lattice Fe(II) by O_2 . Model simulations suggested that the surface catalyzed reoxidation of Fe(II), incorporated in the lattice surface structure, by molecular O_2 is much faster than the published reoxidation rate of adsorbed Fe(II) on goethite [3].

In chapter 6, we observed that photoreductive dissolution of lepidocrocite in the absence of organic ligands was more effective at lower wavelengths (in the UV range), but also occurred in the visible range. In the presence of DFOB, photoreductive dissolution of lepidocrocite at pH 8 was most effective in the visible range (395-435 nm).

In chapter 1 and 5, the effect of light on the dissolution of other iron(III) (hydr)oxide phases (goethite, ferrihydrite, and amorphous ferric hydroxides) was investigated. Ferrihydrite (freeze dried) and lepidocrocite, both intermediate phases between the thermodynamic more stable goethite phase and the less stable amorphous ferric hydroxides, were most affected by photoreductive dissolution in the presence and absence of siderophores. Furthermore, we showed in chapter 5 that light has only a minor effect on the dissolution of amorphous ferric hydroxides in the presence of DFOB.

2. Environmental significance

The experiments in this thesis were conducted under conditions which are not comparable to conditions in remote ocean waters, regarding total iron and siderophore concentrations. However, the results of this thesis still imply that siderophores play a key role in the solubilization of crystalline iron(III) (hydr)oxides phases or iron bearing minerals in sunlit surface waters. To provide more insights into the role of siderophores in iron solubilization in ocean waters at low iron and ligand concentrations, downscaled experiments representing natural conditions are required. In a current downscaled study, iron dissolution from natural dust in natural seawater was investigated (unpublished results, J. Mendez, Caltech). Dissolution of 1 mg/L dust (3.8 % Fe content) in the presence of 51 nM aerobactin in natural seawater led to almost identical initial dissolution rates in the dark and under irradiation as observed in this thesis with 20 mg lepidocrocite and 45 μM aerobactin (chapter 1). In additional downscaled studies, Rijkenberg and co-workers have investigated the photoproduction of dissolved Fe(II) in

natural and artificial seawater spiked with excess Fe(III) (exceeding Fe(III) solubility) [4, 5]. In both artificial and natural seawater samples, they concluded that the amorphous iron(III) hydroxides formed after addition of excess Fe(III) were the major source for the photoproduction of dissolved Fe(II) and that photoproduction of Fe(II) decreased with increasing aging time of the amorphous iron hydroxides in artificial seawater [4, 5]. Additional experiments were performed in the presence of DFOB, but as these researchers focused on the photoformation of Fe(II), no information was provided on the potential increase in total dissolved iron from photoreductive dissolution of amorphous iron(III) hydroxides in the presence of DFOB [5].

The results and conclusions drawn in this study suggest that siderophores play a major role in the transformation of colloidal iron leading to an increase in the pool of dissolved iron. Due to the high response of photoreductive dissolution of lepidocrocite in the presence of DFOB in the visible range (395-435 nm), we suggest that photoreductive dissolution of iron(III) (hydr)oxides may occur deep into the photic zone of oceanic waters (chapter 6). Provided that iron bound in siderophores such as DFOB is available to marine microorganisms, we suggest a strong link between siderophore-promoted solubilization of colloidal iron and biological iron acquisition.

3. Outlook

It was indicated in this study, that intrinsic photochemical mechanisms of the lepidocrocite phase as well as ligand-to-metal charge-transfer (LMCT) reactions of surface complexes of siderophores with coordinated α -hydroxycarboxylate and unexpectedly also hydroxamate groups may contribute to photoreductive dissolution of lepidocrocite at circumneutral pH. To assess the contribution of each of these possible mechanisms, we encourage more molecular level investigations of the interactions of diverse siderophores at the surface of different iron(III) (hydr)oxides. In addition, the determination of rate constants of iron(III) (hydr)oxide dissolution by a greater number of structurally different siderophores may help to assess the dissolution reactivity of these siderophores and to provide more insights into the processes involved at the surface during iron(III) (hydr)oxide dissolution. In addition surface complexation modeling may help to elucidate the conformation and charge distribution of surface species of siderophores on iron(III) (hydr)oxides. We are convinced that the present spectroscopic and macroscopic data of the adsorption of DFOB to lepidocrocite provides a reasonable basis for surface complexation modeling.

Due to the strong light-absorbing iron(III) (hydr)oxide phases, it has not been possible to experimentally measure the absorption spectra of surface species at iron(III) (hydr)

oxides surfaces, e.g., surface Fe(III)-complexes with siderophore functional groups. To bypass these experimental limitations, ab initio or semi-empirical calculations of charge-transfer transitions may help to predict the photoreactivity of surface Fe(III)-species. In this context, it would be highly rewarding to substantiate the hypothesized photoreactivity of surface Fe(III)-hydroxamate complexes. In order to provide more information on the various photochemical processes involved during photoreductive dissolution of lepidocrocite in the presence of DFOB, we recommend further experiments where reactive oxygen species are also measured.

4. References

- [1] Barbeau, K. **2006**. Photochemistry of organic iron(III) complexing ligands in oceanic systems. *Photochem. Photobiol.* 82: 1505-1516.
- [2] Furrer, G. and Stumm, W. **1986**. The coordination chemistry of weathering: I. Dissolution kinetics of δ -Al₂O₃ and BeO. *Geochim. Cosmochim. Acta* 50: 1847-1860.
- [3] Wehrli, B. **1990**. Redox reactions of metal ions at mineral surfaces. In: *Aquatic chemical kinetics*. Wiley-Interscience, New York: 311-337.
- [4] Rijkenberg, M. J. A. (2005). Photochemistry and organic complexation of iron: interactions in the Southern Ocean. PhD Thesis, University of Groningen.
- [5] Rijkenberg, M. J. A., Gerringa, L. J. A., Carolus, V. E., Velzeboer, I. and de Baar, H. J. W. **2006**. Enhancement and inhibition of iron photoreduction by individual ligands in open ocean seawater. *Geochim. Cosmochim. Acta* 70: 2790-2805.

Acknowledgements

This PhD thesis would not have been possible without the help and support of many people. I was lucky to have a bunch of supervisors who gave me the freedom to do experimental work without hardly any boundary conditions. I am very grateful to Ruben Kretzschmar and Stephan Krämer at ETH and Barbara Sulzberger and Stephan Hug at Eawag for supervising my PhD work and for providing excellent facilities at both institutes.

Stephan Krämer originally had the idea of investigating the role of light on the dissolution of iron(III) (hydr)oxides in the presence of siderophores. Without Stephan Krämer's farsightedness, and without the great knowledge of Barbara Sulzberger and Stephan Hug in interfacial photochemistry, this PhD project would not have been initiated and would not have been so successful.

Working at two institutes was sometimes a difficult task. I would therefore like to thank all the people at Eawag and ETH for making research life as pleasant as possible. From Eawag, I would like to thank Thomas Ruettimann, Hans-Ueli Laubscher, Chris Robinson, Christian Rellstab and Christoph Tellenbach for their everyday jokes that really made me smile. Of course there were many people who supported me during my time at Eawag and made research life very pleasant: Linda Roberts, Ioannis Katsoyiannis, Ralf Kägi, Pascal Wunderlin, Michael Dodd, Andreas Peter, Christophe Werlen, Daniel Pellanda, Andrea Ciani, the technicians from the AUA lab and last but not least the members of the Aquatic Ecology group (especially Christine, Christiane, Sarah, Christian, Christoph, Chris, Diane).

Special thanks go to the following people for support in the lab: Hans-Ueli Laubscher, Kurt Barmettler, Richard Illi, Thomas Ruettimann, Iso Christl, Andrea Ciani and Ralf Kägi.

From the beginning of my PhD project, I wished to be part of the Soil Chemistry Group. Many thanks go to Ruben Kretzschmar for making this possible. I would like to thank all the members of this fantastic group for the many scientific and less scientific discussions we had, for the numerous hiking and ski-weekends and for the

uncountable times we enjoyed drinking beer and wine at the Thirstday Beer event and in Palmhof. Many thanks to all of you: Ruben, Kurt, Charlotte, Iso, Stephan, Andreas, Evert, Jan, Jen-How, Yves, Göril, Amandine, Naraya, Jessi, Ruth, Beate, Jakob, Chico (Oli), Mirjam, Felix, Yves, Jakob, Christian, Anke, Laurie, Frank-Andreas, Petra, Irene, Gérome, Scott, Sabina, and the numerous diploma students and hiwis.

Special thanks go to my office mates for coping with my ups and downs during the last phase of my work and for ignoring me when I was talking bullshit (very often)! Thanks Jessi, Anke, Jakob, Yves and Naraya. I also really appreciated the stimulating scientific discussions with Yves, Jakob and Christian. Many thanks go also to Christian and Jakob for reviewing parts of this thesis.

Finally I want to thank my parents who never stopped supporting me.

And last but not least, I am greatly indebted to the financial support from the Swiss tax payers. Without them, research would not be possible. Merci viel mol!

Curriculum Vitae

Paul Michael Borer

Born April 8, 1977 in Bulawayo, Zimbabwe

Citizen of Erschwil (SO), Switzerland

1984-1991 Primary School in Johannesburg, South Africa and in Wolfenschiessen (NW), Switzerland

1991-1998 Matura Typus C, Kollegium St. Fidelis, Stans (NW), Switzerland

1998-2003 Studies in environmental sciences with specialization in environmental chemistry and terrestrial systems at ETH Zürich, Switzerland

2003 Diploma thesis „Effect of siderophores on the light-induced dissolution of iron(III) (hydr)oxides“ at Eawag and at the Institute of Biogeochemistry and Pollutant Dynamics (ETH Zürich)

2004-2008 PhD thesis at Eawag and at the Institute of Biogeochemistry and Pollutant Dynamics (ETH Zürich)

